A PUBLICATION OF THE AMERICAN SOCIETY OF LUBRICATION ENGINEERS

COMPLIMENTARY

ASLE Transactions

VOLUME 2 NUMBER 1

CONTENTS

Page

CARROLL, J. G. and BOLT, R. O., Development of Radiation Resistant Oils 1

KOTTCAMP, C. F., NEJAK, R. P. and KERN, R. T., The Effects of High Energy Ionizing Radiation on Turbine Oil Performance Characteristics 7

FORSTER, E. O. and KOLFENBACH, J. J., Viscoelastic Behavior of Greases 13

WOLF, J. E. and CONNELLY, R. E., Development of Seals for Rocket Engine Turbopumps 25

GLAESER, W. A. and ALLEN, C. M., A Study of Design Criteria for Oscillating Plain Bearings 32

MASON, W. P., Adhesion Between Metals and its Effect on Fixed and Sliding Contacts 39

[Continued on back cover]

PERGAMON PRESS

NEW YORK LONDON PARIS LOS ANGELES

NOTICES

"Readers are invited to submit written discussions on any of the papers contained in this issue. Discussions received by June 15, 1959, will be published in a following issue. Correspondence should be addressed to ASLE Headquarters."

"ASLE Transactions is published semi-annually by Pergamon Press for the American Society of Lubrication Engineers, 84 East Randolph Street, Chicago 1, Illinois."

OFFICERS OF THE SOCIETY

J. D. LYKINS, *President*
A. B. WILDER, *Vice-President at Large*
J. L. FINKELMANN, *Secretary*
J. W. PETERSON, *Treasurer*
J. O. MCLEAN, *Chairman, Presidential Council*
D. F. WILCOCK, *Eastern Reg. Vice-President*
H. W. MCCULLOCH, JR., *Midwest Reg. Vice-President*
R. C. DISHINGTON, *Western Reg. Vice-President*
P. A. ASSEFF, *Central Reg. Vice-President*
S. C. M. AMBLER, *Canadian Reg. Vice- President*
D. M. CLEAVELAND, *Director*
B. T. HARDING, *Director*
D. W. SAWYER, *Director*
A. B. TWO, *Director*
L. O. WITZENBURG, *Director*
E. E. BISSON, *Director*
R. J. TORRENS, *Director*
B. G. SYMON, *Director*

INDUSTRIAL MEMBERS

Alemite Division, Stewart Warner Corp.
Aluminum Company of America
American Brake Shoe Co.
Bendix Prod. Div., Bendix Aviation Corp.
Bethlehem Steel Co.
Bowser, Inc.
The Cincinnati Milling Machine Co.
E. I. du Pont de Nemours & Co., Inc.
The Elco Lubricant Co.
Esso Standard Oil Co.
The Farval Corp.
Gits Bros. Manufacturing Co.
Gulf Oil Corp.
The Hodson Corp.
Inland Steel Co.
E. F. Houghton & Co.
Lincoln Engineering Co.
The Lubri-Zol Corp.
National Cash Register Co.
Republic Steel Corp.
Shell Oil Co.
Sinclair Refining Co.
Socony Mobil Oil Co., Inc.
Sun Oil Co.
Standard Oil Co. of California
Standard Oil Co. of Indiana
The Texas Co.
Timken Roller Bearing Co.
Trabon Engineering Corp.
U.S. Steel Corp.
Westinghouse Electric Corp.

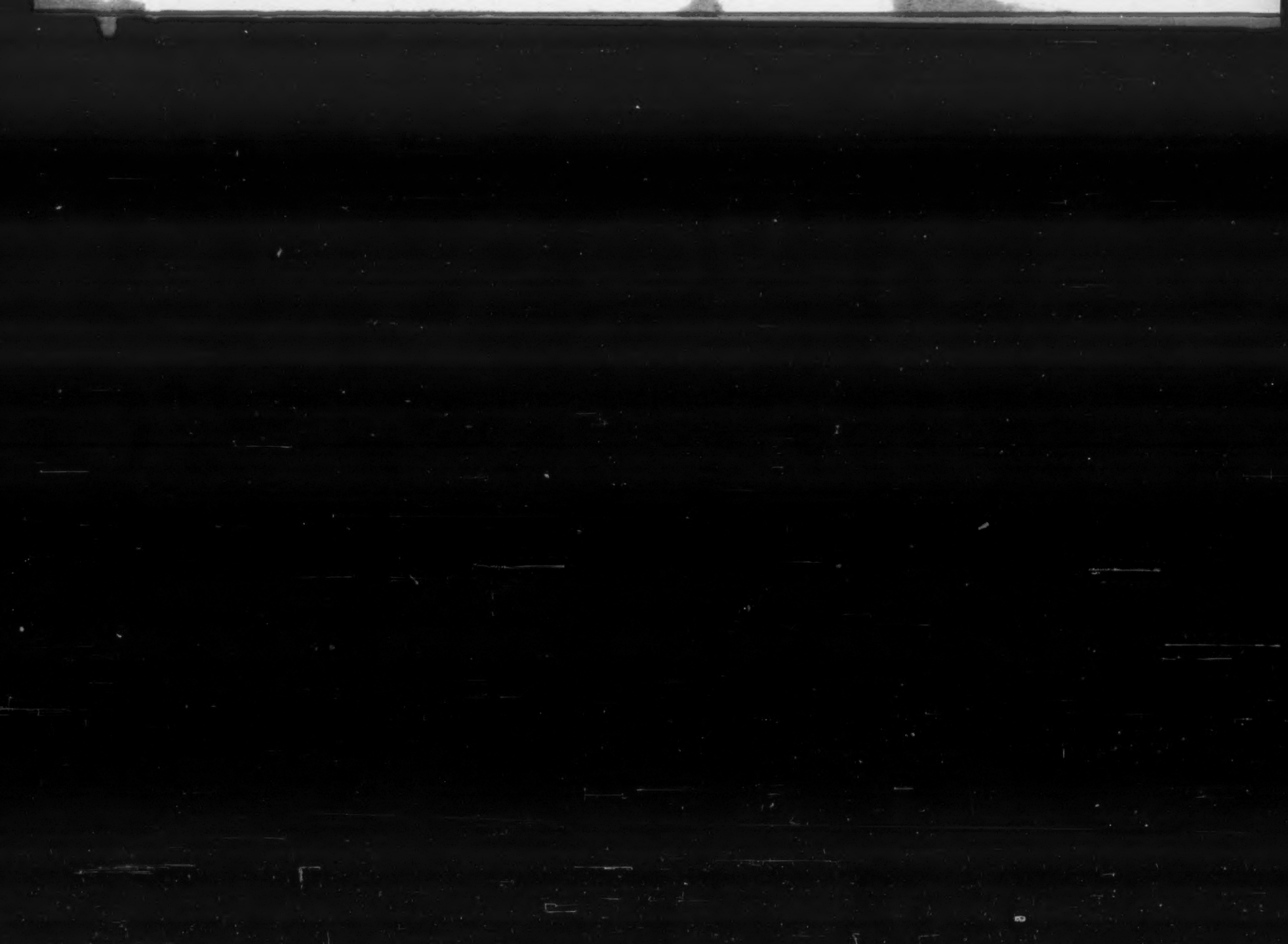

A PUBLICATION OF THE AMERICAN SOCIETY OF LUBRICATION ENGINEERS

ASLE Transactions

VOLUME 2 NUMBER 1

Editor
JOHN BOYD

Editorial Review Committee

E. E. BISSON
A. F. BREWER
A. CAMERON
W. E. CAMPBELL
J. W. GIVENS
D. GODFREY
R. K. GOULD
L. E. HOYER
H.W. McCULLOCH, Jr.
M. E. MERCHANT
E. RABINOWICZ
A. A. RAIMONDI
A. E. SAIBEL
L. B. SARGENT, Jr.
M. C. SHAW

Chairman Publications Committee
D. W. SAWYER

Administrative Secretary, ASLE
C. L. WILLEY

Published by

PERGAMON PRESS

NEW YORK LONDON PARIS LOS ANGELES

PERGAMON PRESS, INC.
122 East 55th Street, New York 22, N.Y.
P.O. Box 47715, Los Angeles, California

PERGAMON PRESS LTD.
4 & 5 Fitzroy Square, London W.1

PERGAMON PRESS, S.A.R.L.
*24 Rue des Écoles, Paris V^e^*

FIRST PUBLISHED 1959

Copyright in Great Britain by
The American Society of Lubrication Engineers

Library of Congress Card No. 58–9688

Subscriptions to ASLE members are available through ASLE headquarters. Subscriptions to non-members are available from Pergamon Press, Inc., 122 East 55th Street, New York 22, N.Y., at $15.00

Printed in Great Britain by J. W. Arrowsmith Ltd.

Development of Radiation Resistant Oils

By J. G. CARROLL[1] and R. O. BOLT[2]

The objective of this work was to develop oils of maximum radiation stability from readily available ingredients. Lubricants in three viscosity grades were made with alkylbenzenes containing selected polymers and additives. Each new oil was subjected to standard tests to determine if it met the specifications for presently used products made from mineral oils. The special oils complied with most requirements, and shortcomings were generally correctable. Both the special and conventional oils were irradiated under water in the Canal Gamma Source at the Materials Testing Reactor (MTR) in Idaho. Most conventional oils were damaged beyond usefulness at 10×10^8 roentgens (r). The alkylbenzene fluids still retained lubricating qualities after 50 to 70×10^8 r and remained fluid well above 100×10^8 r. These results prove the feasibility of making radiation resistant lubricants by this new approach.

Introduction

LUBRICANTS for use in and around stationary and mobile atomic power plants must be stable to the prevailing nuclear radiation. This paper describes one approach to the development of lubricating oils for high radiation resistance. Such lubricants are quite valuable to reactor designers. For example, if these specifically designed lubricants were to be used to the limits of their endurance, the weight of shielding could be reduced.

Of organic compounds, those with aromatic structures (i.e., one or more benzene rings per molecule) are the most stable to radiation (1). The best resistance is shown by polyphenyls without substituent groups; however, these compounds are deficient as base materials in certain respects, e.g., liquid range, viscosity index (V.I.). Thus, radiation resistance is not the only property which must be considered. As a compromise, alkylaromatics are an attractive class of fluids. The alkyl group improves the liquid range and viscosity index of the aromatic which in turn provides radiation stability. The organic selenides are particularly effective as oxidation inhibitors (2) and also as agents which retard radiation damage in those base oils (3).

Most commercially available alkylaromatic fluids are not made for use as lubricant base materials. Thus, they have low viscosities and V.I's. In lubrication practice, viscosity can be raised and viscosity index improved by adding high-molecular weight polymers to an oil (4). However, polymers are affected by radiation. Thus, some experiments were necessary to establish which polymers were satisfactory in solutions exposed to radiation. These polymers were then employed to make new oils from an alkylbenzene which was inhibited with dialkyl selenide. The new oils proved to be resistant to very high radiation dosages. They were tested without radiation against the requirements for conventional mineral oils. Then both the special oils and regular mineral oils were irradiated and evaluated in post-irradiation tests.

Most of the irradiations were made in the Canal Gamma Source at the Materials Testing Reactor (MTR) in Idaho. This source comprises spent fuel elements placed in a frame under 20 feet of water for shielding. Some exposures were also made in a cobalt-60 source (5). Gamma dosages are expressed here in terms of the roentgen (r). The value of r in more familiar units of energy may be expressed as 10^8 r $\cong$ 362 Btu per lb. Measurements in the sources used are determined (6) (by replacing a sample with a monitor) in terms of r. Thus, the unit is familiar and meaningful even though it is properly applied only to the strength of the radiation field rather than to energy absorbed by the sample. The prevailing dose rate at the MTR varied ten-fold to a maximum of about 2×10^7 r/hour, while the rate in the cobalt-60 source was 3.2×10^5 r/hour. The values of dosage from the two sources are accurate to $\pm$ 10% and $\pm$ 5%, respectively.

In most exposures in the MTR source, about 150 ml. of the oil was placed in a sample container open to the air, as described previously (7). A few preliminary irradiations were conducted on 10-ml. oil samples held in magnesium capsules which, in some cases, were sealed under helium (8). Cobalt-60 tests were made in glass vials open to the air. Earlier work showed that the presence of air during irradiation accelerated damage to polyphenyls (9). New data on the materials at hand are shown in Fig. 1. For conditions shown, the presence of air increased degradation by a factor of two as compared to the inert atmosphere.

The physical and chemical properties of the oils and their performances in bench tests were measured by recognized procedures as set forth in the Federal Test Method Standard (10) and ASTM Standards (11).

Presented as an American Society of Lubrication Engineers paper at the Lubrication Conference held in Los Angeles, Calif., October 1958.

[1] Research Engineer, California Research Corporation, 576 Standard Ave., Richmond, Calif.

[2] Senior Research Chemist, California Research Corporation, 576 Standard Ave., Richmond, Calif.

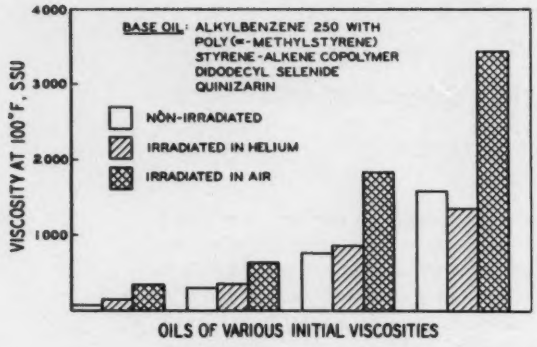

FIG. 1. Effect of air on radiation-induced viscosity change. MTR canal source, 55×10^6 r, magnesium capsules.

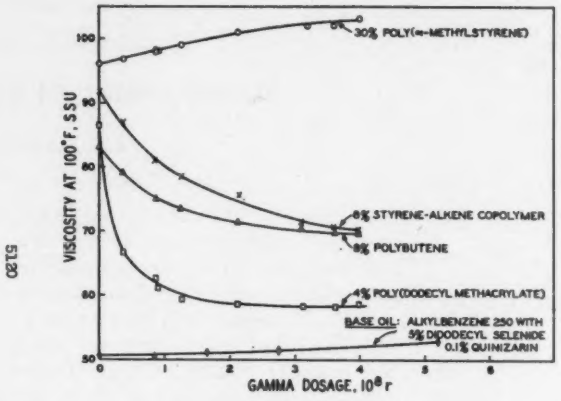

FIG. 2. Effects of radiation on polymer solutions. Alkylbenzene 250 base oil, Co-60 source, capsules open to air.

Selection of lubricants

Two commercially available alkylbenzene mixtures[3] were used for base stocks. These are made by the HF alkylation of benzene with polypropene. Certain properties are listed in Table 1.

TABLE 1

Properties of Mixed Alkylbenzenes

	Alkyl-benzene 250	Alkyl-benzene 350
Average molecular weight	~250	~350
Alkyl carbon atoms	~12	~20
Viscosity, centistokes		
at 210°F	1.78	3.99
at 100°F	6.51	29.6
Viscosity Index	(23)	−40
Pour point, °F	−80	−40
Flash point, °F	260	355
Initial boiling point, °F	520	602

The next step was to increase viscosity and improve V.I. of these base stocks by the addition of high-molecular weight polymers. Selected types were added to samples of the selenide-inhibited alkylbenzenes, and the solutions were irradiated. Results are shown in Fig. 2. The oil containing the polymethacrylate suffered the greatest decrease in viscosity on irradiation. The polybutene and the copolymer solutions were about equivalent in viscosity decrease. The oil containing the more aromatic poly(α-methylstyrene) slowly thickened, as did the base oil. From these data, a combination of the poly(α-methylstyrene) and the copolymer was selected as best for lubricant formulations.

Based on previous work, didodecyl selenide was used as an inhibitor in all formulations. Figure 3 is included to show that additives[4] vary widely in effectiveness and tend to be less effective in more stable fluids.

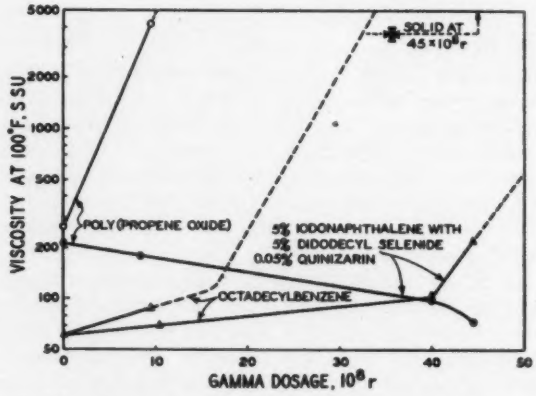

FIG. 3. Influence of additives on radiation-induced thickening of oils. MTR canal source, magnesium capsules sealed under helium.

Tentative formulations were exposed to gamma rays to determine whether they could survive the extremely high dosage of 10^{10} r in a helium atmosphere. They did, as shown in Fig. 4. The polymers detracted but slightly from the stability of the inhibited base oil. Data at only the extremities of the plots in Fig. 4 were obtained. Therefore, the curves are dotted to indicate that their shape is approximate. In order to establish the general shape of the intermediate curves, reference was made to more extensive data, shown in Fig. 5[5], on a similar base oil, *n*-butylbenzene.

[3] Alkylbenzene 250 is a distilled product, mostly monoalkylbenzene; Alkylbenzene 350 is a bottoms product, mostly dialkylbenzene.

[4] The iodine-containing additives were not used in this development; their role is described in reference (3).

[5] Data are from exposures in an atomic pile. Pile dosage was converted to gamma dosage by the following Eq. [12]: 10^{18} slow neutrons/cm^2 = 13×10^6 r. This equation is only approximate. However, errors in dosage conversion will have no effect on the shape of the curve of Fig. 5.

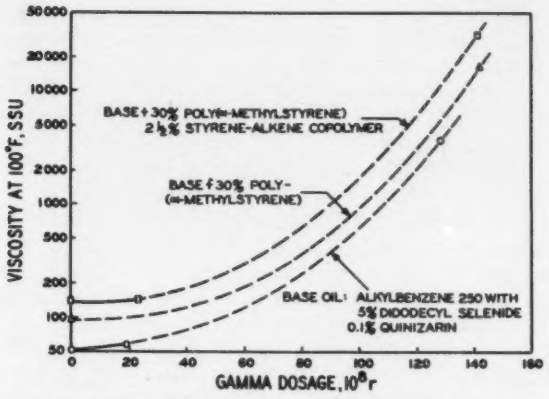
VISCOSITY AT 100°F, SSU
BASE + 30% POLY(α-METHYLSTYRENE) 2½% STYRENE-ALKENE COPOLYMER
BASE + 30% POLY-(α-METHYLSTYRENE)
BASE OIL: ALKYLBENZENE 250 WITH 5% DIDODECYL SELENIDE 0.1% QUINIZARIN
GAMMA DOSAGE, 10⁸r

FIG. 4. Radiation-induced viscosity increase of experimental oils. MTR canal source, magnesium capsules sealed under helium.

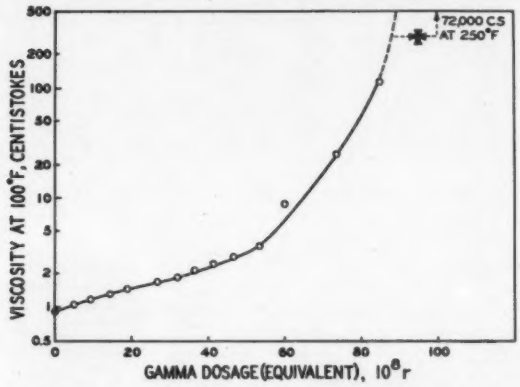

FIG. 5. Radiation-induced viscosity increase of *n*-butylbenzene. MTR VH-3 source, magnesium capsules sealed under helium.

This information established that the tentative formulations had outstanding radiation stability. Next, new oils were made in three viscosity grades as shown in Table 2. Test work on these was to answer the question "will they lubricate?" Polybutene was substituted for the copolymer on the basis of equivalent radiation resistance and limited thermal stability tests, as indicated in Fig. 6.

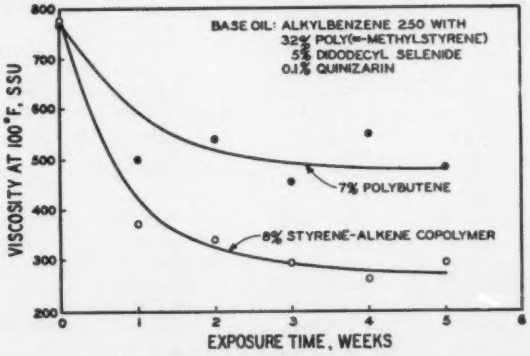
VISCOSITY AT 100°F, SSU
BASE OIL: ALKYLBENZENE 250 WITH 32% POLY(α-METHYLSTYRENE) 5% DIDODECYL SELENIDE 0.1% QUINIZARIN
7% POLYBUTENE
8% STYRENE-ALKENE COPOLYMER
EXPOSURE TIME, WEEKS

FIG. 6. Thermal stability of special oil at 400°F, 410 stainless steel capsules sealed under helium.

TABLE 2

Identification and Properties of Special Oils

	Light O–1.5A	Medium O–2.5A	Heavy O–3.5A
Composition, % by weight			
Alkylbenzene 250	66.2	—	—
Alkylbenzene 350	—	68.95	43.95
Poly(α-methylstyrene)	21.8	18.0	40.0
Polybutene	7.0	8.0	11.0
Didodecyl Selenide	4.95	5.0	5.0
Quinizarin	0.05	0.05	0.05
Viscosity, centistokes			
At 210°F	4.42	9.35	16.9
At 100°F	25.8	108	367
Viscosity, SSU			
At 210°F	40.8	57.1	85.4
At 100°F	123	502	1701
Viscosity Index	82	57	22

For reference standards, 13 typical mineral oils were selected. Three or more were in each of the viscosity grades—light, medium and heavy. These oils are identified in Table 3. Insofar as possible, general purpose lubricants meeting military specifications were chosen.

TABLE 3

Lubricating Oils Tested

Light Grade; 20 to 120 SSU at 130°F	
MIL-L-15016A, Grade 2075	General purpose
MIL-L-15017, Grade 2110H	Hydraulic
MIL-L-644A	Preservative, special
MIL-O-5606	Hydraulic, aircraft
Oil No. O-1.5A	General purpose, radiation resistant
Medium Grade; 55 to 70 SSU at 210°F	
MIL-L-15016A, Grade 2190	General purpose
MIL-L-17331 (Ships), Grade 2190T	Turbine (noncorrosive)
MIL-L-2104A, Grade 30	IC Engine, HD
MIL-L-9000A (Ships), Grade 9030	Diesel engine
MIL-L-6086A, Grade M	Gear, petroleum base
Oil No. O–2.5A	General purpose, radiation resistant
Heavy Grade 85 to 200 SSU at 210°F	
VV-L-765, Grades 90, 140	Enclosed gear, straight mineral
MIL-L-6082A, Grade 1100	Aircraft engine
MIL-L-2105, Grade 90	Gear universal
Oil No. O–3.5A	General purpose, radiation resistant.

Performance of special oils in specification tests, before irradiation

The new oils were tested against the requirements common to conventional oils in each of the three viscosity

grades listed in Table 3. Results are in Table 4. The performance of the special oils is summarized as follows:

1. Outstanding: Oxidation-corrosion at 250°F (light and heavy grades), turbine oil oxidation at 200°F (medium grade).
2. Satisfactory: Flash point (except heavy grade), color, neutralization number, copper corrosion, ash, saponification number, carbon residue, sulfur, and precipitation numbers.
3. Marginal: Foaming, demulsibility, film strength, and pour point.

In general, the new formulations are acceptable lubricants as indicated by the specification tests. The marginal properties are those which normally can be controlled or improved by additives.

Results of irradiations

Both the special and conventional oils were irradiated in the MTR Canal Source for nominal dosages of 5, 10, and 50×10^8 r. The exposures were about 200, 400 and 2000 hours, respectively, at 70°F. Post-irradiation tests were conducted on the limited size samples, and results are summarized qualitatively in Table 5. No mineral oils survived the 50×10^8 r exposure. All were reduced to brittle, plastic solids. Figure 7 illustrates their typical appearance. By contrast, all the special oils were still fluid and only slightly darkened by this level of irradiation.

Viscosity change is a good over-all index of radiation damage and is easily measured. Figures 8, 9 and 10 illustrate radiation-induced viscosity change for light, medium and heavy oils, respectively. Not all oils are shown, but the curves include the best and worst of those tested. The slopes are indicative of the rates of viscosity change. The heavy oils increase in viscosity at a faster rate than the lighter oils. For all grades, aromatic base lubricants were clearly superior.

The effect of radiation on the V.I. of thickened (3, 7) and of unthickened (7) lubricants was reported previously and was confirmed by these results. The possibility of making a "constant viscosity" fluid for a given radiation

TABLE 4

Performance of Special Oils in Specification Tests

Test or property	Range of requirements of oils in Table 3			Test results on special oils		
	Light	Medium	Heavy	Light O–1.5A	Medium O–2.5A	Heavy O–3.5A
1. Specific gravity 60/60	←	Report	→	0.9106	—	—
2. Viscosity, SSU, at 210°F	—	55–70	85–200	40.8	57.1	85.4
130°F	70–120	—	—	73	190	—
100°F	—	—	800–1500	123	502	1701
0°F	10,000 max	200,000	—	—	115,000	—
Viscosity Index	65	—	50–100	82	57	22
3. Pour point, °F	−70 to +15	−20 to +35	0 to +35	+15	+20	+20
4. Flash point, °F	200 to 440	310 to 390	325 to 470	380	340	340
5. Color	<7	<8	—	4½	4½	4½
6. Neutralization no.	0 to 0.20	0 to 1.0	0.10 max	Nil	Nil	Nil
7. Corrosion to copper at 212°F	None	None	None	←	Slight tarnish	→
8. Ash, %	0.003 max	0.003 max	0.05 max	0	0	0
9. Saponification no.	0.5 max	0.5 max	0.5 max	0.35	0.38	0.41
10. Carbon residue, %	0 to 0.80	0.40 max	1.2 max	0.11	0.07	0.10
Nature of carbon	L and F*	L and F	L and F	L and F	L and F	L and F
11. Total sulfur, %	0.50 max	0.50 max	0.50 max	0.41	0.44	0.44
12. Precipitation no.	0.01 max	0.10 max	0.1 max	Trace	0	Trace
13. Foaming (after 10 min)	300 ml	200 ml	200 ml	Pass	Not pa s	Not pass
14. Emulsion at 130°F (after 30 min)	Stable	Stable	—	Not pass	Pass	—
15. Oxidation corrosion (168 hours at 250°F)						
Evaporation loss, %	—	—	—	1.3	—	0.6
Change in 100°F viscosity	−5 to +20	—	—	−0.4	—	0
Change in Neutralization no.	<0.20	—	—	+0.03	—	+0.01
Weight change						
mg/cm²; copper	±0.2 to ±0.6	—	—	0.10	—	+0.08
steel	±0.2	—	—	0	—	+0.02
aluminum	±0.2	—	—	0.01	—	0
magnesium	±0.2	—	—	−0.01	—	+0.02
cadmium	±0.2	—	—	+0.01	—	+0.01
16. Mean Hertz load, kg	—	40 min	—	—	13.5	—
17. Turbine oil oxidation, hrs	—	1000 min	—	—	3800+	—

* Loose and flaky.

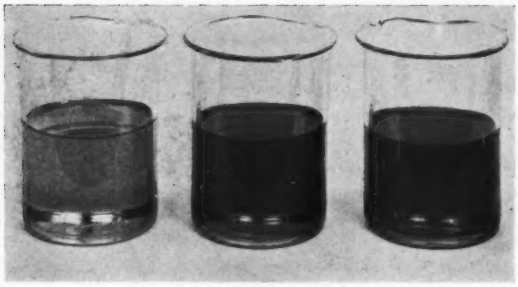

(a)

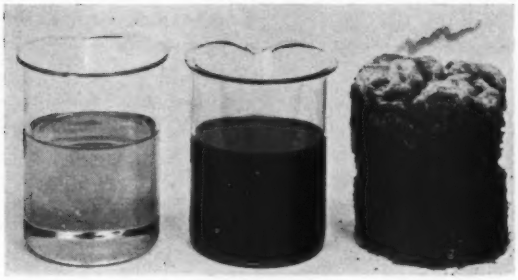

(b)

0 r 10⁹ r 5 × 10⁹ r

GAMMA DOSAGE

FIG. 7. Performance of radiation resistant oil.

(*a*) Based on alkyl aromatic.

(*b*) Based on mineral oil.

TABLE 5

Influence of Gamma Irradiation on Lubricating Oils

Property	How determined	Effect of 10^9 r	
		Conventional oils	Special oils
Color	ASTM	Darken	Darken
Odor	Smell	Sharp, acrid	Sharp, acrid
Appearance	Visual	Clear	Hazy
Corrosivity	Appearance of tin can	No effect from oil; some additives decompose and become corrosive	
	Copper at 212°F	No effect from oil	Selenium is hostile to copper
Sludging	Insolubles	None	None
Acidity	Neutralization no. (micro)	Nil	Nil
Wear	Four-ball machine	No worsening	No worsening
Pour point	ASTM	Raises	Lowers then raises
Evaporation	At 210°F	—	None

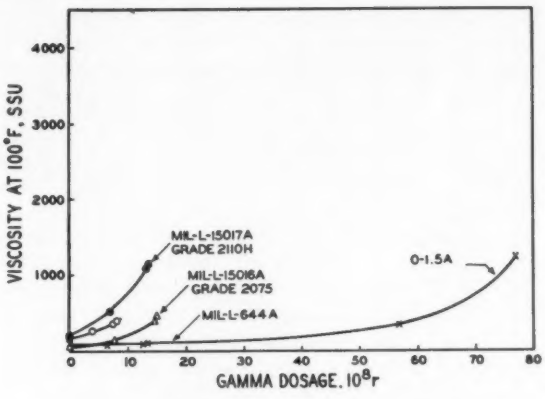

FIG. 8. Variation of viscosity of light grade oils with irradiation. MTR canal source, open to air.

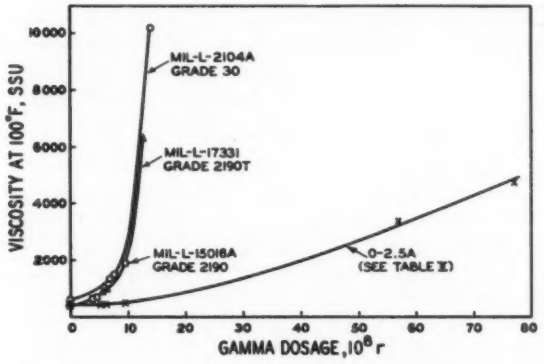

FIG. 9. Effect of irradiation on viscosity of medium grade oils. MTR canal source, open to air.

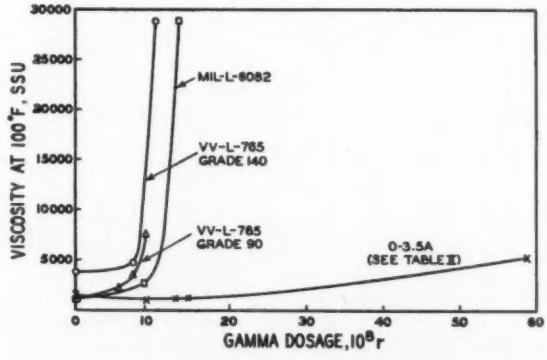

FIG. 10. Change of viscosity of heavy grade oils with irradiation. MTR canal source, open to air.

dosage range, i.e., an oil which would have the same or only slightly different viscosity after exposure to a selected dosage relative to its original value, was also mentioned before (3). Figure 11 illustrates the loss and recovery of

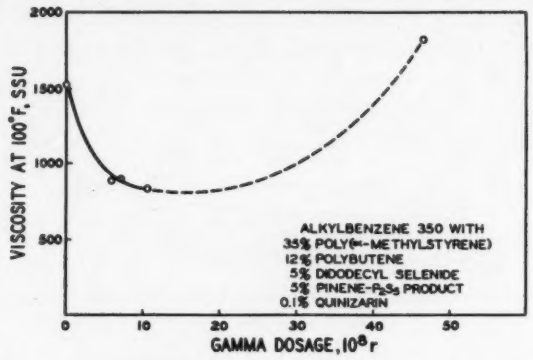

FIG. 11. Radiation-induced viscosity change of a thickened oil. MTR canal source, open to air.

viscosity with gamma irradiation for the type of polymer-in-oil system discussed here. A proper choice of polymers (see Fig. 2) would minimize the initial viscosity decrease shown in Fig. 11 and allow a lubricant to be designed to recover its original viscosity after a given dosage.

Significance of results

The new formulations have outstanding radiation stability. They are still fluid after 5×10^9 r and, for non-critical uses, are probably usable to above 10^{10} r total dosage. This approaches the limits of radiation tolerance for fluid hydrocarbon lubricants. To gain further radiation stability, the next step would be the use of completely aromatic compounds. However, these compounds, e.g., biphenyl, have high melting points.

The special lubricants meet most of the requirements for conventional oils. Most of the deficiencies of the new oils can be corrected by additives. The low temperature viscosity and pour point are impaired by the particular selenide used[6]. As the aromatic base fluids are thermally very stable, it is probable that the polybutene V.I. improvers are the ingredients which would limit thermal stability in these formulations. Inhibitors can also be used to impart rust protection, antifoaming, film strength, etc. For each new ingredient, of course, radiation stability would have to be retested.

In the presence of radiation, the behavior of a solution containing polybutene and poly(α-methylstyrene) is complex. The first polymer undergoes a rapid cleavage, causing loss in viscosity and viscosity index. Meanwhile, the second polymer begins to crosslink, thus tending to increase the viscosity. The base oil also begins to polymerize. After an initial decrease in viscosity, there is a gradual increase in both viscosity and viscosity index of the solution. Eventually, solidification occurs.

In conclusion, the approach of adding an organic selenide and selected polymers to an alkylbenzene was successful for the stated objectives. The resulting formulations (a) have excellent radiation resistance and (b) are acceptable lubricants by conventional standards.

[6] Related work has shown that lower pour points result from use of a branched chain bio-tridecylselenide.

Acknowledgments

The authors express their appreciation to Messrs. S. R. Calish and R. L. Peeler of California Research Corporation for assistance in planning and conducting the test work and to Mr. D. L. Hunke of Phillips Petroleum Company for performing the gamma irradiations in the MTR Canal Source.

The work was sponsored in part by the Atomic Energy Commission on Contract AT(11-1)-174.

REFERENCES

1. SCHOEPFLE, C. S. and FELLOWS, C. H., "Gaseous Products from Action of Cathode Rays on Hydrocarbons," *Ind. & Eng. Chem.*, v. 23, n. 12, December 1931, p. 1396.
2. DENISON, G. H., and CONDIT, P. C., "Oxidation of Lubricating Oils—Dialkyl Selenides as Inhibitors," *Ind. & Eng. Chem.*, v. 41, n. 5, May 1949, p. 944.
3. BOLT, R. O., and CARROLL, J. G., "Radiolysis and Radiolytic Oxidation of Lubricants," *Ind. & Eng. Chem.*, v. 50, n. 2, February 1958, p. 221.
4. KALICHEVSKY, V. A., "Lubricating Oil Additives," *Petrol. Refiner*, v. 28, n. 8, July 1949, p. 125.
5. MANOWITZ, B., "Use of Kilocurie Radiation Sources," *Nucleonics*, v. 9, n. 2, August, 1951, p. 10.
6. HOGG, C. H., "Gamma Ray Dosage Rate Measurements," Office of Technical Services ($0.20), US AEC Document IDO-16205, November 1955.
7. CARROLL, J. G., and CALISH, S. R., "Some Effects of Gamma Radiation on Commercial Lubricants," *Lubrication Engineering*, v. 13, n. 7, July 1957, p. 388.
8. SHIELLS, N. P., BOLT, R. O., and CARROLL, J. G., "Safe Containers Hold Organics for Irradiations," *Nucleonics*, v. 14, n. 8, August 1956, p. 54.
9. BOLT, R. O., and CARROLL, J. G., "Organics as Reactor Moderator Coolants: Some Aspects of Their Thermal and Radiation Stabilities," *Proc. Int. Conf. on Peaceful Uses of Atomic Energy* in Geneva, August 8–20, 1955, United Nations, New York, v. 7, 1956, p. 546.
10. "Federal Test Method Standard No. 791," December 1955.
11. "ASTM Standards on Petroleum Products and Lubricants," ASTM Committee D-2, November 1955.
12. CARROLL, J. G., BOLT, R. O., and BERT, J. A., "A Survey of the Radiation Stability of Hydrocarbon Fuels," *Aeron. Eng. Rev.*, v. 17, n. 3, March 1958, p. 64.

The Effects of High Energy Ionizing Radiation on Turbine Oil Performance Characteristics

By C. F. KOTTCAMP[1], R. P. NEJAK[2] and R. T. KERN[3]

Representative turbine oils and turbine oil components were exposed to electron radiation and evaluated for radiation-induced changes in functional characteristics. The irradiated oils were examined by numerous laboratory techniques including those established by the ASTM Committee C on Turbine Oils. As a result of exposure to radiation, changes were noted in turbine oil viscosity, oxidation stability, rust resistance, foaming susceptibility, color and other properties.

THE increasing application of nuclear energy to electric power production and marine propulsion has necessitated a consideration of the effects of radiation on important plant lubricants. Accordingly, marine and stationary steam turbine oils have been exposed to radiation and examined for changes in important functional characteristics. Numerous laboratory techniques, including those established by the ASTM Technical Committee C on Turbine Oils, were used to index radiation damage.

Turbine oil is the principal lubricant used in conventional and nuclear steam power plants by virtue of quantity requirements and customer sensitivity to changes in working properties. The modern turbine oil is made up of well-refined oil and varying quantities of oxidation stabilizer, rust inhibitor and foam preventive additives. Its function is the adequate lubrication and cooling of turbine bearings and associated equipment. Turbine oils are required to maintain proper viscosity, show resistance to oxidation, protect against corrosion, minimize foaming and maintain good water separation characteristics over a normal service life of 10–20 years or more. Small changes in these critical properties are often viewed with concern.

The extent to which nuclear plant turbine oils may be exposed to radiation in the field is governed by the method of steam generation and the proximity and shielding of the reactor and turbine units. In nuclear plants where steam is generated by heat exchange with primary reactor coolants, turbine oil exposure to radiation is governed by shielding and proximity conditions. The turbine unit can be, and usually is, isolated from a radiation environment in this type of plant. In nuclear plants where steam for the turbine is generated in the reactor (Boiling Water Reactor) the turbine must operate in a radiation field produced by radioactive steam and steam impurities. Investigators have reported radiation dose rates of less than one rad per hour at the steam turbine of small boiling water reactor plants (1, 2). While this constitutes a very low radiation dose rate, it is possible that larger plants of similar or different design may afford considerably higher radiation dose rates at the turbine unit. The rapid and confidential nature of nuclear power plant concept and design details makes for difficulty in anticipating future conditions for nuclear power plant lubrication. Considering this, and the importance of turbine oil performance quality, it appears desirable to understand the limitations imposed on turbine oil by radiation.

Ten turbine oil formulations were used to examine the effects of radiation on fully formulated steam and marine turbine oils, turbine oil base stocks, phenol- and amino-type oxidation stabilizers, rust inhibitors and foam preventive additives. Measurements were made of radiation-induced changes in viscosity, oxidation stability, rust resistance, foaming, emulsification susceptibility, and other properties. The formulations studied were:

- Oil A — A commercially available 150 Saybolt Universal Second turbine oil made up of a highly refined paraffinic base oil, phenol-type oxidation stabilizer, rust inhibitor and silicone-type foam preventive.
- Oil B — An experimental 150 Saybolt Universal Second oil made up of a solvent processed naphthenic base oil and the same additives contained in Oil A.
- Oil C — A commercially available 150 Saybolt Universal Second turbine oil made up of a solvent processed paraffinic base oil and the same additives contained in Oil A, plus an additional corrosion inhibitor.
- Oil D — A fully formulated marine geared turbine oil with extreme pressure properties.
- Oil Base A is Oil A with no additives.
- Oil Base B is Oil B with no additives.
- Oil Base A Plus Phenol-Type Antioxidant.
- Oil Base A Plus Amino-Type Antioxidant.
- Oil Base A Plus Rust Inhibitor.
- Used Oil A—Oil A after 5 years of continuous service in a 200,000 kW Turbine Generator Unit.

Table 1 lists inspections on these oils prior to irradiation.

Presented as an American Society of Lubrication Engineers paper at the Lubrication Conference held in Los Angeles, Calif., October, 1958.

[1] Product Application Engineer, Gulf Research & Development Co., Pittsburgh 30, Penna.

[2] Research Engineer, Gulf Research & Development Co., Pittsburgh 30, Penna.

[3] Chemist, The Gulf Oil Corporation, Refinery Technology Laboratory, Philadelphia, Penna.

TABLE 1

Turbine Oil Inspections Prior to Irradiation

	Oil A	Oil B	Oil C	Oil D	Oil base A	Oil base B	Oil base A plus phenol-type anti-oxidant	Oil base A plus amino-type anti-oxidant	Oil base A plus rust inhibitor	Used Oil A
Inspection:										
Gravity: °API	31.5	27.9	31.6	29.7	31.9	28.0	31.7	31.7	31.9	31.8
Viscosity, SUV: sec										
100°F	152.4	155.1	150.6	413	153.3	156.9	152.4	152.4	152.4	152.9
210	43.8	42.0	43.4	59.2	44.1	42.2	43.9	44.1	44.2	44.3
Viscosity index	108	55	103	100	112	59	110	113	115	116
Color, ASTM union	1.0	<1.0	1.0	1.75	<1.0	1.0	<1.0	1.0	1.0	2.75
Flash										
Pensky-Martin: °F	400	355	405	400	410	350	385	415	425	410
Flash, Open cup: °F	430	370	410	450	430	355	415	420	430	425
Fire, Open cup: °F	485	425	475	520	505	405	495	495	500	495
Pour: °F	0	−55	+10	+5	+5	−30	+10	+10	+10	−5
Neutralization value										
ASTM D 974-55 T										
Total Acid No.	0.09	0.06	0.08	0.15	nil	0.01	0.01	0.01	0.03	0.03

Each turbine oil formulation was irradiated with 1.5 million volt electrons to total dosages of 9, 45, 90 and 270 million rads at a dose rate of about 3.4×10^4 rads/second in a 3 MeV Van de Graff Accelerator facility. The term rad represents a unit of radiation dosage corresponding to the absorption of 100 ergs of energy per gram of material.

Test oil samples were irradiated in a circulating system which consisted of a thin walled radiation cell, a reservoir, heat exchange unit and a pump. The circulating system was thermostatically controlled to maintain a temperature of 145 ±5°F during radiolysis and vented to the atmosphere through a wet test meter to facilitate collection and measurement of efflux gas.

Radiation dosages were considered accurate to ±10% according to an aqueous formic acid dosimetry technique which had been referenced by ferrous sulfate dosimetry (3, 4). The nature of the radiation and the radiation dose rate in this study probably differs considerably from that which might be encountered in the field. It therefore should be assumed that equal absorbed total dosages of radiation lead to similar qualitative and quantitative effects regardless of radiation type and/or dose rate. Several investigators have indicated that this is a reasonable assumption (5, 6).

Viscosity

Turbine oil viscosity must be high enough to give satisfactory lubrication and low enough to minimize bearing power friction loss. The normal viscosity range of a turbine oil for lubricating direct connected turbine generator units is 140–170 Saybolt Universal Seconds at 100°F. In marine geared turbine systems the normal lubricant viscosity range is 400–550 Saybolt Universal Seconds at 100°F.

Table 2 and Fig. 1 illustrate the effect of radiation on turbine oil viscosity. A straight line relationship could be

TABLE 2

The Effect of Radiation on Turbine Oil Viscosity

	Saybolt universal viscosity at 100°F: sec.					Saybolt universal viscosity at 210°F: sec.				
Radiation dosage: rads × 10^6	0	9	45	90	270	0	9	45	90	270
Oil A	152.4	155.1	162.8	174.5	224	43.8	44.1	44.6	45.5	49.2
Oil base A	153.3	157.4	164.6	175.4	228	44.1	44.4	45.0	45.8	49.7
Oil B	155.1	157.8	166.9	176.3	238	42.0	42.2	42.8	43.4	46.9
Oil base B	156.9	159.6	166.4	177.3	236	42.2	42.4	43.0	43.7	46.9
Oil C	150.6	152.4	161.0	171.4	219	43.4	43.5	44.2	44.9	48.5
Oil D	413	410	444	473	651	59.2	59.3	61.0	62.7	73.4
Oil base A plus phenol-type antioxidant	152.4	155.1	163.3	175.4	234	43.9	44.1	44.7	45.7	49.9
Oil base A plus amino-type antioxidant	152.4	155.1	164.2	175.4	236	44.1	44.3	44.9	45.9	50.3
Oil base A plus rust inhibitor	152.4	156.9	165.5	175.4	224	44.2	44.2	44.8	45.4	49.2
Used Oil A	152.9	155.1	163.7	175.4	232	44.3	44.2	44.9	45.8	50.0

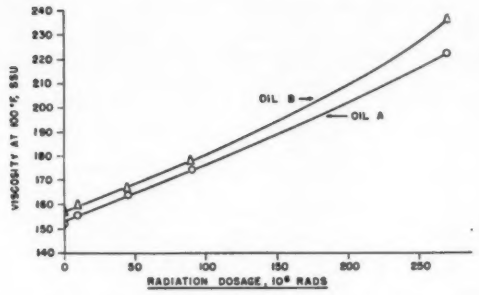

FIG. 1. The effect of radiation on turbine oil viscosity.

drawn between viscosity and radiation dosage at least up to 90 million rads. Over the entire dosage range studied, the logarithm of viscosity varied as a close straight line function of dosage. The presence of phenol and amino-type oxidation stabilizers, rust inhibitor and foam preventive additives had no large effect on the magnitude of radiation induced viscosity change. No appreciable distinction could be drawn between the viscosity response of different base oils and new and used turbine oil.

The increases in viscosity caused by radiation can be attributed largely to a crosslinking of constituent lubricant molecules to form higher molecular weight species.

Oxidation stability

The oxidation of turbine oils eventually leads to the formation of deposits and sludges which are detrimental to proper bearing lubrication. In order to minimize the rate of oxidation, modern turbine oils are formulated with highly refined base oils and oxidation stabilizers.

The ASTM D943-54 Oxidation Test (7), the Continental Oxidation Test and the Rotary Bomb Oxidation Test (8) were used to evaluate the effects of radiation on turbine oil oxidation life. As shown in Table 3, turbine oil resistance to oxidation is rapidly depleted by radiation. In the ASTM D943-54 Oxidation Test all of the fully formulated turbine oils showed losses in oxidation life of 40% or greater after a 45×10^6 rad dosage. Oil A and Used Oil A showed approximately the same percentage reductions in oxidation life over the entire radiation dosage range even though the initial oxidation life of Used Oil A was only about 50% that of Oil A. The phenol oxidation stabilizer appeared more resistant to radiation than the amino-type oxidation stabilizer under the conditions of the Rotary Bomb and Continental Oxidation Tests. On the other hand, the amino-type oxidation stabilizer appeared somewhat superior to the phenol-type under the conditions of the ASTM D943-54 Oxidation Test.

The degradation of turbine oil oxidation stability probably is due largely to the direct destruction of oxidation stabilizer by radiation and the formation of oxidizable entities in the base oil.

Foaming characteristics

Small quantities of silicone polymers are often added to turbine oils to prevent the formation of stable foams which may impede oil flow to turbine bearings. The ASTM D892-46T Foam Sequence Test (7) was used to evaluate turbine oil foaming susceptibility as a function of radiation dosage. As shown in Table 4, foaming tendencies were increased for all the oils after irradiation. With the exception of Oil D at the 90 and 270 million rad dosage levels, all

TABLE 3

The Effect of Radiation on Turbine Oil Oxidation Resistance

	Radiation dosage: rads $\times 10^6$	Oxidation test, ASTM D 943-54 time oxidized: hr. to 2.0 acid no.	Continental oxidation stability test: hr.	Rotary bomb oxidation test time for 25 lb pressure drop: min.
Oil A	0	2250	257	400+
	9	1600	158	375
	45	1060	149	295
	90	610	85	230
	270	220	20	108
Oil base A	0	250	31	135
	9	120	16	84
	45	90	14	73
	90	60	10	65
	270	55	9	64
Oil B	0	1750	253	406
	9	1100	154	304
	45	1090	104	258
	90	500	61	158
	270	70	13	78
Oil base B	0	75	14	93
	9	55	14	82
	45	35	6	53
	90	35	6	48
	270	35	6	48
Oil C	0	1740	394	400+
	9	980	208	288
	45	485	64	185
	90	245	42	105
	270	65	13	50
Oil D	0	1450	186	378
	9	1160	139	272
	45	570	67	197
	90	460	43	155
	270	80	15	72
Oil base A plus Phenol-type anti-oxidant	0	2600+	280	400+
	9	1800	248	380
	45	1300	142	325
	90	900	92	210
	270	230	15	118
Oil base A plus amino-type anti-oxidant	0	2600+	280	400+
	9	2200+	271	350
	45	2200+	141	300
	90	2200+	14	85
	270	240	8	37
Oil base A plus rust inhibitor	0	140	18	92
	9	90	18	68
	45	55	18	65
	90	40	15	65
	270	30	5	60
Used oil A	0	1200	205	325
	9	770	160	242
	45	580	36	230
	90	360	36	150
	270	120	22	93

TABLE 4

The Effect of Radiation on Turbine Oil ASTM D892-46T Foaming Characteristics

	Radiation dosage: rads × 10^6	Volume of foam after 5 minutes' blowing		
		Sequence 1 (75°F)	Sequence 2 (200°F)	Sequence 3 (75°F)
Oil A	0	20	20	30
	9	10	15	10
	45	40	50	70
	90	20	20	150
	270	460	40	380
Oil base A	0	150	20	140
	9	140	30	140
	45	210	25	160
	90	210	30	40
	270	380	30	320
Oil B	0	30	30	20
	9	10	30	110
	45	140	30	60
	90	210	25	280
	270	590	40	540
Oil base B	0	250	40	210
	9	275	30	225
	45	450	20	460
	90	400	40	350
	270	550	30	470
Oil C	0	40	15	20
	9	460	15	60
	45	370	20	240
	90	480	40	390
	270	590	60	530
Oil D	0	30	40	15
	9	30	90	20
	45	130	430	420
	90	530	20	10
	270	410	530	400

oils showed satisfactory recovery from foaming. Changes in foaming susceptibility are partially explainable on the basis of additive destruction and viscosity increase.

Emulsification

Turbine oil water separation characteristics were evaluated as a function of radiation dosage in the Federal 3207.5 Emulsion Test (9) using distilled water at 130°F. With the exception of Oil D at the higher dosage levels, all oils showed satisfactory recovery from emulsification.

Rust prevention

All of the formulations containing rust inhibitor passed the Rust Preventive Test Procedure A at 9 and 45 million rad dosages with the exception of Used Oil A which failed at the 45 million rad dosage level. At 90 million rads only Oil C which contained extra rust inhibitor passed the Rust Preventive Test. All test oils failed at the 270 million rad dosage level.

The loss of rust resistance seemed to result from a degradation of polar rust inhibitors by radiation. This is indicated in Fig. 2 which plots the increase in turbine oil interfacial tension against radiation dosage. Addition of fresh rust inhibitor to oils which failed the Rust Preventive Test at the higher dosage levels resulted in passing rust tests.

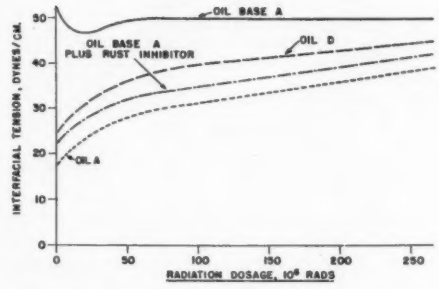

FIG. 2. Effect of radiation on turbine oil interfacial tension.

Other radiation effects

Each turbine oil formulation evolved gas during radiolysis as shown in Fig. 3. According to mass spectrographic

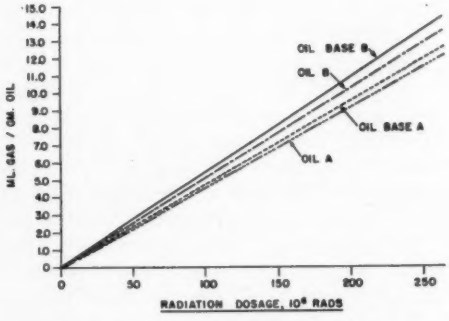

FIG. 3. Effect of radiation on turbine oil gas evolution.

analyses of gas samples taken at about the 45 million rad dosage level, the evolved gas was composed of greater than 90% hydrogen and small quantities of methane, ethane, propane, ethylene and other hydrocarbons.

Each new oil formulation darkened in color slightly as a result of exposure to radiation. In no instance did color exceed an ASTM Union Color Test (7) rating of 3. Used Oil A, with an initial Union Color of 2.25, lightened to a 1.75 rating at 9, 45 and 90 million rads then darkened to 2.25 at 270 million rads.

Turbine Oil ASTM D974-55T Neutralization Values (7) were not significantly affected by radiation. If anything, total acid values were slightly reduced.

The load carrying capacities of Marine Turbine Oil D and the fully formulated Steam Turbine Oils were adversely affected by radiation as shown in Table 5. This effect probably resulted from destruction of load carrying additives.

TABLE 5

The Effect of Radiation on Turbine Oil Wear Characteristics[a]

	Radiation dosage: rads × 10^6	Average coefficient of friction	Average scar diameter, mm
Oil A	0	0.101	0.28
	9	0.092	0.33
	45	0.086	0.37
	90	0.084	0.40
	270	0.113	0.48
Oil base A	0	0.088	0.70
	9	0.094	0.58
	45	0.074	0.59
	90	0.092	0.52
	270	0.110	0.54
Oil B	0	0.099	0.35
	9	0.084	0.37
	45	0.093	0.45
	90	0.110	0.58
	270	0.112	0.61
Oil base B	0	0.098	0.70
	9	0.091	0.66
	45	0.088	0.65
	90	0.093	0.62
	270	0.093	0.58
Oil C	0	0.085	0.29
	9	0.090	0.32
	45	0.086	0.38
	90	0.110	0.46
	270	0.097	0.52
Oil D	0	0.093	0.30
	9	0.094	0.29
	45	0.10[illegible]	0.60
	90	0.109	0.60
	270	0.102	0.66

[a] Test run according to MIL-L-17331A Specification in the 4-Ball Wear Test Apparatus.

All of the turbine oil formulations listed showed directionally the same changes in API Gravity, Pour Point, Flash Point and Fire Point and other physical properties shown for Oil A in Table 6.

Summary and conclusion

Each of ten turbine oil formulations was irradiated to 9, 45, 90 and 270 million rad radiation dosages and examined for changes in critical properties. The results of this study showed that:

1. Turbine oil viscosity was increased as a result of exposure to radiation. The relationship of turbine oil viscosity and radiation dosage appeared to be linear at least to 90 million rads.
2. The oxidation stabilities of turbine oils were markedly reduced by radiation. It appeared that radiation functioned to destroy the oxidation suppressor additives.
3. The foaming susceptibility of turbine oils was increased by radiation but not critically.
4. The water separation characteristics of turbine oils generally remained good after irradiation.
5. Turbine oil rust prevention characteristics were degenerated markedly at radiation dosage levels greater than 45 million rads. It was possible to regenerate the rust prevention characteristics by addition of fresh rust inhibitor additive.
6. All of the formulations studied evolved about 0.05 ml. of gas per gram of oil per 10^6 rads of radiation. Hydrogen was the principal component of this gas.
7. Turbine oil wear properties were degraded by radiation.

Considering the overall data, it appears that radiation becomes limiting to the performance quality of unused turbine oils at dosage levels of 45 million rads or more.

TABLE 6

The Effect of Radiation on Turbine Oil A Physical Properties

	Radiation dosage: rads × 10^6				
	0	9	45	90	270
Inspection:					
Gravity: °API	31.5	31.5	31.3	31.4	30.7
Viscosity, SUV: sec.					
100°F	152.4	155.1	162.8	174.5	224
210	43.8	44.1	44.6	45.5	49.2
Viscosity index	108	110	110	109	112
Color, ASTM union	1.0	1.0	1.25	1.25	2.5
Flash, Pensky-Martin: °F	400	365	315	250	166
Flash, open cup: °F	430	410	405	415	295
Fire, open cup: °F	485	470	475	485	475
Pour: °F	0	0	0	+10	+10
Neutralization value ASTM D 974-55 T					
Total acid No.	0.09	0.04	0.03	0.01	0.01

REFERENCES

1. HAUSMAN, R. F., and BOOSER, E. R., "Application Problems with Petroleum Lubricants in Nuclear Power Plants," *Lubrication Engineering*, v. 13, April 1957, pp. 199–202.
2. Anon., "Significance of the EBWR," *Nucleonics*, v. 15, n. 7, July 1957, pp. 54–57.
3. HARDWICK, T. J., and GUENTNER, W. S., "Aqueous Formic Acid Dosimetry," unpublished data.
4. WEISS, J., "Chemical Dosimetry using Ferrous and Ceric Sulfates," *Nucleonics*, v. 10, n. 7, July 28, 1952.
5. CALKINS, V. P., "Radiation Effects on Reactor Materials: Nonmetals," *Nucleonics*, v. 12, No. 9.
6. SCHULER, R. H., *J. Am. Chem. Soc.*, v. 79, 1957, p. 273.
7. ASTM Standards on Petroleum Products and Lubricants, 1957.
8. "The Rotary Bomb Oxidation Test for Inhibited Steam Turbine Oils," *ASTM Bulletin* No. 186 (December 1952.)
9. Lubricating Oil Emulsion Test Federal Method 3201.5, Federal Test Method Standard No. 791.

Viscoelastic Behavior of Greases

By E. O. FORSTER[1] and J. J. KOLFENBACH[2]

1. Introduction

THE mechanical properties of greases are usually examined either under steady state conditions at relatively high shearing stresses or under static conditions involving very small shearing stresses. The steady state conditions, such as encountered in the capillary pressure viscometer, are selected in the belief that they represent the conditions under which the greases will have to operate. The static conditions such as those encountered in the grease penetrometer are usually employed as specification tests to permit rapid comparisons between materials having the same chemical composition. Relatively few investigations have been made of the behavior of greases which reflect the time dependent behavior of these materials. Vinogradov and Klimov (1) examined calcium soap greases with a torsional elastometer and found that under low shear stresses, greases behaved like an elastic solid body. At higher shear stresses they found that these elastic deformations were accompanied by irreversible plastic deformations and that description of the mechanical behavior of greases required a knowledge of the shear modulus, as well as the viscosity, as a function of time. Carver and Van Wazer (2) and Goldberg and Sandvik (3) studied aluminum gels using a concentric cylinder type viscometer which could be made to rotate suddenly at a constant speed or to oscillate mechanically at frequencies ranging from 10 to 6000 cycles per second. Both research teams found that the aluminum soap gels had elastic as well as viscous properties and resembled linear amorphous polymers in their mechanical behavior. Hutton and Matthews (4) investigated simple sodium and lithium soap greases in a parallel plate plastometer under compression and confirmed again that these greases had elastic as well as viscous properties.

In the present paper, the behavior of a mixed soap and a complex soap grease is described under cyclic shear stresses resulting in cyclic deformations. The results of this investigation support earlier findings that greases are viscoelastic bodies and that their response to shear stresses is very time dependent. From the study of the frequency dependence of these materials under a wide range of frequencies, the distribution of relaxation times has been deduced. Evidence has been obtained of the existence of three different types of relaxation mechanisms which are believed to correspond to different types of displacement that can take place within greases. These results are interpreted as providing further evidence of the structure of greases postulated by Hutton (4), Forster and Kolfenbach (5)—namely, that greases are made up of a three-dimensional soap fiber network in which the oil is immobilized.

2. Experimental techniques

The mechanical properties of viscoelastic materials can be studied with three types of rheological instruments according to the specific interest of the investigation. If only the flow properties of a viscoelastic material are to be studied, viscometers such as the Couette or Pochettino coaxial cylinder type can be used. On the other hand, if one is interested in viscoelastic effects that occur in times longer than about 10 sec, one can use static (transient) experiments in which either the strain is observed under constant stress (creep measurements) or the stress is observed under constant strain (relaxation measurements) using instruments such as the elastometer or plastometer. Finally, if investigations are to be made of the viscoelastic effects occurring in times shorter than 10 secs, dynamic measurements have to be made. Naturally there exists among these methods a certain amount of overlap with regard to the time scale.

The majority of dynamic tests are based upon vibrating systems in which stress and strain vary sinusoidally with time. The time scale involved ranges from about 10^{-8} sec up to 10^{4} sec (6). The dynamic measurements can be grouped into three classes based upon the ratio of wavelengths of the elastic waves generated to the dimensions of the sample. If these dimensions are small compared to the wavelength, one uses the method of vibration with additional mass. In order to set up vibrations, an additional mass is fixed to the sample and the system permitted to vibrate freely or forced to vibrate at certain frequencies. If the dimensions of the sample are of the same order of magnitude as the wave lengths, one uses vibrations without additional mass. In this case, standing waves, which are dominated by the mass of the sample, are built up. If the dimensions of the sample are very large compared with the wavelengths, elastic waves are propagated through the medium and one employs wave propagation methods.

In the work of Vinogradov (1), static experiments were conducted to examine the stress relaxation of a grease. Carver (2) in his study of aluminum soap gels used a Couette type viscometer to study the flow properties, and Goldberg (3) used a similar arrangement to which he added a forced oscillatory motion, thus performing an experiment of the forced vibration type with additional mass. Hutton (4) subjected his grease to compression and performed essentially creep measurements. The present investigation employed forced vibrations with additional mass similar to

Presented as an American Society of Lubrication Engineers paper at the Lubrication Conference held in Los Angeles, Calif., October 1958.

[1] Research Associate, Esso Research and Engineering Co., P.O. Box 51, Linden, New Jersey.

[2] Research Associate, Esso Research and Engineering Co., P.O. Box 51, Linden, New Jersey.

that of Goldberg (3) but unlike Goldberg, the imposed frequencies were very low compared to the resonance frequency of the sample. This non-resonance method was selected because it appears to be the most appropriate method for measuring large energy losses in viscoelastic materials.

A. *Theory*

Before the difference between the resonance method and the non-resonance method can be appreciated, it appears advisable to discuss briefly the theoretical background of the dynamic test method. A viscoelastic material which is subjected to sinusoidal shearing stresses of maximum amplitude τ_0 will reach a balance of stresses and deformations in a few cycles. At any particular time, t, the stress can be written as

$$\tau = \tau_0 \sin \omega t \qquad [1]$$

where ω is angular frequency of vibration. The corresponding strains will also vary sinusoidally with the same frequency with an amplitude γ_0 and with a certain phase difference δ. At any time, t, the shear strain will be given by the equation

$$\gamma = \gamma_0 \sin(\omega t - \delta) \qquad [2]$$

Thus, it can be seen that the strain will lag behind the stress. The phase angle that exists between the two is called the loss angle δ. The ratio between stress and strain amplitudes is called the absolute dynamic modulus, $|G|$,

$$|G| = \tau_0/\gamma_0 \qquad [3]$$

The absolute dynamic modulus together with the loss angle are sufficient to describe the dynamic behavior of a viscoelastic material.

For reasons of convenience, one introduces two other characteristic functions for the description of vibration experiments. The first one, G_1, is called the storage modulus or modulus of rigidity. The second one, G_2, is called the loss modulus. This loss modulus is directly related to the dynamic viscosity η' by the equation

$$\eta' = \left(G_2/\omega\right) \qquad [4]$$

The stress–strain relationship can then be expressed in the following manner:

$$\tau = \gamma_0[G_1(\omega) \sin \omega t + G_2(\omega) \cos \omega t] \qquad [5]$$

The first term in this expression is the component of the stress in phase with strain and determines the elastic reactive forces. The second term represents the part of the stress which is 90° out of phase with the strain and represents the dissipative forces. The relationships between the absolute modulus, the loss angle and the storage and loss moduli are given in the following equations

$$G_1 = |G| \cos\delta;\ G_2 = |G| \sin\delta;\ \tan\delta = G_2/G_1 \qquad [6]$$

The meaning of the loss modulus can be best illustrated by the calculation of the dissipation of energy due to viscoelastic losses in the material. The energy dissipated during one cycle is

$$W = \int \tau d\gamma = \pi G_2(\omega)\gamma_0^2 = \pi\tau_0\gamma_0 \sin\delta \qquad [7]$$

while the total energy expended during one cycle, E, is given by

$$E = \pi\tau_0\gamma_0 \qquad [8]$$

The storage and loss moduli are sometimes expressed also as a single complex quantity, the complex shear modulus, $G^* = G_1 + iG_2$, where the moduli are the real and imaginary parts of the complex modulus.

With this background in mind, one can now appreciate the difference that exists between the method of forced vibrations operating at a frequency close to the resonance frequency of the material and the non-resonance case. In the resonance case, one can handle only conditions under which $\tan\delta$ is much smaller than 1. In this case, the moduli vary only slowly with frequency and one measures the amplitude as a function of the frequency ω in the neighborhood of the resonance frequency ω_0. In the non-resonance case the tangent of the loss angle is not restricted to being much smaller than 1. In this case, force and deformation are compared with respect to amplitude and phase. As a matter of fact one will find in most text books dealing with this subject, that the discussion of vibration measurements including definitions of storage and loss modulus are based upon non-resonance forced vibrations and the resonance case is only considered as a special limited application.

B. *Apparatus*

The vibration tester used in this investigation was developed by W. Philippoff (7) and has not been described in detail elsewhere. Basically, the instrument consists of two concentric cylinders, the outer one referred to as the cup and the inner one is called the plunger. With this setup, the material is pumped by movement of the inner cylinder. The plunger is mounted in a frame which is connected through a dynamometer to a driving cam which imparts sinusoidal motion in the direction of the long axis of the plunger. The cup is solidly clamped to the base of the machine. Between the cam and the frame, as well as between the cup and the frame, strain gages are mounted to permit the measurement of the stress and the movement of the frame. Two linear-variable transformers were used in conjunction with these strain gages. The output of these transformers, properly amplified and rectified, was applied to the horizontal and vertical plates of an oscilloscope. The resulting stress–strain ellipse traced on the screen of the oscilloscope was photographed and the picture used to obtain the necessary experimental information. The details of the analysis of this ellipse and the method used to calculate the moduli are shown in Appendix I. When frequencies below 10^{-3} cycles per sec were used, the output of the strain gages was recorded on a two-pen recorder rather than an oscilloscope because the long exposures necessary to record a complete cycle produced poor pictures.

The range of forces and deformations that can be

measured with this equipment varies from a few grams to 10 kilograms force and from 10 to 1000 microns double amplitude of deformation. The frequencies covered with this instrument range from 10^{-4} to 10 cycles per second and the test temperature ranges from −17°C to 50°C.

C. *Procedure*

Two sets of plungers were used with two different cups, thus providing clearances ranging from 2/32 to 8/32 inches. The plunger and cup sets were calibrated with a National Bureau of Standards oil. From this calibration, the instrument constants were obtained. These calibration values are shown in Table 1 together with the values that were obtained from theoretical calculations based on the geometry of the cup and plunger arrangement. The details of these calculations are shown in Appendix I.

TABLE 1

Calibration Values

Gap, inches	Constants in dyn × microns cm^2 kg	
	Calculated	Experimental
2/32	1.035×10^4	1.185×10^4
3/32	3.26×10^4	3.24×10^4
7/32	4.98×10^5	5.07×10^5
8/32	7.15×10^5	6.31×10^5

It can be seen from this comparison that there exists good agreement between these two sets of values.

Once the instrument was calibrated, the grease samples were carefully packed into the cup to avoid any entrapment of air and any unnecessary working. The sample was then brought up to the desired temperature and was ready for testing.

D. *Materials*

Two greases were used in this investigation. Grease A was a mixed calcium-lithium soap grease of NLGI grade 2 and Grease B was a complex calcium soap grease of NLGI grade 1. Both greases contained naphthenic type base oils with Grease A containing a slightly more viscous oil than Grease B. The composition and physical properties of these greases are shown in Table 2.

TABLE 2

Composition and Physical Properties of Test Greases

Composition	*Grease A*	*Grease B*
Soap type	Lithium/ Calcium	Complex Calcium
% Soap content	12	22
Base oil viscosity, SSU at 210°F	70	60
V.I. of base oil	35	35
Physical Properties		
Penetration, mm/10 at 77°F		
Unworked	275	274
Worked 60 strokes	280	310
Worked 10,000 strokes	320	333
Unworked at 210°F	350	300

The main difference between these two greases existed in the shape and size of their constituent soap fibers as shown in Fig. 1. From the electron micrographs, it can be seen that grease A has fibers with a length to diameter ratio of about 1000 to 1 or more, while in grease B this ratio is of the order of 10 to 1. These micrographs were made from the samples of the two greases after homogenization.

(a)

(b)

FIG. 1. Comparison of soap structure, 10,000×

It should be kept in mind that all the following results were obtained from these homogenized samples.

3. Experimental results

Both greases were examined in the vibration tester to determine their dependence on frequency, amplitude, temperature, and the geometry of the testing equipment.

A. *Reproducibility of Sample Preparation*

Before proceeding with the above mentioned measurements, it was necessary to determine the reproducibility of the measurements as affected by sample preparation. Fresh samples of greases A and B were examined at several frequencies and the values so obtained for G_1 and G_2 were subjected to a statistical analysis. From this analysis, it was concluded that the reproducibility of samples was very good and that one could obtain the values of the moduli with an accuracy of $\pm 5\%$ at 90% confidence level.

When measurements were repeated after a whole sequence of tests had been run with the same sample, significant changes outside the experimental error were observed. This behavior of the greases is a reflection of their sensitivity to working and is illustrated in Table 3.

TABLE 3

Effect of Working on Rigidity and Viscosity of Test Greases

(Frequency $f = 0.034$ c/s, 25°C)

	Grease A			Grease B		
Run No.	G_1'	G_2[a]	η'[ab]	G_1[a]	G_2[a]	η'[b]
1	3.81	1.88	8.85	2.54	1.61	7.52
2	4.14	1.62	7.60	2.03	1.23	5.75

[a] In 10^3 dyn/cm^2.
[b] $\eta' = G_2/2\pi f$ in 10^3 poises.

There was a difference of two days between the first and the second run during which period the grease sample had been subjected to a complete frequency and amplitude analysis.

These observations point out the need for careful control of the conditions when testing greases, since the properties of these materials depend on their previous history. Such behavior had been noticed earlier by Singleterry and Stone (8).

B. *Frequency Dependence*

The frequency dependence of the two greases was studied at four different temperatures using a reasonably constant deformation amplitude ($\gamma = 8\%$). The results for greases A and B are shown in Figs. 2 and 3, respectively. From these figures it can be seen that the moduli G_1 and G_2 increase only by a factor of about 10, while the frequency is increased ten thousandfold. In the case of grease A, it is interesting to note that the G_1 remains larger than G_2 over the whole frequency range and at temperatures below 35°C. With grease B, G_1 becomes consistently smaller than G_2 at

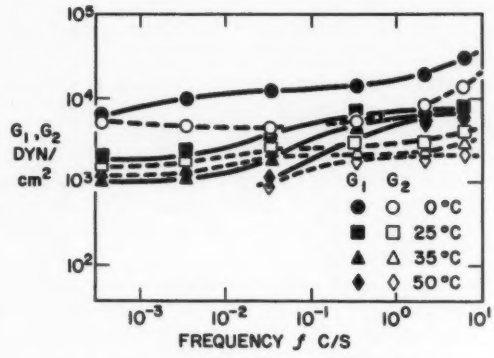

FIG. 2. Frequency dependence of Grease A.

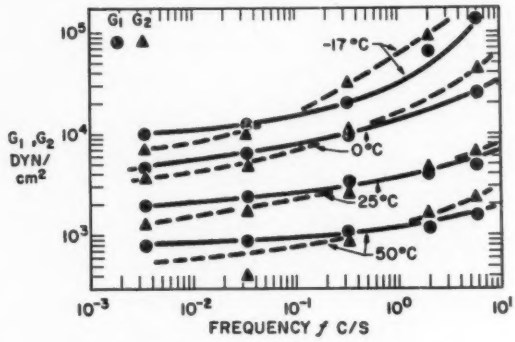

FIG. 3. Frequency dependence of Grease B.

higher frequencies and at all temperatures tested. This indicates that the viscous response of this grease increases consistently in importance and predominates at higher frequencies.

C. *Amplitude Dependence*

The amplitude dependence of the two greases was examined at various frequencies and at three temperatures, −3°, 25° and 50°C. The results are shown in Figs. 4 and 5 for greases A and B, respectively. In both cases a very strong dependence on the extent of deformation is noted, which is quite different from the previous observation made of the frequency dependence. From a comparison of these two figures, one notes again that for grease B, G_1 decreases in magnitude more rapidly than G_2 indicating that the viscous response increases with increasing deformation.

From the shape of the curves and the photographic pictures obtained in determining the amplitude dependence of the two greases, it was noticed that there existed a non-linear region, i.e. a region in which the response of the materials to sinusoidal stressing was non-linear. This appears in the figures as a change in slope and in the photographs as a distortion of the normally observed ellipse. This region of non-linearity seems to extend from very low shear strains of about 0.3% to about 5% and occurs for both greases in approximately the same region. A harmonic analysis was made to determine whether the

stress or the strain or both are non-linear. This was done by separating the stress and strain curves and analyzing each one separately. To obtain higher sensitivity for this study, grease B was tested at −3°C at 0.0034 cycles per sec. The reason for selecting grease B for the study was based on the fact that it showed the stronger non-linear response of the two samples. The low frequency of 0.0034 cycles per sec was selected because it permitted the use of a two-pen recorder to trace force and deformation versus time. These curves are shown in Appendix 2 together with the details of the calculations. The deformation curve was found to be perfectly sinusoidal and, therefore, the entire non-linearity had to be present in the force curve. It was also established that this observed non-linearity was not due to any superposition of higher harmonic motions but was characteristic of the fundamental wave. This confirmed the assumption on which the procedure outlined in Appendix 1 is based—namely, that only fundamental waves were being measured and that the results so obtained can be used to calculate the stress as the function of strain. The surprising factor of this analysis was the indication that the non-linearity resides in the loss modulus, the viscous behavior, which is contrary to what one usually expects.

D. *Temperature Dependence*

As was noticed already in Figs. 2 and 3, an increase in temperature caused a decrease in the value of the storage and loss moduli over the whole frequency range indicating a decrease in rigidity and viscous response. A similar condition prevailed when the amplitude dependence of the grease was tested at different temperatures as was shown in Figs. 4 and 5. An additional peculiarity that could be

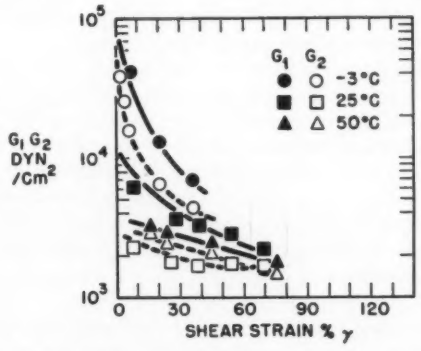

FIG. 4. Amplitude dependence of Grease A (Frequency = 0.34 cps)

observed was the fact that for grease A an increase in temperature to 50°C increased rather than decreased the value of the loss modulus over that at 25°C, particularly at lower shear strains. The amplitude dependence of the two greases remained quite similar at different frequencies as shown in Figs. 6 and 7 for greases A and B, respectively. From these figures it can be seen that increasing the frequency over the same range of shear strains produces essentially similar effects to decreasing the temperature.

The strong amplitude dependence evidenced by these two greases makes it somewhat difficult to compare their true

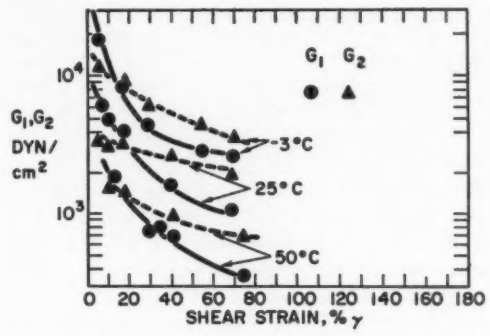

FIG. 5. Amplitude dependence of Grease B (Frequency = 0.34 cps).

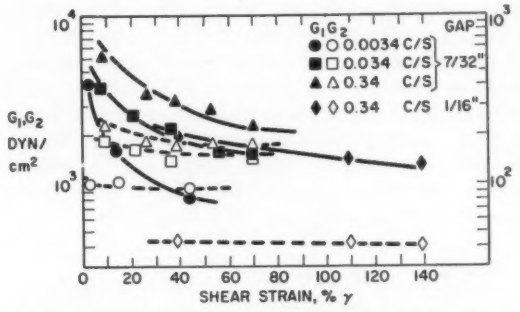

FIG. 6. Effect of frequency and geometry on amplitude dependence of Grease A (25°C).

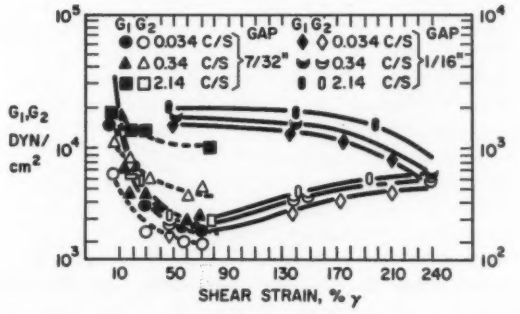

FIG. 7. Effect of frequency and geometry on amplitude dependence of Grease B (−3°C).

frequency dependence. Ideally, one would have to examine the greases at all frequencies at 0 amplitude. Practically, this is not possible but one could use very small amplitudes and assume them to be practically negligible. Unfortunately, when working at these low frequencies, it is impossible to achieve this condition because the greases are too soft and the instrument is not sensitive enough to resolve the small forces necessary. Also, one is more interested in the behavior of the greases at large deformations and hence large amplitudes, since these represent more realistic conditions under which the greases are expected to operate.

E. *Effect of Geometry*

Two different clearances were used in performing the

series of experiments. In one case a wide opening of 7/32 of an inch was used, while in the other case a relatively narrow gap of 1/16 of an inch was used. The resulting differences in amplitude dependence have been incorporated into Figs. 6 and 7. It can be readily seen that by narrowing the gap the greases will be much more severely deformed and hence more structural breakdown occurs. Under these conditions, the greases have smaller storage and loss moduli than when the wide opening is used, indicating considerable softening. With this narrow clearance, one cannot approach properly the region of small deformations necessary for the investigation of the region on non-linearity. But these narrow clearances can be used to point out the behavior of the test greases under large deformations and indicate unusual occurrences in that region. This point is clearly shown in Fig. 7 for grease B. It can be noticed that G_2 remains smaller than G_1 over a wide range of deformations and increases only at very large deformations, whereas G_2 for grease A remains essentially unchanged. It is for this reason that these values of G_1 and G_2 have not been shown over the same extended range for grease A. Thus, results obtained with these two clearances supplement each other and provide information over a wide range of deformations.

F. *Principle of Reduced Variables*

In the preceding discussion, it was pointed out that increasing the frequency or decreasing the temperature produced similar results. This trend suggests an equivalence between frequency and temperature. Ferry (9) recognized this relationship and introduced the concept of "reduced variables" in which he assumed that each mechanical response of the system has an identical temperature coefficient. The validity of reduced variables has been experimentally verified for many systems, particularly polymers, and permits measurements at different temperatures and different frequencies to be reduced to one temperature, in this case 25°C, while covering a much wider range of frequencies.

In practice the isothermal curves of G_1 and G_2 are plotted against the frequency on a log–log plot. The "reduced" curve is produced by sliding each isothermal curve along the frequency axis until the points line up with the reference curve at 25°C to give a continuously smooth curve. The amount of horizontal shift necessary to obtain coincidence is a measure of the temperature dependence of the material and is referred to as the shift factor, log a_T.

An attempt was made to apply this principle to both greases. While it was possible to do this reduced variable treatment for grease A, it was not applicable for grease B under prevailing circumstance. Apparently mechanical responses, the reactions of the material to external deformation are not equally affected by temperature changes. One cannot shift these curves parallel to each other as can be readily appreciated from Fig. 3. The graph of the reduced variable plot for grease A is shown in Fig. 8. One can see that G_1 is always larger than G_2 over the extended frequency range.

In order to check the validity of the method of reduced

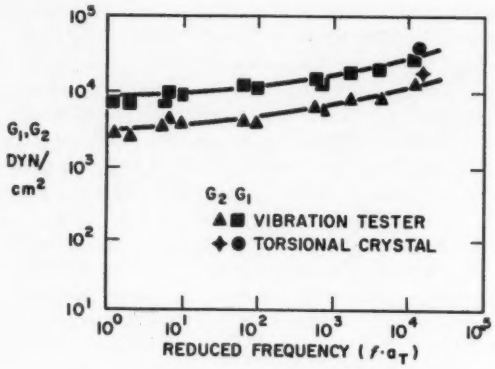

FIG. 8. Reduced curve, 25°C Grease A.

variables for this grease system, the dynamic behavior of grease A was measured at high frequencies with a torsion crystal using the Mason Technique (10). The torsion crystal was brought into contact with the grease with the bottom of the crystal just touching the material to be measured. The technique and the evaluation are outlined in the literature (11). The ambient temperature of the measurements was 28.5°C and the shear was so small that it was assumed to be 0. In order to compare these results with the ones obtained in the vibration tester, it was necessary to correct for the shear dependence using the results obtained previously from the amplitude dependence. After this correction and the correction for different temperatures were made, it was found that the moduli so found fit very closely on the reduced frequency curve as shown in Fig. 8.

An interesting piece of information from this reduced variable principle can be obtained by plotting the shift factor log a_T versus $1/T$. The slope of this curve yields an apparent activation energy of viscous flow. The physical meaning of this activation energy is somewhat vague at the present time since it refers to moles of flow units, and it is impossible to define the meaning of moles in this case. This plot is shown in Fig. 9, indicating that there exists an essentially straight line relationship between 0 and 50°C. The slope of this line indicates an activation energy of about 22 kcal/mol.

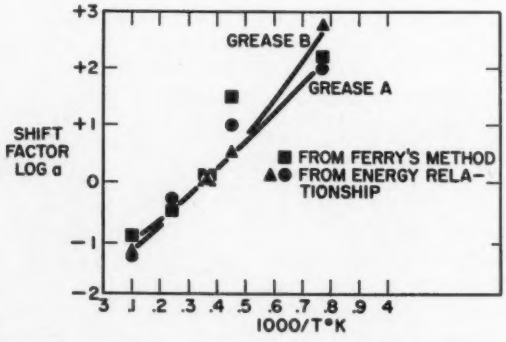

FIG. 9. Temperature dependence of test greases.

G. *Relationship of Total to Dissipated Energy*

Another interesting piece of information can be obtained from a study of the relationship that exists between the total energy expended and energy dissipated per cycle. These data have been obtained using the Equations [7] and [8], given in Part 2, and are shown in detail in Fig. 10

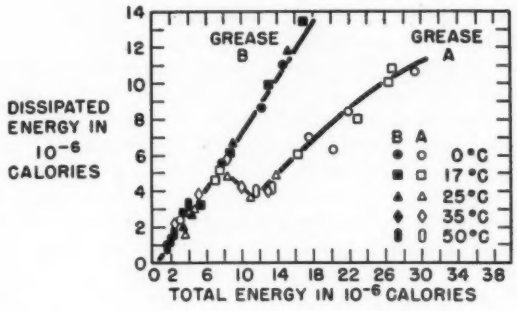

FIG. 10. Relationship between total energy and dissipated energy.

for both greases. For grease A one can see that there exists a maximum at low energy input. At higher energy inputs the dissipated energy increase is practically linear. In the case of grease B there is a continuous increase in the relationship between energy input and energy dissipated indicating that a different mechanism is involved in the mechanical response of this system to strain. This is another way of confirming the previous statement that the two greases respond differently to deformation forces. In both cases the curve appears to start somewhat to the right of the common zero point, indicating that no flow will occur until a finite amount of energy is put into the system. From an extrapolation of both curves to the abscissa one gets approximately 30 dyn/cm^2 as the minimum stress necessary to produce flow.

This method of plotting energy input against energy dissipation can also be used to verify the concept of reduced variables previously advanced. From the amount of overlap that exists between measurements made at the same frequencies but at different temperatures, a similar shift factor can be deduced which when plotted against $1/T$ gives identical results with the one obtained previously for grease A as shown in Fig. 9. Such procedure yields also information on the thermal behavior of grease B where the method proposed by Ferry does not work because of the peculiar shape of the frequency isotherms, as shown also in Fig. 9. From this plot, the activation energy of grease B is found to be roughly the same as that for grease A—namely, 22 kcal/mol between 17 and 50°C. Below that temperature the relationship between shift factor and reciprocal temperature is no longer linear and the slope increases rapidly to much higher values. This is considered further evidence of the aforementioned different behavior of grease B as compared to grease A.

4. Interpretation and discussion of experimental results

Once the response of the two greases to time dependent stresses had been experimentally determined, it became desirable to establish the extent to which these results reflect the known properties and performance characteristics. Also, it was felt that these results should be examined to see whether they could be used to classify the behavior of greases in terms of other well-defined systems such as polymers.

A. *Comparisons of Vibration Tester Results with Known Physical Properties*

The vibration tests were performed at low shear rates, consequently only grease properties, such as consistency, which are measured at low shear rates would be expected to correlate.

1. *Consistency*—The effect of small deformations in the vibration tester can be compared to the effects produced in the penetration test as shown in Table 4.

TABLE 4

Comparison of Vibration Test Results with Penetration Results

Properties	Grease A	Grease B
Unworked penetrationat 25°C, in mm/10	275	274
Extrapolated value of G_1 at 0%γ at 25°C, 0.34 c/s, in dyn/cm^2	1.1×10^4	1.1×10
Minimum stress in dyn/cm^2 to produce movement (τ_1)	30	30
Change in penetration after 60 strokes in ASTM grease worker at 25°C mm/10	5	36
d(log G_1)/dγ for small values of γ at 25°C	−0.16	−0.23

The similar consistency of the two greases as evidenced by their unworked penetration is reflected in two values which were obtained from the amplitude dependence of the greases in one case and the energy relationship (see Fig. 10) in the other case. The change in penetration upon working is well reflected in the rate of change of log G_1 with deformation which is determined from the amplitude dependence of these two greases. If the measurements were carried out to bigger deformations, they would probably permit further correlation with prolonged working in the ASTM grease worker.

2. *Temperature Effects*—The effect of temperature on the behavior of the two greases as determined in the vibration tester compares quite favorably with the change in unworked penetration and apparent viscosity with temperature as shown in Table 5.

TABLE 5

Comparison of Observed Temperature Effects

	Grease A	Grease B
Increase in unworked penetration, in mm/10 (increase in temperature from 25 to 100°C)	75	26
Change in apparent viscosity with temperature (between 25 and 100°C)	large	small
Shift in loss angle minimum, in cycles/sec (increase in temperature from 0° to 50°C) (See Figs. 11 and 12)	0.024to4.4	0

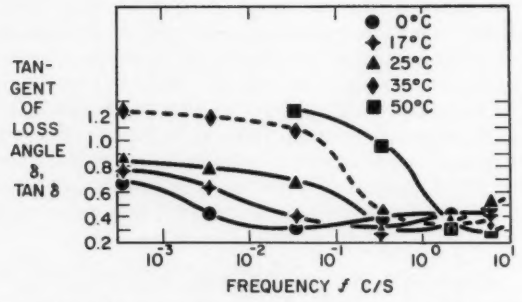

FIG. 11. Effect of temperature on loss angle–frequency relationship, Grease A.

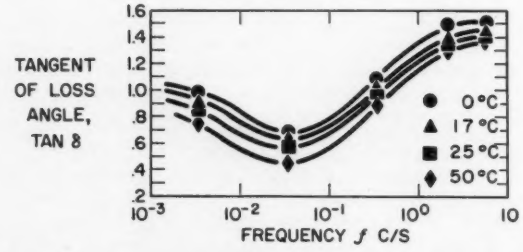

FIG. 12. Effect of temperature on loss angle–frequency relationship, Grease B.

It should be recalled that the tangent of the loss angle represents the ratio of loss modulus to storage modulus and hence represents the ratio of energy dissipated to energy stored per cycle. Since the loss angle–frequency relationship does not shift with temperature for grease B, the structural changes responsible for the movement of this grease appear to be unaffected by temperature changes. This suggests that the results from the vibration tester might be used to uncover in more detail the relationship that exists between the structure of greases and their physical properties.

3. *New Information*—The data presented earlier were analyzed with regard to possible new information that could be obtained from them and several interesting observations were made.

(a) *The existence of two yield stresses*—It has been shown earlier in discussing the relationship between total energy input and amount of energy dissipated, that both greases require a minimum stress τ_1 of 30 dyn/cm² to produce movement. On the other hand, an analysis of the region of non-linearity of the stress–strain relationship indicates the existence of a "yield stress" of 560–650 dyn/cm² for grease A and 670–710 dyn/cm² for grease B. These data indicate the existence of two yield stresses, τ_1 and τ_2, and hence two types of grease movement, namely bulk movement and plastic flow. If one keeps in mind the fact that any movement of grease will require a rupture of contact points among soap fibers, one can explain these two types of movement as follows: Between τ_1 and τ_2 the rate with which contact points are broken is smaller than the rate with which these contacts reform or heal, so that the net effect is the movement of the grease in bulk or creep. At τ_2 the two rates become equal, and above τ_2 the rate of rupture exceeds that of healing. As the shearing stresses further increase, these ruptures lead to smaller and smaller soap fiber aggregates until the apparent viscosity of the grease will approach that of the base oil. The apparent similarity of the behavior of the two greases at the small deformations produced in the vibration tester is not surprising since these deformations are not expected to produce any noticeable damage to the soap structure. One would expect that the structural differences become more noticeable at higher stresses or at lower stresses applied at elevated temperatures.

(b) *Relaxation time distribution*—From Fig. 10, it can be seen that about 40 to 90% of the total energy was dissipated under the prevailing experimental conditions. This means that from 60 to 10% of the total energy has been stored in a more or less reversible fashion. This energy can be stored by stretching bonds, changing bond angles, coiling or uncoiling of molecular aggregates or just simply displacing molecules or molecular aggregates from their equilibrium position. After the deforming stresses have been released, these displacements and molecular changes will be reversed within a definite time interval. This time interval is called the relaxation time and the molecular changes involved are referred to as relaxation mechanisms. In complex systems such as greases, there are many ways and means of storing energy and hence a large number of relaxation times. From the results obtained with the vibration tester, one obtains an approximation of the distribution of relaxation times, $[H(t_r)]$, using Ferry's first approximation method (9). The results are shown in Figs. 13 and 14 for greases A and B, respectively. It is immediately apparent that the two greases behave differently. Grease A has a rather sharp well-defined maximum similar to those observed in amorphous polymers which shifts with temperature from 50 sec at 0°C to 0.2 sec at 50°C, while grease B has a maximum at 1.5 sec that is barely visible at 17°C, is well developed at 25°C and again hardly noticeable at 50°C and does not shift with temperature. Such behavior is believed to be unique among polymers as well as greases and indicates that temperature changes have a different effect on this material than on grease A.

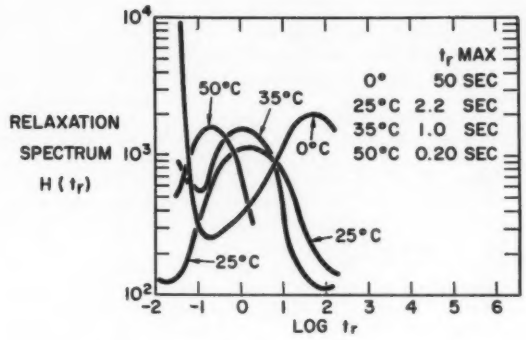

FIG. 13. Relaxation spectrum of Grease A.

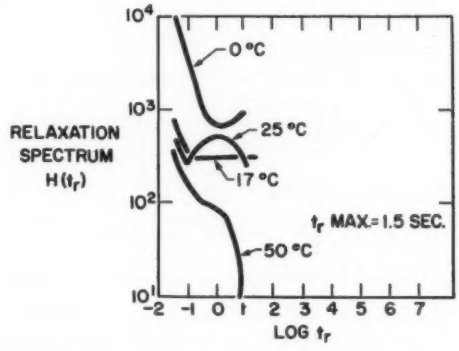

FIG. 14. Relaxation spectrum of Grease B.

The shape of the relaxation distribution curves suggests the existence of two further peaks both at longer and shorter times. Relaxation times of 1600 and 10,000 sec have been previously reported (4) for sodium and lithium soap greases, respectively, when exposed to small compressive deformations. Eyring (12) reported relaxation times of 3 sec at 30°C for an AN-G-25 type grease. These data were obtained in concentric cylinder type viscometers. No data have as yet been reported on the very shortest relaxation times.

The significance of the observed relaxation time in terms of molecular processes can only be guessed at as yet. It is possible that this time interval represents the movement of soap aggregates from one equilibrium position to an adjacent one. In the two greases these soap aggregates are quite different in size and accordingly will take different times to carry out this movement. This tentative assignment of this movement of soap aggregates is made largely on the basis of the electron microscope evidence available. As has been shown in Fig. 1, grease A has the long thin fibers typical of regular soap type greases while grease B has short, well-formed needle-like fibers that do not wrap around each other. The displacement of such needle-like fibers will be quite different from those long fibers which behave like an amorphous polymer.

B. *Comparison of Greases with Polymers*

Once the response of these two greases to time dependent stresses had been experimentally determined, it became desirable to classify this behavior in terms of other well-defined systems such as high polymers. A comparison of greases and high polymers had been suggested earlier when studying the structure of greases (5). If one makes, therefore, this comparison one finds that greases resemble amorphous linear polymers, which also show a relatively small frequency and large amplitude dependence. Like greases, these polymers show a large amount of non-linear, irreversible behavior. An examination of the structural differences existing between greases and amorphous linear polymers suggests the possible explanation of their similar mechanical behavior.

Obviously, greases resemble linear polymers in as much as most soaps usually form long thin fibers. Greases also resemble amorphous polymers because these fibers do not always line up in a geometric fashion but are randomly oriented and entangle with each other. While the crystalline regions within the fiber remain intact, the space occupied by the fibers is not crystalline. The forces holding this network of fibers together will be similar to those holding polymer molecules together except for the additional contribution of the polar groups in the soap fiber which will provide for additional attractive forces in the case of greases. One might, therefore, expect some advantage in this respect over the amorphous polymer. On the other hand, the polymer molecules themselves are made up of monomers which are held together by strong chemical bonds. In the soap fibers, only ionic type forces together with van der Waals forces help to hold the soap molecules together. This condition would give a greater structural stability in at least one direction to the polymer system, which indeed they are known to have. The net effect of this situation is difficult to assess, but one would expect that these differences just pointed out would not cause significant differences in the mechanical properties of these two systems. The effect of fiber length can be held responsible for the different behavior of the two test greases. The short fibers of grease B cannot entangle like those of grease A and any movement will depend more on the forces holding the fibers together than on their disentanglement.

5. Summary and conclusions

On the basis of the experimental results, it can be concluded that the vibration tester method, developed for the study of viscoelastic materials, can be successfully applied to greases. It was shown that the moduli of greases change little with frequency but change considerably with changes in amplitude and temperature. Decreases in the clearance used in deforming the grease were found to decrease the value of the moduli and reflect the shear sensitivity of greases.

Since the vibration tester operates at low shear rates, only those known grease properties that are measured at similar low shear could be correlated with the experimental results. Thus, the consistency of the two greases as reflected in their unworked penetration was correlated with the

extrapolated value of the modulus of rigidity, G_1, and with the minimum stress required to produce grease movement. Similarly the effect of working the greases for 60 strokes in the ASTM worker was correlated with the rate of change of log G_1 with increasing deformation. The effect of temperature on the consistency of the two greases was found to be reflected in the shift of the loss angle tangent with temperature.

In addition to these correlations, it was established that both greases have two yield stresses which reflect the existence of two types of movement, bulk movement and plastic flow. In the bulk movement, fiber contacts are broken, but reform at such a fast rate that the bulk of the grease remains unchanged. In plastic flow, contacts are broken faster than they can reform and the bulk of the grease will soften.

The structural differences existing between the two greases are particularly reflected in the change of the relaxation time distribution with temperature. While grease A has a maximum that shifts with temperature from 50 sec at 0°C to 0.2 sec at 50°C, grease B shows only a clear maximum of 1.5 sec at 25°C which does not shift with temperature but merely tends to disappear with both increasing and decreasing temperature.

The behavior of the two greases in the vibration tester resembles that of amorphous linear polymers. This resemblance is particularly striking for grease A, while it is less pronounced for grease B. This is taken as further confirmation of the difference in soap fiber structure that exists between the two greases. Thus the vibration tester confirms the significance of the relationship between structure and physical properties of greases. More detailed work is now being planned to establish this relationship more quantitatively.

6. Acknowledgment

The authors wish to acknowledge the help of Dr. W. Philippoff of the Franklin Institute in performing the experimental part of this investigation and the many suggestions that have been advanced by him and his coworkers in support of this project.

REFERENCES

1. VINOGRADOV, G. V., and KLIMOV, G., "Rheological Properties of Calcium Greases," *J. Tech. Phys.*, vol. 18, 1948, pp. 355–376.
2. CARVER, E. K., and VAN WAZER, T. R., "Sudden application of a Constant shearing Motion to Anomalous Fluids," *J. Phys. & Coll. Sci.*, vol. 51, 1947, p. 751 ff.
3. GOLDBERG, H., and SANDVIK, O., "Instrument for Measuring Rheological Properties of Elastic Fluids," *Anal. Chem.*, vol. 19, 1947, p. 123 ff.
4. HUTTON, J. F., and MATTHEWS, J. B., "Viscoelastic Behavior of Lubricating Greases," HARRISON, V. G. H., *Proc. 2nd Int. Congress on Rheology*, Academic Press, New York, 1954, p. 408 ff.
5. FORSTER, E. O., and KOLFENBACH, J. J., "Fibers, Forces, and Flow," *NLGI Spokesman*, vol. 20, No. 3, 1956, p. 16 ff.
6. STUART, H. A., *Physik der hochpolymeren*, vol. IV, Springer Verlag, Berlin, 1956, p. 85 ff.
7. PHILIPPOFF, W., "Mechanical Investigation of Elastomers in a Wide Range of Frequencies," *J. Appl. Phys.*, vol. 24, 1953, p. 685.
8. SINGLETERRY, C. R., and STONE, E. E., "Rheological Properties of a Lubricating Grease, *J. Coll. Sci.*, vol. 6, 1951, p. 171 ff.
9. FERRY, J. D., FITZGERALD, E. R., JOHNSON, M. F., and GRANDINE, L. D., JR., "Temperature Dependence of Dynamic Properties of Elastomers; Relaxation Distributions," *Ind. & Eng. Chem.*, vol. 44, 1952, p. 703 ff.
10. MASON, W. P., "Measurement of the Viscosity and Shear Elasticity of Liquids by Means of a Torsionally Vibrating Crystal," *Trans. ASME*, vol. 69, 1947, p. 359 ff.
11. PHILIPPOFF, W., SITTEL, K., FERRY, T. D., and PLAZEK', D. T., "Dynamic Investigations on Polymeric Solutions using Different Methods," *J. Soc. Plastic Engrs.*, vol. 11, n. 7, September 1955, p. 41 ff.
12. HAHN, S. J., REE, T., and EYRING, H., "A Theory of Thixotropy and Its Application to Grease," *NLGI Spokesman*, vol. 21, n. 3, June 1957, p. 12 ff.
13. SMITH, T. L., FERRY, T. D., and SCHREMP, F. W., "Measurements of the Mechanical Properties of Polymer Solutions by Electromagnetic Transducers," *J. Appl. Phys.*, vol. 20, 1949, p. 144 ff.
14. PHILIPPOFF, W., "Further Dynamic Investigations of Polymers," *J. Appl. Phys.*, vol. 25, 1954, p. 1102 ff.

APPENDIX I

Calculation of instrument constant and moduli

The formulas used for the calculation of the maximum shearing stress τ_0 and the maximum shear strain γ_0 are for this arrangement (13, 14):

$$\tau_0 = \frac{F}{2\pi L R_i} \cdot \frac{1-c^2}{1+c^2}$$

$$\gamma_0 = \frac{D}{R_i} \cdot \frac{1-c^2}{1+c^2} \cdot \frac{1}{\ln\frac{1}{c} - \left(\frac{1-c^2}{1+c^2}\right)}$$

where R_i = radius of inner cylinder (plunger in cm).

$c = R_i/R_0$ and R_0 is radius of outer cylinder (cup), in cm.

D = deformation, displacement of inner cylinder with respect to outer cylinder, in microns.

F = force required to move inner cylinder with respect to outer cylinder against the drag of the material contained in the gap $R_0 - R_i$, in kg.

L = length of inner cylinder in cm.

since $|G| = \tau_0/\gamma_0$ it follows that $|G| = E/D \cdot K$ where K is the instrument constant and given by the expression

$$K = \frac{1}{2\pi L} \cdot \left[\ln\frac{1}{c} - \left(\frac{1-c^2}{1+c^2}\right)\right]$$

and has the dimensions of $(\text{dyn/cm}^2) \times (\text{microns/kg})$.

The values of F and D are obtained from the geometry of the hysteresis loop as shown in Fig. 16.

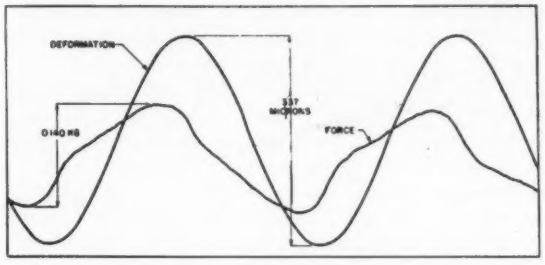

FIG. 15. Force–deformation relationship for Grease B (0.0034 cps, −3°C).

APPENDIX 2

Harmonic analysis of non-linear response

Using a two-pen recorder, traces of force and deformation as a function of time were obtained for grease B at 0.00340 cycles per sec and −3°C. These curves are shown in Fig. 15 and indicate that the deformation curve is perfectly sinusoidal. The entire non-linearity is present in the force curve. A harmonic analysis of this curve gave the following relationship:

$$F = 61{\cdot}0\sin(\omega t + 52°40') - 7{\cdot}6\sin(3\omega t + 83°15') + \\ + 1{\cdot}04\sin(5\omega t + 80°38'')$$

or approximately

$$F = 37\sin\omega t + 48{\cdot}5\cos\omega t - 7{\cdot}6\cos 3\omega t \\ + 1{\cdot}04\cos 5\omega t$$

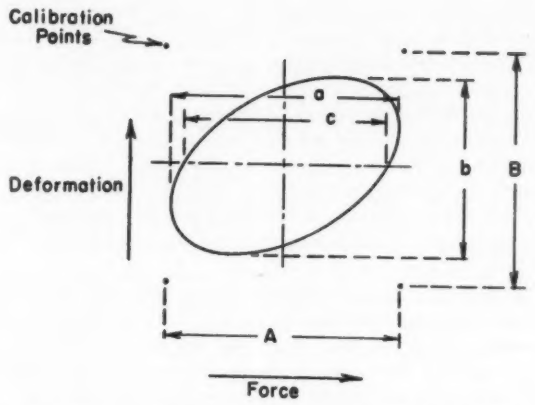

FIG. 16. Stress–strain ellipse. (Thus $F = a/A$, $D = b/B$, $\sin\delta = c/a$, and $G_1 = (KF\cos\delta)/D$, $G_2 = (KF\sin\delta)/D$).

where the constants are in millimeter of travel on the graph, ω is the angular frequency, and t the time in seconds.

If the usual approximation is used, of taking the peak values and one measures the phase shift of these peaks, one obtains

$$F = 62\sin(\omega t + 53{\cdot}0°)$$

in good agreement with the result of the harmonic analysis. The presence of the higher harmonics as cosine terms indicates that the non-linearity resides in the loss modulus rather than the storage modulus.

DISCUSSION

B. W. HOTTON (*California Research Corporation, Richmond, California*):

This paper does a thorough and stimulating job of showing how some of the techniques and theories of polymer research can be applied to lubricating greases. The fact that the stresses and strains of these techniques are gentler than those in a fast-running bearing should be no deterrent to their continued use: they are providing clues to the fundamental structure of greases that are valuable for a better understanding of their use under all conditions. The following questions and comments are suggested by the paper.

Experimental Technique—Details of the radius, length, and orientation of the test cell would be helpful in judging the uniformity of shearing of the grease across the annulus, and comparing the vibration tester with parallel plate instruments.

Experimental Results—The sensitivity of greases to working raises the question of whether one sample should be used for a series of tests of a varying condition or whether a fresh sample should be used for each point. If a single sample was used for a series of variations, how much are later points displaced because the sample was work-softened during measurement of the earlier points?

The inverse temperature dependence of the elastic modulus may offer a clue to the nature of the elastic strain. Bulk crystalline materials also decrease in elasticity with increasing temperature, whereas many rubbery materials behave oppositely. This suggests that more of the elastic strain in greases is within the individual soap crystallites than in the cross links among them, which may be more rubbery in nature. The concurrent change of the oil viscosity with temperature complicates such interpretations, but this variable could be isolated if tests were made on a greater variety of greases.

Equation 4 defining dynamic viscosity should read $\eta' = G_2/\omega$. In the present form, dynamic viscosity would increase with frequency (shear rate). However, shear viscosity decreases with shear rate.

Interpretation of Results—The new information obtained on yield stresses may be compared more directly with penetrations if the penetrations are converted to the same units. We calculate the unworked penetration of Grease A to be 14,800 and that of Grease B 15,000 dynes/sq cm. These values are much higher than the 560–650 and 670–710 dynes/ sq cm obtained from the stress–strain curves and very much higher than the 30 dynes/sq cm obtained from the energy dissipation.

The relaxation time distribution may be partly the

result of the complex distribution of magnitude and direction of shear strain across the annulus, as well as the result of a variety of relaxation mechanisms.

The elastic property of greases studied in this paper is principally the rigidity and not the extensibility. By analogy, the technique of this paper would show that steel has a high elastic modulus (i.e. it is rigid) whereas rubber would have an elastic modulus several orders of magnitude lower. Both the rigidity and the extensibility are useful and necessary quantities to convey the overall elastic nature of matter.

The authors suggest that dynamic viscoelastic studies as a function of temperature permit one to analyze when changes occur in the structural segments involved in deformation. We agree, but we feel that conventional capillary or concentric cylinder shear data as a function of temperature are easier to obtain and to interpret for this purpose.

Acknowledgment—I am thankful to Dr. D. W. Criddle for contributing to the discussion of this interesting paper.

AUTHORS' REPLY:

In response to the questions raised by the discussors regarding the experimental techniques used, we present the following details. The two cups used had inner radii (R_0) of 1.6871 and 1.5314 inches, respectively. The two plungers which were used with either of the two cups had outer radii (R_1) of 1.4694 and 1.4371 inches, respectively. The motion of the plunger was in the vertical direction.

With regard to the question of using one sample for a series of tests rather than a fresh sample for each determination, the following statement might be useful to elaborate what has been already said in the text under Section 3.A. If the frequency dependence of a grease is determined, we found that one sample could be used for a normal sequence of five tests. This was partially due to the fact that only small amplitudes were used in our frequency determinations. The sequence of frequencies did not matter in this study. Thus, we would obtain the same results when starting at about six cycles per second and going down to about 10^{-4} cycles per second as we would get if we would start at the lower end. A different situation exists in studying the amplitude dependence. Here we found that in order to get accurate results, we had to adhere to a given test sequence of increasing amplitudes. Apparently running the grease at small amplitudes does not significantly affect subsequent runs at larger amplitudes. The converse, however, is not true. We believe that our procedure of using one sample in making determinations in a sequence of increasing amplitudes yields a reliable picture.

The point raised by the discussors regarding the low yield-stress values observed by us deserves some attention. Messrs. D. W. Criddle and J. L. Dreher (Yield Points of Lubricating Greases, paper presented at Annual Meeting of NLGI, 27–29 October, 1958) points out that the yield stress of a grease depends on at least three variables: the rate of deformation, the type of deformation and the work history of the grease. Obviously, one cannot directly compare penetration data with the yield stresses found under the prevailing experimental conditions. One can, however, as we suggested in our paper, compare penetration data of two or several greases and the yield stresses of these greases obtained with the vibration tester or other similar instruments. Such a comparison indicates the similarity or dissimilarity, as the case may be, of the physical properties of the greases under consideration.

It is true that one can obtain information of structural changes in capillary or concentric cylinder viscometers, but these latter instruments do not yield at the same time the desired information on the viscoelastic properties. Our suggestion of using these studies for structural changes was meant to illustrate the inclusiveness of the vibration test method used and was not meant to detract from the other well-known test methods.

Development of Seals for Rocket Engine Turbopumps

By JAMES E. WOLF[1] and ROBERT E. CONNELLY[2]

Introduction

THE rocket may be defined as a heat engine in the same sense as the steam turbine or the internal combustion engine. Fuel is burned and the resulting high pressure and high temperature gases, instead of impinging on turbine buckets or a piston, are released through an aperture in the device and the resulting reaction is the propulsive effort.

Small short range rockets are usually of the solid propellant types where a chemical solid is surface combusted at a very rapid rate. Larger sized rockets can use either solid or liquid propellants; at the present writing the larger rockets are usually of the liquid propellant type.

Liquid propellants are stored in tanks and are fed to the rocket nozzle either by pressurizing the tanks or by means of pumps. The smaller sized units use pressurized tanks.

Figure 1 shows a schematic of a small liquid propellant rocket engine. The tanks shown are filled with liquid oxygen and fuel and are pressurized, thus forcing the fuel and oxidizer to the combustion chamber where they are combined in the proper proportions, ignited and burned.

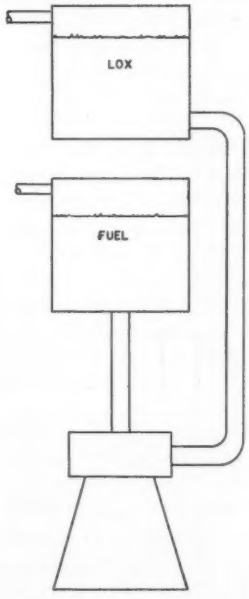

FIG. 1. Schematic of a liquid rocket engine with pressurized tanks

When the rocket reached large proportions the weight of pressurized tanks became prohibitive. Dr. Robert Goddard in the U.S.A. and Herman Oberth in Germany had both independently, and at an early date, envisioned the use of pumps to do the job. It was not until the rocket reached the size of the V2 that it became necessary to tackle the problem, and the problem seemed almost insurmountable. The pumps had to be able to pump the fuels, one of them a liquid gas at −300°F with a delivery pressure of approximately 300 psi and a flow rate of between 2000 and 3000 gal. per min. They had to be simple enough to eliminate any malfunctions and they had to be light. The only redeeming feature was that the operational life was measured in minutes. These requirements indicated the use of centrifugal pumps and the requirements of weight and space and the availability of high strength H_2O_2 dictated the choice of a gas turbine to drive the pumps.

Figure 2 is a schematic of a large sized liquid propellant rocket engine. The fuel and oxidizer tanks are kept at a minimum weight by not pressurizing them and the low pressure fuel and oxidizer are fed to the centrifugal pumps driven by a gas turbine. The pumps then raise the pressure to the required levels and feed the propellants to the combustion chamber.

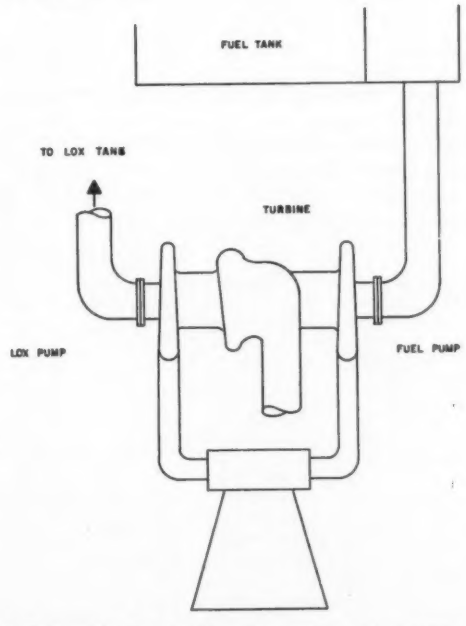

FIG. 2. Schematic of a liquid rocket engine with turbine driven pumps.

Presented as an American Society of Lubrication Engineers paper at the Lubrication Conference held in Los Angeles, Calif., October, 1958.

[1] Supervisor, Turbomachinery, Rocketdyne, Canoga Park, California.

[2] Senior Engineer, Research, Rocketdyne, Canoga Park, California.

Since World War II many firms in the U.S. have been actively engaged in the development of rocket engines. There have been many technical advances and the size of the engines has increased tremendously: however, the basic configuration of a centrifugal pump and a turbine to drive it has remained the same.

The combination of the pump and turbine is naturally called a turbopump and for optimum overall efficiency each turbopump must be designed with a particular rocket engine application in mind. For example, the ideal turbopump for a one minute duration engine would probably not look anything like the ideal turbopump for a ten minute duration engine.

In order to obtain the maximum efficiency of a turbine it should generally be made as small as possible and be operated at as high a speed as possible. The operating characteristics of a centrifugal pump for maximum efficiency naturally do not match those of the turbine. A compromise is therefore in order. This compromise establishes two basic types of turbopumps, the direct drive unit and the geared unit.

Figure 3 is a sketch of a direct drive unit. The pumps and turbine are all attached to a single shaft. The turbine may be in between the pumps as shown or at one end.

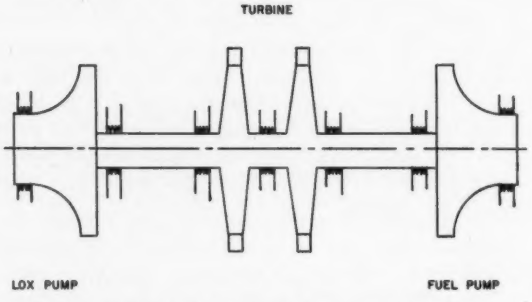

FIG. 3. Schematic of a direct drive type turbopump.

Figure 4 shows schematically a geared unit. The pumps operating at relatively slow speed are driven by a high speed turbine through a gear box. The pumps may be on one shaft as shown or on separate shafts.

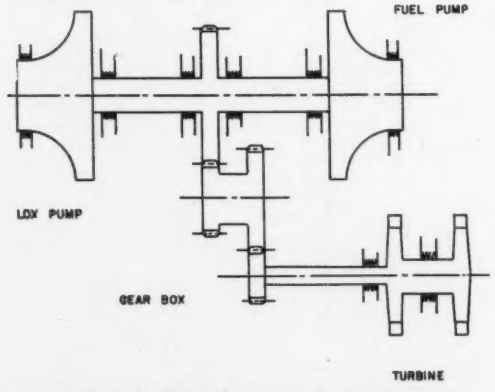

FIG. 4. Schematic of a geared type turbopump.

In the geared unit both the turbine and the pumps operate at their most efficient speed. However, we have introduced an additional piece of equipment that not only adds weight but complexity. By adding a gear box we have added gears, more bearings, more seals and perhaps an additional lubrication supply. In order to make a proper selection, however, the added weight and complexity of the gear box must be balanced against the lower efficiency of a direct drive unit with its greater turbine mass flow and the increased weight of the turbine assembly.

Sealing problems

Although reliability is of prime importance, compactness and light weight must also be achieved, consequently such non-essentials as bearings and seals are begrudged space and weight. Looking again at Fig. 4 the jobs the seals have to perform can be more clearly seen.

Mounted on a shaft at one side of the gear box, the farthest side from the turbine, is the liquid oxygen pump. The liquid oxygen pump is turning at 5000 to 10,000 rpm pumping the −300°F liquid gas at a relatively high pressure. It is mandatory that we not allow the liquid oxygen to leak either into the engine compartment or to the gear box as this would cause at the least a fire and most likely an explosion.

On the opposite end of this shaft on the other side of the gear box is mounted the fuel pump. The fuel is being pumped at a more reasonable, though not ideal temperature. The fuel pump exit pressure is also relatively high and this high pressure fuel must also be prevented from entering either the engine compartment or, although not so important, the gear box.

Both the liquid oxygen pump and the fuel pump are of the centrifugal type developing substantial heads. To maintain good efficiencies the differential pressure between the inlet and outlet must be sealed. The seal is usually placed as close to the impeller inlet as possible.

Connected to the input end of the gear train is the high speed turbine operating at temperatures up to 1800°F and speeds of over 40,000 rpm. The high temperature and high pressure gases used to drive the turbine must be controlled and prevented from overheating and damaging the turbine and gear box bearings.

If the turbine is of the pressure compounded type using two or more stages, the stages must be sealed with respect to one another. Furthermore, if the turbine is designed with reaction or free vortex type blading, the blade tips should be sealed to maintain good turbine efficiencies.

Finally, the gear box containing high speed rolling contact bearings and heavily loaded gears must be lubricated and the accessory pad shafts must be sealed to prevent oil leakage to the engine compartment and even more important the main pump shaft must be sealed to prevent lubricating oil from coming in contact with the oxidizer.

In summary there are four basic types of seals.

A. Oxidizer seals
B. Fuel seals
C. Gas seals
D. Oil seals

The operating conditions of some typical turbopump seals are shown in Table 1 and the allowable static leakage rates are shown in Table 2. In order to satisfactorily operate rocket engines seals had to be developed to overcome these sealing problems and the discussion now presents some of the solutions.

TABLE 1

Operating Conditions of Turbopump Seals

Seal type	Temperature °F	Pressure psig	Rubbing velocity ft/min
Oxidizer seal	—300	200	5000–8000
Fuel seal	100	200	5000–8000
Turbine seal	1800	150	20,000–30,000
Oil seal	250	50	5000–8000

TABLE 2

Seal Leakage Rates for Several Types of Seals

Seal type	Allowable static leakage	Test fluid
Shaft riding seal	500 cu. in./min. at ΔP of 30 psia	Air at 70 $\pm$10°F
Floating ring seal	4 cu. ft./min. at ΔP of 30 psia	Air at 70 $\pm$10°F
Face seal	6 cu. in./min. at ΔP of 30 psia	Gaseous nitrogen

Oxidizer seals

First, the oxidizer seal: Over the past 10 years a face type seal with satisfactory characteristics has been developed. A cross-section of a face type seal is shown in Fig. 5.

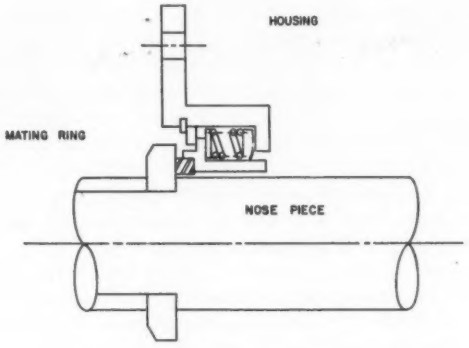

FIG. 5. Face type liquid oxygen seal.

The seal consists of a rotating part or mating ring that is fastened to the shaft and rotates with the shaft and a stationary member that is retained in the turbopump housing.

The sealing is accomplished between the rotating mating ring and a nose piece in the stationary part. A great many different materials can be used in these seals and numerous combinations were tested. Table 3 lists a number of different combinations of materials that have been tested along with comparative results.

TABLE 3

Face Type Seal Materials Evaluation

(Test conditions: Surface speed = 8000 fpm, Test pressure = 200 psi, Test fluid = LN_2).

Materials		Wear, in.		Time, min.	Notes
Nose piece	Mating ring	Nose	Ring		
Carbon	Nitralloy	0.006	0.0002	5	Low leakage
Carbon	Chrome plate	0.005	0.0001	5	Low leakage
Bronze	Nitralloy	0.001	0.0005	3	Severe scoring of bronze and excessive leakage
PTFCE	Nitralloy	0.042	NMW	1	Seal failure
PTFE	Nitralloy	0.018	NMW	0.5	Seal failure
Carbon	Titanium-carbide composition	NMW[a]	NMW	5	Low leakage
Aluminum (hard anodized)	Chrome plate	—	—	10 sec	Complete failure chrome ring galled anodized case worn through

[a] No measurable wear

The evaluations were made using a seal tester and operating under the following conditions:

(a) Surface speed 8000 fpm
(b) Test fluid pressure 200 psi
(c) Face loading 100 psi
(d) Test fluid LN_2

The combinations of carbon and nitralloy, carbon and chrome plated steel, and carbon and titanium-carbide show acceptable wear rates and good sealing characteristics. The PTFCE[3] and PTFE[4] combinations were found to be unsatisfactory, both the seals failing in an extremely short period of time. Aluminum as a nose piece material also proved unacceptable, failing in less than 10 sec. Other material combinations investigated include carbon and bronze, carbon and copper, nickel-chrome-iron alloy and nitralloy and various silver plated materials running with nitralloy and chrome plated materials.

One of the two main parts of the seal, either the rotating or the stationary member must be mounted to permit axial movement. This is necessary because of the stackup of these parts and also to take care of bearing axial movement when the turbopump is operating. Usually the stationary part is allowed to move axially and because of this axial movement a secondary seal is necessary. The secondary seal may be of the lip type as shown, or it can be a piston ring, or a chevron type.

A spring is used to insure initial contact between the mating faces; however, most of the load between the faces is from the pressure of the sealed fluid.

The rocket engine turbopump is working in an area of relatively high pressure and extremely high rubbing velocities. The mating face forces must be adjusted to be an optimum value which is a compromise between seal efficiency and wear. Although the operating conditions are severe, the operating life is of extremely short duration.

The face seal is balanced by varying the location of the mating face diameter and the area of the seal acted upon by the high pressure fluid. A wide range of face pressures can thus be obtained and an optimum established for a given installation.

Fuel seals

The fuel seal on the opposite end of the shaft is almost identical to the oxidizer seal although it is much less critical as the operating conditions are not nearly as severe.

A small amount of fuel leaking into the gear box is not necessarily harmful as the conventional fuel usually has some lubricating properties and some lubrication of the fuel seal parts can be expected. Compatible materials, seal pressures and rubbing velocities are therefore not as important at the fuel pump location as when sealing liquid oxygen.

Seal installation

Efficient sealing of the face type seal not only depends upon the proper choice of materials but also upon the correct installation.

[3] Polytrifluorochloroethylene.
[4] Polytetrafluoroethylene.

Parallism and normalities of the various parts must be held to close limits.

The seal shell is normally flanged and bolted to the turbopump housing and sealed at the bolted joint with a gasket in the case of the liquid gas and with an "O" ring in the fuel application.

Correct mounting of the rotating part or mating ring is of the utmost importance. The mating face of the ring is lapped to a flatness of a few helium light bands and this flatness must be maintained when installed.

The basic ring installation is shown in Fig. 6(a) where

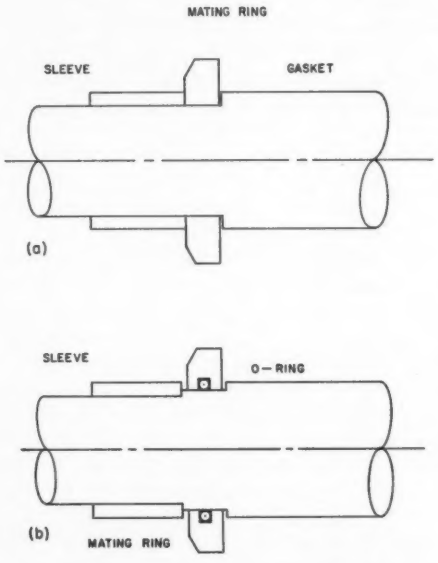

FIG. 6. Turbopump seal mating ring installations.
(a) Clamped mating ring.
(b) Floating mating ring.

the ring is clamped between flat shoulders. It is important that the shoulders in both sides of the ring be of equal height to prevent distortion. The shims should be ground shims if shims are necessary to position the seal and maintain the proper operating length. A gasket is also required to prevent leakage between the I.D. of the ring and the shaft.

A superior installation is shown in Fig. 7(b) and is called a floating mating ring. This type of installation, however, may not be used in areas where temperatures are too severe to utilize elastomers to effect the seal between the ring and the shaft. The advantage of this installation is that no clamping of the ring is required and therefore there is much less possibility of distortion of the ring.

For slow speed operation the "O" ring friction is sufficient to drive the mating ring. For high speed operation and in applications where rapid accelerations are encountered the ring must be keyed to the shaft.

Impeller seals

The volumetric efficiency of a centrifugal pump is a function of the leakage loss occurring between the rotating

impeller and the stationary housing at the impeller eye and can be expressed as:

$$\eta_V = \frac{Q}{(Q + Q_L)}$$

η_V = Volumetric efficiency
Q = Capacity measured (vol/unit time)
Q_L = Leakage capacity

Methods of calculating the amount of leakage as well as discussions of the various types of wear ring seals are covered in detail in the standard texts dealing with centrifugal pumps.

Although various types such as face type seals and floating ring seals have been tested the best results to date have been obtained using a labyrinth seal. The labyrinth seal may be of various well known types and will be discussed later in somewhat more detail in dealing with the compressible fluids handled by the turbine.

Hot gas seals

Another important area where sealing is a problem is in the vicinity of the turbine. Instead of a liquid gas at −300°F, combustion products at pressures of over 500 psig and temperatures up to 1800°F must be sealed. In addition to the high pressure and temperatures the combustion products contain a high percentage of contaminants in the form of carbon particles.

One of the most common types of hot gas seals is the labyrinth seal. The labyrinth seal consists of alternating constrictions and enlargements arranged in sequence in such a way that the kinetic energy developed by flow through the constriction is dissipated by turbulence and expansion in the succeeding chamber. When steady flow has been established through the labyrinth, there will be a throttling of the gas decreasing the pressure from the initial pressure P_t to the exit pressure P_r.

In order to bring the exit pressure P_r down to the ambient pressure P_e at the exit of the last stage, a certain minimum number of constrictions are required depending on the overall pressure ratio P_t/P_e.

A labyrinth seal as described above is subject to the following conditions.

(a) The same weight flow of gas will flow through each constriction, but the volume flow will be increased through each constriction.
(b) If all of the clearances have the same area, the velocity will increase at each successive throttling, requiring a greater enthalpy drop each time to produce this greater velocity. The pressure ratio across each constriction will therefore decrease from inlet to exit.
(c) The greatest velocity that can be attained will be Mach 1 and this will occur at the last restriction only.
(d) With the optimum number of restrictions established, any further decrease in ambient pressure P_e will not change the leakage flow as the leakage flow is only a function of inlet pressure P_t. Raising the ambient pressure will, however, decrease the flow as this will unchoke the last constriction.
(e) A small leakage loss must be accepted.

An effective labyrinth is shown in Fig. 7(a). The gas, after flowing through a minimum clearance area, must leak

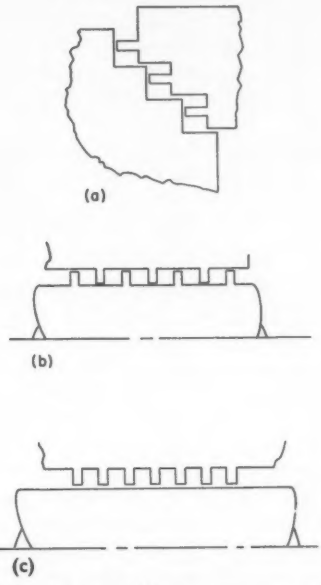

FIG. 7. Turbopump high temperature gas seal.
(a) Stepped labyrinth.
(b) Interlocking labyrinth.
(c) Standard labyrinth.

radially inward against the action of centrifugal force to get to the next expansion chamber.

If the turbomachine can be designed with split casings, the labyrinth can be of the configuration as shown in Fig. 8(b), however, most flyable turbomachinery cannot afford the luxury of the added weight usually associated with split casings; the labyrinth must therefore look like Fig. 8(c) and is not nearly as effective.

Sealing between the first stage turbine wheel and the inboard bearing is the most important and difficult job. The temperature and pressure are higher in this area than further downstream and the temperature that the bearing can stand is considerably below the inlet gas temperature.

Because of the extremely high pressure and limited space in this area a satisfactory labyrinth could not be designed and it was therefore necessary to develop some other type or combination of types of seals. Face type seals were investigated and because of the high temperatures several types of ceramic seals were tested, ceramic running against ceramic and ceramic running against steel and carbon. All of the ceramics experienced the same general type of failure. The wear characteristics were excellent but they could not withstand the vibrating loads and developed numerous cracks and subsequent complete failure in a relatively short period of time. Best results were achieved with a combination labyrinth and shaft riding seal. Various types of shaft riding seals were investigated and three were found that gave satisfactory results. One shown in Fig. 8(a) consists of a series of segmented carbon rings that ride on

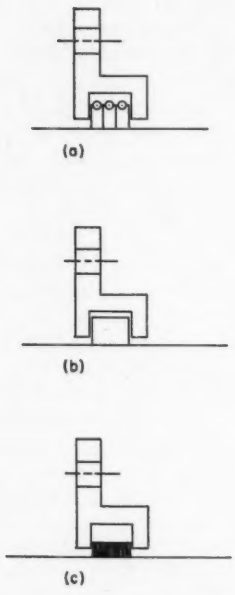

FIG. 8. Turbopump high temperature shaft seals.
(a) Segmented ring seal.
(b) Floating ring seal.
(c) Brush seal.

the hardened turbine shaft. The carbon rings are held against the shaft by high temperature garter springs. Another type shown in Fig. 8(b) is a floating carbon ring seal that also rides with minimum clearance on the turbine shaft. A third type of seal that has worked well is a brush seal shown in Fig. 8(c). This consists of a series of small wires rubbing on the shaft, and the best description would be to visualize an ordinary wire brush that is wrapped around the shaft. The seal becomes more effective as running time is increased, as the brush catches the carbon particles (from turbine gases) which decreases the flow area through the seal.

Between the turbine stages normal practice has been to utilize the labyrinth type of seal. Even though space is not available to accommodate the critical number of restrictions the loss in efficiency due to the extra gas leakage is far less than the penalty of the added weight of lengthening the turbopump. Further work is being done in the development of a shaft riding seal in this area.

Sealing the blade tips of the turbine wheels is accomplished in several ways:

(a) The O.D. of the turbine wheel and I.D. of the housing are held so that minimum clearance is established under operating conditions.

(b) Honeycomb type rings of high temperature steel are mounted in the turbine housing and the turbine blade tips actually rub and wear in the honeycomb ring. The honeycomb may be likened to a form of labyrinth seal.

(c) Shrouded turbine blades are also used in some instances to decrease the tip losses when it is not possible to run minimum required blade tip clearances.

Oil seals

The gear box oil seals have not presented any new problems. The fluid to be sealed has good lubricating properties, the rubbing velocities and pressures to be sealed are well within operating conditions of standard lip type seals.

Testing and development

Although the final evaluation of any seal must be in actual operation, it would be too expensive and time-consuming to do all of the development work on an actual turbopump. For this reason a number of seal test rigs have been built. These test rigs can be used both for material investigations or actual seal development. A photograph of one of the low temperature fluid test rigs is shown in Fig. 9. It consists of a test head where the seal configuration to be tested is mounted, a 10 h.p. variable speed drive capable of speeds to 15,000 rpm and a test fluid reservoir mounted directly over the test head. The fluid system is capable of operating at pressures up to 250 psig.

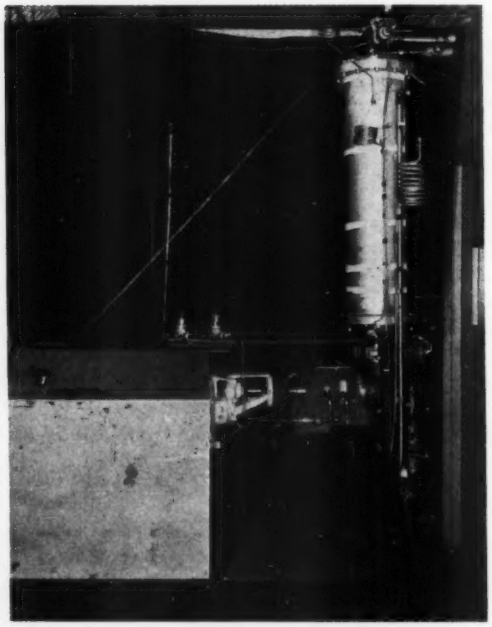

FIG. 9. Low temperature seal test.

A schematic diagram of the test system is shown in Fig. 10. The system is filled with the test fluid through the valve 2 at the bottom of the test head and forced up into the reservoir under a pressure of 10 to 15 psig. During filling, the vent valve 3 is open and the manual control valve and bypass valve 1 closed. The expansion tank is

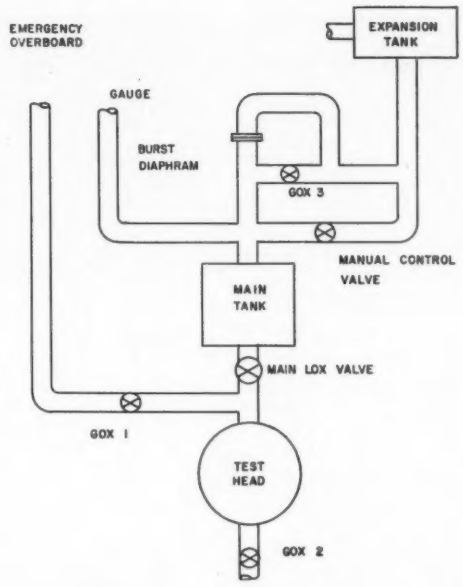

FIG. 10. Diagram of low temperature seal test apparatus.

installed to insure that no liquid is vented overboard. Height of fluid in the reservoir is measured by a series of thermocouples attached to the outside of the reservoir.

When the tank is filled the vent and fill valves 5, 2 and 3 are closed. The pressure in the reservoir and test head is self-generated by the boiling of the liquefied gas and is regulated with the manual control valve.

To protect personnel and equipment a burst diaphragm is used to prevent excessive pressure build-up. A lox valve is provided between the test head and the reservoir to isolate the reservoir from the test head in case of fire in the test head. When the lox valve is closed, valve 1 is opened simultaneously and the fluid in the test head is dumped overboard.

Leakage from the seal is measured with a rotameter, the fluid first passing through a heat exchanger to convert all the fluid to gas.

Conclusion

Progress is continually being made in the development of new and more powerful propellants and oxidizers. The seal development program is therefore a continuous process. As soon as a new fuel or oxidizer is made available seals must be developed to handle them. Materials and designs that work satisfactorily in one medium may be entirely unsatisfactory in another. Lubricating properties of the fluids must be evaluated and compatabilities determined. As space in a rocket vehicle is at a premium the seals must be designed as compact and as light as possible. The seal not only must seal properly, but it must seal under the operating conditions of the missile. It must withstand the flight maneuver forces, the temperatures and the vibrations encountered in a flight.

Successfully launching a satellite, an IRBM or a rocket to the moon can all depend on how well seal problems have been solved.

A Study of Design Criteria for Oscillating Plain Bearings

By W. A. GLAESER[1] and C. M. ALLEN[2]

The load-life and friction characteristics of sleeve-bearing materials have been determined under conditions simulating airframe operation. The bearings were grease lubricated, and operation was oscillatory (±45-degree amplitude). All bearing evaluations were conducted at room temperature. Design charts relating bearing load and wear to life in terms of cycles of oscillation were constructed from the data. Frictional characteristics were also studied. Aluminum bronze was found satisfactory as a bearing material when used with hardened SAE 4340 steel shafts for loads up to 15,000 psi. Steady-state load conditions were found more severe than reversing-load conditions.

Introduction

RELIABILITY of mechanical devices in aircraft has become increasingly essential in the past decade as advances in power plants and in aerodynamic design have increased the speed of flight. Specifically, airframe bearings, used in control-surface hinges, pivots in actuation linkages, and moving-structure joints have presented a special problem to designers owing to the lack of good bearing-design information. Plain bearings (sleeve bearings) have been used in many airframe applications where space is cramped and heavy bearing loads are encountered. In the past, these applications were satisfactorily dealt with by using standard AN bolts and housing dimensions sufficient to provide ample margins of safety for crushing or shear tear-out of the bushings. However, with the high-speed aircraft came heavier loads and the problems of "stuck" bearings owing to galling, seizure or failure of the lubricant. Many bearings now are in critical control assemblies where one bearing failure can mean the loss of a plane. No longer is it sufficient to use rule-of-thumb methods in applying plain bearings to airframe design. The dynamic bearing properties have become as much a necessary part of the designer's knowledge as the tensile properties of structural materials.

At the suggestion of the ANC-5 Committee, a research program was initiated to obtain empirical data on airframe bearing materials commonly used; these data were to be compiled in such a form as to be directly applicable to design problems. In addition, the limitations and performance characteristics of these materials were to be studied. A survey was made of Government and industrial organizations having direct experience in airframe-bearing applications. The results of the survey were used to establish the range of operating conditions considered compatible with most airframe design requirements. The following conditions were set up as standard parameters to be investigated:

Bearing motion	Oscillatory, 12 cycles per minute
Rubbing speed	8 to 12 feet per minute
Bearing oscillation	±45 degrees
Type of loads	Steady-state radial and reversing radial
Load range	5000 to 40,000-psi bearing stress
Bearing materials	MIL-B-6946 aluminum bronze and SAE hardened steel
Shaft or bolt materials	SAE 4340 hardened steel; chromium-plated SAE 4340 steel
Lubricant	MIL-G-3278 grease
Bearing design	Circumferential groove; $L/D = 1.0$ and 0.8

Experimental apparatus and procedure

Photographs of the bearing-evaluation machine and sample test bearings are shown in Figs. 1 and 2. A drawing of the test bearing is shown in Fig. 3.

In the bearing-evaluation machine shown in Fig. 1, test shafts are rotated while the bushings are held stationary in a link or housing. The link is held between two clevises, one clevis fixed and the other attached to the end of a hydraulic piston. The test shafts are held in the clevises by heavy-duty needle bearings of a non-skewing design. Test shafts are oscillated by driving shafts that are connected through a rigid coupling. The drive shafts are oscillated by a rack-and-gear arrangement actuated by a hydraulic cylinder. The amount of rack displacement and, hence, amplitude of oscillation of the test shaft is controlled by limit switches which are placed at either end of the ram stroke. Shaft torque is measured by strain gages attached to the drive shaft in a configuration sensitive to twisting and insensitive to bending. The drive shafts are hollow and the torque-transducer lead wires are threaded through them so that flexing of the wires during shaft oscillation is kept to a minimum. Load is applied to the bearings by the hydraulic cylinder with the yoke attached to its piston. The applied load is measured both by strain gages attached to the hydraulic piston rod and from hydraulic oil-pressure gage readings.

Presented as an American Society of Lubrication Engineers paper at the Lubrication Conference held in Los Angeles, Calif., October, 1958.

[1] Project Leader, Bearing-Lubrication Section, Battelle Memorial Institute, Columbus, Ohio.

[2] Division Consultant, Engineering Mechanics Division, Battelle Memorial Institute, Columbus, Ohio.

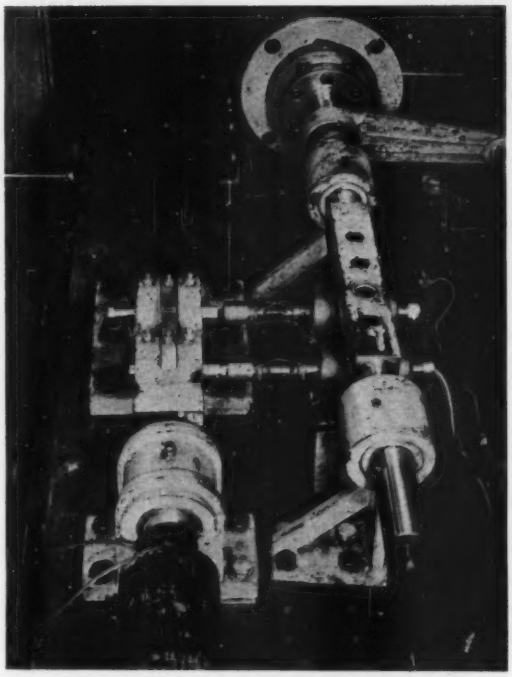

FIG. 1. Bearing-evaluation apparatus showing one shaft uncoupled from drive shaft.

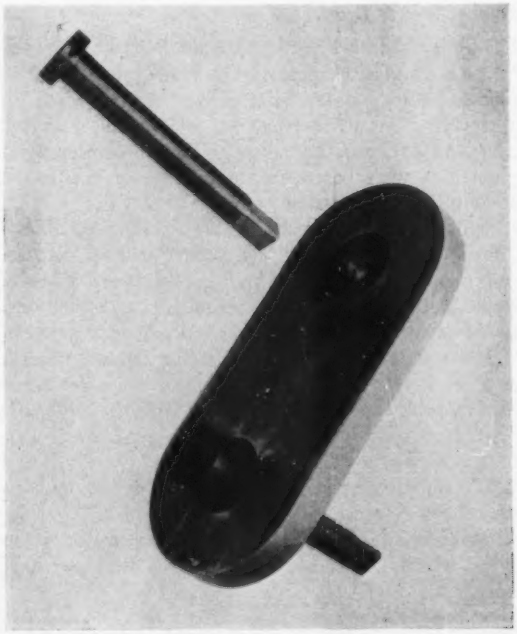

FIG. 2. Shafts and bearings with bearing housing.

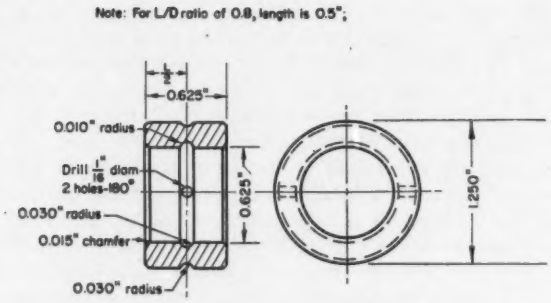

FIG. 3. Bearing details.

Experimental Method

Using one bearing-and-shaft material combination and one oscillation amplitude, wear and friction characteristics as a function of cycles of operation were determined at each of several bearing loads. The bearing loads investigated included 7500, 15,000, 20,000, 30,000 and 45,000 psi of nominal bearing stress. Nominal bearing stress was calculated by using the applied load in pounds acting on the projected area of the bearing in square inches. Figure 4 shows a sample chart recording of bearing load and shaft

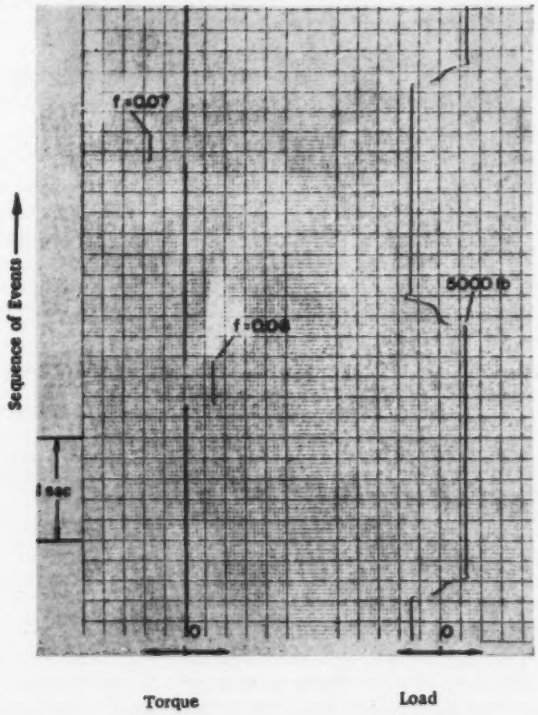

FIG. 4. Sample chart showing bearing torque and applied load as a function of time.
Reversing bearing load—15,000 psi.
Bearing—aluminum bronze.
Shaft—4340 hardened steel.

torque demonstrating the sequence of events during a reversing-load operation. Total bearing wear was determined by dimensional measurements made before and after test using an electrolimit comparator in conjunction with precision gage blocks. Periodic bearing-play measurements were made during a test using a standard reversing load and measuring the movement of the bearing relative to the shaft with the shaft held stationary. Torque measurements and bearing-play measurements were taken frequently during the first 5000 and 10,000 cycles or wear-in period. As soon as wear-in was accomplished, as noted by a leveling off of friction, torque measurements were taken every 5000 cycles. Bearings were greased at each 5000-cycle interval. In greasing the bearings, care was taken to apply enough grease to flush out the wear debris contained in the old grease.

Bearing Materials

The bearing and bolt materials evaluated are listed, together with their composition and properties, in Table 1.

TABLE 1

Airframe Bearing Materials used in Evaluations

Material	Analysis wt. %	Pretreatment
MIL-B-6946 alum. bronze[a]	Cu 90.80 Al 7.03 Si 1.92	As received.
SAE 4340 steel[b]	C 0.40 Mn 0.71 Si 0.30 Cr 0.77 Ni 1.76 Mo 0.23	Heat treated to R_C 46
SAE 4340 steel	Ditto	Heat treated to R_C 46 and plated with industrial hard chromium plate.
Ditto	Ditto	Heat treated to R_C 46 and plated with CR-600 chromium plating process; baked for 2 hr at 550°F
Ditto	Ditto	Heat treated to R_C 46 and coated with commercial resin-bonded MoS_2-graphite.

[a] Tensile strength = 90,000 psi, yield strength = 46,100 psi.
[b] Electric furnace quality, tensile strength = 230,000 psi (as heat-treated).

Experimental results

Wear and friction characteristics and galling tendencies were investigated for aluminum bronze over a load spectrum from 7500 to 40,000 psi. Both reversing and steady-state conditions were included in the investigation. SAE 4340 steel, heat treated to a 230,000-psi tensile strength or R_C hardness of 46, was used as a shaft or bolt material. The results of these evaluations are summarized in the design charts Figs. 5 and 6 and the curves for coefficient of friction shown in Figs. 7 and 8. Other materials studied were chromium-plated steel and dry-film-coated steel. These were operated at representative load levels and their performance compared with the aluminum bronze.

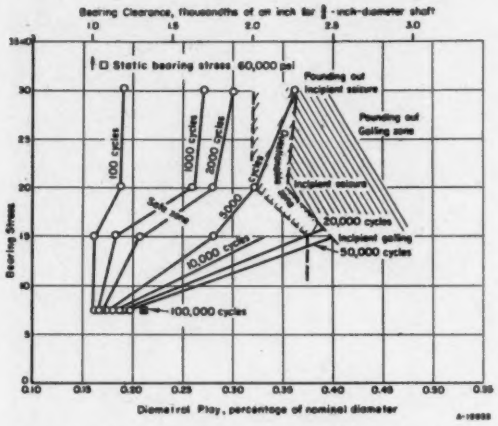

FIG. 5. Design chart for aluminum bronze bearings under conditions of oscillating load at 80°F.
Based on data from duplicate runs on ¾-inch bearings with an $L/D = 1$.
Shaft oscillating ± 45 degrees.
Hardened SAE 4340 steel shafts (R_C 47 ≃ 230,000-psi tensile strength).
MIL-G-3278 grease applied every 5000 cycles.
The initial percentage of diametral play was 0.16.
Shaft finish 10 to 15 microinches, rms.
Bearing finish 20 to 30 microinches, rms.

Aluminum Bronze Bearings

The design charts (Figs. 5 and 6) summarize the load-life characteristics of aluminum bronze bearings for two load conditions: steady-state radial and reversing radial. The design charts show the variation of bearing play with bearing stress for various values of cycles completed. The original data were based on the average of two runs at each condition of operation.

It will be noted that wear rates are significantly different for both types of loading. This effect will be discussed later. Areas have been located on these charts and delineated by cross hatching to denote zones of safe operation, questionable performance, galling, and seizure and pounding out. These zones are based on bearing failures observed after operation for a given number of cycles at a given load. Excessive wear was not used as a criterion for bearing failure since airframe applications have widely varying wear specifications. Thus, the designer, given a bearing load and an estimate of total cycles of operation before overhaul, can determine a bearing size which will give him a safe operating bearing stress and can estimate the amount of wear which might occur during the lifetime of the bearing.

An example of the use of this chart might be as follows: A 13,000-pound oscillatory load is to be supported by a hinge joint. Envelope dimensions will allow a ¾-in. bore

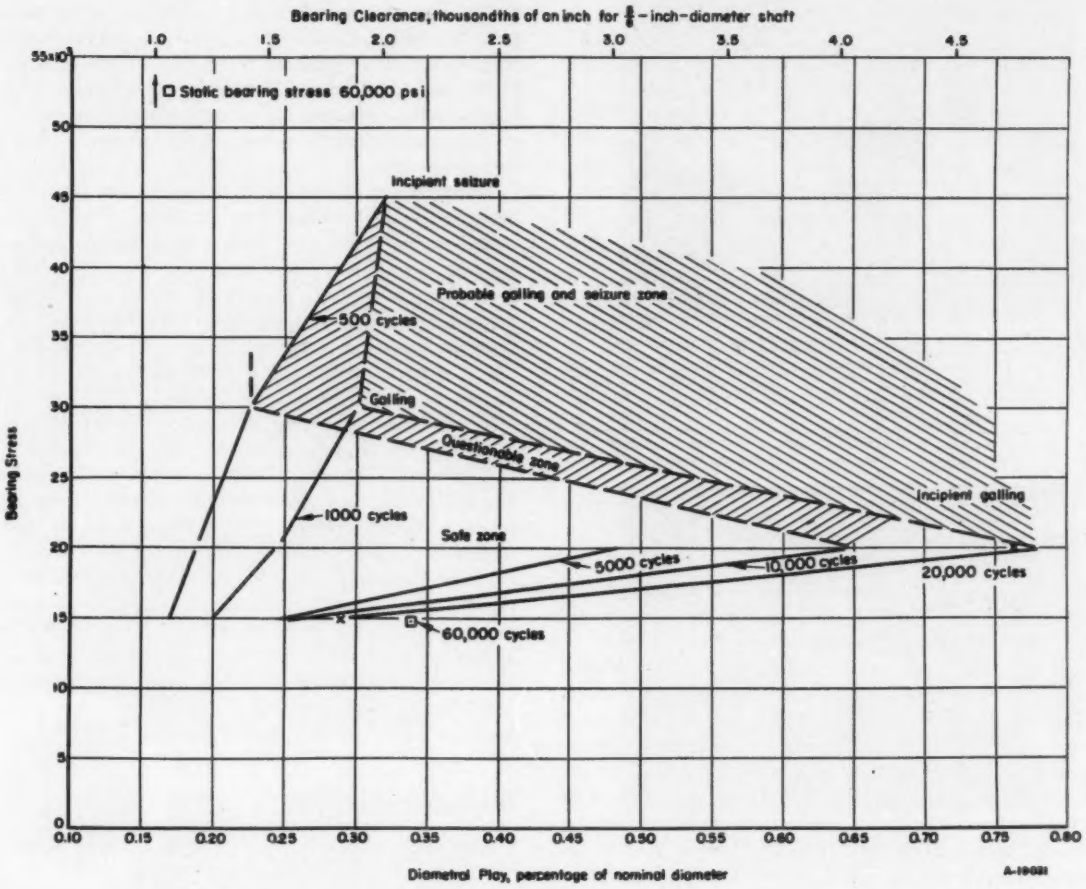

FIG. 6. Design chart for aluminum bronze bearings under conditions of steady-state radial load at 80°F. Based on data from duplicate runs on ⅜-in. bearings with an $L/D = 1$. Shaft oscillating ± 45 degrees. Hardened SAE 4340 steel shafts (R_C 47 ≃ 230,000-psi tensile strength). MIL-G-3278 grease applied every 5000 cycles. The initial percentage of diametral play was 0.16. Shaft finish 10 to 15 microinches, rms. Bearing finish 20 to 30 microinches, rms.

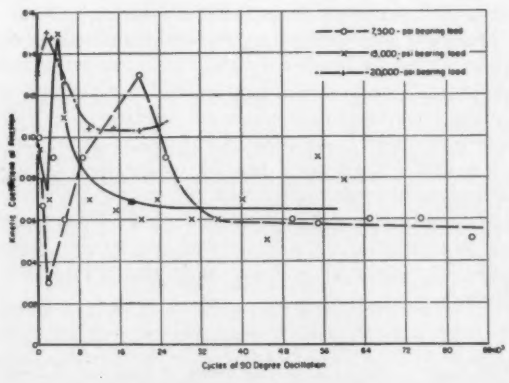

FIG. 7. Coefficient of friction vs. cycles completed for bearing life over 10,000 cycles.

bearing of aluminum bronze to be used. The problem is to determine the bearing area required and the wear or bearing clearance increase for a life of 20,000 cycles. Referring to Fig. 5, it can be seen that the maximum safe allowable bearing stress for a 20,000 cycle life is 15,000 psi. The required bearing area is

$$\frac{13{,}000 \text{ lb}}{15{,}000 \text{ psi}} = 0.823 \text{ sq. in.}$$

Since good design practice requires an L/D ratio of not greater than 1.0, and assuming a single circumferential grease groove, the maximum projected area of a single ⅜-in. bore bearing is 0.33 sq. in. It follows that the hinge joint should consist of three bearings which would have a total area of 0.99 sq. in. This will provide a calculated stress of 13,200 psi. It will be noticed that the intercept of the 13,200-psi stress level and the curve of a 20,000-cycle life provide a final bearing clearance of about 0.0022 in. or

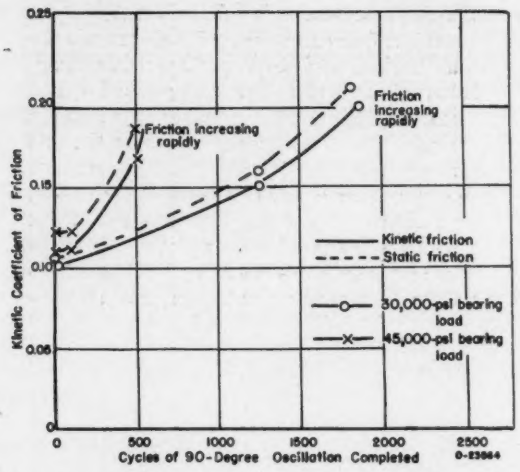

FIG. 8. Coefficient of friction vs. cycles completed for bearing life under 5000 cycles.

an increase in clearance (wear) of about 0.0012 in. It can be seen that if only two bearings are used, the stress would be 19,500 psi and the life would be about 5000 cycles.

The values for coefficient of friction, as shown in Figs. 7 and 8, increase as the applied load is increased. Friction coefficients for loads up to a 15,000-psi steady-state range between 0.06 and 0.07 after the initial higher friction wear-in period. Friction coefficients for reversing loads in the 7500 to 15,000-psi range are lower, ranging between 0.04 and 0.05. Above these load levels, friction values become erratic for both loading conditions and usable bearing life become short. It will be noted, however, from Fig. 8 that before the period of rapid increase in friction, even at a 30,000-psi bearing load, the bearings have some 1000 cycles of useful life. The chart in Fig. 8 was included for short-life applications.

Steel Shaft and Steel Bearing

Shafts made of heat-treated SAE 4340 steel were operated with steel sleeves made of the same material with the same heat treatment. The lubricant used was MIL-G-3278 and it was applied every 5000 cycles. This material combination was operated at 7500 and 15,000-psi load levels using both reversing and steady-state load conditions. In all cases, friction was high at the beginning of the run and increased rapidly followed by gross seizure and severe galling after a few cycles of oscillation. This material combination was considered unsatisfactory for oscillating bearings under the conditions investigated.

The galling tendency of the steel bearings was reduced by chromium plating the shafts or by using a dry-film lubricant on the shaft. Fatigue failures of the shafts, however, were encountered when industrial hard chromium plate was used. Failures were obtained at 20,000 psi after 7000 cycles of reversing load application.

Recent studies on the mechanisms of fatigue failures of chromium-plated steel have revealed that the fatigue strength of the steel is related to the type of stress in the plate deposit[3]. A plating process has been developed which will produce a chromium deposit with compressive stresses in the skin. It is claimed that this deposit results in a much higher fatigue strength for hardened steel than other types of chromium plate possessing residual tensile stresses in the outer skin.

The above-mentioned process was used to plate shafts of hardened SAE 4340 steel for evaluation. The shafts were plated to size and no postplating finishing operations were performed on them. These shafts were baked at 500°F for 2 hours after plating. They were run at a reversing load level of 30,000 psi using hardened SAE 4340 bearings. The bearings operated successfully for 840 cycles and then galled. Coefficient of friction before galling was about 0.06. In operating this same combination at a 25,000-psi load level, the bearings were successfully operated for over 40,000 cycles. No fatigue failures were encountered.

Coating the bearing shafts with a commercial resin-bonded MoS_2 and graphite film increased the life of bearings operating above a 15,000-psi stress, but the improvement was not as significant as that observed with chromium plating. Dry-film coated bearings failed more rapidly when grease was used as a supplemental lubricant as compared with operation without grease. The grease apparently tended to soften and dissolve the resin binder, facilitating the wearing away of the coating. Since these evaluations, new coating formulations have become available which are resistant to lubricating oils.

Discussion of results

Aluminum bronze proved to be satisfactory as an oscillating plain bearing material for bearing stresses of 15,000 psi and under. This stress was selected on the basis of a 50,000-cycle bearing life. Above this stress, bearings subjected to a steady-state load tended to gall and wear rapidly while bearings subjected to reversing load tended to pound out. This material will operate at heavier loads for short periods of time. It was also noted that in none of the bearing failures did the aluminum bronze cause freezing of the bearing to the shaft. The coefficient of friction would rise from about 0.1 to about 0.2 to 0.3 during galling.

The use of steel as a bearing material permitted operation at higher bearing stresses with less wear and no pounding out, but performance was less reliable. Unless protective coatings were used to separate the steel surfaces, seizure occurred suddenly and resulted in freezing of the bearing to the shaft, making the bearing inoperative. Protective coatings investigated did not prove entirely satisfactory. Chromium plating if not carefully controlled was found to contribute to shaft fatigue failure and dry-film coatings tended to wear away and expose fresh steel surfaces to galling.

---

[3] STARECK, J. E., *et al.*; "The Effect of Different Chromium Deposits on the Fatigue Strength of Hardened Steel," *Proc. Amer. Electroplaters Soc.*, 42nd Annual Convention, 1955, pp. 129–135.

Factors other than bearing-material compatibility were found to influence oscillating-bearing performance. These included the type of loading (reversing or steady state) and the amplitude of oscillation. Generally reversing loads provided better performance than steady loads. Small angles of shaft oscillation, ± 10 degrees, provided less wear than large angles, ± 45 degrees, of oscillation for the same load and total number of life cycles.

Effect of Load Type

It has been pointed out that for aluminum bronze bearing-wear rates were higher under steady-state load than they were under reversing-load conditions. Friction characteristics were also different for both types of loading as was found in a study of torque traces. Sample torque records showing typical frictional behavior for bearings subjected to the two types of loading are shown in Fig. 9. A well-defined torque peak at breakaway can be observed

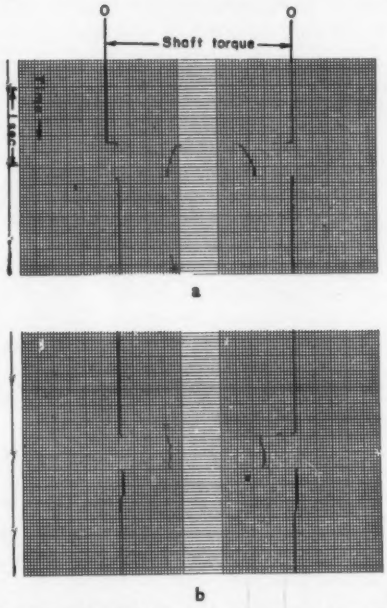

FIG. 9. Friction characteristics of the same aluminum bronze bearings under two different conditions of load (7500 psi).
(a) Steady-state radial load. (b) Oscillating radial load.

in the steady-state load trace, while little if any breakaway can be detected in the reversing-load trace. It was apparent, therefore, that for each oscillation, bearings subjected to steady-state load were overcoming a greater tangential force before turning than the bearings subjected to reversing load. It was presumed that this effect might be traceable to the influence of load on the effectiveness of the lubricant in the bearing. Studies were made using a glass bearing and a polished steel shaft. By illuminating this bearing with ultraviolet light, the grease was made to fluoresce and the relative thickness of the film in various locations could be estimated. Some photographs showing the effects of shaft movement on the grease film are shown in Figs. 10 and 11. Figure 10

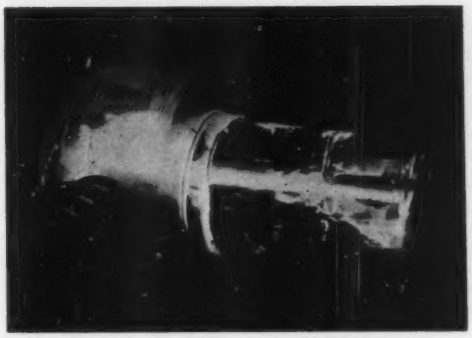

FIG. 10. Transparent bearing, shaft rotating toward the viewer at 10 rpm. Note buildup of lubricant film in load area as shown by fluorescent light.

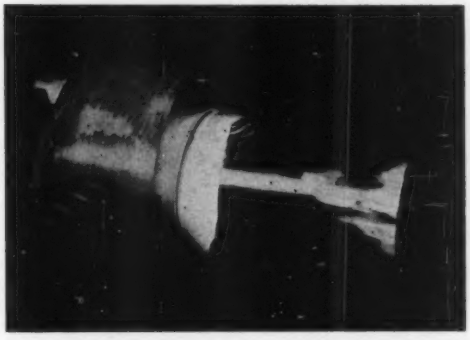

FIG. 11. Transparent bearing, shaft oscillating away from the viewer.

shows the relatively thick film built up in the bearing load area for the condition of steady-state load and slow continuous rotation (10 rpm). Figure 11 shows how the film in the load area is torn apart and removed from the load area under conditions of slow shaft oscillation and steady-state load. The results of this study seem to indicate that grease-lubricated bearings operating under conditions of steady-state load (for instance, preloading bearings) starve themselves of lubricant in the area of rubbing contact. Reversing the load tends to distribute the lubricant to loaded areas in the bearing. Therefore, under steady-state load, more metal-to-metal contact would occur, resulting in higher breakaway friction.

Another interesting effect noted during evaluation of aluminum bronze was the tendency for the aluminum bronze to "dealuminize" during operation at steady-state load. Bearings examined after being subjected to steady-state load conditions were observed to have a copper-colored film covering the surfaces subjected to rubbing. This film was also observed on the mating steel surfaces. Analysis of these films by electron-diffraction techniques identified them as pure copper. Little if no dealuminization was observed under reversing-load conditions.

Conclusions

In the process of obtaining airframe-bearing data suitable for use in airframe-bearing design, it was found that sleeve-bearing materials popularly used show decided limitations as oscillating bearings. Although aluminum bronze showed certain definite advantages when used at loads up to 15,000 psi, it cannot be recommended for heavier loads. Since space requirements in hypersonic aircraft—especially in very thin wing sections—make it necessary for small-section bearings to carry heavy loads, there is a pressing demand for the development of new materials capable of use as airframe bearings at loads of 50,000 psi and higher. This calls for imaginative materials development where, instead of adapting existing materials to bearing requirements, new materials are developed specifically for airframe bearings. Ideally, these materials should be self-lubricating, have low friction and wear, and exhibit high strength and toughness over a broad temperature range.

Acknowledgments

The research described was carried out as part of a continuing program for the Navy Bureau of Aeronautics, Experimental Structures Unit, Air Frame Design Division, with Mr. A. P. Cowles, the project officer. The paper is published by permission of the Department of Navy.

The authors wish to thank Mr. Sam Gordon of Battelle Memorial Institute for his assistance and suggestions for presentation of data and Mr. William Stanton of Battelle, who was laboratory technician in charge of operation and maintenance of the apparatus.

Adhesion Between Metals and its Effect on Fixed and Sliding Contacts

By WARREN P. MASON[1]

Recent studies of adhesion between metals measured as a function of pressure, temperature and time have resulted in a quantitative understanding of the process. Creep causes the spaces between the point contacts to be filled in and molecular seizure occurs.

Recent work by O. L. Anderson has shown that seizure can occur between two sets of metals if a twist is superposed on a compression. By this technique, the area of contact is increased over that resulting from compression alone, and a large enough area of contact results so that the adhesive stresses overbalance the elastic stresses which tend to disrupt the adhesive bond. Hence seizure occurs. By studying the coefficient of adhesion as a function of the applied stress, Amonton's law of friction has been verified from the adhesion side, thus confirming the Bowden–Tabor theory of stick-slip friction.

Adhesion between metals due to compression, occurring over a finite time, is essential for such connections as the solderless wrapped connection and is important for contacts left under pressure in the same position for a length of time as in printed circuit type connections. Adhesion between metals caused by both compression and shear is the cause for mechanical seizure, plowing and wear experienced in sliding contacts. Direct force measurements have shown the nature of the slip-stick process.

1. Introduction

WHEN permanent and semi-permanent electrical contacts are employed, as in screw connections and the solderless wrapped connection (1, 2), it is desirable that a permanent adhesion occur between the two parts of the contacts. Such adhesion will resist the effect of stress relaxation, that always occurs as a function of time, and the effect of vibration in breaking the contact. Hence adhesion will improve the durability of the contact.

For very fast acting relays, adhesion is not desired but nevertheless sometimes occurs, particularly if there is any tangential motion between the contacts. Such sticking sets a lower limit to the amount of electrical energy that is required to operate a relay. Furthermore, the adhesion between contacts is a source of wear of the contacts. Hence a knowledge of the causes and quantitative values of adhesion, is essential for an understanding of electrical contacts.

It is the purpose of this paper to describe experiments which show that adhesion can occur between two metals under compression as a function of temperature and time. Furthermore if a shearing stress is superposed on a compression, adhesion can occur instantaneously. The adhesion occurring under either condition, as measured by the force to break the contact, is directly proportional to the applied normal force. This ratio between the breaking and normal forces, called the coefficient of adhesion, varies between metals, but has a value of the order of unity. Calculations are given based on dislocation theory, which account for the temperature and time effects of adhesion.

Presented as an American Society of Lubrication Engineers paper at the Lubrication Conference held in Los Angeles, Calif., October, 1958.

[1] Head, Mechanics Research, Bell Telephone Laboratories, Murray Hill, New Jersey.

2. Adhesion between metals under compression

It has been a qualitative observation for many years that two metals, pressed together with a moderate pressure, have a tendency over a period of time to adhere to each other, even at room temperature. This tendency is considerably increased at high temperatures as is evident from the experience of a blacksmith who is able to weld together two pieces of metal by blows at temperatures much under the melting point of the metal. Conversely, by going to pressures so high that flow occurs, it is possible to cold weld two pieces of metal. The same process occurs in extrusion.

It has only been recently that quantitative data have been obtained which allow an analysis of the process to be made. Figure 1 shows the rate (1) for which copper makes a bond with a nickel silver terminal. The copper rod, 0.080 in. in diameter, was pressed on the two 90° wedges of nickel silver with a force of 4 lb. At a temperature of 245°C it takes a time of 1.8×10^4 sec before any adhesion is observed between the copper rod and the nickel silver double wedge, as measured by the force to pull the rod off the wedge. The force increases with time until it amounts to about 2.5 lb at the end of 1.5×10^5 sec. Another curve is given for 175°C and it is seen that it takes a longer time to attain a given force at a lower temperature. From the time difference and the equation

$$\frac{t_2}{t_1}=\exp\left\{+\frac{E}{R}\left(\frac{1}{T_1}-\frac{1}{T_2}\right)\right\} \qquad [1]$$

where R is the energy required to increase the temperature of one gram mole by 1°C, t_2 and t_1 are the times required

to attain a given force at the absolute temperatures T_2 and T_1, it is possible to measure the activation energy E for the process. Figure 2 shows the activation energy plotted against the time. One can obtain some idea of the size of the area caught by looking at the region of bright spots appearing after the rod is lifted off and it appears that 2.5 lb corresponds to about 6% of the apparent area of contact.

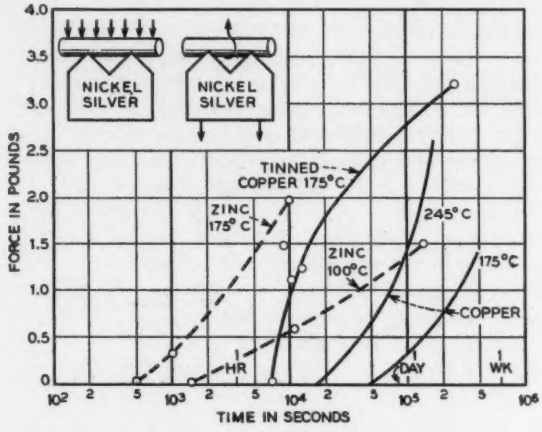

FIG. 1. Rate for which adhesion develops between a metal wire and a nickel silver terminal.

Figure 1 shows also the rate for which force builds up for a very pure zinc rod, $\frac{1}{10}$ in. in diameter, with a force of 2 lb pushing it down on the nickel silver double wedge. This joining occurs at a lower temperature and the activation energy for the process is lower as can be seen from Fig. 2. Measurements (1) have also been made by a strip-off technique for actual solderless wrapped connections and it is found that platings such as tin and zinc can reduce the time of the joining process.

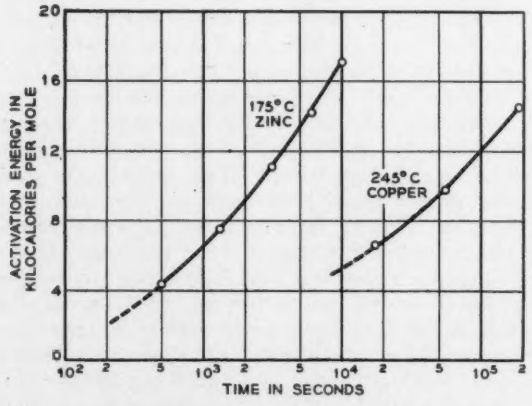

FIG. 2. Activation energies measured as a function of time.

In order to make use of this process in such connections as the solderless wrapped connection, it is necessary to demonstrate that a compressive stress is going to be maintained for a sufficiently long time so that adhesion can take place between the parts of the connection. The rate for which stress relaxes was measured by wrapping 100 turns of number 24 gage (0.020 in. in diameter) of OFHC copper wire round a steel spring terminal with a tension of 1300 grams. This tension of about 9000 psi was maintained in the wire, as in the solderless wrapped connection, because the wire can only come unwrapped to the extent of a half turn on each end as has been shown by photoelastic investigations (2). This tension causes the spring to twist through an angle of about 25°, since the wire advances a wire diameter for each turn, and hence a residual torque is impressed on the spring which is proportional to the wire tension. By observing the angle of twist of the clock spring, as a function of time and temperature, one can evaluate how fast the stress relaxes.

Measurements were made at a series of temperatures by putting a number of such springs in a temperature controlled box with a glass front and observing the angular decrease as a function of time. For oxygen-free high-conductivity copper, the ratio of the angle to the initial angle is shown plotted by Fig. 3 for temperatures of 100°C, 150°C, 175°C and 200°C. A few long time measurements were also made at room temperature which was assumed to be about 25°C. To eliminate transient creep, the terminals were inserted one day after they were formed and it was found that the initial starting stress was about 8000 lb per sq. in. The rate for which the stress decreased could be represented well by a relation derived from dislocation theory

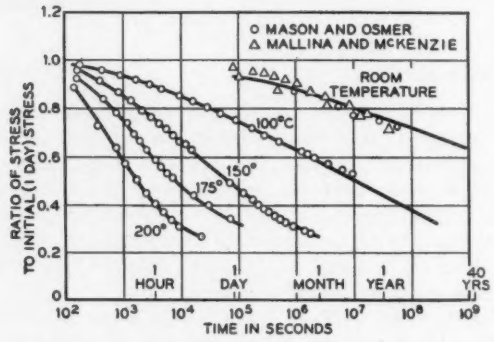

FIG. 3. Stress relaxation to copper wire measured as a function of time and temperature.

$$\sigma_{11_0} - \sigma_{11} = K \log_e(1 + t/t_0) \qquad [2]$$

where σ_{11_0} is the initial tensional stress, σ_{11} the tensional stress of time t, t_0 is a time separating the linear decrease with time from the logarithmic decrease which occurs for large values of t. The solid line of Fig. 3, for the 100°C curve, shows that the measurement agrees well with this formula with a value of $K = 2.5 \times 10^7$ and $t_0 = 320$ sec. For stresses below 0.5 of the initial relaxed stress, the measured curve begins to diverge from the theoretical, indicating that the material is beginning to harden.

By employing Eq. [1], the activation energy for stress relaxation can be determined and is shown plotted as a

function of stress by Fig. 4. If one extends the curve through the measured values out to zero stress, one obtains an indicated activation energy of 53 kcal per mole. The most recent measurement of the activation energy of diffusion for copper is 49 kcal per mole, but this was measured at a higher temperature for which the value should be lower. Hence the conclusion appears to be that the activation

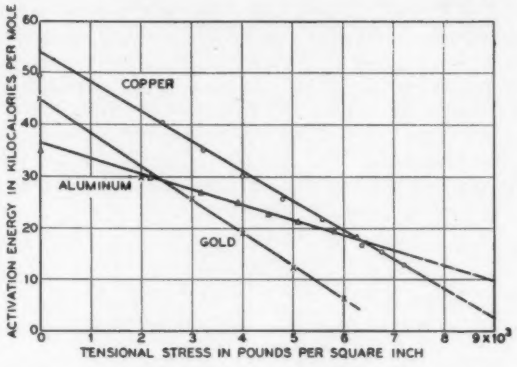

FIG. 4. Activation energies for stress relaxation plotted as a function of the tensional stress.

energy for stress relaxation is the self diffusion energy reduced in proportion to the applied stress. This conclusion is verified by two other measurements made for 2S aluminum wire (1) and 99.97% pure gold (3), whose activation energy-stress curves are shown by Fig. 4. An extension to the zero stress axis gives activation energies that are only slightly higher than the self diffusion energies measured directly at somewhat high temperatures.

3. Theoretical discussion of creep and stress relaxation curves

Since creep and stress relaxation are believed to be the primary causes for the formation of the thermocompression bonds and shear compression bonds, it is the purpose of this section to consider in detail how these processes occur. Creep and stress relaxation are usually considered to occur by a number of processes which include slip inside grain boundaries, slip along grain boundaries, polygonization (cell formation) and recovery. For the pure metals and the relatively low temperatures considered here, Mott (4) has shown that the rate determining process is connected with slip alone. Slip occurs by dislocations being dragged through the material. The rate process is determined by the time required to drag jogs through the material when they are biased by the applied stress. It is the purpose of this section to show that the measured values agree with these theoretical considerations.

In the unstrained state, dislocations are assumed to form nets with nodal points formed by the joining of three dislocations in different planes, as shown by Fig. 5. Stress can bow dislocations about their nodal points but the sum of the forces on the three dislocations cancel at the nodal

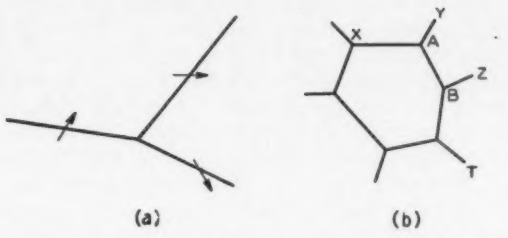

FIG. 5. Dislocation networks in metal crystals (after N. F. Mott)

points so that these are stationary in the crystal. Impurity atoms can settle along dislocations and act as pinning points, but for stresses of interest for creep, the dislocations will have broken away from the impurity atoms and it is the reactions of the loop lengths between nodal points that are responsible for creep and stress relaxation. When a shearing stress is applied to the metal, a dislocation will bow out between nodal points, as shown by Fig. 6(a), because a force per unit length is applied to the dislocation. This has a value (5) of

$$F = \tau b \qquad [3]$$

where τ is the shearing stress and b the value of the Burger's vector; 2.55×10^{-8} cm for copper. This force will always act at right angles to the dislocation direction. The amount normal to the dislocation rest direction is

$$F = \tau b l_i \qquad [4]$$

where l_i is the distance between nodal points. This force is resisted by the tension of the dislocation which tends to contract the loop into the shortest distance between D and D'. This tension has been shown to be (5)

$$T = \frac{\mu b^2}{2} \qquad [5]$$

where μ is the shearing modulus of the metal. For small strains, the displacement of the dislocation loop is elastic and it can be shown that the presence of these loops lowers the effective elastic stiffness μ of the metal. However, when the stress gets sufficiently large, the loop becomes unstable and goes through the successive states shown in Fig. 6(a), to (e). Up to semicircular form the loop is stable, but for any increase in size beyond this, instability results. This critical condition results when the resolved normal force is equal to twice the tension, i.e.

$$\tau b l_i = 2T = \mu b^2 \text{ or } \tau = \mu b / l_i. \qquad [6]$$

The succeeding states of the dislocation can only occur if there is no obstruction to prevent the dislocation from moving.

For creep resistant materials these obstructions are usually in the form of precipitates in the body of the materials, but for the relatively pure materials considered here, the principal type of obstructions are cross dislocations in other planes, as shown by Fig. 7. For the large size

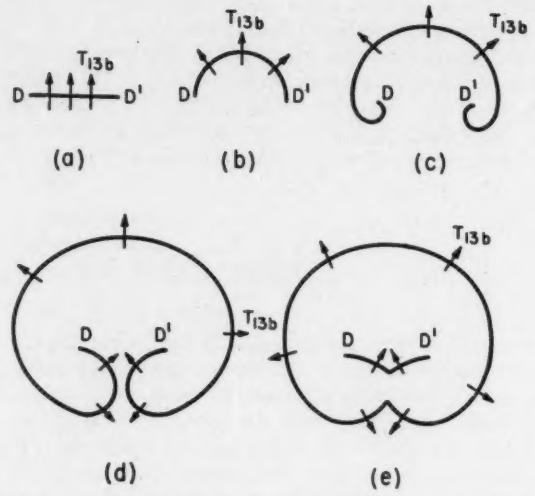

FIG. 6. Action of a Frank–Read source (after W. T. Read).

dislocations activated by the lower stresses used in stress relaxation measurements, the cross dislocations will be closer together than the distance l_i. The force acting on such a cross dislocation will be in the order of

$$(\tau b l_i - \mu b^2) = F \qquad [7]$$

since twice the tension of the loop has to be supported by the applied stress acting on the dislocation. When the force

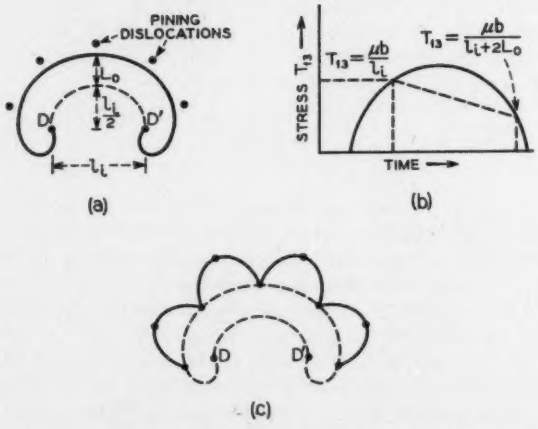

FIG. 7. Frank–Read source held up by cross dislocations.

F is large enough, the dislocation can cut through the obstructing dislocation by producing a jog (a dislocation of unit length b with its direction along the Burger's vector of the cut dislocation) on both the moving and the fixed dislocations. The process by which this is accomplished is shown by Fig. 8, which shows the jog resulting on the moving screw dislocation when it has cut another screw. Since the jog is a piece of dislocation one Burger's vector

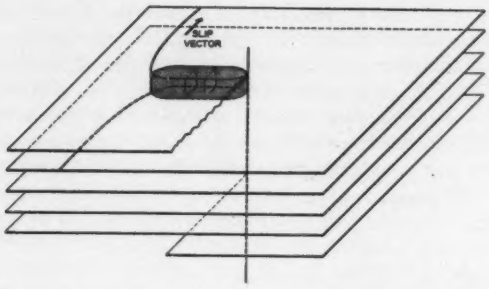

FIG. 8. Generation of a dislocation jog when one screw dislocation cuts another (after W. T. Read).

long, one would expect the energy[2] to produce a jog would be the tension times the distance b or

$$E = Tb = \frac{\mu b^3}{2} \qquad [8]$$

Hence the stress required to produce a cut is in the order of

$$(\tau b l_i - \mu b^2)b = \mu b^3 \text{ or } \tau = \frac{2\mu b}{l_i} \qquad [9]$$

which is larger than that to produce an unstable loop. Hence although a number of dislocations may be cut through, it appears that the larger sized loops will end up against cross dislocations, as shown by Fig. 7(a), rather than to go through the multiplicative process of Fig. 6.

This conclusion is verified by some recent studies of the internal friction (6, 7) of a metal as a function of stress amplitude. For oxygen-free high-conductivity copper, the internal friction curve versus longitudinal stress is shown by Fig. 9.

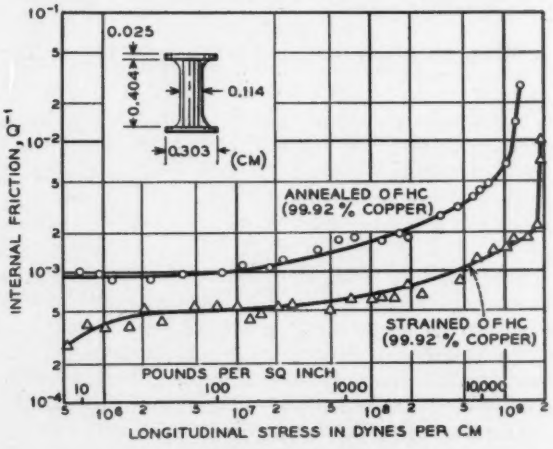

FIG. 9. Internal friction for an annealed and strained OFHC copper.

[2] There is, however, no agreement on the energy required to produce a jog. Seegar and Mott give values several times that suggested above. On the other hand Friedel (Les Dislocations) Paris, Gauthier Villars (1956) has suggested values smaller than the above.

The top curve is for annealed copper while the bottom one is for strained copper. The rise in internal friction for the annealed copper, between 10^7 and 10^9 dynes per sq. cm, has been analyzed on the basis that it is due to the longer loops becoming unstable, and restrained from reproducing themselves by the cross dislocations. They are held in this form until the stress reverses and hence the stress–strain curve occurs in the form of a hysteresis loop, which abstracts energy from the vibration. Calculations based on these premises have been used to evaluate the distributions of Frank–Read sources, versus loop length, with results shown in Fig. 10. In this figure the loop length distribution

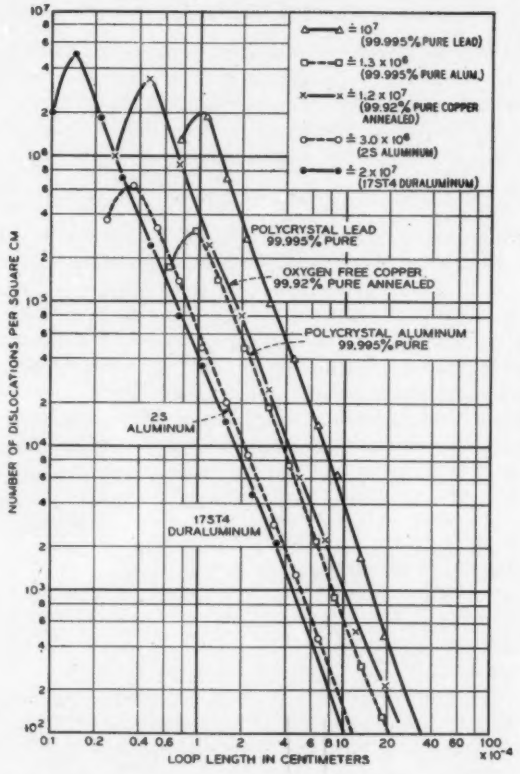
≐ 10^7 (99.995% PURE LEAD)
≐ 1.3 x 10^6 (99.995% PURE ALUM.)
≐ 1.2 x 10^7 (99.92% PURE COPPER ANNEALED)
≐ 3.0 x 10^6 (2S ALUMINUM)
≐ 2 x 10^7 (17ST4 DURALUMINUM)
POLYCRYSTAL LEAD 99.995% PURE
OXYGEN FREE COPPER 99.92% PURE ANNEALED
POLYCRYSTAL ALUMINUM 99.995% PURE
2S ALUMINUM
17ST4 DURALUMINUM
NUMBER OF DISLOCATIONS PER SQUARE CM
LOOP LENGTH IN CENTIMETERS
x 10^-4

FIG. 10. Distribution functions for dislocations for several metals.

is shown in the form of the number of dislocations per sq. cm for a logarithmic interval of loop length sizes. The intervals cover a range of loop lengths between two loop sizes which are smaller and larger than that for the value plotted. For example, between 0.4×10^{-4} and 0.62×10^{-4} cm loop length there are 3.5×10^6 dislocations (for annealed OFHC copper). Since the number of dislocations is the number of loops times their average length, there are 6×10^{10} separate Frank–Read sources in this loop interval. Figure 10 shows also the distribution measured for polycrystal lead and for aluminum of various states of purity.

As the stress becomes greater than 10^9 dynes/cm^2, for annealed OFHC copper, another source of internal friction appears which increases very rapidly with stress. This was shown to be connected with dislocation loops of length less than the peak length cutting through the pinning dislocations and producing jogs, vacancies and an uncontrolled number of Frank–Read loops. The large amount of slip associated with the extra loops causes a large increase in the plastic compliance. This region is the flow region for which extrusion and cold welding occurs. For alternating stresses, fatigue in metals can occur in this region (6, 7).

When the stress is lower than this, for example 5.5×10^8 dynes/cm^2 for which the stress relaxation curves of Fig. 3 were measured, dislocations that are long enough to become unstable will be held up by cross dislocations, as indicated by Fig. 7, and will not be able to proceed further at the absolute zero of temperature. At higher temperatures, thermal agitation can add to the effect of stress and occasionally the thermal and mechanical energy will be sufficient to cause the dislocation to be cut and it can proceed further. If the process that limits the motion of dislocations through the metal is the cutting of cross dislocations, as suggested in Mott's theory (8) of exhaustion creep, the activation energy for the process, i.e. the energy that has to be overcome by thermal motion, is the jog energy, taken as $\frac{1}{2}\mu b^3$, minus the work done on the jog by the applied stress. This energy rather than twice the value for two jogs is taken since a dislocation with a jog is a stable entity. Hence it will be produced by thermal agitation much more often than two jogs simultaneously. To proceed further, another jog has to be formed. This requires only twice the time to produce one jog rather than the much longer time to produce two jogs simultaneously. When one dislocation presses on the cross dislocation, two thirds of the energy goes into stretching the dislocation, if only one jog is formed (as can be seen from Eq. [9]). Hence the activation energy should be

$$E=(\tfrac{1}{2}\mu b^3-\tfrac{1}{3}\tau b^2 l_i) \qquad [10]$$

Consequently stress can lower the activation energy for jog diffusion and the jog can move in a reasonable time if E is comparable to kT.

This is not the only possibility for the rate determining process since when a screw dislocation cuts another screw dislocation, as shown by Fig. 8, the moving dislocation has a jog which will not glide with the screw dislocation. For one sign dislocation, the motion of the jog produces vacancies, while for the other sign it produces interstitial atoms as it is dragged through the metal. The latter process requires much more energy than the first and hence such a jog cannot move in creep but acts essentially as a nodal point. When the dislocation is part screw and part edge, it has been argued that it is more likely to glide off at an angle rather than to produce vacancies[3]. Nevertheless two physical measurements favor the hypothesis that vacancy production occurs in creep. The first of these is the agreement of the activation energy of creep with that for self diffusion. When the jog creates a vacancy, the activation energy for the process will be the energy to create a vacancy

[3] Recent measurements by W. C. Dash show, however, that both screw and mixed dislocations can produce vacancies—*J. Appl. Phys.*, v. 29, 1958, p. 705.

plus the energy to move it, which together make up the self diffusion energy. The other piece of experimental evidence is that when a tin plated wire is held under stress for 400 hours at 180°C, there is evidence (9) of diffusion of the tin from the plating into the copper for a distance of 0.0025 cm. With an activation energy of tin into copper of 41 kcal per mole, a diffusion of this depth would not occur at 180°C in this time by normal diffusion processes. However, if dislocations travel from the tin into the copper generating vacancies from jogs, the most diffusible component, tin, will be carried along by the motions of the dislocations.

Assuming that the motion of jogs through the metal is the rate determining process, the creep rate can be calculated as follows. Since the self diffusion energy W is close to $\mu b^3/2$, Eq. [10] will represent the activation energy reduced by stress if W replaces $\mu b^3/2$. The number of jumps forward that a jog can make per second will be

$$\nu \exp -(W-\tfrac{1}{3}b^2\tau l_i)/kT \qquad [11]$$

where ν is the vibrational frequency of the jog (about 10^{12} per sec). If the jog advances by one Burger's vector b for each jump, the area of the loop will increase by about $bl_i/2$. The creep strain introduced by the displacement of one dislocation loop is

$$S = Ab \qquad [12]$$

where A is the area associated with the forward jump. Hence the time rate increase of the creep strain is

$$\frac{dS}{dt} = \nu b \sum_i N_i A_i \exp[-(W-\tfrac{1}{3}b^2\tau l_i)/kT]$$
$$= \frac{b^2\nu}{2} \sum_i N_i l_i \exp[-(W-\tfrac{1}{3}b^2\tau l_i)/kT] \qquad [13]$$

The distance l_i between jogs will be in the order of the separation of the peak distance l_0 between dislocations (about 7×10^{-5} cm for copper) and $\Sigma N_i l_i$ will be in the order of 5×10^6 copper from Fig. 10. It can be shown (7) that the average shear strain will equal the longitudinal strain, while the average shear stress will equal one-third of the longitudinal stress. Hence the equation for longitudinal creep should be of the form

$$\frac{dtS_l}{dt} = \frac{b^2\nu \sum_i N_i l_i}{2} \exp[-(W-\tfrac{1}{3}b^2\sigma l_0)/kT] \qquad [14]$$

For a constant applied stress σ, the creep strain will increase in proportion to the time in agreement with measurements for secondary creep.

For stress relaxation, however, the stress σ decreases continually as the strain decreases. For any particular degree of strain, there is a relation between the stress and strain of the form

$$\sigma = Y_0{}^P S_l \qquad [15]$$

where $Y_0{}^P$ is the slope of the stress strain curve. Measurements for 8000 psi indicate that its value is about 10^{10} dynes/cm^2 for copper. With the substitution

$$\frac{d\sigma}{dt} = \frac{b^2\nu Y_0{}^P \Sigma N_i l_i}{2} \exp[-(W-\tfrac{1}{3}b^2 l_0\sigma)/kT] \qquad [16]$$

Assuming $Y_0{}^P$ is nearly a constant, a solution for this equation is

$$\sigma_0 - \sigma = \frac{9kT}{b^2 l_0} \log_e(1+\frac{t}{t_0}) \text{ where}$$
$$t_0 = \frac{18kT \exp[(W-\tfrac{1}{3}b^2 l_0\sigma_0)/kT]}{\nu b^4 l_0 Y_0{}^P \Sigma N_i l_i} \qquad [17]$$

The most likely value for $b^2 l_0/9$ can be obtained from Fig. 4 which shows that the activation energy for stress relaxation approaches zero when the applied stress is about 10,000 psi $= 6.9\times10^8$ dynes/cm^2. With this value and the value $b = 2.55\times10^{-8}$ cm for copper, one finds for l_0 the value

$$l_0 = 0{\cdot}74\times10^{-4} \text{ cm} \qquad [18]$$

which is in fair agreement with the value shown by Fig. 10. With this value of l_0, and $W = 3.68\times10^{-12}$ ergs corresponding to $W = 53$ kcal per mole, and taking $\Sigma N_i l_i = 10^6$ since only loops on the long side will be activated by this stress, one finds for t_0 a value of 6 sec compared to a measured value of 320 sec. Since the result depends very critically on the activation energy and hence the loop length l_0, this can be considered a reasonable agreement. The other constant that can be checked is the value

$$K = \frac{9kT}{b^2 l_0} = 10^7 \qquad [19]$$

compared to the measured value of 2.5×10^7. A somewhat better check is obtained for the 2S aluminum of Fig. 4 of reference (1). This gives t_0 calculated 3×10^3 sec, compared to 130 sec measured, and $K = 1.6\times10^7$ calculated compared to 2.05×10^7 measured. The conclusion appears to be that the largest part of creep for these materials is accounted for by slip caused by dislocations dragging jogs through the metal under combined stress and thermal activation.

4. Theoretical discussion of thermocompression bonds

The activation energies observed for the rates for which metals adhere to other metals under the action of pressure and temperature (thermocompression bonds) are given by the quantitative results of Fig. 2. These are the same order as those observed for stress relaxation and creep suggesting that we are dealing with the same process. It appears that the most likely reason that metals adhere to each other is that creep occurs at high pressures and temperatures until all the spaces between the metals disappear for regions around the points of initial contact. If the two surfaces are within atomic dimensions, adhesion can occur by the exchange of electrons between adjacent atoms as in other metallic bonds such as welding and soldering.

Even very smooth copper or other metal surfaces have asperities in the order of several microns high (one micron = 10^{-4} cm) and when two smooth surfaces are pressed together, as shown by Fig. 11(b), they contact at only a

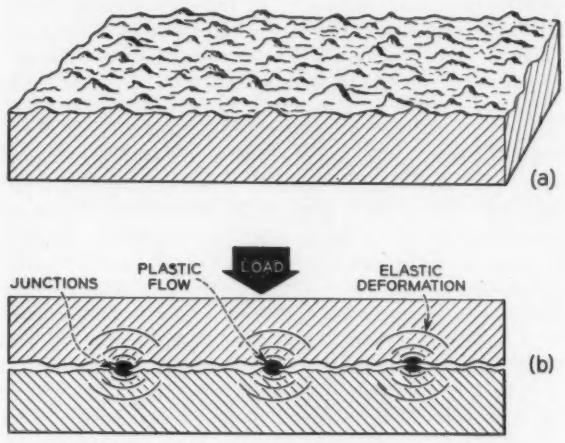

FIG. 11. Type of contact between smooth metals.

few spots. When a load is applied to one surface, plastic flow occurs at the asperities until a large enough area results to support the load. There is a certain maximum pressure P_m that the material will support, and the area of contact grows until the area times P_m equals the load. There will be elastic deformation under the asperities and in the surrounding regions and if the load is taken off, the release of the elastic deformation is usually sufficient to break any bonds between surfaces except in such soft materials as indium. This metal is known to make contact with other metals under applied pressures alone. By using gold balls to simulate the action of asperities, this process has recently been studied by O. L. Anderson (10). Figure 12 shows the diameter of contact of the gold ball pressing on an aluminum alloy plane, plotted against the resistance of the contact in ohms, as measured by the voltage drop across the contact. (The slope is nearly -2 showing that the resistance measured is determined mostly by the aluminum film whose thickness decreases slightly as the pressure increases.) The gold was pure and well annealed and was more ductile than the alloy. The force applied was also plotted against the displacement and had a similar relation to the diameter of contact with an exponent of -2.3, showing that the gold was hardened somewhat by the plastic flow. The limiting pressure was about 30,000 lb per sq. in. During the compression cycle, no adhesion took place between the gold ball and the aluminum or even between two gold balls, showing that the stored elastic energy was sufficient to break any bonds.

The elastic stresses in a ball pressing on a semi-infinite plane have been calculated and they are high over the contact area and decrease about as the square of the distance from the contact area center. Some idea of the

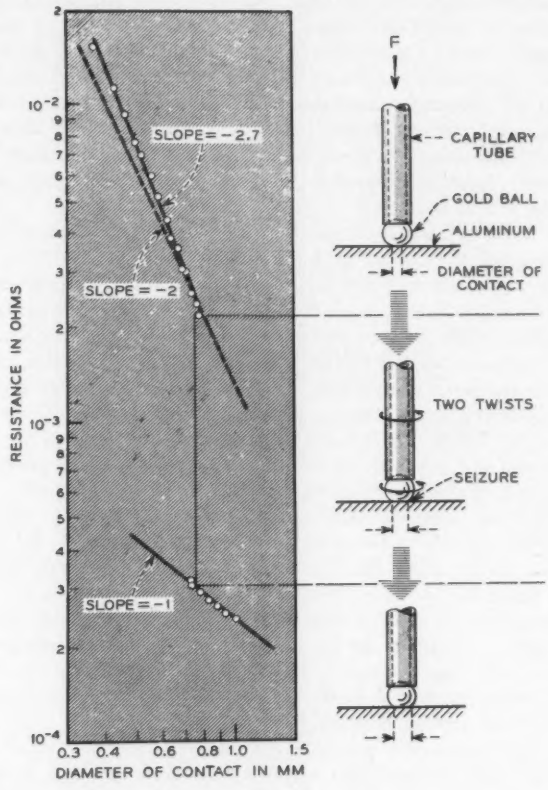

FIG. 12. Resistance of contact vs. diameter of contact of a gold ball on an aluminum plate (after O. L. Anderson).

distribution of these stresses can be obtained from a solution of the stresses of a sphere pressing against a plane, as discussed by Love (11). Figure 13 shows the directions of

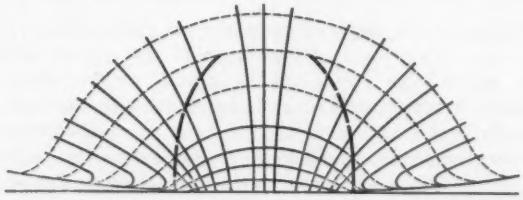

FIG. 13. Calculation of principle stresses in a sphere pressed against a plate (after A. E. H. Love).

the principal stresses in the sphere. Solid lines indicate compression while dotted lines indicate tension. Directly under the area of contact all the stresses are compressive and when the stress is taken off, the release of this energy is sufficient to break any bonds that have been formed, which tend to hold the ball in its deformed position.

The maximum shearing stresses can be determined from the principal stresses from the relation

$$\tau = (\sigma_2 - \sigma_1)\frac{\sin 2\theta}{2} \qquad [20]$$

where σ_2 is the longitudinal stress along one of the principal axes, σ_1 the longitudinal stress along the other and θ the angle between σ_2 and the direction that the shearing stress is to be measured. This will be a maximum when $\theta = 45°$. If one stress is compressive and the other tensile, the shearing stress is larger than if both are of the same sign. The dot-dash lines show the estimated path for the maximum shearing stress and it is seen to occur just outside of the area of contact.

After all the instantaneous plastic flow has occurred, shearing stresses will be high near the edges of the contact areas and according to Eq. [11], one can expect a creep in which the outer planes beyond the area of contact creep down to fill the gap between the asperities and the plane. On account of the higher stresses, metal near the edge of the contact area will have the lower activation energy and will creep down more rapidly than more distant planes. Nevertheless, if time is allowed, these will also creep down, increasing the area of contact. As the area of contact grows, the elastic forces tending to break the contact decrease while the bonding forces increase in proportion to the area. Hence at some time t_0 for a given temperature T_0, the bonding force will be larger than the breaking force and it requires a force to separate the two parts. For large times, the force increases, but on account of the rapid drop off in the creep rate as the activation energy increases, one reaches a maximum force which does not increase much with time. The ratio of the pull-off force to the load applied is called the coefficient of adhesion.

If the asperity were perfectly elastic it can be shown that the adhesive bond will always be broken down to a very small radius. This follows from the stress distribution that will result (12) from a lifting force applied to counteract the downward load. If the surface is bonded and does not move, this will result in a tensional distribution

$$\sigma_L = \frac{F_L}{2\pi a_0 \sqrt{a_0^2 - r^2}} \qquad [21]$$

where a_0 is the radius of contact, r the radius vector, and F_L the lifting force. At the edge of the contact circle, $r = a_0$, and the tension will be infinite. As the radius of contact became smaller, as F_L became larger, the infinite tension region will move toward the center and will break the bond down to a small radius near the center. Hence it is only if plastic strain occurs to change the elastic nature of the asperity, that a bond can be made.

While no calculations have been made of the tension distribution that will occur when account is taken of plastic strain, it appears reasonable that the tension will approach a constant across the contact area. The high stress indicated on the edges by Eq. [21] will induce instantaneous plastic flow. This in turn will lower the tension on the edge and increase it in the center in order to support the total force F_L. On such an assumption one can calculate coefficients of adhesion that agree reasonably well with those measured.

If the lifting tension is stronger than the bonding tension P_B, as it is in most metals, then no adhesion takes place. When, however, the radius grows to a_1, due to plastic creep along the sides of the area of contact, then, since the load remains the same, the lifting tension σ_L decreases and a point is reached for which $\sigma_L = P_B$. Some indications of this value of a_0/a_1 can be obtained from the experimental values of Fig. 2. For zinc, the activation energy of bonding is about 4.5 kcal per mole when the force to remove the bar is just measurable, while for copper it is about 6.8 kcal per mole. The activation energy takes the form of the equation

$$(W - b^2 l_0 \tau) = E \qquad [22]$$

where τ is the shearing stress at the point of interest. Right at the edge of the area of contact the activation energy should be initially nearly zero since the edge is the last region for which plastic flow can occur instantaneously. Hence,

$$W = b^2 l_0 \tau_0 \qquad [23]$$

Calculations show that the activation energy decreases about as the square of the distance from the center of the area of contact assuming that the average loop length remains constant. Actually, due to cold work, the loop length should be smaller near the area of contact than it should at some distance away and hence the activation energy should fall off less rapidly than inversely proportional to the square of the radius ratio. Neglecting this effect, the activation energy for a radius $r > a_0$ is

$$E = b^2 l_0 \tau_0 \left[1 - \left(\frac{a_0}{r}\right)^2\right] = W\left[1 - \left(\frac{a_0}{r}\right)^2\right] \qquad [24]$$

Hence, the radius a_1 for which the lifting tension is just equal to the bonding tension is

$$\left(\frac{a_0}{a_1}\right)^2 = 1 - \frac{E}{W} = 1 - \frac{4.5}{28} \text{ or } a_1 = 1.085\, a_0 \text{ for zinc} \qquad [25]$$

since the self diffusion energy W is about 28 kcal for zinc. For copper, $E = 6.9$ kcal and $W = 53$ kcal, giving $a_1 = 1.072\, a_0$.

For a longer period of time the radius r increases until it has a value a_2. For the longest times shown for the highest temperatures of Fig. 1, the ratio of a_0/a_2 can be obtained from [25] by using the highest values of activation energies shown by Fig. 2. For these cases

$$\left(\frac{a_2}{a_0}\right) = 1.63 \text{ for zinc}; \quad \frac{a_2}{a_0} = 1.19 \text{ for copper} \qquad [26]$$

The coefficient of adhesion is the force required to break the bond, divided by the load. This is given by the equation

$$K_A = \frac{\pi a_2^2 P_B - \pi a_0^2 \sigma_L}{\pi a_0^2 \sigma_L} = \left(\frac{a_0}{a_1}\right)^2 \left(\frac{a_2}{a_0}\right)^2 - 1 \qquad [27]$$

since $P_B = \sigma_L (a_0/a_1)^2$. From the values given above, the coefficient of adhesion should be 1.25 for zinc and 0.23 for copper compared to the measured results of 1.0 and 0.625. A better agreement for copper is obtained if one assumes that the activation energy falls off inversely as the radius. Since copper can strain harden, loops close to the contact area should be shorter than those at a distance. Zinc, being a hexagonal structure, does not strain harden.

Since the lift-off tension is the result of elastic stresses locked in the metals, it might be expected that those should decrease with time or annealing and the bonds would become stronger. Experimental evidence for this effect has been found with indium. Another question raised by the observations (see reference 9) that tin can diffuse into copper across their common interface, is the question of whether diffusion is necessary to obtain a thermocompression bond. This question has been answered in the negative by the work of Anderson, Christensen and Andreatch (13) on thermocompression bonds between a metal and a semiconductor such as silicon and germanium. Here dislocations cannot be created or moved in the semiconductor at any of the pressures or temperatures used for thermocompression bonding. No signs of diffusion of the metal into the semiconductor have been found. Since a strong bond is formed between the metal and semiconductor, it can be concluded that diffusion between the two parts is not necessary. All that is required is atomic contact between the parts.

Since the asperities extend only a small distance from the surface and the stress pattern does not extend deeply into the metal, it is evident that a small layer on the surface will determine the properties of the thermocompression bond. As discussed in reference (1), platings in the order of 1 mil in. thick can change the character of the bond. On account of the complex nature of the stress pattern associated with the pressing of a sphere on a plane, it is difficult to calculate the time required for a given amount of adhesion. Since the activation energies and the times are in the same order as those for creep and stress relaxation, it appears likely that it is the same phenomena operating.

5. Adhesion caused by compression and shear stresses

It is a well known fact that when both compression and shearing stresses are applied between two metals, they tend to adhere to each other. In fact, the most promising theory of friction, known as the "Adhesion Theory of Friction" (14), makes use of the idea that the friction between two solids is primarily due to the tangential force required to break the points of adhesion that form between the solids under the combined action of compression and shear. Since the area of contact is proportional to the load, the coefficient of friction, which is defined as the ratio of the tangential force to the normal force, is independent of the load. This relation is known as Amonton's law.

A verification of the nature of slip-stick forces is shown by the force oscillograms (15) of Fig. 14. These show the tangential forces measured between a metal wire and a phenolic plastic, under a steady weight of 40 grams, as the motion of the wire increases from 0.05 mil in. to 2.0 mil in. For low amplitudes, gross slide does not occur and a sinusoidal force is measured. For larger amplitudes, there are indications that the point of contact has changed from one position to another. This agrees with the idea that friction is due to a definite bonding between points of contact between the two materials. When these are broken by their relative motions, a friction force is required. New

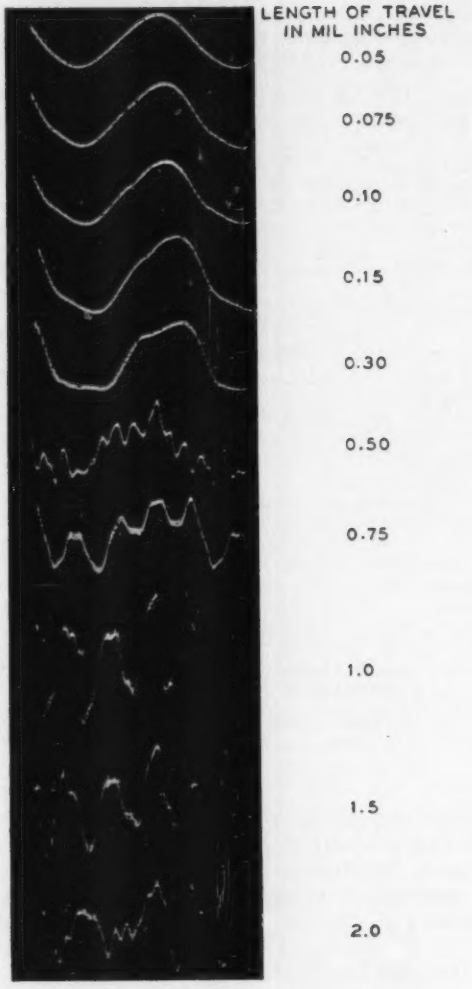

FIG. 14. Force between wire and plastic measured as a function of the relative motion.

points of contact are then made and an irregular frictional force occurs.

The nature of the contact formation between metals has recently been studied by O. L. Anderson (10, 16) and the results will be summarized here. If the gold ball of Fig. 12 is given a twist, the resistance drops by a factor of 10. For a further increase in pressure, the resistance drops in proportion to the contact diameter, evidencing pure contact resistance between metals and a rupture of the surface films. Furthermore, the gold ball is now found to have an adhesion to the aluminum plate. The development of this adhesion has been studied by putting two pieces of copper rod in the head stock and tail stock of a lathe. The ends are squared off and pressed together with a known force. If they are immediately separated, they have no tendency to adhere. If, however, they are pressed together, and one of the rods is given a twist with respect to the other, they develop an adhesion. It then takes a definite

force to pull them apart. If one plots the logarithm of the coefficient of adhesion against an accumulated number of tries on standard Gaussian probability paper, as shown by Fig. 15, nearly a straight line results. The nearly straight

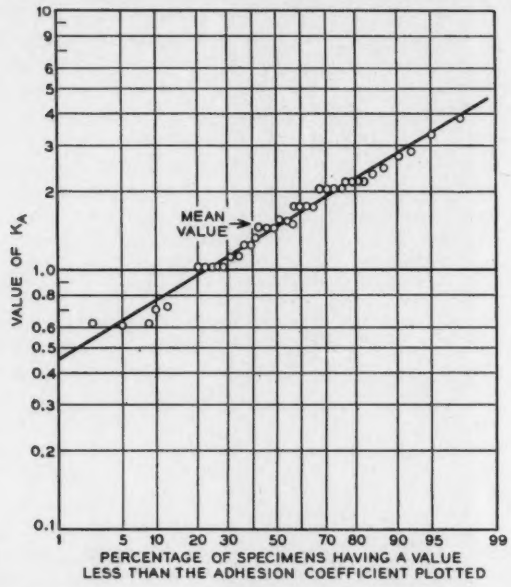

FIG. 15. Coefficient of adhesion between two copper rods plotted as a function of the number of tries (after K. M. Striny and O. L. Anderson).

line indicates that there are a number of variables, which add logarithmically to determine the mean coefficient of adhesion. This is about 1.5 for copper but may be higher for such materials as gold on gold. Approximately the same coefficient of adhesion and the same dispersion were obtained for a number of normal forces. When the force to break the bond was within 0.5 of the tensile strength of the copper, a decrease was observed in the coefficient of adhesion for larger forces.

The principle variable affecting the adhesion is probably the amount of film removed. The largest values of adhesion measured—around 4—agree quite well with the coefficient of friction measured for a degassed and heated wire and cylinder of copper (17). Hence the largest values probably correspond to surfaces for which practically all the film has been removed. The spread in values probably represents the effect of partial removal of the film from the parts that are brought into contact.

The probable reason for the bonding under combined normal and tangential loads, acting on the asperities, is that the combined loads produce considerably more plastic flow than the normal load alone and the area of contact is enlarged[4]. When the tangential load is taken off, there is no stress, such as the lifting tension σ_L, to break the bond. Hence, the bonding pressure over the larger area is sufficient to override the lifting tension σ_L due to the normal load, giving a positive coefficient of adhesion K_A. The traction across a circular boundary has been calculated (18) for the conditions of a normal force N and a tangential force T acting together on two spherical surfaces pressed together. The traction is a shearing stress which has the same form as Eq. [21] with F_L replaced by T. It was suggested (18) that the infinite value of traction near the edge would cause slip between the surfaces over a circular area near the edge and evidence for this was found experimentally (19). Such a traction would also add to the shearing stress in the body of the material and would cause more plastic flow, resulting in a larger area of contact than for a normal stress alone. When the tangential force is withdrawn, there is no resulting stress pattern which tends to pull the two surfaces apart. Hence, since the area of contact is larger than that occurring for pressure alone, then by virtue of the considerations in the last section and Eq. [27], a positive coefficient of adhesion should result. This is evidenced by the curves of Fig. 15. The higher the normal force, the higher the bonding strength. By putting on sufficient force to cause a slight enlargement of the area at the point of contact, the bond can be made as strong as that in the body of the material. The relation between the adhesion obtained with normal and tangential forces to the Bowden–Tabor theory of friction is obvious.

6. Effects of adhesion on electrical contacts

For permanent and semi-permanent contacts, the advantage of adhesion between the two parts of the contact is great. In the solderless wrapped connection (1, 2), the adhesion occurring with time, resists the deleterious effects of stress relaxation and vibration. The adhesion caused by normal and tangential forces explains the success attained with the widely used screw connection. The two parts are bonded together and resist the effects of stress relaxation of the screw and the effects of vibrations of the joint.

For more mobile types of contacts, the adhesion caused by normal and tangential forces is a source of sticking and a source of wear. Figure 16 is a photomicrograph of a

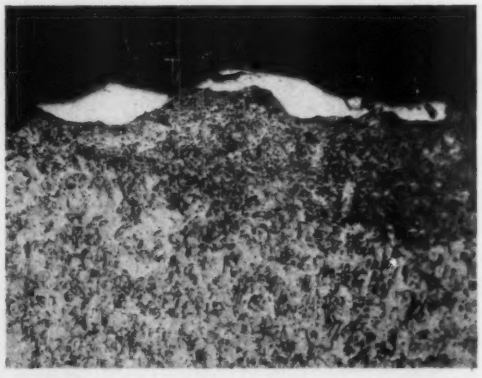

FIG. 16. Joint between copper and aluminum formed by compression and shear (after O. L. Anderson).

[4] For example, if one uses the von Mises criterion for plastic yielding, $\sigma^2+3\tau^2 = Y^2$, where σ is the normal compressive stress, τ the shear stress and Y is the yield stress of the material in tension or frictionless compression, it is evident that the area is increased by the factor $\sqrt{1+3\tau^2/\sigma^2}$.

copper–aluminum bond, made by normal and tangential forces, which has been pulled apart. Pieces of aluminum are seen to adhere to the copper, showing that the bond is stronger than the strength of the softer aluminum interior. In this way, metal can be transferred from one contact to the other and can be the source of mechanical wear. The force to break such bonds is a source of sticking in the relay. Both of these effects can be minimized if the tangential force can be kept very small. Similar results (15) were found for the wear of plastic materials encountered in the wire spring relay.

For high current carrying relays, a tangential motion is desirable in order to obtain a low contact resistance, but is usually accompanied by a larger amount of wear.

REFERENCES

1. Mason, W. P., and Anderson, O. L., "Stress Systems in the Solderless Wrapped Connection," *B.S.T.J.*, vol. 33, September 1954, pp. 1093–1110.
2. Mason, W. P., and Osmer, T. F., *B.S.T.J.*, vol. 32, May 1953, pp. 557–590.
3. Anderson, O. L., and Andreatch, P., "Stress Relaxation in Gold Wire," *J. Appl. Phys.*, vol. 26, n. 12, December 1955, p. 1518.
4. Mott, N. F., "A Discussion of Some Models of the Rate-Determining Process in Creep," Symposium on Creep and Fracture of Metals at High Temperatures, Nat. Phys. Laboratories, June 1954, and *Nature, London*, vol. 75, n. 4452, Feb. 26, 1955, p. 365.
5. Cottrell, A. H., *Dislocations and Plastic Flow in Crystals*, Oxford Univ. Press, 1953, pp. 19 and 53.
6. Mason, W. P., "Internal Friction and Fatigue in Metals at High Strain Amplitudes," *J. Acoust. Soc. Amer.*, vol. 28, Nov. 1956, p. 1207.
7. Mason, W. P., "Internal Friction, Plastic Strain and Fatigue in Metals and Semiconductors," Amer. Soc. Testing Materials, Symposium on Fatigue, June 1958.
8. Mott, N. F., *Phil. Mag.*, 7th Series, v. 44, 1953, pp. 742–765.
9. Mason, W. P., and Osmer, T. F., "Solderless Wrapped Connections Part II," *B.S.T.J.*, vol. 32, May 1953, pp. 557–590, see Fig. 19.
10. Anderson, O. L., "Adhesion of Solids, Principles and Applications," *Bell Laboratory Record*, Nov. 1957, pp. 441–445, Fig. 6.
11. See *The Mathematical Theory of Elasticity*, Cambridge Univ. Press, 4th ed., 1934, p. 198, Fig. 15.
12. Timoshenko, S., *Theory of Elasticity*, McGraw-Hill Co., 1934, p. 338.
13. Anderson, O. L., Christenson, H., and Andreatch, P., "Techniques for Connecting Electrical Leads to Semiconductors," *J. Appl. Phys.*, vol. 28, Aug. 1957, p. 923.
14. Bowden, F. P., and Taber, D., *The Friction and Lubrication of Solids*, Oxford, 1950.
15. Mason, W. P., and White, S. D., "New Techniques for Measuring Forces and Wear in Telephone Switching Apparatus," *B.S.T.J.*, vol. 31, May 1952, p. 469, Fig. 9.
16. Further data and conclusions are in course of publication.
17. Bowden, F. P., and Tabor, D., *The Friction and Lubrication of Solids*, Oxford Univ. Press, 1954, see Fig. 55c, p. 147.
18. Mindlin, R. D., "Compliance of Elastic Bodies in Contact," *J. Appl. Mech.*, Sept. 1949, p. 529.
19. Mindlin, R. D., Mason, W. P., Osmer, T. F., and Deresiewicz, H., "Effect of an Oscillating Tangential Force on the Contact Surfaces of Elastic Spheres," *Proc. 1st Nat'l Cong. of Appl. Mech.*, 1952, pp. 203–208.

Transition Temperatures in Sliding Systems

By R. S. FEIN[1], C. N. ROWE[2], K. L. KREUZ[3]

A pin-on-disk type of apparatus is used to study the effect of operating variables on transition temperatures with dilute solutions of pure fatty acids in pure paraffinic hydrocarbons and with a straight paraffinic mineral oil. It is found that the temperature at which the sudden transition from low to high friction and wear occurs increases with sliding speed, decreases with load, and is otherwise independent of operating variables. Empirically, the reciprocal of the absolute transition temperature varies linearly with the logarithm of the ratio of load to speed. The absence of conventional hydrodynamic lubrication in this system is demonstrated.

It is concluded that these results are inconsistent with the widely accepted concept that boundary lubricants must form a "solid" adsorbed film to be effective. It appears necessary to adopt a modified view of the role of the boundary lubricant, in which rheological and other diverse physical characteristics must be considered, and not simply the state of matter in which it exists. In addition, it appears necessary to consider the interrelated kinetics of boundary film formation and welding between asperities.

Introduction

SUDDEN transitions from effective to ineffective lubrication have frequently been observed when some operating variable was changed during sliding experiments carried out in the presence of boundary (for example, fatty acid) lubricants. Usually, the transitions have been observed experimentally under changing temperature conditions, and the critical temperatures have been called transition temperatures (1, 2, 3, 4).

The most generally accepted explanation of this transition phenomena appears to be that developed by Bowden and his school (1, 5, 6), and applied subsequently by Zisman (3, 7) and co-workers, among others. They attribute the sudden onset of high friction and wear to the "softening" or "melting" of adsorbed monomolecular films of the fatty materials, or of the product of their reaction with the surface. Below the transition temperature, effective lubrication is provided because the adsorbed film is "solid" and capable of keeping the two surfaces apart. The transition temperature corresponds closely to the bulk melting or softening point of the boundary lubricant.

The concept of effective lubrication by a solid surface film which has a fairly well defined softening or melting point implies that friction and wear transition temperatures should be determined solely by the physical nature of the adsorbed film and hence by the particular lubricant–metal combination employed. That is, the transition temperatures should be independent of operating conditions such as sliding speed, load, and bearing surface configuration, provided that frictional heating is negligibly small.

The above picture has been based on and supported by results of studies carried out under a highly circumscribed set of operating conditions using the Bowden–Leben type of apparatus in which a spherically-ended rider makes a single pass over a flat plate at very low (usually ≤ 0.01 cm/sec) speeds. The boundary lubricant was applied as a thin film of the bulk material or in the form of isolated monolayers. These studies did not consider the effect of pure boundary lubricant versus dilute solutions, of single versus repeated traversal of the wear track, or of variables such as load and speed on transition temperature phenomena.

Scattered literature references indicate that transition temperature phenomena should be interpreted in broader terms than indicated above. Frewing (8), investigating solutions of fatty materials in white oil with a Bowden–Leben machine, found no apparent relation between transition temperature and bulk melting point of the boundary lubricant, but believed that polarity of the molecule was important.

A few studies (2, 6, 9, 10, 11) involving both single and multiple traverse systems have shown transition temperature to be affected by changes in speed and/or load. Rabinowicz (6), for example, using a pin-on-disk in single pass operation, found transition temperature to increase with increasing speed. In some of these cases transition temperatures have been observed with lubricants not related to fatty acids and not usually classified as boundary lubricants. Thus, Coffin (2) reported transition temperatures with such materials as ethanol or hexane; in these cases transition temperatures increased with sliding speed but were independent of load over the limited range studied. Cowley, Ultee and West (9), working with a straight mineral oil and with an organo-silicone copolymer concluded that transition temperature (measured in the bulk lubricant) decreased with both load and speed. In related experiments, Beeck, Givens and Smith (12), and Burwell and Strang (13) and Murray and Burwell (14) working at constant temperature, found sudden decreases in friction

Presented as an American Society of Lubrication Engineers paper at the Lubrication Conference held in Los Angeles, Calif., October, 1958.

[1] Project Leader, Texaco Research Center, Beacon, New York.
[2] Chemist, Texaco Research Center, Beacon, New York.
[3] Project Leader, Texaco Research Center, Beacon, New York.

when a critical speed characteristic of the lubricant was exceeded.

The available information concerning transitions in boundary lubrication thus indicates these phenomena to be more general in occurrence and more complex in their dependence on constitutional and operational variables than is implied in the simple picture currently accepted.

The present studies were undertaken to clarify the effect of operational variables on transition temperature in a closely controlled multiple-traverse sliding system using a dilute hydrocarbon solution of a fatty acid as a simple model lubricant. For this investigation a pin-on-disk type apparatus was used to determine transition temperatures for steel-on-steel with several lubricants over a wide range of operating conditions. For 0.43% stearic acid/cetane similar determinations were made with copper-on-copper and silver-on-silver.

Apparatus and Materials

The pin-on-disk type apparatus is shown in Figs. 1 and 2

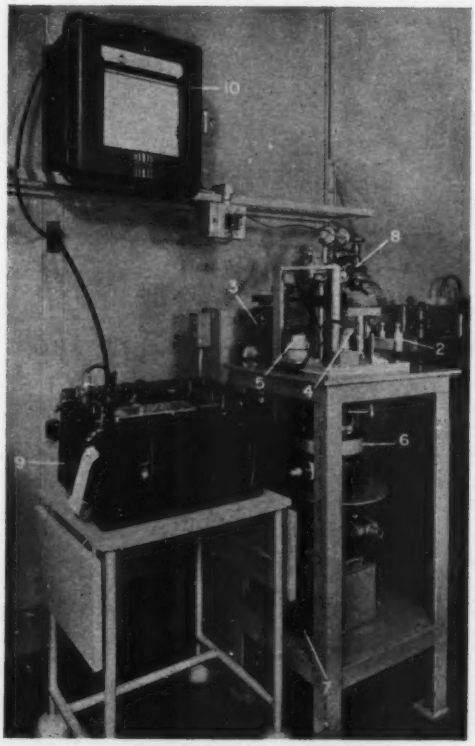

FIG. 1. General view of apparatus.

with the various parts identified in Table 1. The machine, patterned after one used by Murray, Johnson and Bisson (11) offers controlled coverage over wide ranges of variables considered basic to friction and wear phenomena.

The metals and lubricants used for this study are listed in Table 2.

FIG. 2. Close-up of test pot.

TABLE 1

Principal Parts of Pin-on-Disk Friction and Wear Machine.

1. Test pot.
2. Dead weight load.
3. Variable speed drive.
4. Strain ring (friction measurement).
5. Revolution counter (sliding distance measurement).
6. Hot plate (lubricant heat supply).
7. Variac (hot plate control).
8. Gas supply (atmosphere control).
9. Friction recorder.
10. Temperature recorder.
11. Rotating shaft.
12. Rotating flat specimen.
13. Load and friction transmitting shaft.
14. Bullet or rider specimen.
15. Lubricant.
16. Thermocouple.

TABLE 2

Materials

Metals	Diamond pyramid hardness	
	Disk	Rider
1. AISI 4140 steel. Austenitized, quenched and tempered	273	293
2. Copper	91	111
3. Silver (fine)	49	89
Lubricants	**Viscosity, centipoises**	
	100°F	210°F
1. Cetane. Percolated over silica gel and alumina, filtered.	2.3	0.9
2. Dodecane. Percolated over silica gel and alumina, filtered	1.2	0.5
3. 0.43% Stearic acid (m.p. 66°C) in 1	2.3	0.9
4. 0.43% Stearic acid (m.p. 66°C) in 2	1.2	0.5
5. 0.26% Capric acid (m.p. 30°C) in 1	2.3	0.9
6. Paraffinic mineral oil (solvent-refined mid-continent distillate oil)	27.6	4.4

Experimental Procedure

The apparatus was washed with pentane and then acetone; in the latter part of the work *iso*octane replaced the pentane. The test pot was scrubbed with soap and water and then dried with acetone.

Disk specimens were prepared by abrading in air on a metallographic grinder. Successively finer grades of emery paper down to 3-0 paper were used (except for silver disks which galled with 2-0 and 3-0 paper). A random surface finish was obtained by continuously moving the specimen "upstream" on the rotating grinding disk. About a 2 microinch RMS finish on the steel resulted from this operation. No attempt was made to check the wettability of the disk surface by water since water can affect the surface action of boundary lubricants (1). However, since surfaces prepared in this manner generally are wet by water, the disk specimens can be assumed free of surfactive organic matter. The disk specimens were washed with *iso*octane after grinding to remove any grinding debris.

The lathe-turned pin specimens were prepared by washing with pentane or *iso*octane and acetone. In general, they were not abraded since the tip shape is too easily changed in an abrasion process. It is reasoned that any contaminating film will be quickly removed in the wear process since the tip of the pin is always in contact with the opposing disk.

Immediately after preparation, specimens were installed in the apparatus and submerged in the test lubricant. During the runs, dry air (containing $< 1/1200$ atmosphere H_2O) at atmospheric pressure was either passed over or bubbled through the lubricant.

Experimental results

Most of the transitions were determined by raising the bulk lubricant temperature while maintaining speed and load constant. Figure 3 shows a typical friction trace.

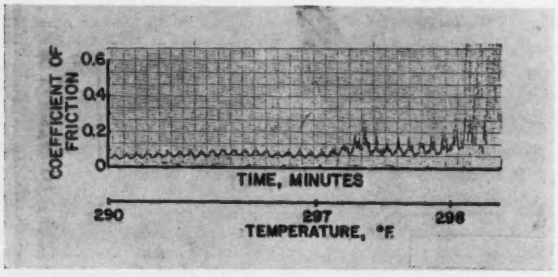

FIG. 3. Typical friction transition (0.43% stearic acid/docedane, ~1 cm/sec, 1200 g).

Below the transition, the friction trace is smooth showing a cycle corresponding to the period of rotation of the disk. At the transition, there is a sudden increase in friction and the friction trace becomes rough (in the case shown) or stick-slip (relaxation oscillation) occurs. As expected, the tendency to stick-slip is dependent on load, speed and the compliance of the strain ring used for friction measurements.

At the transition, there is also an abrupt increase in wear rate[4] by a factor of the order of 10^2 to 10^5. The median wear particle size increases from the order of a fraction of a micron to the order of a fraction of a millimeter (the order of a 1000-fold increase). The wearing surfaces, as illustrated in Fig. 4, change from a scored surface (for steel-on-steel after run-in) to a severely torn or galled surface. For copper-on-copper, the well run-in wear track is so sufficiently smooth (only rare fine scratch marks) that it is difficult to locate visually below the transition, but it is similar in appearance to the steel surfaces above the transition. Visually, the nature of the galled surfaces was the same regardless of whether the transition resulted in rough irregular friction or stick-slip.

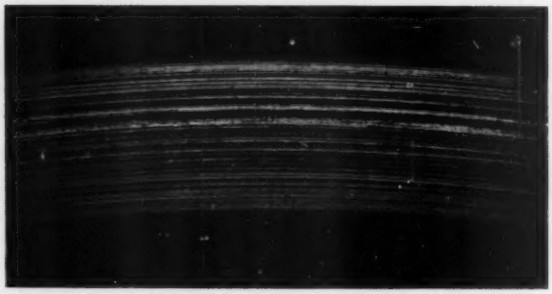

(4a)

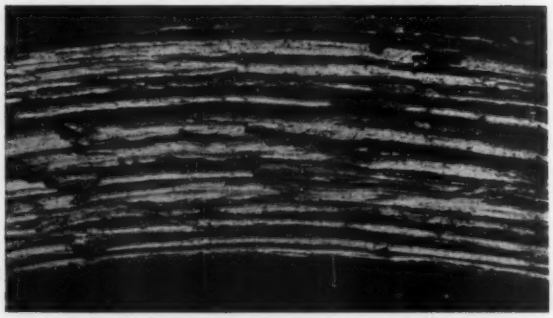

(4b)

FIG. 4. Typical flat-specimen wear scars (AISI 4140 steel, 30×, reduced by ½). (a) Effective lubrication. (b) Ineffective lubrication.

From both friction and wear it is apparent that the transition represents a change from effective to ineffective boundary lubrication—qualitatively this change appears to be similar in nature to the change from "mild" to "severe" metallic wear reported by Archard and Hirst (15) and Kerridge and Lancaster (16) under dry sliding conditions.

Results with 0.43% Stearic Acid/Cetane

The 0.43% stearic acid/cetane system was studied extensively over the range of the operating variables listed

[4] Approximate wear rates below the transition were determined by weight loss while above the transition they were determined by the rate of change of rider length measured by a dial gage on the shaft which transmits load and friction.

in Table 3. As shown in Figs. 5 and 6, marked dependence of the transition temperature on both load and speed was found. (Table 4 explains the symbol coding on the figures in this paper.) Increasing load lowered the transition temperature, while increasing speed raised it.

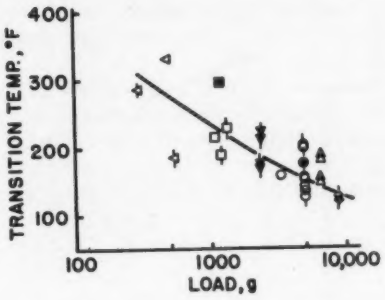

FIG. 5. Variation of transition temperature with load (0.43% stearic acid/cetane, AISI 4140 steel, speed 1 cm/sec).

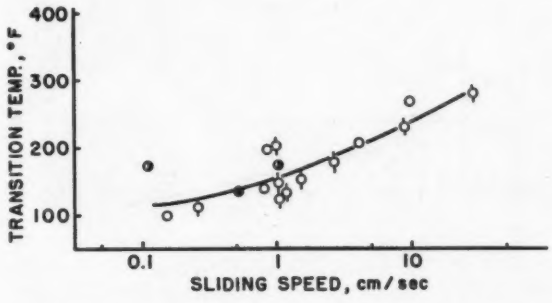

FIG. 6. Variation of transition temperature with speed (0.43% stearic acid/cetane, AISI 4140 steel, load 4900 g).

TABLE 3

Ranges of Operating Variables Studied

Temperature	85–350°F
Load	302–8728 g
Mean Hertz Pressure	
Cylindrically ended riders	0.074–68.1 kg/mm²
Spherically ended riders	97–187 kg/mm²
Sliding Speed	0.070–29.2 cm/sec
RPM	0.26–108
Sliding distance per revolution	4.24–16.2 cm
Strain ring constant	0.0492–0.285 (Recorder Deflection)/(Torque, g-cm)
Pin or Rider Specimen Configuration	
Cylindrically ended	0.012–0.090 in. diameter
Spherically ended	¼ in. radius

TABLE 4

Code for Points Used in Transition Temperature Plots

Load, g	*Point shape*
300– 700	◁
701–1500	□
1501–2500	▽
2501–5000	○
5001–7500	△
7501–8700	◊

Rider Configuration	*Point Shading*
0.090 in. diam. cylinder	None
0.030 in. diam. cylinder	Bottom shaded
0.012 in. diam. cylinder	Fully shaded
0.250 in. diam. spherical	Right shaded

Stain Ring	*Line Through Point*
Compliant	Vertical
Stiff	None

In general, the transitions were reversible in that recovery to low friction and wear could be achieved by lowering the temperature or load or by raising the speed. Exceptions to this reversibility were encountered at combinations of high load and speed (favoring frictional heating) with the steel and copper systems, and all loads and speeds with the silver system. With the high load and speed combinations, the lack of reversibility may be attributed to frictional heating above the transition; otherwise, frictional heating effects appear to be negligible in this work[5]. With the silver system, no explanation of the irreversibility is apparent.

Empirically, it was found that the reciprocal of the transition temperature (absolute, Rankine) increased linearly with the logarithm of the ratio of load to speed. (Admittedly, the logarithm of the absolute temperature would also give a linear plot, but the reciprocal of the absolute temperature has some theoretical basis.) This is shown in Fig. 7 where the reciprocal scale is plotted increasing downwards so that the transition temperature increases upwards in the usual manner. Data shown in this figure were obtained over a period of about one year by several different operators. In this period of time, the machine was completely disassembled, moved and reassembled.

From Fig. 7 and the symbol code of Table 4, it may be deduced that with the exception of the load–speed ratio dependence, there are no systematic trends of the transition temperatures with (a) load or sliding speed alone, (b) rider configuration or apparent area of contact, or (c) strain ring stiffness. In addition, although not shown in the figure, there are no systematic trends with the diameter of the wear track on the disk (sliding distance per revolution), lubricant history, and whether air was bubbled through the

[5] Negligible frictional heating is implied by reversibility of the transition despite the several-fold change in friction coefficient accompanying the transition. Negligible heating is also implied by lack of dependence of transition temperatures on the product of load and speed which, along with the coefficient of friction, determine the temperature rise at the sliding surface.

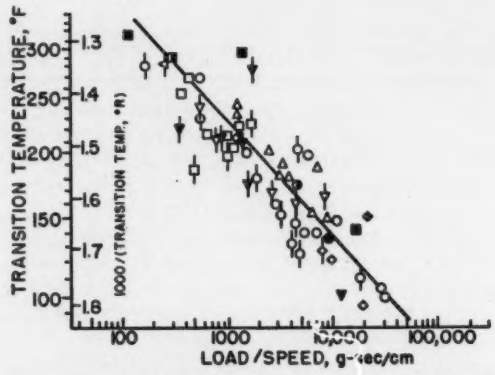

FIG. 7. Transition dependence on load–speed ratio (0.43% stearic acid/cetane, AISI 4140 steel).

lubricant or passed over the surface. Slight oxidation of the lubricant (as indicated by appearance of hydroxyl and intensification of carbonyl bands in infrared spectra) had no effect on the transition temperatures. In addition, specimen surface condition had no influence on the transition temperature. That is, the same dependence of transition temperature on load–speed ratio was found with new specimens without appreciable running in, well run-in new specimens, or specimens that had been badly torn by previous transitions (by nature of the experiment, some running in always occurs before the transition is reached).

Thus, over the ranges of variables studied, the transition temperatures for this system appear to depend only on load–speed ratio. These results compare with data in the literature. Figure 8 shows the line from Fig. 7 along with transition temperature data of Murray, Johnson and Bisson (11) and that of Frewing (8). Murray and co-workers used

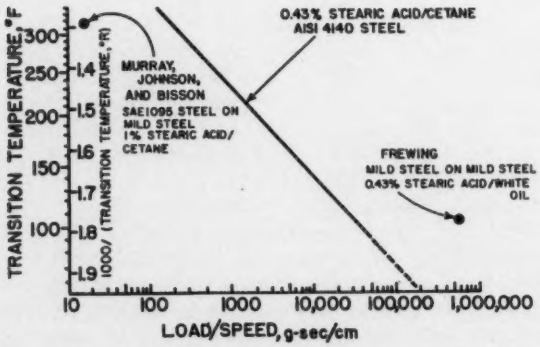

FIG. 8. Comparison of transition temperatures.

a machine similar to the pin-on-disk machine used for the present work while Frewing used a Bowden–Leben machine. Considering that different steels were used, that the lubricants were not exactly the same, and that the relatively high sliding speeds used by Murray *et al.* probably caused some frictional heating effects, the results of the present work appear to be in good agreement with diversely obtained results in the literature. In fact, these apparently uncorrelated results in the literature now appear to fit into an overall pattern of transition temperature dependence on load–speed ratio.

Figures 9 and 10 show a similar dependence of transition temperature of 0.43% stearic acid/cetane on load–speed

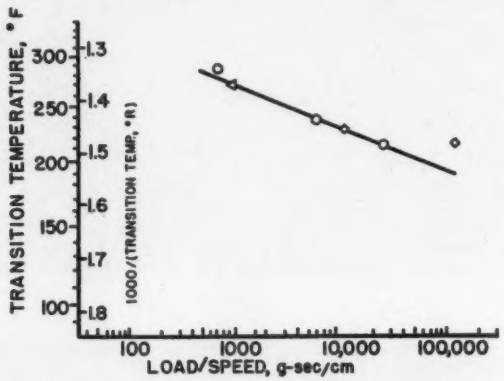

FIG. 9. Transition dependence on load–speed ratio (0.43% stearic acid/cetane, copper).

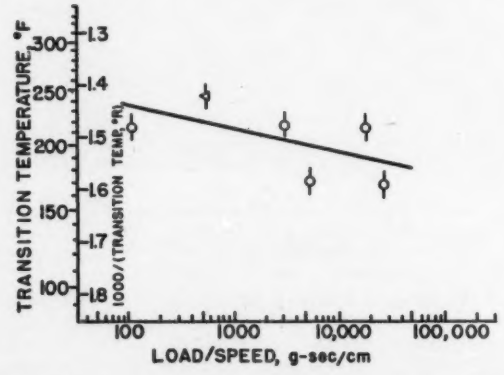

FIG. 10. Transition dependence on load–speed ratio (0.43% stearic acid/cetane, fine silver).

ratio with copper sliding on copper and silver on silver. However, these latter systems showed much smaller changes in transition temperature with load–speed ratio, with that for silver being barely detectable within the precision of the data.

In all the systems, including the silver, metal soap was found in the used lubricant (soaps were identified by infrared absorption). In the copper system the soap appeared (by color and by infrared spectrum of the used lubricant) to be formed in copious quantities when operating at temperatures above the transition. In the steel and silver systems, a very small quantity of soap was separated from used lubricant by centrifuging and/or filtering. The presence of soap in the silver system is in agreement with the studies of Smith and McGill (17), who found soap on freshly formed surfaces and in disagreement with Bowden and Tabor (1). No difference in transition temperature was

found between fresh and used lubricants, even with the copper system in which the soap was quite soluble. In addition, with the steel system, runs made with new metal specimens and used lubricant gave the same results as new specimens and lubricant or used specimens and lubricant. This implies that, if soap is the effective boundary lubricant, sufficient quantities are formed on the surfaces below the transition to overwhelm the influence of the bulk lubricant soap concentration.

Results with Paraffinic Mineral Oil

In order to check the generality of the relationship of transition temperature to load–speed ratio, several runs with steel on steel were made with a straight paraffinic mineral oil. As shown in Fig. 11, this lubricant also gave a

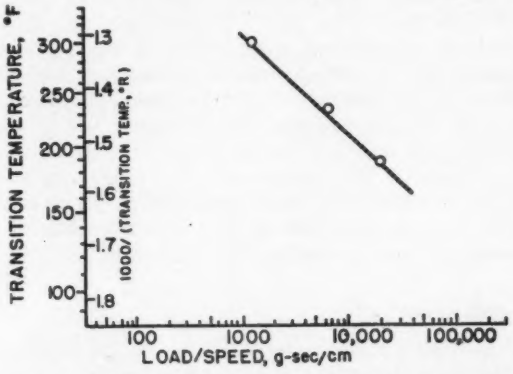

FIG. 11. Transition dependence on load–speed ratio (paraffinic mineral oil, AISI 4140 steel).

similar dependence of transition temperature on load–speed ratio. Although the temperatures are higher, the slope of the curve is about the same as that for stearic acid/cetane with steel on steel.

Effect of Viscosity

The exponential dependence of transition temperature on load–speed ratio naturally suggests the familiar dependence of friction of ZN/P which is found in hydrodynamic lubrication[6] even though, in the present case, load and not pressure is the critical variable. Figure 12 shows transition temperatures obtained with steel on steel with 0.43% stearic acid/dodecane. The line on this figure is that shown on Fig. 3 for 0.43% stearic acid/cetane. Although the viscosity of the dodecane solution is about half that of the cetane solution, it is apparent that the transition temperatures are the same. This agrees with the result of Beeck, Givens and Smith (12) and Burwell and Strang (13); they found that bulk lubricant viscosity did not influence the critical speed at which transition to high friction occurred.

Effect of Boundary Lubricant Component

In order to check the effect of the boundary lubricant component of the system, attempts were made to obtain

[6] Z = lubricant viscosity, N = speed, P = apparent pressure.

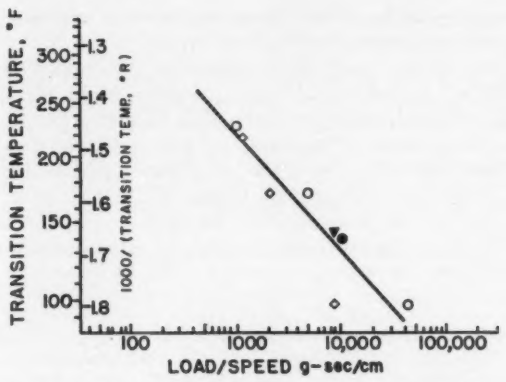

FIG. 12. Transition dependence on load–speed ratio (0.43% stearic acid/dodecane, AISI 4140 steel).

transition temperatures with cetane alone in the steel system. However, at room temperature, even at the lowest obtainable load–speed ratio, friction was high and irregular. Thus, if cetane does show a transition, it must be lower than room temperature. It is a curious fact that, with cetane at comparable conditions, the surface damage was much less than was observed with stearic acid/cetane above its transition temperature.

Runs were also made with 0.26% capric acid/cetane (same molar concentration as 0.43% stearic acid) in the steel system. Figure 13 shows these data. Comparison with

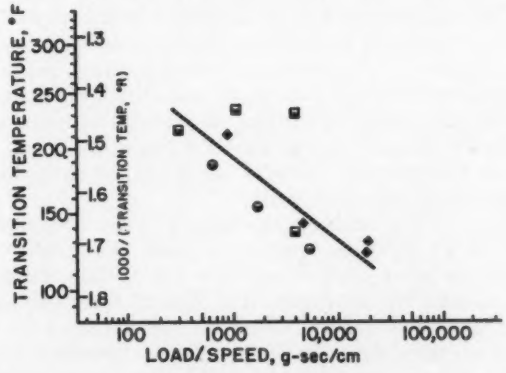

FIG. 13. Transition dependence on load–speed ratio (0.26% capric acid/cetane, AISI 4140 steel).

Fig. 7 indicates that capric acid may give slightly lower transition temperatures than stearic acid at lower load–speed ratios.

Discussion of Results

A variety of metal-lubricant systems show transition temperatures that decrease with increasing load–speed ratio. In all of the systems, this decrease is such that the reciprocal of the absolute transition temperature is, at least to a first approximation, linearly dependent on the logarithm of the load–speed ratio. This relationship is in the form of the typical expression of temperature dependence,

$A \exp(-E/RT)$, for chemical and physical reaction-rate and equilibrium constants, viscosity, etc.

The friction and wear transition phenomena must occur by physical or chemical processes which are temperature, load, and speed dependent. The energy, E, and the proportionality constant, A, corresponding to such processes were calculated from the observed relationships of Figs. 7 through 13 and are shown in Table 5. Both the energy and the proportionality constant appear to depend on the particular boundary lubricant–metal combination.

TABLE 5

Empirical Constants in Equation $W/V = A \exp(-E/RT_t)$

System			g-sec
Metal	Lubricant	E, cal/mol	A, cm
Steel	Paraffinic mineral oil	−13,500	1×10^{-4}
Steel	0.26% Capric acid/cetane	−15,800	3×10^{-7}
Steel	0.43% Stearic acid/dodecane	−11,500	2×10^{-4}
Steel	0.43% Stearic acid/cetane	−11,500	3×10^{-4}
Copper	0.43% Stearic acid/cetane	−31,600	8×10^{-15}
Silver	0.43% Stearic acid/cetane	−54,400	2×10^{-20}

W = load, g
V = speed, cm/sec
A = constant, g-sec/cm
E = energy, cal/mol
R = gas constant = 1.987 cal/mol—°K
T_t = transition temperature, °K

One process that must be important is that of welding between opposing asperities since it promotes metal transfer and tearing which are characteristic of the transition. This process undoubtedly involves the visco-elastic deformation of the metal to bring surfaces of opposing asperities into intimate contact followed by bond formation across the contact area to form a weld. Load, speed and temperature could readily affect this process.

The welding process, which tends to promote the transition, must be opposed by one or more of the following processes which tend to minimize the welding and thus afford effective lubrication. The first of these processes one might consider and one which could account for the load and speed dependence of transition temperature is one of conventional hydrodynamic action. This would prevent welding by a fluid film separating the surfaces and it would have a temperature coefficient determined by the energy of activation for viscous flow (18). This process can be discarded here, however, since the transition temperature is load dependent and not dependent on the apparent area or bulk lubricant viscosity.

Another process that must be considered is that suggested by Beeck, Givens and Smith (12). In this process a thick layer enriched in boundary lubricant provides effective lubrication because the lubricant is trapped by the contours of sliding surfaces. The effectiveness of the trapped material in keeping the surfaces apart would depend on its rheological properties, which in turn would be dependent on temperature, stress and strain rate. If the trapped material is a generated soap, the kinetics of its formation and dissolution would also enter in the above relation. It must be concluded that this process involving trapping is rationally compatible with the observed interrelationships among the operating variables.

The lubricant may also exist at the surface simply as an adsorbed monolayer. The monolayer would function to prevent welding by physical separation or surface contamination or by controlling the level and extent of oxidation of the metal substrate. The important surface processes in such a case are expected to be identified with adsorption–desorption, surface mobility, or deformability (rheology) of the monolayer; any of these can rationally be considered to depend on temperature, sliding speed, load and physical state of the film.

Any one or a combination of these processes could account for the observed relationship between transition temperature and load–speed ratio[7]. Undoubtedly, the sudden transitions occur when some critical balance is reached between the competing processes of welding and weld prevention by the lubricant. At this critical balance condition, the welding becomes self-accelerating and produces the high and unsteady friction and wear characteristic of severe wear. It thus appears necessary to incorporate the kinetics of welding, and other rheological properties as well as the mere physical state of the undisturbed film in the present concept of boundary film lubrication.

Conclusions

The temperature corresponding to the transition from low to high friction and wear increases with sliding speed and decreases with load. The reciprocal of the absolute transition temperature varies linearly with the logarithm of the ratio of load to speed.

The dependence of transition temperature on load–speed ratio cannot be explained by conventional hydrodynamic lubrication or by the concept of effective lubrication by a "solid" film of boundary lubricant. It appears necessary to adopt a modified view of boundary lubrication which includes other rheological properties of the boundary lubricant, as well as the interrelated kinetics of boundary film formation and welding between asperities.

REFERENCES

1. BOWDEN, F. P., and TABOR, D., *The Friction and Lubrication of Solids*, Oxford Univ. Press, London, 1954.
2. COFFIN, L. F., "A Transition Temperature for Surface Damage in Sliding Metallic Contact," *Lubrication Engineering*, vol. 13, n. 10, 1957, pp. 399–405.
3. COTTINGTON, R. L., SHAFRIN, E. G., and ZISMAN, W., A., "Physical Properties of Monolayers at the Solid/Air Interface," Part III, "Friction and Durability of Films on Stainless Steel," *J. Phys. Chem.*, vol. 62, n. 5, 1958, pp. 513–518.
4. RABINOWICZ, E., and TABOR, D., "Metallic Transfer Between Sliding Metals: An Autoradiographic Study," *Proc. Roy. Soc.*, vol. A 208, 1951, pp. 455–475.

[7] The idea of multiple effects is supported by recent work by Cottington, Shafrin and Zisman (3). They attributed large differences in performance of boundary lubricants on glass–steel and steel–steel sliding couples to differences in the deformability and weldability of the two systems.

5. RABINOWICZ, E., "An Autoradiographic Study of the Surface Damage of Sliding and Impacting Metals," submitted to the University of Cambridge for the degree of Doctor of Philosophy, 1950.
6. RABINOWICZ, E., "Theoretical Criteria for the Effectiveness of a Lubricant Film," presented to 12th Annual ASLE Meeting, April 16, 1957, Detroit, Michigan.
7. LEVINE, O., and ZISMAN, W. A., "Physical Properties of Monolayers Adsorbed at the Solid/Air Interface," Part I, "Friction and Wettability of Aliphatic Polar Compounds and Effect of Halogenation," *J. Phys. Chem.*, vol. 61, n. 8, 1957, pp. 1068–77. Part II, "Mechanical Durability of Aliphatic Polar Compounds and Effect of Halogenation," *J. Phys. Chem.*, vol. 61, n. 9, 1957, pp. 1188–96.
8. FREWING, J., "The Heat of Adsorption of Long-Chain Compounds and Their Effect on Boundary Lubrication," *Proc. Roy. Soc.*, vol. A 182, 1944, pp. 270–285.
9. COWLEY, C. W., ULTEE, C. J., and WEST, C. W., "Influence of Temperature on Boundary Lubrication," presented to Third Annual ASME–ASLE Joint Lubrication Conference, October 9, 1956, Atlantic City, N.J.
10. KINGSBURY, E. P., "The Influence of Bulk Temperature on Metallic Friction and Wear," submitted to Massachusetts Institute of Technology for the degree of Doctor of Philosophy, 1957.
11. MURRAY, S. F., JOHNSON, R. L., and BISSON, E. E., "Limiting Bulk Fluid Temperatures for Effective Boundary Lubrication by Synthetic Lubricants," *Lubrication Engineering*, vol. 10, n. 4, 1954, pp. 193–198.
12. BEECK, O., GIVENS, J. W., and SMITH, A. E., "On the Mechanism of Boundary Lubrication," Part I, "The Action of Long-Chain Polar Compounds," *Proc. Roy. Soc.*, vol. A 177, 1940, pp. 90–102.
13. BURWELL, J. T., and STRANG, C. D., "The Incremental Friction Coefficient—A Non-Hydrodynamic Component of Boundary Lubrication," *J. Appl. Phys.*, vol. 20, n. 1, 1949, pp. 79–89.
14. MURRAY, S. F., and BURWELL, J. T., "Measurement of the Incremental Friction Coefficient of Several Homologous Series of Straight-Chain Hydrocarbon Compounds," *Ann. N.Y. Acad. Sci.*, vol. 53, 1951, pp. 906–918.
15. ARCHARD, J. F., and HIRST, W., "An Examination of a Mild Wear Process," *Proc. Roy. Soc.*, vol. A 238, 1957, pp. 515–528.
16. KERRIDGE, M., and LANCASTER, J. K., "The Stages in a Process of Severe Metallic Wear," *Proc. Roy. Soc.*, vol. A 236, 1956, pp. 250–264.
17. SMITH, H. A., and MCGILL, R. M., "The Adsorption of *n*-Nonadecanoic Acid on Mechanically Activated Metal Surfaces," *J. Phys. Chem.*, vol. 61, n. 8, 1957, pp. 1025–36.
18. GLASSTONE, S., LAIDLER, K. J., and EYRING, H., *The Theory of Rate Processes*, 1st ed., McGraw-Hill, New York, 1941, pp. 477–516.

Wear and Friction of Filled Polytetrafluoroethylene Compositions in Liquid Nitrogen

By DONALD W. WISANDER[1], CHARLES E. MALEY[2] and ROBERT L. JOHNSON[3]

Wear and friction behavior of slider materials at cryogenic temperature is important to the development of seals and bearings for missile powerplants. Data were obtained in liquid nitrogen (−320°F) with a series of molded and extruded polytetrafluoroethylene (PTFE) compositions containing various filler materials. A $\frac{3}{16}$-in. radius rider specimen (PTFE materials) was caused to slide in a circumferential path on the flat surface of a rotating 2½-in. diameter disk specimen (usually type 304 stainless steel). The sliding velocity was usually 2300 ft per min and the load was 1000 grams.

As compared with reference steels and carbons used in conventional seals and bearings, the filled PTFE compositions gave low wear and friction (friction coefficients from 0.06 to 0.13) in liquid nitrogen. Several extruded compositions have particular promise for seal and bearing materials. An extruded glass-filled material gave wear and friction that was essentially unaffected by sliding velocities to 6000 ft per min.

Introduction

CRYOGENIC fluids of various types are of primary importance in liquid rocket propulsion systems. Fuels, oxidants, and inert working fluids can be advantageously handled in liquid form. The turbopump systems must have reliable seals for the cryogenic liquids, and the use of bearings lubricated by the pumped fluid is highly desirable.

The selection of seal and bearing material for rubbing surfaces lubricated by cryogenic liquids can be very critical. The physical and chemical properties of most cryogenic liquids of interest are such that they might be expected to have very poor lubricating ability. Initial studies of cryogenic systems were performed with liquid nitrogen because of convenience and freedom from hazard. Previous NACA research (1) has shown that surface welding occurs very readily with metals sliding submerged in liquid nitrogen at −320°F. In fuels and inert liquids the surface failure problem would be accentuated by the lack of surface films such as oxides on the wearing surfaces. Other friction studies (2) suggest that the adhesion concept of sliding friction is useful at liquid helium temperature (4.2°K) and at increasing temperatures (to 600°K) to those more common in friction studies.

The low temperatures associated with cryogenic fluids of interest (boiling point around −300°F or lower) provide cooling capacity that is helpful to slider materials. For example, the failure of PTFE compositions in slider applications at room temperature has been associated with thermal degradation accentuated by poor thermal conductivity (3). In liquid nitrogen, however, wear data (1) showed that a carbon-filled PTFE material was a good slider material over a substantial range of sliding velocities. Further, the PTFE composition gave friction in liquid nitrogen that was in the same range as effectively boundary lubricated metal surfaces at room temperatures. The preliminary results of (1) indicated sufficient promise for PTFE compositions in liquid nitrogen to merit the more detailed investigation reported herein.

This investigation was conducted to study the wear and friction of several experimental and commercial filled PTFE compositions in liquid nitrogen. The materials were used as purchased and were formed by conventional molding and extruding methods. The fillers including carbon, graphite, metal salt, glass, fiber, metals, and a ceramic, were used in concentrations up to 25% by weight. The data were obtained with a sliding friction apparatus consisting of a hemisphere-tipped ($\frac{3}{16}$-in. rad.) rider specimen sliding in a circumferential path on the flat surface of a rotating disk (2½-in. dia.) submerged in liquid nitrogen. Usual surface speed was 2300 ft per min. The test load of 1000 grams gave an initial Hertz surface stress of approximately 150,000 lb per sq. in. with steel specimens.

Apparatus and procedure

The apparatus used in this investigation is shown in Fig. 1. The basic elements consist of a rotating-disk specimen 2½-in. diam., ½ in. thick) and a hemisphere-tipped ($\frac{3}{16}$-in. rad.) rider specimen. The rider specimen slides in a circumferential path on the lower flat surface of the rotating disk. Unless otherwise specified the specimens were run submerged in liquid nitrogen.

The disk specimen was driven by a 5-horsepower hydraulic motor through a 6:1 speed increaser. Surface speed was usually 2300 ft per min (5000 rpm) for the data reported herein; some data are reported for other speeds. Two sets of helium-purged shaft seals were used to seal leakage from the test chamber. In the case of nitrogen,

Presented as an American Society of Lubrication Engineers paper at the Lubrication Conference held in Los Angeles, Calif., October, 1958.

[1] Aeronautical Lubrication Research Engineer, NACA, Lewis Flight Propulsion Laboratory, Cleveland 11, Ohio.

[2] Aeronautical Research Facilities Engineer, NACA, Lewis Flight Propulsion Laboratory, Cleveland 11, Ohio.

[3] Head of the Lubrication Research Section, National Advisory Committee for Aeronautics, Cleveland 11, Ohio.

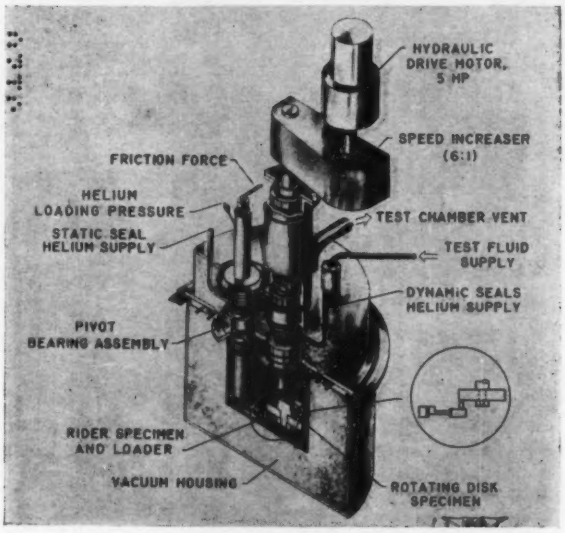

FIG. 1. Cryogenic friction apparatus.

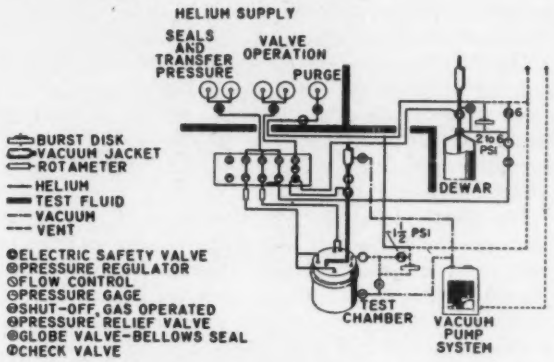

FIG. 2. Cryogenic friction apparatus fluid transfer system.

control of shaft seal leakage is not important, however, but fuels or oxidants seal leakage can be very important.

The rider specimen was supported by an arm assembly that allowed the measurement of friction force outside the test chamber. The vertical shaft of this assembly was pivoted through a bearing assembly mounted in the top housing. The shaft was sealed at the top and bottom of the pivot by flexible metallic bellows. In operation, the enclosed volume between the bellows was pressurized (7 psig) with helium. Friction force was measured by a strain-gage dynamometer ring connected to the top of the shaft. The deflection necessary for friction measurement was so small (0.003 in. at the top) that the restraining spring action of the bellows was negligible.

The rider specimen was loaded with a helium-pressurized piston assembly. The loading piston and rider holder were one part. Two polychlorotrifluoroethylene "O" rings were used as piston rings to minimize helium leakage, one being mounted on the lower edge of the piston and the other at the upper edge of the cylinder. Helium leakage through the loader into the test chamber was less than 2 cu. ft per hr corrected to standard conditions. Helium pressure of 95 in. of mercury above atmospheric gave a load of 1000 grams. The internal pressure of the test chamber was held at a gage pressure 1½ lb per sq. in. by a pressure relief valve in the vent line (Fig. 2).

The top housing of the apparatus was insulated by foamed-in-place polyurethane. The lower housing and transfer line were vacuum jacketed. The vent line was insulated by block polyurethane foam from the top of the test chamber (for 4 ft). The static heat leak resulted in vaporization of less than ½ liter of liquid nitrogen per hour. In operation, however, the vaporization was primarily a result of friction heat from the test specimens and the shaft seals. A 100-liter Dewar of liquid nitrogen was usually sufficient for up to four 1-hr runs or one 5-hr run.

The liquid nitrogen was transferred to the test chamber through the closed systems shown in Fig. 2. The Dewar was pressurized from 2 to 6 lb per sq. in. to transfer the liquid. About 2 liters of liquid were required in the test chamber for proper operation. The liquid level was determined by a copper-constantan thermocouple and two carbon resistors at different levels in the test chamber. It was possible to maintain the desired flow rate for the proper liquid level during an experiment (about 3 in. above the test specimens) by controlling the Dewar pressure.

The filled PTFE compositions used in these studies are listed in Table 1. The PTFE compositions were run as rider specimens sliding against type 304 stainless steel disk

TABLE 1

Polytetrafluoroethylene (PTFE) Compositions

NACA designation	Availability	Method of forming	Filler material
O-M	Commercial	Molded	(No filler)
10GR-M	Commercial	,,	About 10% graphite
10C-M	Commercial[a]	,,	10% coke flour
25C-M	,,	,,	25% coke flour
15GL-M	,,	,,	15% glass fiber
25GL-M	,,	,,	25% glass fiber
13XGL-M	,,	,,	5% coke+7½% glass
22XBR-M	,,	,,	9% coke+13% bronze
10GR2-M	Experimental[a]	Molded	10% graphite
25GR-M	,,	,,	25% graphite
10M-M	,,	,,	10% MoS_2
25AG-M	,,	,,	25% silver
25CU-M	,,	,,	25% copper
O-E	Commercial	Extruded	(No filler)
C-E	Experimental	,,	Carbon base filler
10GR-E	Commercial	,,	Approx. 10% graphite
M-E	,,	,,	MoS_2
M2-E	,,	,,	MoS_2
20[illegible]-E	,,	,,	CaF_2 (20%)
5A-E	,,	,,	Ceramic (5% Al_2O_3)
25GL-E	,,	,,	25% glass fiber
10XGL-E	,,	,,	10% glass fiber+ $CaSiO_4$+pigment
XGL-E	,,	,,	Glass fiber+pigment
20Cu-E	,,	,,	Cu (20%)

[a] Especially processed for NACA.

specimens. The several reference materials used have common commercial designations or are described in (1).

The metal disks were all finish ground on the test surface and had surface roughness from 4 to 8 microinches root mean square as measured with a profilometer. The rider specimens were finished on a lathe. The radius ($\frac{3}{16}$ in.) of each rider specimen was checked with a radius gage and a strong light source prior to use.

The metal specimens were cleaned by the following procedure: (a) washed with acetone, (b) repeated scrubbing with moist levigated alumina, (c) washed in tap water, (d) washed in distilled water, (e) washed in 95% ethyl alcohol or (c.p.) acetone, and (f) dried in clean warm air and stored in a desiccator.

The PTFE specimens were cleaned with (c.p.) acetone and stored in a desiccator. The test chamber was cleaned with (c.p.) acetone just prior to each run.

After the experimental specimens were installed, the lower housing was securely bolted in place. The seals were pressurized with helium, and the transfer tube, the test chamber, and the vent were purged for at least 15 min with gaseous helium. Another 10 to 20 min was required after the storage Dewar was pressurized to obtain the the required 2 liters of liquid in the test chamber. The initial helium purge is very important. Experience in (1) suggested that quenching the specimen from atmospheric air into liquid nitrogen without a purge left a frozen film of adsorbed moisture on the specimens. Wear of a carbon material on type 304 stainless steel was 10,000 times greater when the system was carefully purged than when there was no purge.

After stabilization of the liquid level, the drive motor was adjusted to the proper speed. The load was then applied to begin the experiment. Frictional force was measured by a recording potentiometer used as a strain indicator. The usual run was of 1-hr duration.

Following the run, the lower housing was removed and the specimens and test chamber were heated with an electric air heater to minimize condensation of atmospheric moisture. The test specimens were usually removed from the apparatus as quickly as possible to minimize the possibility of corrosion.

The wear and friction data reported are from typical runs with the various materials. Typical runs were selected from the 3 to 5 repeat runs made with each material. In most instances, with the specially prepared PTFE materials, friction coefficient was reproduced within ± 0.01 and wear data checked within $\pm 10\%$. With other materials, the data scatter in some cases was twice as large.

The wear of the rider specimens was determined by measuring the diameter of the wear scar and calculating wear volume. The specimens were carefully studied and photographed at low magnification using oblique illumination.

Results and discussion

Reference Materials

Data contained herein must be evaluated on a comparative basis. Therefore, to obtain the basis for evaluation of the filled PTFE compositions, data are presented in Figs. 3 and 4 for a series of other materials. These reference data were established with a cryogenic structural material (type 304 stainless), a conventional bearing steel (SAE 52100), a

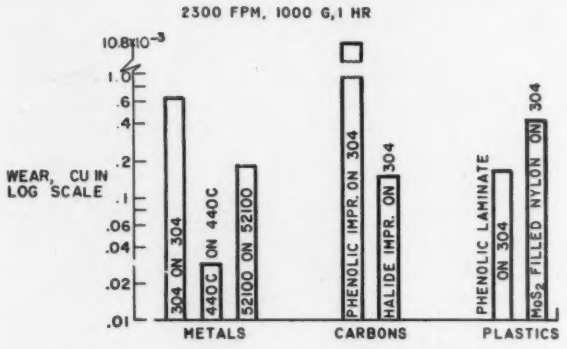

FIG. 3. Wear of reference materials in liquid nitrogen.

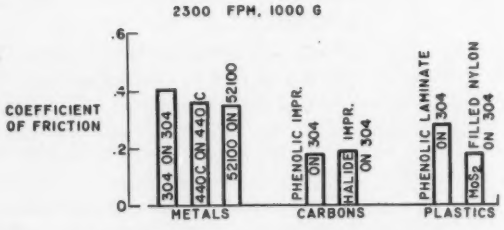

FIG. 4. Friction of reference materials in liquid nitrogen.

stainless steel that has been used in cryogenic bearings and seals (type 440-C), carbons of types considered for both conventional (phenolic impregnated), and cryogenic (metal halide impregnated) seals, a phenolic laminate of a type used for cages of high-speed rolling contact bearings, and a molded nylon containing MoS_2.

It is of interest that two well-established values for 304 on 304 could be reported. The data obtained in short runs (less than 10 min) reported in (1) indicate wear rates up to 10 times greater than those in runs continued for 30 min or more as reported herein. Metal transfer and other forms of surface deterioration continued in both cases (Fig. 5a). Continued running, however, caused the friction coefficient to be reduced substantially from the 0.78 reported in (1). Reductions in both wear and friction that were noted with continued sliding of 304 on 304 may be a result of the transformation of sliding surface structure from the original austenite to martensite. This transformation has previously been studied in terms of structural problems (4). In the present instance the probability of the transformation was suggested by increased magnetic susceptibility of the run surface, as observed after the run.

Both of the bearing steels (440-C and 52100) gave relatively low wear as compared with austenitic stainless (304) (in Fig. 3). Wear was primarily of the adhesive type that is

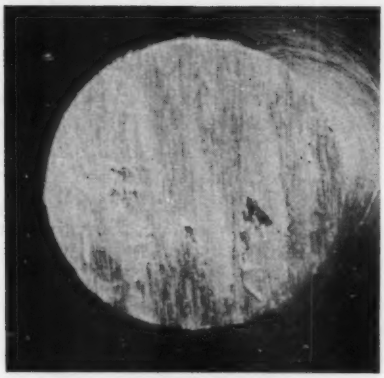

304 RIDER

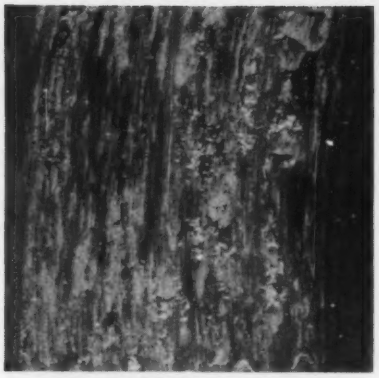

304 DISK

(a)

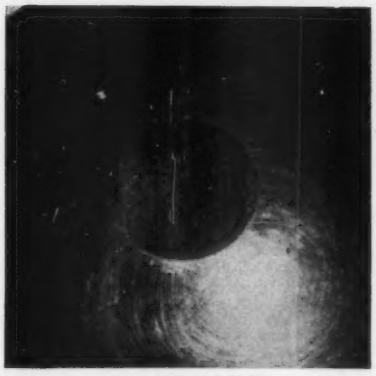

440 C RIDER

440 C DISK

(b)

52100 RIDER

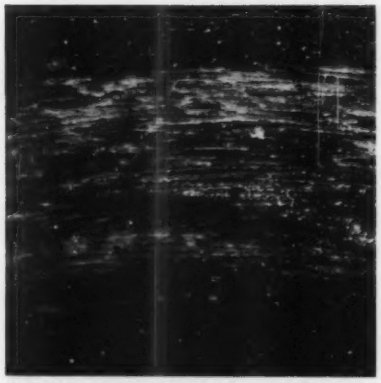

52100 DISK

(c)

Halide Impr. Carbon Rider

304 DISK

(d)

FIG. 5. Surfaces of reference materials after sliding in liquid nitrogen. Load, 1000 grams, 10×.

characterized by the removal of fine particles; however, some surface welding and metal transfer were noted (Figs. 5b and c).

The wear of carbons against 304 stainless steel was discussed in some detail in (1). It is sufficient here to note that conventional seal carbons wear extremely rapidly in liquid nitrogen. A metal halide impregnant can reduce wear appreciably. Friction of the carbons with a phenol impregnant and with a metal halide impregnant are not greatly different (Fig. 4). The wear surfaces (Fig. 5d) show no evidence of failure except normal adhesive wear.

Results for the reference plastic materials are also presented in Figs. 3 and 4. Laminated phenolics are of interest primarily for cages of rolling-contact bearings. Uses for nylon materials may develop in cryogenic applications because they have relatively good mechanical properties, as compared with other non-metallic materials. Both wear and friction with the plastic materials are within the range of values of the other reference materials.

Molded PTFE Compositions

Reference (1) showed that several PTFE compositions give low wear and friction. The results were not as consistent as might be expected. It was considered that much of the data scatter could have resulted from the method of processing the materials. In particular, variations in density and poor dispersion of the filler materials were found important. Aggregates of both PTFE and filler materials were noted in the compositions previously studied.

A series of specially milled and molded compositions was procured. These materials are described in Table 1. Every reasonable precaution was taken by the processor to obtain a homogeneous material, although conventional processing methods were used. The compositions were molded to the approximate size ($\frac{3}{8}$-in. dia.) of the rider specimens.

Wear data obtained with the specially molded compositions are reported in Fig. 6. The reproducibility of the

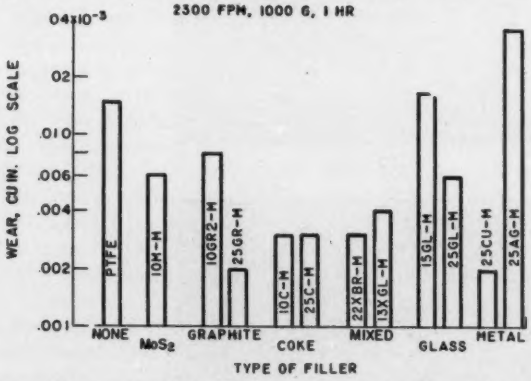

FIG. 6. Wear of molded PTFE compositions in liquid nitrogen.

wear data (usually within $\pm 10\%$) was much improved with the specially molded materials. Previous commercial products reported in (1) gave variations in wear of about 10 to 1 in duplicate runs. In general, the wear values reported herein were not only more consistent but were substantially lower than data on similar compositions of (1). Wear rates of about 0.003×10^{-3} cu. in. per hr are common (Fig. 6) for several materials. This approaches the lowest wear value for a single run of any material (0.0013×10^{-3} cu. in./hr) reported in (1). It should be noted that the ordinate scale of Fig. 6 is different than that of Fig. 3.

As compared with the reference materials, the results obtained with the specially molded materials were consistently good regardless of the type of filler. Copper, glass fiber, and solid lubricants including graphite and MoS_2 gave good results as fillers in the molded PTFE compositions. Silver was not as effective a filler as the other materials employed.

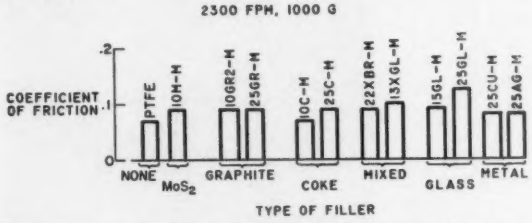

FIG. 7. Friction of molded PTFE compositions in liquid nitrogen.

As shown in Fig. 7, the friction coefficients of these materials were between 0.07 and 0.10 except when glass fiber was the filler material. With glass fiber in the molded compositions, friction coefficients up to 0.13 were measured.

Surface films of PTFE compositions were formed on the mating metal surface with all these materials. Thus sliding was between the molded material and a surface film of similar composition. This is consistent with the mechanisms of sliding for PTFE bodies suggested in (3). In some instances with glass-filled compositions the film on the mating surface was abraded and friction was somewhat higher, as noted previously.

Extruded PTFE Compositions

Commercial filled PTFE compositions are available in both molded and extruded form. Economic considerations probably have been more important in determining the desired method of forming than any performance parameter. Reference (5) reported that the method of molding and the thermal history, such as shock-cooling, are important in determining mechanical properties. For example, shock cooling may reduce crystallinity and improve resistance to brittle fracture. Some further discussion of crystallinity and its relation to properties of molded PTFE is given in (6). As compared with molding methods, extrusion forming of small cross-sections probably imposes severe shock cooling and therefore should give low crystallinity and good mechanical properties. Wear resistance can be influenced by mechanical properties. Therefore, it might be expected that extruded compositions would have wear resistance different from the usual molded materials.

Several extruded PTFE compositions with various types of fillers are described in Table 1. Because they are commercial products and proprietary interests are involved, it is not possible in most cases to present exact compositions. Wear data on the extruded compositions are presented in

Fig. 8; friction data for the same materials are in Fig. 9. In most instances the specimens used were made from rod extruded to very near the final diameter of the rider

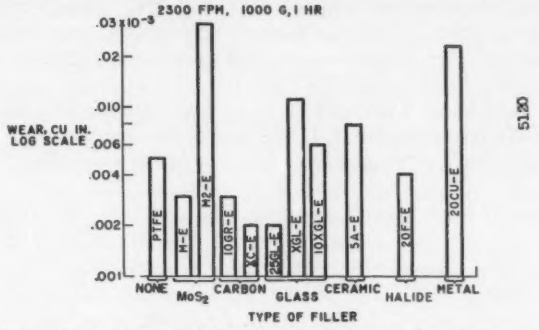

FIG. 8. Wear of extruded PTFE compositions in liquid nitrogen.

specimens ($\frac{3}{8}$-in. dia.). Unreported results showed that specimens made from different parts of large extruded (or molded) sections are apt to give inconsistent wear data.

As compared with the reference materials of Fig. 3, all the extruded PTFE compositions of Fig. 8 gave low wear (note different ordinate scales for Figs. 3 and 8). The lowest wear was obtained with a carbon-type filled material (XC-E) and a glass-filled composition (25GL-E). Comparable results were obtained however with MoS_2 filled (M-E), and another carbon-filled (10GR-E) extruded materials. The friction coefficients with these materials were usually in a range from 0.07 to 0.09. The highest friction coefficient of Fig. 9 (0.13 for 25GL-E) is well within the range

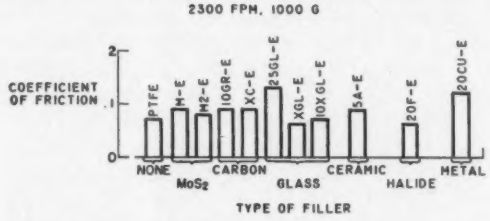

FIG. 9. Friction of extruded PTFE compositions in liquid nitrogen.

normally experienced (0.10 to 0.20) in effective boundary lubrication of metal surfaces with petroleum oils.

The worn surfaces of the disk and rider specimens were similar with all of the filled PTFE compositions. Figure 10 presents photographs for two of the better materials. The

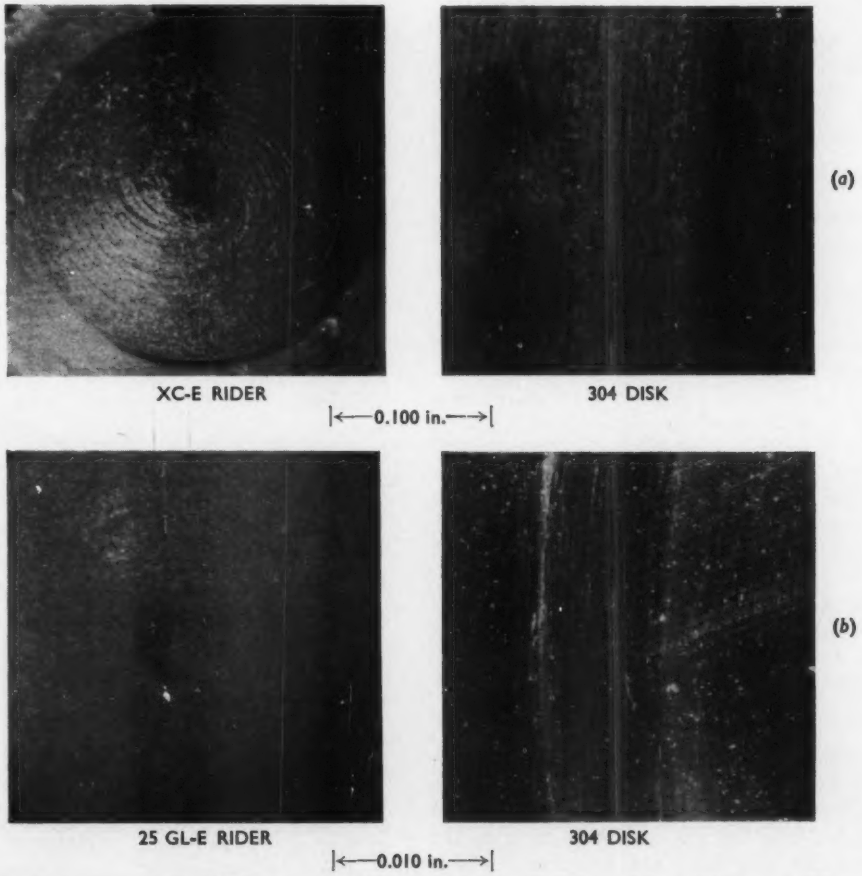

FIG. 10. Surfaces of filled PTFE materials after sliding in liquid nitrogen. Load, 1000 grams, 10 ×.

appearance is similar to that for the other compositions. A thin film of PTFE was established on the disk surface with all the extruded as well as the molded compositions. With 25GL-E extruded glass-filled composition, the amount of transfer film abrasion by glass particles was much less than had been noted with the molded glass-filled materials (15GL-M and 25GL-M of Table 1); either the type of glass fiber or the orientation of the fibers and the orientation of the PTFE could have influenced this result.

Comparison of wear and friction data for molded (Figs. 6 and 7) with that for extruded (Figs. 8 and 9) compositions shows that, in general, the extruded materials give better results. A more direct comparison of molded and extruded materials run in both liquid and gaseous nitrogen can be made in Figs. 11 and 12. The molded materials 10C-M (carbon) and 25GL-M (glass) are generally equivalent to the extruded materials XC-E (carbon) and 25GL-E (glass).

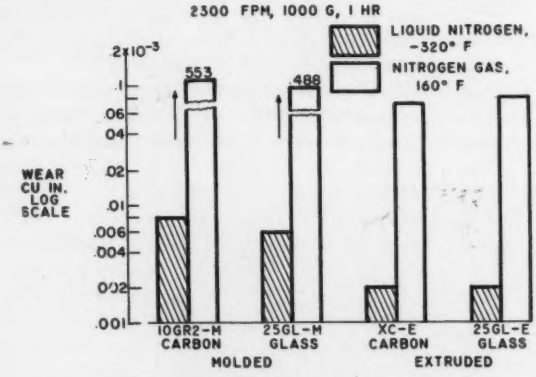

FIG. 11. Wear of PTFE compositions in liquid and gaseous nitrogen.

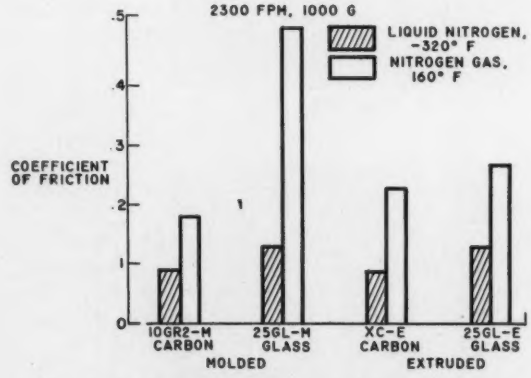

FIG. 12. Friction of PTFE compositions in liquid and gaseous nitrogen.

With both carbon- and glass-filled compositions, wear (Fig. 11) of extruded materials was substantially less than similar molded compositions in either liquid or gaseous nitrogen. Friction (Fig. 12) was more dependent on the fluids (and possibly their associated temperature differences) than on type of forming and composition. As discussed in (1), the cooling effect of the liquid nitrogen is important to the performance of PTFE composition as slider materials. Although data are reported herein for only four compositions, most of the materials of Table 1 were run in gaseous nitrogen; the four materials were among the better slider compositions in gaseous nitrogen (160°F) and in liquid nitrogen (−320°F).

The effect of sliding velocity on wear of a graphite filled PTFE material (10GR-E of Table 1) was reported in (1). Those data are presented for comparison purpose in Fig. 13.

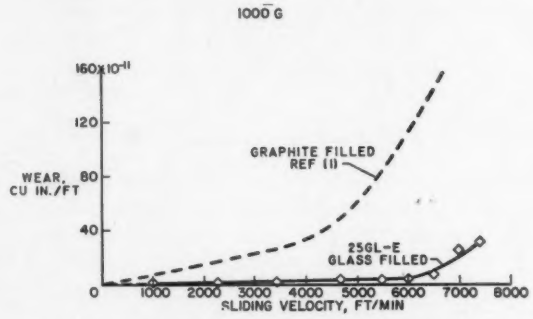

FIG. 13. Wear of PTFE compositions in liquid nitrogen at varied sliding velocities.

Wear increased rapidly at sliding velocities above about 3000 ft per min for the graphite filled PTFE. The increase in wear at high sliding velocity was considered a result of thermal softening by frictional heating. Thermal softening is also probably responsible for the more rapid wear of the compositions of Fig. 11 in warm gaseous nitrogen than in liquid nitrogen. The data obtained in nitrogen gas, some of which are reported in Fig. 11, show that the extruded glass-filled composition (25GL-E of Table 1) had as good resistance to wear as any of the materials. The effect of sliding velocity on wear of the extruded glass-filled PTFE was also determined and is presented in Fig. 13. Wear rates of this material were not significantly influenced by sliding velocities up to 6000 ft per min. Wear values were always very much lower than for the graphite-filled material (10GR-E of Table 1). Friction of 25GL-E in liquid nitrogen (Fig. 14) was not changed significantly by sliding velocities from 300 to 7550 ft per min and loads from 500 to 1000 grams. It should be noted that the glass-filled composition probably has greater strength and hardness than the other PTFE base materials, but thermal conductivity may not be significantly improved.

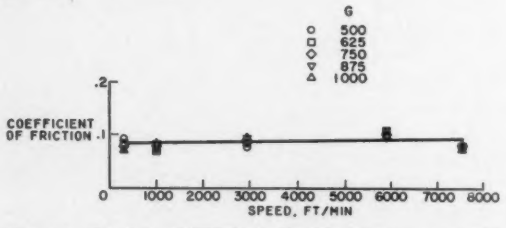

FIG. 14. Friction of PTFE in liquid nitrogen at varied sliding velocities.

Evaluation of Results

Boundary lubrication studies with conventional petroleum and synthetic oils usually show friction coefficients for steel surfaces around 0.10 and up to 0.20. Friction data for hardened steel surfaces in liquid nitrogen show friction coefficients from 0.30 and much higher. Under conditions of load and speed similar to those reported herein, many liquids of very low viscosity are capable of preventing metal transfer or other forms of surface failure (7). In liquid nitrogen, metal transfer and varying degrees of surface failure as well as relatively high friction were observed with all metal combinations of this study and in (1). These results emphasize the point that liquid nitrogen cannot be considered as a boundary lubricant. It does, however, provide an excellent heat sink for frictional energy.

The PTFE compositions almost always gave less wear and lower friction than the reference materials (metals, carbons and plastics). The low temperatures and heat sink provided by the liquid nitrogen are considered vital for the use of PTFE materials for slider surfaces at relatively high loads and surface speeds. The room temperature properties of PTFE are typical of plastic materials as a class. At cryogenic temperatures (e.g. −320°F), however, (8) shows that fabricated PTFE has mechanical properties similar to those for metals such as non-worked aluminum. PTFE does not show a brittle point at temperatures as low as 4°K (9).

More consistent and better results were obtained in this investigation than in previous studies (1) with PTFE compositions. Uniform and careful processing of molded materials and the use of extruded materials formed to the approximate size of the final specimens are believed to have been helpful in obtaining reproducible data. It is probable that further improvement in consistency of results could be gained by heat treatment to control crystallinity.

The data of this study show that extruded materials were generally more resistant to wear than molded compositions. In one specific case, a commercial composition was available in both extruded (10GR-E) and molded (10GR-M) forms; the extruded material had less than one-tenth the wear of the molded form (0.003 and 0.039×10^{-3} cu. in. per hr). Disregarding the influence of the fillers, it is of interest that pure PTFE in the extruded form gave about one-third as much wear (Fig. 8) as the same material in the molded form (Fig. 6). The greater wear resistance of extruded materials may be associated with crystal orientation effects or with low crystallinity of the PTFE in this form. As mentioned in (5) and (8), thermal histories of PTFE materials influence crystallinity and mechanical properties. Equivalent cooling rates give similar crystallinity in both molded and extruded materials (8). Detailed discussions of the relation between crystallinity and physical characteristics of PTFE are in (6) and (8). Many of the mechanical properties that may influence wear are affected by crystallinity. Low crystallinity can be obtained by shock cooling (5) such as might be expected in the extrusion of small sections. Studies of the influence of PTFE crystallinity on wear of these materials in liquid nitrogen would seem highly desirable. If low crystallinity is helpful as this discussion suggests, the use of PTFE in intermittent contact for cryogenic applications could be beneficial. In the present apparatus PTFE disks or PTFE coated disks would be subject to shock cooling by frictional heating and subsequent quenching in the cryogenic fluid as the surface of the disk wear track leaves sliding contact with the rider specimen.

Low friction is important to the successful use of PTFE materials at high sliding velocity. Poor thermal conductivity makes heat dissipation for the slider difficult, and thus it is important to generate as little frictional heat as possible even in a cryogenic fluid. Reference (10) shows that no filled PTFE compositions had friction lower than pure PTFE. This was the basis for selection of the low filler concentrations used in these studies. In most instances, within the range of filler concentrations employed (25% or less), there was little difference in friction coefficients for all the materials. None of the compositions gave friction that was significantly lower than the pure PTFE materials. In some instances glass- and metal-filled compositions gave slightly higher friction than other materials. Some abrasion of the transferred PTFE films on disks suggested that solid contact of glass particles with the disk metal may have contributed to the friction force.

The friction data of Fig. 14 showed that friction coefficient was not significantly affected by sliding velocity up to 7550 ft per min with 25GL-E. Only limited data for one composition are reported herein (Fig. 14) on the effect of load (W) on friction coefficient (f_k). A comprehensive survey on this factor over a wide range of loads is reported in (3) showing that friction coefficient $f_k = 0.178\ W^{-0.15}$ for pure PTFE. The friction coefficient in air for 1000 grams load with PTFE in (3) is the same (0.07) as that reported herein for the same load in liquid nitrogen.

The addition of fillers to PTFE compositions usually decreased wear in liquid nitrogen for molded materials. One exception was the molded composition containing 25% silver (Fig. 6). This result is consistent with experience reported in (11) where high wear of silver-filled PTFE was attributed to breakup of conglomerations of silver particles. The extruded compositions containing a MoS_2 filler, carbon type fillers or a glass fiber filler had very good resistance to wear under the conditions of these experiments. The glass-filled material probably provides higher strength and hardness than the carbon-filled material but may have the disadvantage of lower thermal conductivity. The lack of influence of sliding velocity up to 6000 ft per min on wear of the glass-filled material is worthy of special note. This composition should be studied over a wider range of experimental conditions.

Summary of results

The wear and friction of several experimental and commercial filled PTFE compositions were investigated in liquid nitrogen. Most of the data were obtained at a sliding velocity of 2300 ft per min and a load of 1000 grams with a PTFE hemisphere ($\frac{3}{16}$-in. rad.) sliding on the flat surface of a rotating disk (type 304 stainless steel). The following results were obtained:

1. In liquid nitrogen, filled PTFE compositions of various types gave low wear and friction (friction coefficients from 0.06 to 0.13) as compared with conventional bearing and seal materials. Several extruded compositions have particular promise for seal and bearing materials.

2. Two identical compositions were used in both molded and extruded forms. The extruded materials gave the lower wear. Method of forming had no significant influence on friction for the two materials. This was true in gaseous nitrogen at 160°F as well as in liquid nitrogen at −320°F. It is suggested that the lower wear for the extruded materials may have resulted from the improved mechanical properties that accompanied lower crystallinity. The thermal history of small extruded sections is favorable for obtaining low crystallinity.

3. Liquid nitrogen cannot be considered as an effective boundary lubricant. It does, however, serve as an effective heat sink for frictional energy. This is particularly important to PTFE compositions because low thermal conductivity makes dissipation of heat relatively difficult. Failure of PTFE in slider applications usually results in thermal softening. One composition that showed promise in other experiments had a wear rate that was essentially unaffected by sliding velocities up to 6000 ft per min.

REFERENCES

1. WISANDER, D. W., HADY, W. F., and JOHNSON, R. L., "Friction Studies of Various Materials in Liquid Nitrogen," NACA TN 4211, 1958.

2. SIMON, I., MCMAHON, H. O., and BOWEN, R. J., "Dry Metallic Friction as a Function of Temperature Between 4.2° and 600°K," *J. Appl. Phys.*, v. 22, n. 2, Feb. 1951, pp. 177–184.

3. ALLAN, A. J. G., "Plastics as Solid Lubricants and Bearings," *Lubrication Engineering*, v. 14, n. 5, May 1958, pp. 211–215.

4. KULIN, S. A. and COHEN, MORRIS, "The Martensite Transformation at Temperatures Approaching Absolute Zero," *J. Metals Trans.*, v. 188, 1950, pp. 1139–1143.

5. DOBAN, R. C., SPERATI, C. A., and SANDT, B. W., "The Physical Properties of 'Teflon' Polytetrafluoroethylene," *J. Soc. Plastics Engrs.*, v. 11, n. 9, Nov. 1955.

6. THOMAS, P. E., LONTZ, J. F., SPERATI, C. A., and MCPHERSON, J. L., "Effects of Fabrication on the Properties of Teflon Resin," *J. Soc. Plastics Engrs.*, v. 12, n. 6, June 1956.

7. JOHNSON, R. L., SWIKERT, M. A., and BISSON, E. E., "The Lubrication Characteristics of Synthetic Lubricants at High Sliding Velocities," *Lubrication Engineering*, June 1953, pp. 144–149.

8. ANON., "Mechanical Properties of TEFLON at High and Low Temperatures," Dupont Polychemicals Department Booklet A-6659, March 1958.

9. CORRUCCINI, R. J., "Properties of Materials at Low Temperatures," *Chem. Engng. Prog.*, August 1957, v. 53, n. 8, pp. 397–402.

10. TWISS, S. B., WILLSON, P. J., and SYDOR, E. J., "Friction of Polytetrafluoroethylene Dry Bearings, *Lubrication Engineering*, v. 14, n. 6, June 1958, p. 251.

11. WHITE, HUBART S., "Small Oil Free Bearings," *J. Res. Nat. Bur. Stds.*, v. 27, n. 4, Oct. 1956, pp. 185–204.

The Conduction of Current in Bearings

By H. N. KAUFMAN[1] and J. BOYD[2]

Introduction

In spite of general agreement that it is not good for bearings to carry current, there are many instances in which they are called upon to do so. In some cases, they are expected to carry current since they act as part of an electrical circuit as in the trolley wheel of a streetcar. In other cases, bearings carry current because they operate under conditions which unintentially subject them to various sources of electrical potential. An example of this would be the bearing on a motor with a grounded rotor.

The magnitude of the currents involved varies over wide limits as does the damage which they cause to the bearings. However, large current does not necessarily mean large bearing damage, for a trolley wheel bearing can operate quite satisfactorily with currents of many amperes whereas a current of only one ampere may seriously damage a motor bearing.

The literature on the subject of bearing currents has repeatedly pointed out the harmful effects that can result. However, little has been written about the specific factors which influence bearing damage and how these factors are related, sometimes producing a negligible effect and sometimes resulting in catastrophic failure.

This paper presents the results of an investigation which was made to obtain a better understanding of the problems concerned with the conduction of current through bearings. Because of the somewhat random nature of the phenomena, the information gained is necessarily more qualitative than quantitative. Nevertheless, it indicates relationships which are useful in understanding the variables involved so that corrective steps may be taken to minimize damage. The results may also be of interest in the cases of commutation and spark machining.

Factors influencing bearing damage

Although other effects may also exist, the principal effect of bearing currents is the damage caused by arcing across the bearing and journal surfaces. High voltages are not necessary for arcing to take place and damage can occur at potentials well below one volt. The main consequence of arcing is the wear of the bearing and journal due to the removal of fused metals in the arc, but mechanical wear can be considerably accelerated by the roughening of the surfaces produced by arcing. An additional consequence is the deterioration of the lubricant produced by arcing and the contamination of the lubricant and the lubricating system by arc debris.

On the basis that damage due to bearing currents is primarily due to arcing, the factors which can be expected to influence the phenomena can be set down. These include the supply voltage, the resistance in the circuit, the oil film thickness, the bearing and journal materials and their surface finishes, the composition of the lubricant and the relative velocity between the journal and the bearing. The unit load on the bearing need not be included since its only effect is to influence the film thickness and this has already been specified.

While it is recognized that the composition of the bearing, the journal and the lubricant affect the phenomena, these factors were not studied specifically in this investigation. Since the project was mainly concerned with babbitt-lined journal bearings, tin base babbitt was used for the bearing material, carbon steel for the journal material and turbine oil for the lubricant. Other materials would probably give somewhat different results, but it is felt that the main trend of the conclusions would be the same.

Wear rate apparatus

Since it is inconvenient to measure wear-rates on an actual bearing, the special apparatus shown in Fig. 1 was

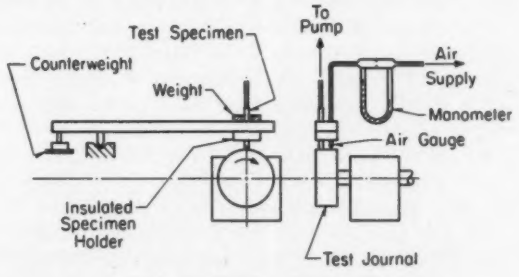

Fig. 1. Wear-rate apparatus.

set up. The specimen representing the bearing was an annular area of tin base babbitt with an I.D. of 0.187 in. and an O.D. of 0.250 in. (see Fig. 2). The specimen was held in an insulating holder attached to a lever supported by a knife edge. The specimen rested on the cylindrical surface of a steel disk which represented the journal. The disk was 7 in. in diameter and was mounted on precision ball bearings. It was ground in position on its own bearings and had a run-out of less than 0.1 mil. The load applied to the specimen was adjusted by weights which were

Presented as an American Society of Lubrication Engineers paper at the Lubrication Conference held in Los Angeles, Calif., October, 1958.

[1] Research Engineer, Westinghouse Research Labs., Churchill Borough, Pittsburgh 35, Penna.

[2] Manager, Bearings and Lubrication Section, Westinghouse Research Labs., Churchill Borough, Pittsburgh, 35, Penna.

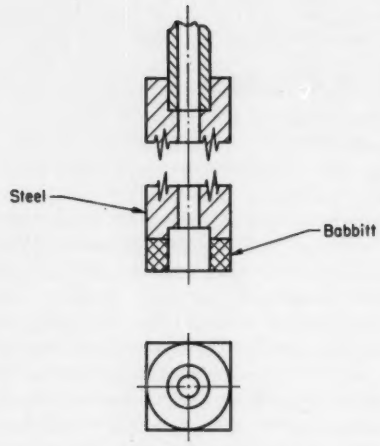

FIG. 2. Babbitt test specimen.

placed on the lever in such a manner as to be concentric with the specimen. This prevented bending of the lever or edge loading of the specimen. Tests were run with a unit load of 25 psi on the specimen.

The film thickness between the specimen and the disk was measured with an air gage consisting of a $\frac{1}{16}$-in. diameter nozzle in series with a 0.0515 in. diameter orifice. With a pressure of 50 psi applied, a movement of 0.1 mil of the nozzle gave a change of about 0.2 in. on a mercury manometer connected across the orifice. The nozzle was mounted on the lever beside the specimen so that the reading of the manometer was proportional to the length of the specimen. The air gage was calibrated against a dial gage graduated in 0.0001 in. divisions.

In order to control the film thickness with the desired degree of accuracy, the oil for the film was supplied to the center of the specimen and flowed outward over its annular surface. Attempting to control the film thickness by regulating the oil pressure supplied to the specimen would result in unstable operation since the pressure multiplied by the supported area must be in equilibrium with the load on the specimen which was held constant. To avoid this difficulty, the oil was supplied by a positive displacement pump whose speed could be varied to give controlled rates of flow and hence provide controlled film-thickness. Because of the low flow rates required, a special piston-type pump was constructed. The pump piston, which had a diameter of $\frac{3}{4}$ in. and a length of 6 in., was actuated by a screw which was connected to a variable speed drive.

Changes in film-thickness due to the specimen riding-up on the lubricant carried around by the shaft were eliminated by blowing the excess oil off the shaft with an air blast.

The electrical circuit for the apparatus is shown in Fig. 3. The voltage was supplied to the specimen by a transformer which had an auto-transformer in its primary circuit. This was done to avoid any change of resistance of the circuit with voltage. A copper–graphite brush riding on a copper slip-ring was used to pick up the current from the shaft. A variable resistance R, which will be referred to as

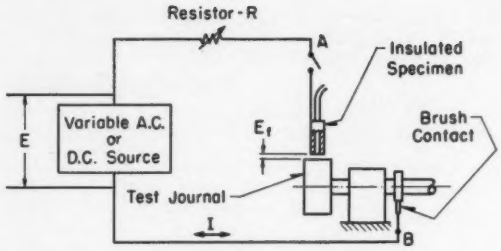

FIG. 3. Electrical circuit.

the external resistance in the circuit, was used to limit the current.

As used in this investigation, the term "supply voltage" will be defined as the voltage across points A and B before the switch was closed.

Conditioning of test specimens

In order to obtain consistent results, it was necessary to make sure that the babbitt specimens were properly conformed to the shaft diameter and that the shaft was reproducibly smooth before the start of each test. It turned out that the simplest method of doing this was to (a) pre-pit the specimen; (b) polish the shaft with 4/0 polishing paper; (c) flush the specimen and shaft clean; (d) wear-in the specimen to the shaft with high load and almost no oil film; and (e) again flush the specimen and shaft clean. With these precautions the wear-rate due to mechanical wear was essentially negligible for the test loads, and the wear-rates with current could be duplicated with reasonable accuracy considering the perverse nature of thin films and the difficulty of making electrical measurements under arcing conditions.

Because of the higher melting point of the shaft material and the much larger area of the shaft compared to the specimen, wear of the shaft was negligible. It was found possible to restore the shaft to its original smoothness by light application of 4/0 paper.

Pitting specimen apparatus

Since the wear-rate apparatus of Fig. 1 did not lend itself well to the preparation of specimens for pitting illustrations, the equipment shown in Fig. 4 was employed. In this

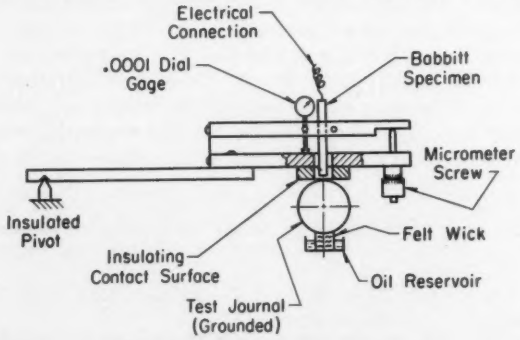

FIG. 4. Pitting specimen apparatus.

machine, a lever with an insulated contact surface rested on the test journal at one end and on an insulated pivot at the other. The journal had a diameter of 2.125 in. and was run at a speed of 1725 rpm. The bearing specimen which was a $\frac{3}{8}$-in. diameter rod of babbitt was held in a clamp so that it could be positioned at any desired distance from the test journal by adjustment of the micrometer screw. The end of the specimen was flat and not conformed to the journal as is the case of the apparatus of Fig. 1. A dial gage mounted as shown permitted measurements of the specimen setting and the specimen wear to be made.

Tests were conducted by first adjusting the specimen to a fixed distance above the journal (usually 0.1 mil), then turning on the voltage and allowing pitting to continue until the arc would no longer jump the gap. The gap thickness was then measured and the specimen photographed.

Wear rate curves

Typical wear-rate curve obtained with the apparatus of Fig. 1 is shown in Fig. 5. It was run at a fixed lubricant

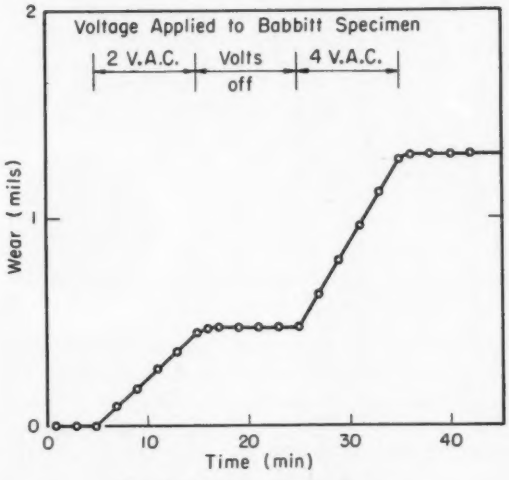

FIG. 5. Typical wear-rate curve.

flow-rate thus keeping the film-thickness constant. It will be seen that the wear-rate prior to the application of current was negligible but when 2 V a.c. was applied, the wear-rate abruptly increased to a readily measurable value which quickly became constant. When the current was interrupted the wear-rate again became negligible. When 4 V a.c. was applied, the wear-rate rose to a new constant value which was appreciably greater than that at 2 V.

Applying d.c. potential to the specimen produced the wear-rate curves shown in Fig. 6. It will be seen that wear-rate was approximately the same when the babbitt specimen was supplied with 2 V a.c. or 2 V d.c. positive. It will also be seen that when the specimen was supplied with 2 V d.c. negative, the wear-rate was considerably less than the positive value. The latter result

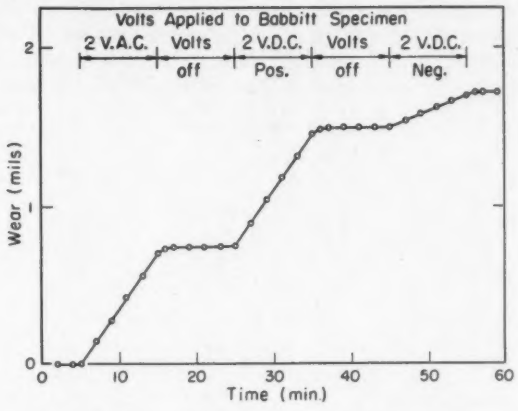

FIG. 6. Wear-rate curve for a.c. and d.c. voltages.

agrees with the usual experience on electrical brush wear but this phase of the investigation was not carried further since the main interest was on a.c. potentials.

Effect of sliding velocity

It was found early in the investigation that the wear-rate was zero if there was no sliding velocity. This indicates that motion is necessary to cause sustained pitting. It appears that small filaments of current start flowing when high points on the asperities of the journal come close to or contact similar points on the bearing or when conducting particles pass through the oil film. When these conducting paths are broken as the asperities become separated either by motion due to rotation, vibrational effects, or a combination of both, arcing results. Arcing will also result as conducting particles in the film are rearranged by relative motion of the parts.

At very low speeds (about 0.03 rpm) the wear-rate was also essentially zero. At 200 rpm, however, the wear-rate was considerable but it was not altered appreciably by increasing the speed to 1000 rpm. This would indicate that as long as a certain minimum speed is exceeded, wear-rate is not greatly affected by speed, provided, of course, that the film thickness and other factors are held constant. Unless otherwise noted, all of the tests in this investigation were run at 220 rpm (4400 in. per min.). Although speed did not greatly influence the wear-rate, it did have a marked effect on film thickness for a given flow rate. By keeping the speed the same throughout the tests, the influence on the flow was kept constant.

Typical test data

When the lubricant flow was shut off so that the film thickness was zero, it was found that the babbitt specimen readily conducted current, the amount conducted being directly proportional to the supply voltage. Although very large currents could be carried, the wear-rate under this condition was negligible.

As soon as there was a definite film-thickness, however, the situation was quite different, as shown by Figs. 7 and 8,

which show test results obtained at two different film-thicknesses and are typical of the many tests which were made. They indicate that when a film was present the current did not begin to flow until a certain threshold voltage was reached. Thereafter, the current increased approximately linearly with supply voltage. A study of many tests showed that the threshold value was proportional to the film-thickness.

The curves also indicate that when the supply voltage was less than the threshold value, the wear-rate was zero. When the voltage exceeded this value, the wear-rate increased with the supply voltage.

The voltage across the film and the corresponding film resistance as calculated from voltage and current measurements are shown in Figs. 7 and 8. It can be seen that the resistance across the film, which was quite high initially, rapidly fell to a low value as the supply voltage was increased.

Figure 9 shows how the wear-rate varies with film-thickness for different supply voltages. It is immediately apparent that for each supply voltage there is a film-thickness at which the wear-rate is a maximum.

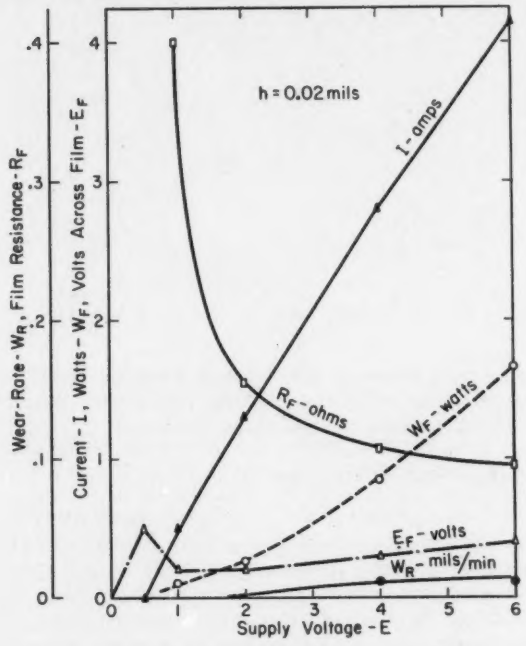
h = 0.02 mils
I - amps
R_F - ohms
W_F - watts
E_F - volts
W_R - mils/min
Wear-Rate - W_R, Film Resistance - R_F
Current - I, Watts - W_F, Volts Across Film - E_F
Supply Voltage - E

FIG. 7. Wear test data for film-thickness of 0.02 mils.

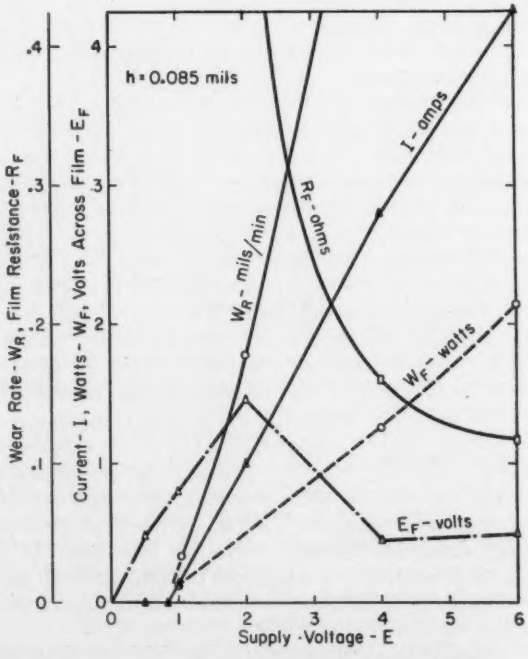
h = 0.085 mils
I - amps
W_R - mils/min
R_F - ohms
W_F - watts
E_F - volts
Wear Rate - W_R, Film Resistance - R_F
Current - I, Watts - W_F, Volts Across Film - E_F
Supply Voltage - E

FIG. 8. Wear test data for film-thickness of 0.085 mils.

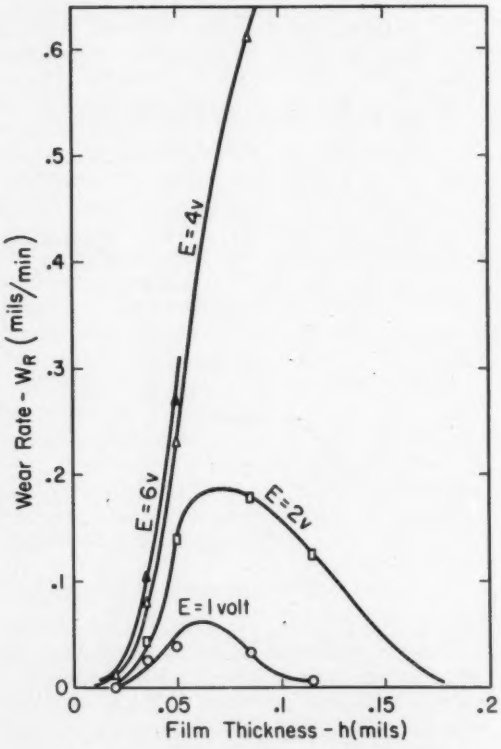

FIG. 9. Curves of wear-rate vs. Film-thickness for different voltages.

Generalizations with regard to the wear phenomena

The main relationships of the wear phenomena can be expressed in the following two equations which are developed in the appendix. The first is the equation for the current I which can be written

$$I = a(E-b) \qquad [1]$$

where E is the supply voltage, a a factor which depends on the circuit resistance, and b a factor which depends upon the film-thickness.

The second relation is the equation for the wear-rate W_r which can be stated

$$W_r = g(E-b)^p \qquad [2]$$

where p varies with the film-thickness and g depends on the film-thickness and the circuit resistance.

Both of these equations can be combined and the overall relations of the wear phenomena shown in three-dimensional plots which makes it possible to graphically represent the effect of the factors which influence the wear-rate.

Figure 10 shows how the wear-rate, the current and the supply voltage are related assuming that the external

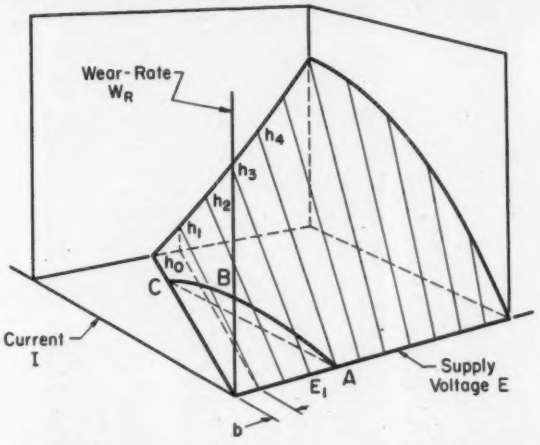

FIG. 10. Wear-rate as a function of current and supply voltage.

resistance R is constant. The lines h_0, h_1, h_2, etc., are lines of constant film-thickness with h_0 being the line for zero film-thickness. The point where each line intersects the E axis gives the term b in Eqs. [1] and [2].

It will be seen that the wear-rate is zero if the film-thickness is zero (line h_0). There is also no wear for any given film-thickness, say h_3, if the voltage is less than the value at which the line for the film-thickness intersects the E axis. For all values of the film-thickness less than h_3 there will be wear, the value of which depends upon the values of E_1, I and h.

If the figure is cut with a plane representing a constant value of E, the curve, ABC will result. The curve has a zero wear-rate at A and C and a maximum wear-rate at B. It is related to the constant E curves of Fig. 9 and the construction of Fig. 10 shows why maxima exist for the latter curves.

Figure 11 shows how the wear-rate varies with the film-thickness and the supply voltage assuming R to be constant. The lines of constant film-thickness are shown as h_0, h_1, h_2, etc., and again it will be seen that if there is no film-thickness (line h_0) there is no wear. There is also no wear if the supply voltage is lower than the value at which the line for the film-thickness intersects OA.

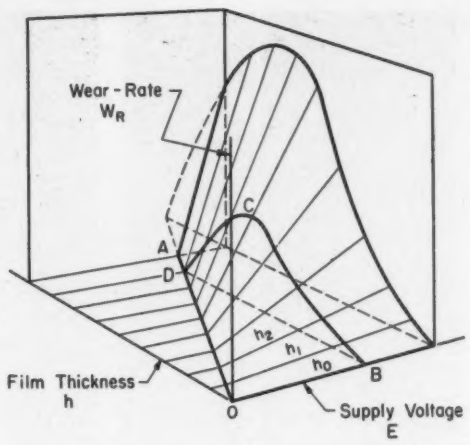

FIG. 11. Wear-rate as a function of film-thickness and supply voltage.

A constant E plane placed on Fig. 11 gives the curve BCD and it will be recognized that this curve, when viewed looking from E toward O, is one of the family of curves in Fig. 9.

Generally speaking, increasing the external resistance R, decreases the wear-rate more or less proportionally throughout the diagram, but the relation is complicated somewhat by other factors, as is pointed out in the appendix.

As a result of the previous discussion, it is evident that there are three main ways of reducing wear from bearing currents. These are: (a) lowering or eliminating the supply voltage, (b) raising the external resistance, and (c) altering the film-thickness either by decreasing the film-thickness so as to operate in the neighborhood of point B, Fig. 11, or raising the film-thickness so as to operate in the neighborhood of point D. Since points C and D may be difficult to evaluate in an actual case, one should either make large changes in film-thickness to be sure of avoiding the maximum wear region or should be prepared to cut and try until an improved condition is obtained.

Pitting specimens

Several series of pitting specimens were run on the apparatus of Fig. 4 to provide a visual reference for comparing examples of pitting damage. Figure 12 shows one such series with the supply voltage ranging from 1 to 20 V a.c. and with the external resistance set at 1 Ω. As previously mentioned, the test was run by setting the film-thickness at 0.1 mils and turning on the voltage and allowing the pitting to proceed and the film-thickness to increase until the arc would no longer bridge the gap. The supply voltage and the starting current are indicated on the figure. It will be seen that the size of the pattern also increased with voltage. The latter effect might be different in an actual bearing, however, since the test specimen was a flat surface in contact with a cylinder whereas the bearing would involve two cylinders.

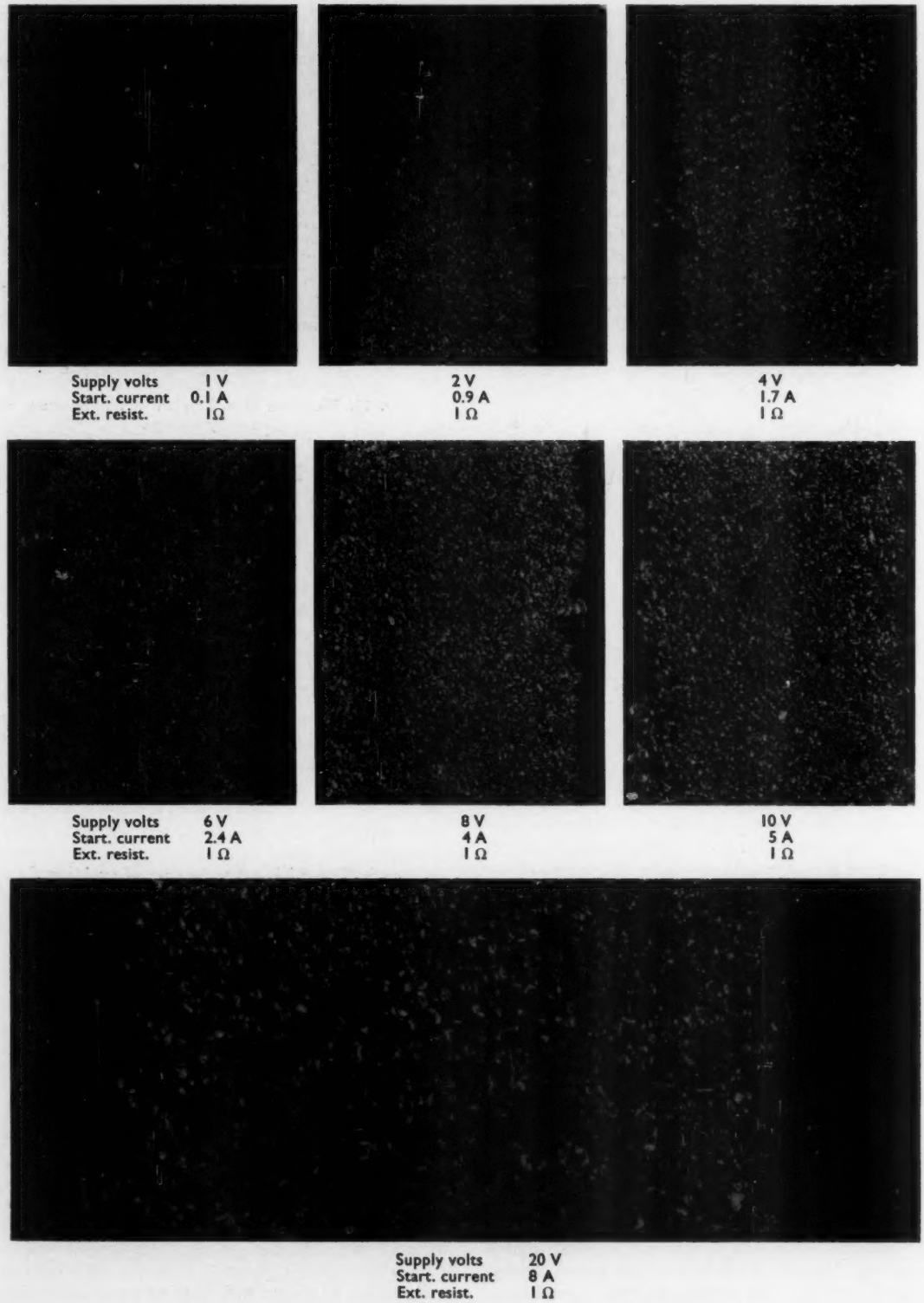

FIG. 12. Relative pitting damage on Babbitt at various voltages, ×25.

In general, the journal surface was much less damaged due to pitting than the babbitt surface. This is as might be supposed considering the greater area and the higher melting point of the former. Figure 13 shows the relative pitting of the journal at 6 and at 20 V a.c. While the pitting removed material from the journal surface, a more serious effect was the roughening produced by the built up debris. This roughening greatly increases mechanical wear which occurs in the absence of a film or under conditions of boundary lubrication.

That the supply voltage alone does not define the extent of pitting is evident from Fig. 14. Here it will be seen that increasing the external resistance from 1 to 8 Ω considerably reduced the pitting.

That the current alone does not define the extent of pitting is shown by Fig. 15. In this case, both specimens carried an initial current of 1.7 A but the pitting with 40 V and 25 Ω was much more severe than the pitting with 4 V and 1 Ω. The greater pitting should occur in the first case may be expected on the basis of greater average film-thickness (0.15 mil final film-thickness at 4 V, 0.75 mil thickness at 40 V).

That watts alone (i.e. watts dissipated within the film) do not define the extent of pitting may be deduced from

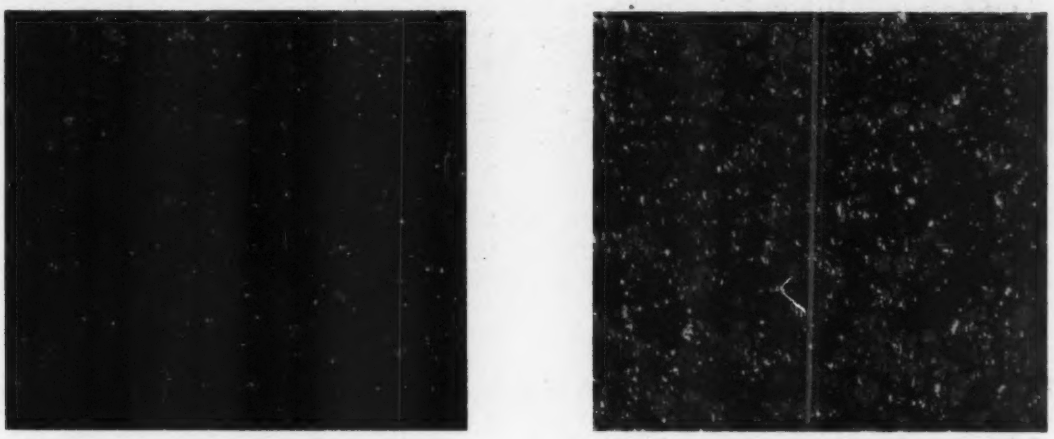

Supply volts	6 V	20 V
Start. current	2.7 A	7.5 A
Ext. resist.	1 Ω	1 Ω

FIG. 13. Relative pitting damage on steel journal at different voltages, ×25.

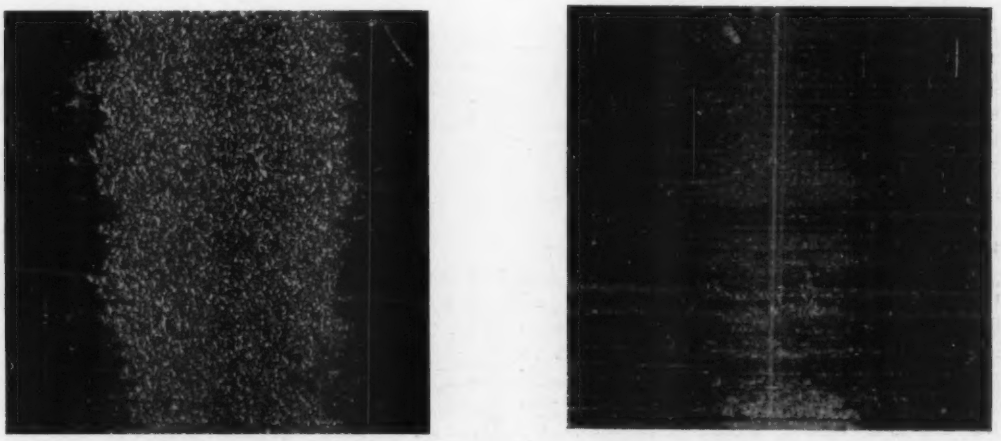

Supply volts	6 V	6 V
Start. current	3.25 A	0.35 A
Ext. resist.	1 Ω	8 Ω

FIG. 14. Relative pitting damage at constant supply voltage and different external resistances, ×25.

Figs. 7 and 8 which show that although the watts (as calculated from volts × amps) were not greatly different, the wear-rate for a film-thickness of 0.085 mils was much greater than the wear-rate for a film-thickness of 0.02 mils.

The effect upon pitting caused by positive and negative polarities of d.c. voltages is shown in Fig. 16. The figure indicates that larger pits were formed with positive polarity than with negative polarity.

To obtain pitting specimens at high voltages, an insulation tester with a circuit resistance of one megohm was employed. This was used for the tests at 1000 and 10,000 V d.c. shown in Fig. 17. Since the wear-rate was quite small because of the low current, the high-voltage tests were stopped after two minutes rather than being allowed to run until the voltage was no longer able to bridge the gap. Although the high external resistance greatly limited the extent of pitting, it will be seen that the pitting increased with voltage at constant film-thickness and increased with film-thickness at constant voltage as was the case for lower voltages. It will also be noted that at the higher film-thickness the arcing tended to concentrate at certain points producing fairly large pits.

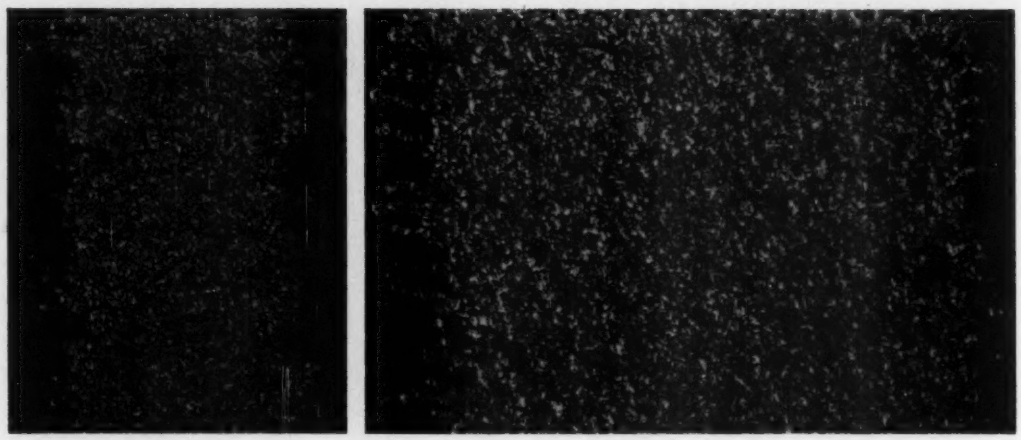

Supply volts	4 V	40 V
Start. current	1.7 A	1.7 A
Ext. resist.	1 Ω	25 Ω
Final film-thick.	0.15 mils	0.75 mils

FIG. 15. Relative pitting damage at constant current and different voltages and external resistances, ×25.

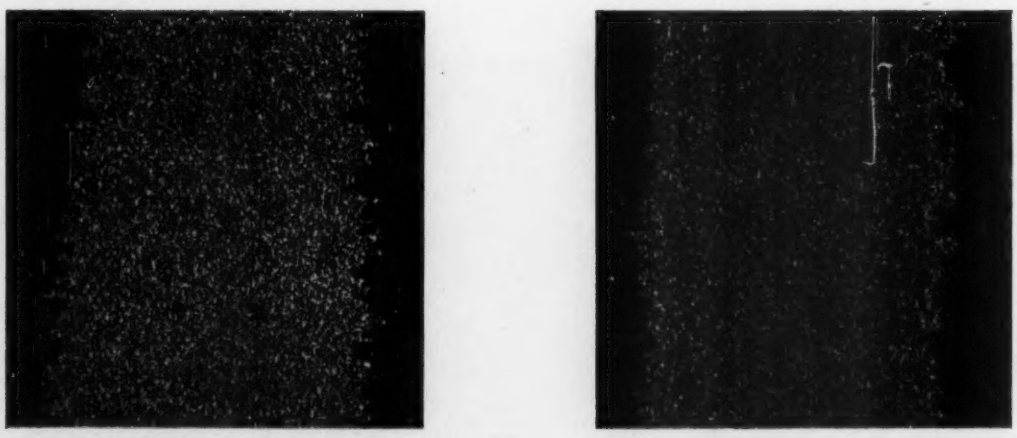

Supply volts	6 V d.c.	6 V d.c.
Babbitt polarity	Pos.	Neg.
Start. current	3.3 A	4.1 A
Ext. resist.	1 Ω	1 Ω

FIG. 16. Relative pitting damage at different babbitt polarities, ×25.

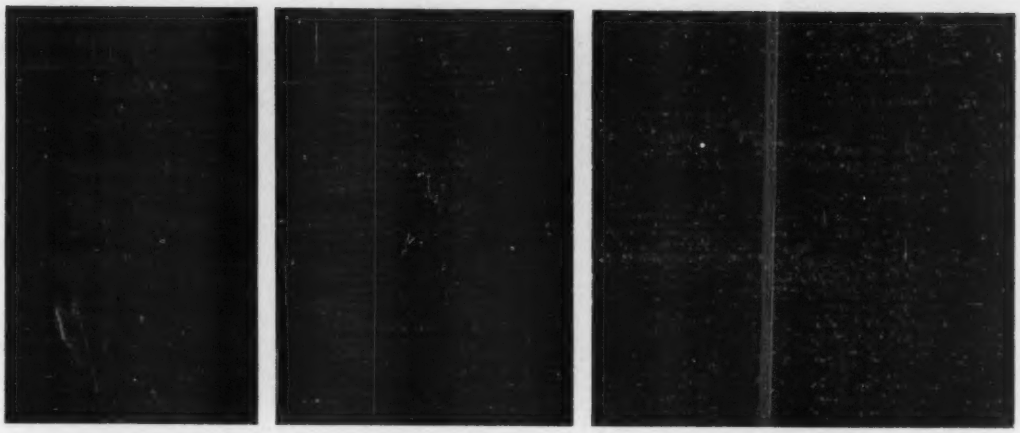

Supply volts	1000 V	10,000 V	10,000 V
Start. current	9 μA	90 μA	12 μA
Ext. resist.	1 megohm	1 megohm	1 megohm
Film-thick. (Initial)	0.1 mil	0.1 mil	1 mil

FIG. 17. Relative pitting damage at high supply voltages and different film-thicknesses, $\times 25$.

Effect of film-thickness on voltage at which arcing ceases

The effect of the film-thickness on the voltage at which arcing will no longer take place was determined from the pitting tests. The results are plotted in Fig. 18 which shows

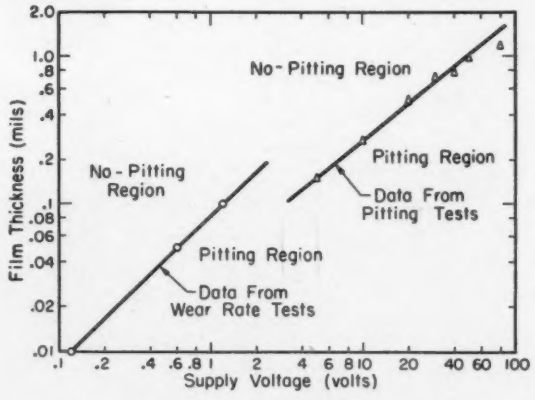

FIG. 18. Voltage necessary to produce pitting vs. Film thickness at which pitting will occur.

how large the film-thickness has to be to prevent arcing at various voltages or how much voltage is necessary to cause arcing at various film-thicknesses. The values given will not necessarily be quantitatively valid for actual bearings, however, because of differences in geometry, etc. It will be observed that the data from the wear-rate tests can also be placed on the same plot. That the curve is not continuous is attributed largely to different specimen geometry.

Visual evidence of pitting

Since pitting is an arc phenomena, visual sparking might be expected to provide a clue as to whether pitting is present and, if so, what its magnitude might be. From the tests it was observed that when there was no pitting wear there was no sparking. Sparking was found to increase in intensity with voltage and the film-thickness which was being bridged. At high voltages with high external resistance sparking was quite pronounced but the wear-rate was quite low.

Conclusions

The investigation has shown that the wear-rate due to electrical pitting is not a function of any single factor such as voltage, current, or wattage, but is dependent on a combination of many factors including the voltage, the circuit resistance, and the film-thickness.

If the film-thickness is zero, the current is proportional to the voltage and large currents can be carried at negligible wear-rates.

If the film-thickness is not zero but has some value, say h_n, there is a threshold value of the voltage below which current will not flow and below which there will be no wear. The threshold value of the voltage is related to the film-thickness.

Wear will take place for all values of the film-thickness between zero and h_n at all voltages greater than the threshold value at h_n. The amount which will occur will depend upon the values of E, R, and h.

For each supply voltage there is a value of the film-thickness for which the wear-rate is a maximum.

Wear from bearing currents can be reduced in three main ways: (a) lowering or eliminating the supply voltage,

(b) raising the circuit resistance, and (c) altering the film-thickness, either by increasing it to the point where the current will no longer bridge the gap or decreasing it to very low film-thicknesses.

BIBLIOGRAPHY

While the text makes no reference to specific prior literature on the subject of bearing currents, the following references are listed for those who may wish to study the matter at greater length.

1. ALGER, P. L. and SAMSON, H. W., "Shaft Currents in Electric Machines," *Trans. A.I.E.E.*, February 1924, v. 43, pp. 235–245.
2. PEARCE, C. T., "Bearing Currents—Their Origin and Prevention," *Electric J.*, August 1927, v. 24, pp. 372–376.
3. RIGGS, L. W., "How Much Shaft Current Can a Bearing Carry Safely?" *Power*, February 1944, pp. 103–105.
4. HOOVER, D. B., "Heating and Failure of Bearings Due to Little Appreciated Causes," *Water Works and Sewerage*, October 1945, v. 92, n. 10, pp. 297–299.
5. WILCOCK, D. F., "Bearing Wear Caused by Electric Current," *Electrical Manufacturing*, February 1949, pp. 108–111.
6. "Static Charges Might Cause Turbine Bearing Failures," *Power Engineering*, May 1954, v. 58, pp. 73–74.
7. RUDORFF, D. W., "Principles and Applications of Spark Machining," *Proc. Inst. Mech. Engrs.*, 1957, v. 171, n. 14, pp. 495–512.

APPENDIX

The equations presented in the text were derived from relationships observed in the test data. The following shows the manner in which the equations were developed.

Variation of current with voltage

If the inductance and the capacity of the circuit are negligible, as they are likely to be in many instances, the current can be expressed in terms of the supply voltage E, the external resistance R, and the film resistance R_f, by the ohmic relation:

$$I = \frac{E}{R+R_f} \qquad [1a]$$

Although R remained fixed as E varied, R_f changed over wide limits (see Figs. 7 and 8) being very high at low values of E and falling rapidly after some threshold value was reached. This can be shown by Fig. 19 where the line A represents the initial condition when R_f is large compared to R and the line B represents conditions after R_f has fallen to a value which is low compared to R. The threshold point, which is illustrated by point C, is a function of the film-thickness (but no doubt also varies with the surface finish and the quantity of contaminating or conducting particles in the oil). The curve OCF is drawn for a film-thickness h_1 and the curve ODG for a larger film-thickness, h_2.

For convenience in handling the test data and because of the wide variation of R_f, it was assumed that the curve OCF could be replaced by a straight line with the equation,

$$I = a(E-b) \qquad [2a]$$

where b is a function of the film-thickness, h, and a is a function mainly of the resistance R.

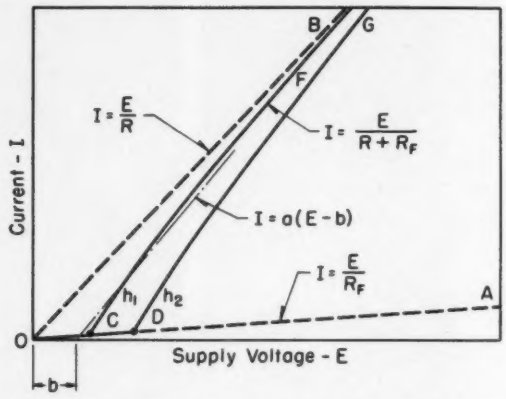

FIG. 19. Assumed form of curves of current vs. Supply voltage.

The intercept b was found to be related to the film-thickness by the relation

$$b = c\,h^n \qquad [3a]$$

where the values of c and n which fitted the test conditions were 12.0 and 1.0, respectively.

The slope a was not quite linear with R but varied according to the relation

$$a = \frac{d}{R^m} \qquad [4a]$$

The values of d and m for the test conditions were 0.73 and 0.8, respectively. It will be noted from the equations that if the film-thickness is kept constant, changing R changes the slope but not the intercept. Idealized curves representing Eq. [2] are shown in Fig. 20.

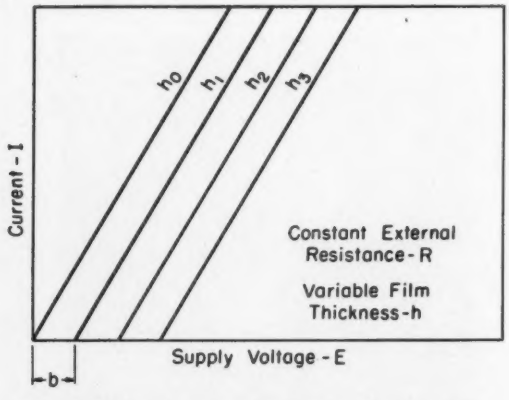

FIG. 20. Idealized curves of current vs. Supply voltage.

Variation of wear-rate with voltage

Figures 7 and 8 show that the wear-rate increased with E for different values of the film-thickness and had an intercept on the E axis. Since there can be no wear if there is no current, it will be assumed that the intercept for the

wear-rate curve is the same as for the I vs. E curve having the same film-thickness. A survey of many curves like those of Figs. 7 and 8 indicated that the wear-rate W_R can be approximated by a relation of the form

$$W_R = g(E-b)^p \qquad [5a]$$

where p varies in a somewhat complicated manner with h, and g is a function of h and R of the form

$$g = \frac{kh^l}{R^q} \qquad [6a]$$

The terms k, l and q were more or less constant but p varied from 0.5 at low film-thicknesses to 2.5 at the high film-thicknesses. Idealized curves representing Eq. [5a] are shown in Fig. 21.

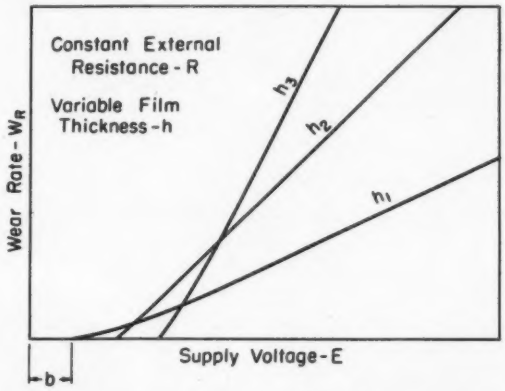

FIG. 21. Idealized curves of wear-rate vs. Supply voltage.

The relation between W_R, I, h and R

One might expect that the wear-rate for a given film-thickness would depend upon the current and would not be influenced by the manner in which the current was obtained (i.e. by adjusting the supply voltage and the resistance in the circuit). This was true for the test conditions at low values of the film-thickness but was not true for the higher film-thickness as can be deduced from Fig. 22. It will be noted that a current of one ampere, for

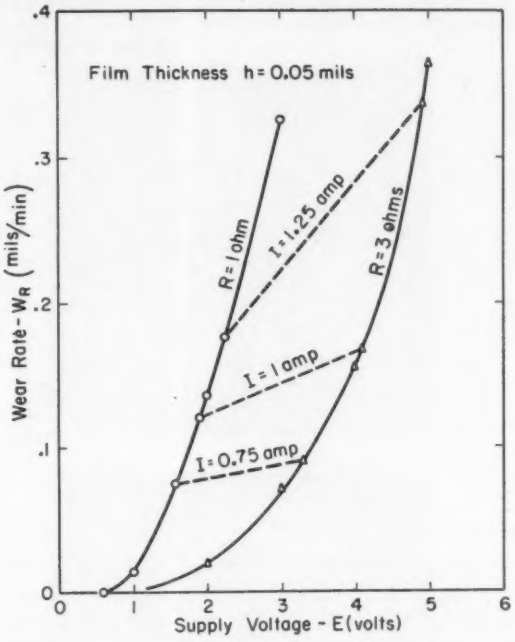

FIG. 22. Wear-rate vs. Supply voltage showing lines of constant current.

example, produced a greater wear-rate for the test with $R = 3\ \Omega$ than for the test with $R = 1\ \Omega$. That this can be the case can be deduced qualitatively from the equations which have been presented by substituting Eqs. [2a], [4a] and [6a] in Eq. [5a] giving

$$W_R = \text{const}\, h\, R^{(pm-q)} I^p \qquad [7a]$$

From this it can be seen that if $pm = q$ the wear-rate, at constant I, is independent of R. If $pm > q$ the wear-rate, at constant I, increases with R.

A Surface Effect Associated with the Use of Oils Containing Zinc Dialkyl Dithiophosphate

PAUL A. BENNETT[1]

It is shown that the operation of engines on crankcase oils containing appreciable amounts of zinc dialkyl dithiophosphate can increase the small-scale roughness of the lifter-foot surfaces. In addition, the small-scale roughness can be reduced by subsequent operation of the same engine parts on oils containing no zinc dialkyl dithiophosphate. This change in roughness coincides with a change in reflectivity that can be detected visually.

A similar effect of the additive has been demonstrated in a bench test machine. The increase in roughness which accompanies the operation on the additive-treated oil occurs rapidly and is maintained to high contact loads although some smoothing may occur at high loads.

The evidence suggests that the change in roughness results from a reaction of additive decomposition products with the metal surface. The mechanism responsible, however, is not completely understood.

Introduction

ALTHOUGH zinc dialkyl dithiophosphate additives are widely used as antiscuff agents in automotive engine lubricants, little has been published concerning the mechanism of action of these materials. It would seem, however, that the most probable mechanism may parallel that established for other phosphorus, chlorine, and sulfur (1, 2, 3, 4) compounds; namely, that under suitable temperature conditions additive or additive decomposition products react with the metal to form a tenacious solid film which reduces surface damage under boundary lubrication conditions. This mechanism of action of "extreme pressure" lubricants can reconcile such apparently contradictory observations as reduced scuffing and wear under some conditions (5, 6) and increased wear in others (7, 8).

Some recent publications have furnished evidence that the zinc dialkyl dithiophosphates do react with metal surfaces. For example, the retention of zinc and phosphorus (9, 10) on metal surfaces following tests using zinc dialkyl dithiophosphate additives has shown that these materials are attached to the surface in such a manner that they could not be removed by mild abrasion, solvents, or other treatments. These results further indicate that some chemical combination of the additive and the surface is involved.

Thus, although the mechanism is not completely understood, it is generally accepted that the surface effects of the additive are important factors. This paper presents the results of studies of a surface effect associated with the use of a commercial zinc dialkyl dithiophosphate additive.

Presented as an American Society of Lubrication Engineers paper at the Lubrication Conference held in Los Angeles, Calif., October, 1958.

[1] Supervisor, Tests and Operations, Fuels and Lubricants Department, Research Staff, General Motors Corp., Detroit 2, Michigan.

Equipment and procedures

The engine wear tests were conducted at no load, 1000 rpm, in a popular make 1954 6-cylinder engine at normal valve spring loads and jacket water temperatures of 170°F. Production unlubrited hardened alloy cast iron (HCI) and special lubrited[2] 5120 steel valve lifters were used on a production lubrited HCI cam.

The bench tests were conducted using the General Motors Tappet Test Machine (12). The camshafts and valve lifters were production 1954 and 1955 V-8 engine parts. Lubrited steel and both lubrited and unlubrited HCI valve lifters were used on an unlubrited HCI cam. The cam speed was held constant at 1250 rpm and the lubricant flow rate was set at 2 drops per sec.

The lifters were washed in a solvent consisting of a mixture of equal parts of chloroform, acetone, and toluene prior to weighing or taking microinterferograms.

Grube and Rouze (13) have described the principle of operation of an interference microscope which is similar to the instrument used in this work. The instrument is basically an optical microscope with a beam-splitting prism between the light source and the ocular. The light beam is divided into two parts, one part being reflected from the surface to be examined and the other reflected from a mirror. The light beams are brought together and viewed simultaneously through the ocular. When the path traveled by the two beams differs in length by multiples of half wavelengths, interference fringes are seen in the image. Any deviation of these fringes from straight lines indicates an irregularity or lack of flatness in the surface. The particular instrument used will also serve as an ordinary light microscope.

Figure 1 is a microinterferogram of a smooth surface containing a scratch and a hole. The surface had been

[2] A wear-resistant phosphate coating, see reference (11).

polished on a six micron diamond wheel and the relatively straight fringes are characteristic of relatively smooth surfaces. The dark bands are essentially profiles of the surface being viewed. A variation of a fringe from a straight line is an indication of a surface irregularity. A deflection of one band interval corresponds to a change in elevation of one half the wavelength of the light used as the source. For the work reported in this paper, a thallium lamp was used as the light source and one band interval corresponds to a 0.27 micron change in elevation. A "contour map" effect is visible in the hole shown in Fig. 1.

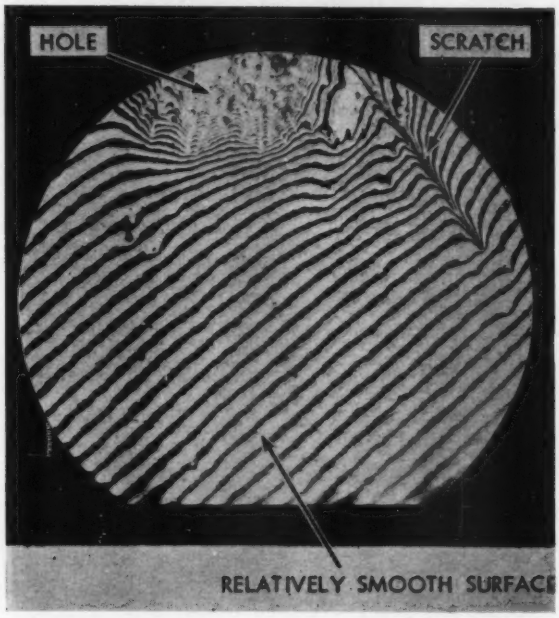

FIG. 1. Microinterferogram of a polished steel surface. The straight fringes are indications of a relatively smooth surface. A deflection of one fringe interval corresponds to a 0.27 micron (0.0000106 in.) change in elevation.

Where a series of interferograms was made of a given lifter, an effort was made to view the same area for each succeeding record. This was done as follows: during the preparation of a lifter for test a Rockwell impression was made on the lifter foot surface. This impression was used as a "landmark" in locating a particular area for study. The lifter was oriented on the microscope so that the Rockwell impression was visible on the edge of the circular area viewed by the microscope at the lowest magnification of the instrument as shown in Fig. 2(a). At this low magnification the microscope viewed an area on the lifter surface about 2.1 mm in diameter. The magnification was then increased to the highest setting attainable. At this setting the area viewed was a circle about 0.35 mm in diameter as shown in Fig. 2(b). The interferogram of this area was then obtained as shown in Fig. 2(c). Except as indicated in the figures, all the interferograms were obtained at this high magnification.

The micrograms of Fig. 2 show very dramatically the numerous pits on the surface. In addition, a few scratches are apparent in Fig. 2(b). However, the nature of the rubbing surface is not as well defined in Fig. 2(b) as in Fig. 2(c). The microinterferogram not only provides an indication of the general contour of the contacting areas,

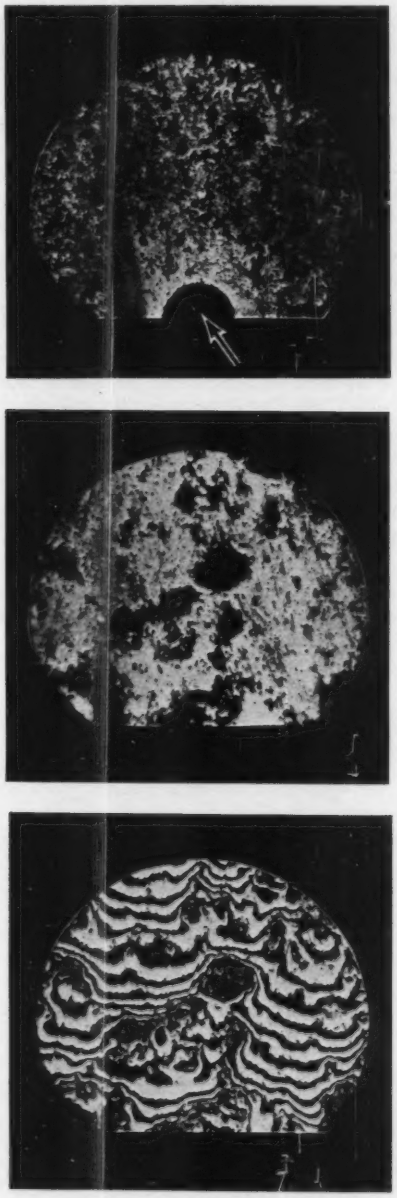

FIG. 2. Valve lifter orientation on microscope. The valve lifter was located on the microscope using the Rockwell impression as a "landmark" as in picture (a). The magnification was increased as in picture (b) and the interferogram (c) taken.

(a) Low magnification (actual area 2.1 mm in dia.) microgram of general area showing the Rockwell impression.
(b) High magnification (actual area 0.35 mm in dia.) microgram of central area of picture (a).
(c) Microinterferogram corresponding to picture (b).

but also emphasizes clearly the surface scratches. For example, the fringes indicate that the deeper scratches (far left, roughly vertical) are of the order of 0.1 micron deep.

Lubricants

Table 1 summarizes the oil inspection data for the lubricants used. Two of the lubricants were CRC reference oils that have been widely used in engine wear studies. Three of the oils were well-known commercial products, and one was a 10W solvent refined Mid-Continent 97 VI mineral oil. The remainder was blended specially for this work.

The special blends were usually mixtures of the mineral oil blended with 5% of a commercial detergent-inhibitor additive package and/or 1% of a commercial zinc dialkyl dithiophosphate. The addition of 1% zinc dialkyl dithiophosphate in the special blends provided a metal content of 0.08% phosphorus and 0.09% zinc in the finished oil. In some cases, the same zinc additive was blended with the CRC reference oils.

In some of the bench tests the lubricants were diluted with kerosene. This dilution increased the wear rate and tended to exaggerate differences in performance of different lubricants. Dilution increased the surface contact temperatures as evidenced by the change in appearance of test parts run with a given cam-lifter load. Also, dilution may reduce the additive concentration below an effective level and, accordingly, result in a lack of correlation with full-scale engines. In general, kerosene dilution was used to exaggerate differences where it could be shown that similar trends were observable with the undiluted lubricant.

Results

Review of Some Bench and Engine Wear Test Results

Wide differences in the appearance of valve-lifter-foot surfaces have been observed among engine parts operated in various bench and engine wear tests. Engine parts operated on different lubricants may display a variety of hues, some of which seem to be associated with the lubricant used. In addition, some lubricants produce shiny surfaces whereas others result in relatively dull surfaces. This paper is concerned only with these differences in reflectivity.

The writer first observed differences in appearance of lifter-foot surfaces several years ago during an inspection of the results of a series of bench and engine tests. Figure 3 illustrates the difference in reflectivity that was observed

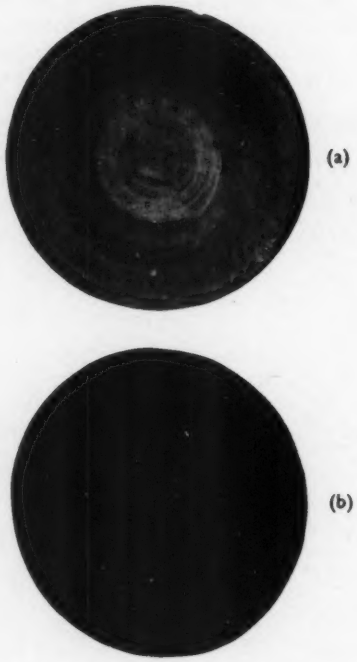

FIG. 3. Valve-lifter-foot surfaces. 1954 6-cylinder engine. 5120 steel lifters—1000 rpm.

(a) Direct photograph of a lifter-foot surface after 14 hr of operation with REO 131.

(b) Direct photograph of a lifter-foot surface after 8 hr of operation with REO 131 containing 1% zinc dialkyl dithiophosphate.

TABLE 1

Oil Inspection Data

Oil	Viscosity, SUS		Metal content, wt.%			
	100°F	210°F	Ba	Ca	P	Zn
REO 128 10W–30	338	62	0.7	—	—	—
REO 131 10W–30	322	60	0.6	—	—	—
Oil A, commercial 10W	193	48	0.8	—	0.09	0.10
Oil B, commercial 5W–20	170	50	0.5	0.05	0.08	0.04
Oil C, commercial 20–20W	325	57	0.7	—	0.07	0.07
Oil D, solvent refined Mid-Continent Mineral Oil, 10W	185	45	—	—	—	—
Oil E, Oil D plus 5% of a commercial detergent-inhibitor additive package	188	46	0.12	0.16	—	—

with different lubricants in engine tests. Figure 4 presents a comparison of the reflectivity of some HCI and 5120 steel lifter-foot surfaces after operation with several lubricants in the Tappet Test Machine. The differences in reflectivity are obvious on both the steel and HCI lifters. In general, the bench tests showed the greatest differences in reflectivity.

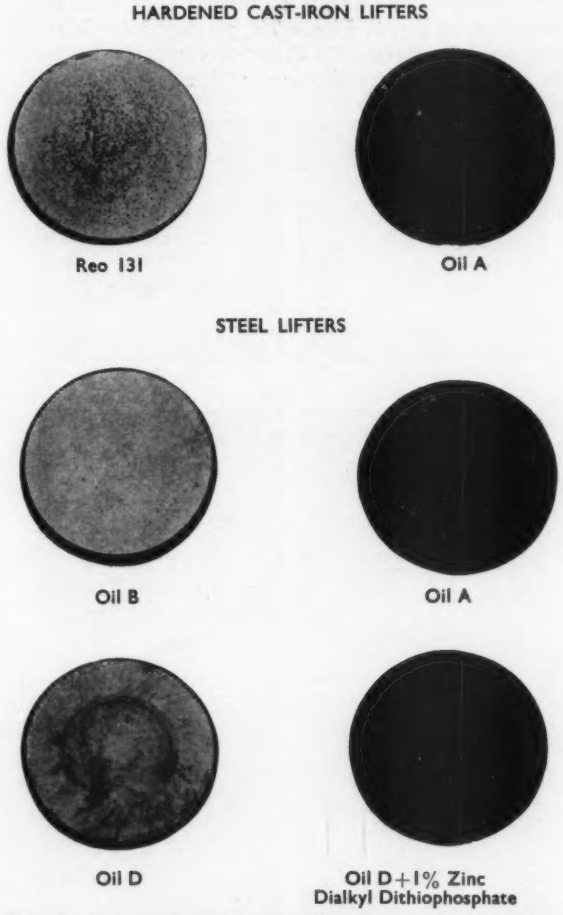

FIG. 4. A comparison of valve-lifter-foot surfaces (lubricant diluted 50/50 with kerosene) illustrating (1) difference in reflectivity observed with different oils, and (2) similarity of appearance of steel and hardened alloy cast-iron parts.

A comparison of the data of Figs. 3, 4, and 5 suggests that the oils which give relatively high wear rates may show the greater tendency to produce shiny lifter-foot surfaces. Compare, for example, Oil B with Oil A in Fig. 5. Inspection of parts operated on a number of oils from bench and engine tests confirmed this trend and indicated that lifters with dull, milky, non-reflective surfaces had been operated on oils resulting in low wear rates.

Further analysis of the oil inspection data suggested that the differences in appearance and rate of wear might correlate with the presence or absence of an appreciable amount of zinc dialkyl dithiophosphate in the lubricant. For example, it was observed that oils containing zinc dialkyl dithiophosphate were generally associated with the low wear-rate parts and resulted in relatively non-reflective lifter surfaces. On the other hand, high wear-rate lifters were associated with oils containing none, or at most, small amounts of the additive. This is illustrated by Fig. 3 and the two pictures of Fig. 4[8]. The results indicate that

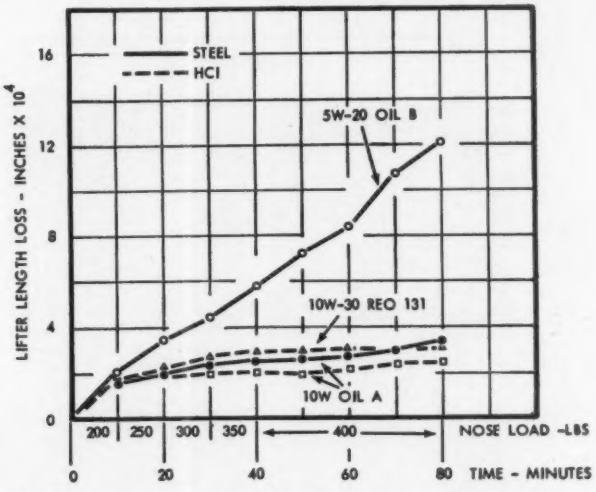

FIG. 5. A comparison of the bench test wear rates observed with four of the parts included in Fig. 4. All oils diluted 50/50 with kerosene.

the differences in reflectivity observed were in some way associated with the presence or absence of this additive.

In attempting to rationalize these observations it seemed that the differences in reflectivity of lifter-foot surfaces operated on different lubricants could be explained on the basis of a difference in surface roughness resulting from:

(a) A combination of an initially rough (lubrited) surface and differences in wear-rate,
(b) Some action of the additive which resulted in the non-uniform removal of material from the surface,
(c) Some combination of the additive or additive decomposition products with the surface resulting in a non-uniform addition of material to the surface,

or some combination of the above.

The relationship among lifter-foot appearance, wear-rate, and lubricant additive content appeared worthy of further study. The results of an investigation of the roughness of

[8] The lifter operated on Oil D (Fig. 4) was somewhat unusual in that the test was stopped at the point of incipient failure. The ring on the lifter surface had a "scorched" appearance under the microscope. The mass at about the 7 o'clock position is believed to be camshaft material which welded to the lifter-foot at failure. This observation is supported by the fact that this mass extended above the surrounding lifter-foot surface and, further, by the observed loss of metal from the cam.

hydraulic valve-lifter-foot surfaces as affected by the presence or absence of a commercial zinc dialkyl dithiophosphate is presented in the following sections.

Large-Scale Roughness

As mentioned above, it is possible that the observed differences in reflectivity could be due to differences in surface roughness. Accordingly, representative surface profiles of the steel lifters which had operated on Oils A and B (Figs. 4 and 5) are shown in Fig. 6.

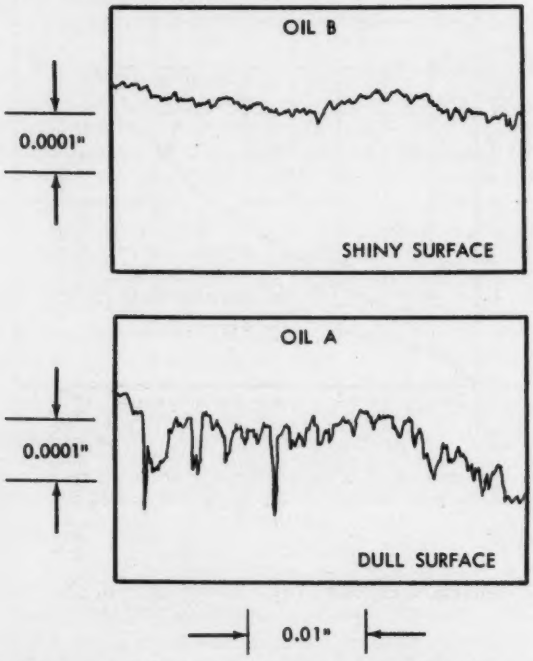

FIG. 6. A comparison of the relative surface roughness of the steel valve lifters run in the bench test (Figs. 4 and 5) with oils A and B.

The profilometer tracings indicate a definite difference in surface roughness for the two lifters. This could result from the difference in wear-rate observed for these oils in that a tracing of a new lubrited lifter indicated a roughness about five times that for the lifter after operation with Oil A. High wear-rate oils result in removal of sufficient metal to remove the pits resulting from the lubriting process with consequent improvement in smoothness of the surface. Thus, lifters operated with oils resulting in low wear rates would retain more of the original surface pits and explain the difference indicated by Fig. 6.

Differences in surface roughness of the type illustrated in Fig. 6 are referred to as "large-scale" in this paper. In general, the profilometer records are a measure of the hills and valleys of the surface which appear as the holes and plateaus of Fig. 2. The interference microscope provides a measure of what will be referred to as the "small-scale" roughness, which may be thought of as the relative roughness of the top of the plateau.

Engine Test Results

In the background work described up to this point it was observed that lifter-foot surfaces were dull after operation on oils containing zinc dialkyl dithiophosphate and shiny with non-zinc oils. In subsequent engine test work it was found possible to make a shiny reflective lifter surface dull by merely changing the lubricant from one resulting in high wear to a lubricant containing sufficient zinc dialkyl dithiophosphate additive to reduce the wear rate. This is illustrated in Fig. 7. Figure 7(a) presents microinterferograms of both steel and HCI lifter-foot surfaces after operation in an engine for six hours with a non-zinc oil. The

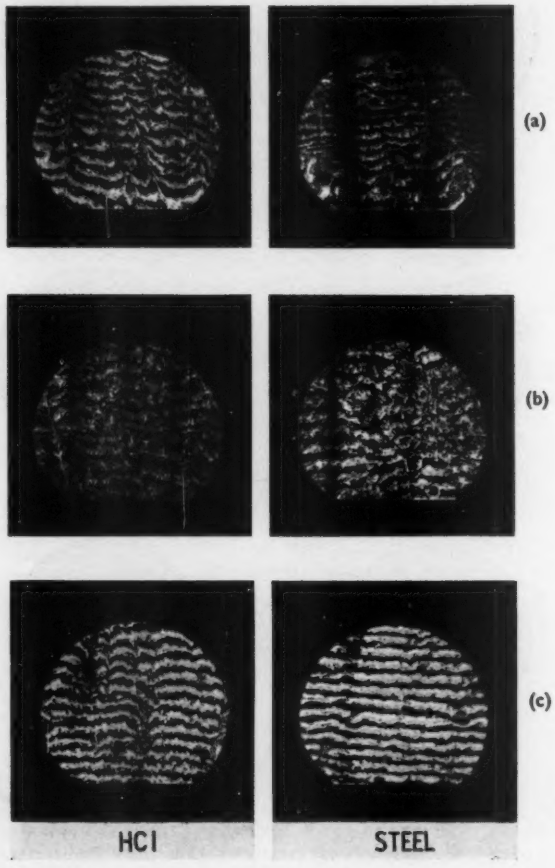

FIG. 7. Surface effect of zinc dialkyl dithiophosphate. 1954 6-cylinder engine, hardened alloy cast-iron and 5120 steel lifters.

(a) Lifter-foot surface after 6 hr operation on REO 128.

(b) After 8 hr of subsequent operation with REO 128 containing 1% zinc dialkyl dithiophosphate.

(c) After an additional 2 hr operation on REO 128.

surfaces were relatively reflective and the fringes reasonably well-defined for both lifter materials, indicating that the surfaces were relatively smooth. The dark vertical streaks on some of the microinterferograms are a peculiarity of the optical system of the instrument and should be ignored.

After a period of operation on the same lubricant containing zinc dialkyl dithiophosphate, the reflectivity of the surface was reduced and the fringes (Fig. 7b) broken up, indicating an increase in the small-scale roughness of the surface. While there are indications of an increase in roughness with both lifter materials this change is most definite with the steel lifter.

Figure 7(c) shows that after an additional two hours of operation on the non-zinc oil the surface has markedly improved in smoothness. Again, the change is most striking with the steel lifter with the final record indicating a possible improvement in smoothness over that of Fig. 7(a). While the roughness differences are small (Fig. 7a vs. 7c), inspection of a number of records indicates that the surface following removal of the small-scale roughness resulting from the use of zinc dialkyl dithiophosphate has fewer irregularities than the surface prior to the use of the additive.

Bench Test Results

Figure 7 has shown that the small-scale roughness of valve-lifter-foot surfaces is increased by operation of the part in an engine on an oil containing zinc dialkyl dithiophosphate, and this roughness is reduced by subsequent engine operation on an oil which does not contain this additive. This effect can also be demonstrated in the Tappet Test Machine as is illustrated by the data of Fig. 8.

The data of Fig. 8 were obtained using equal parts of mineral Oil D and kerosene as the base lubricant. A new cam and lifter were run-in ten minutes at each of a series of gradually increasing nose loads ranging from 160 to 260 lb in twenty-pound increments. Following the run-in, 1% of a commercial zinc dialkyl dithiophosphate additive was added to the Oil D–kerosene mixture and the parts run an additional fourteen ten-minute periods at 200 lb nose load. The lubricant was then changed to the zinc-free oil–kerosene mixture and the parts run for an additional eleven ten-minute periods at constant load.

A microinterferogram of the lifter-foot surface after run-in at 260 lb load with the non-zinc lubricant is shown at the top of Fig. 8. The surface was highly reflective and smooth as indicated by the straight fringes. The center pictures show that after ten minutes of operation with the additive-treated oil a considerable increase in small-scale roughness had occurred, and the surface roughness was relatively unchanged following additional operation. The lower pictures indicate that the small-scale roughness persisted for some time following the change to the non-additive oil. In this case, about 110 minutes of operation on the non-zinc oil were required to obtain a uniformly smooth and reflective surface. This smooth-rough-smooth cycle has been repeated several times on a given lifter.

Figure 8 has shown that the increase in roughness resulting from operation with a lubricant containing zinc dialkyl dithiophosphate persists for some time after changing to a non-zinc oil. As a check on the effect of higher loads on the small-scale roughness, tests were run with the results shown in Figs. 9 and 10. New cams and lifters were run in for ten minutes on Oil E at each of a series of gradually

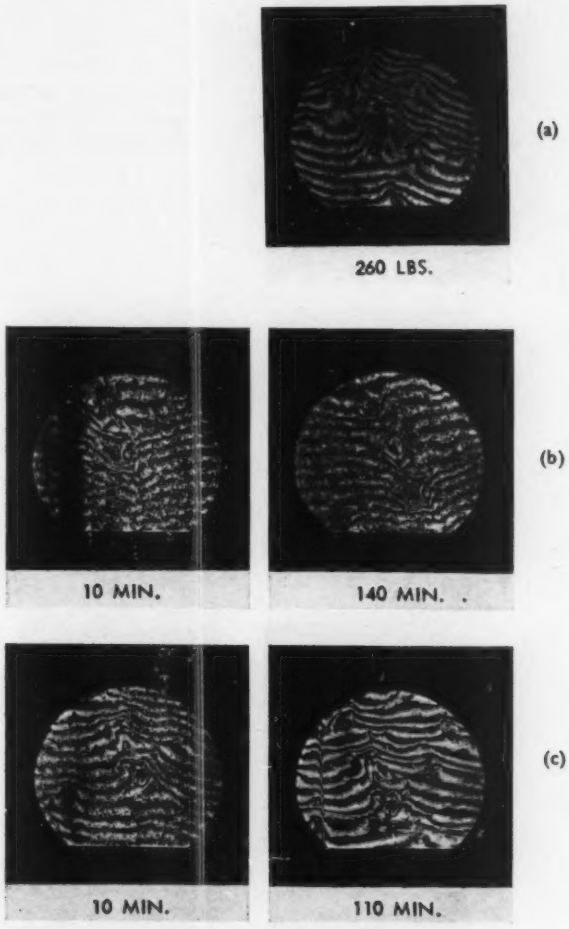

FIG. 8. Surface effect of zinc dialkyl dithiophosphate. (Bench test machine, steel lifter).

(a) Lifter-foot surface after a 60 min. run-in at gradually increasing loads. Base oil D diluted 50/50 with kerosene.

(b) After subsequent operation at 200 lb load with the oil D–kerosene lubricant containing 1% zinc dialkyl dithiophosphate.

(c) After additional operation at 200 lb load with the oil D–kerosene lubricant.

increasing loads ranging from 160 to 320 lb in twenty-pound increments. Following this run-in, 1% zinc dialkyl dithiophosphate was added to the lubricant and a second series of ten-minute runs made at loads ranging from 160 to 660 lb. Microinterferograms were taken after each twenty minutes of operation.

Figure 9 presents the results obtained using a steel valve lifter. An increase in small-scale roughness of the lifter-foot surface is apparent after 20 min of operation (after the 180-lb run) on the zinc-treated oil. The data indicate that the surface roughness changed little up to 500 lb while at higher loads some smoothing was observed. This smoothing

LIFTER-FOOT SURFACE AFTER A 90-MIN RUN-IN AT GRADUALLY INCREASING LOADS ON OIL E.

LIFTER-FOOT SURFACE AFTER SUBSEQUENT OPERATION AT GRADUALLY INCREASING LOADS ON OIL E CONTAINING 1% ZINC DIALKYL DITHIOPHOSPHATE

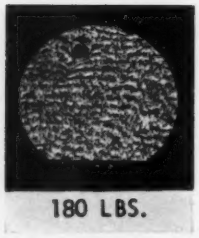

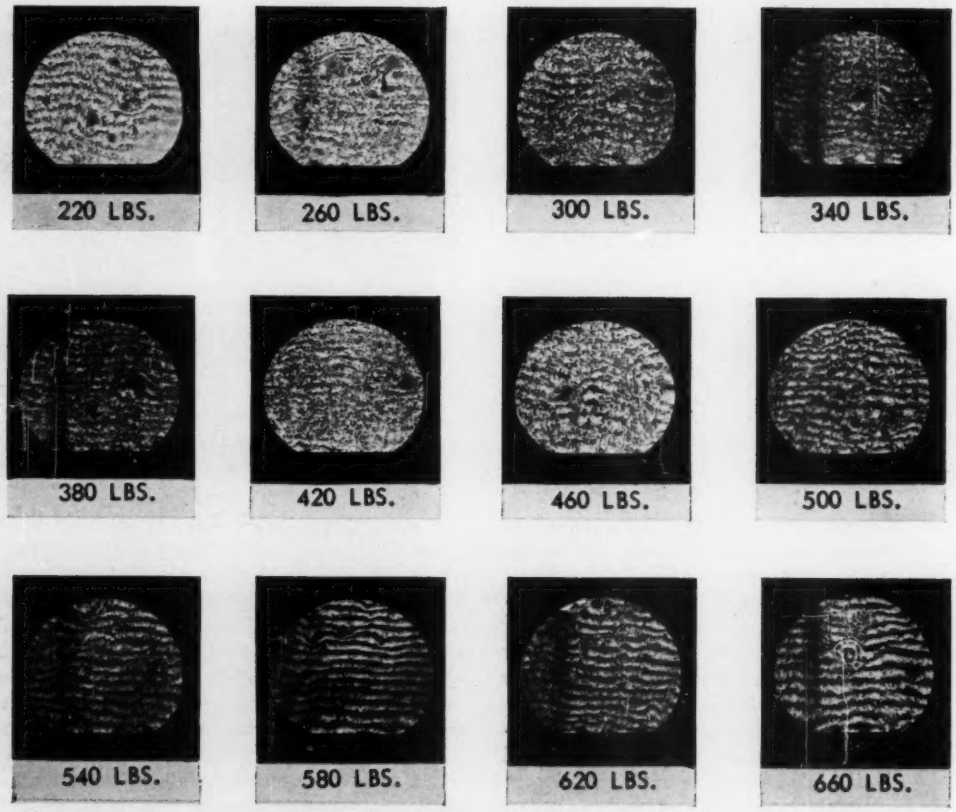

FIG. 9. Effect of load on lifter-foot surface microinterferogram. Bench test machine. Lubrited 5120 steel valve lifter.

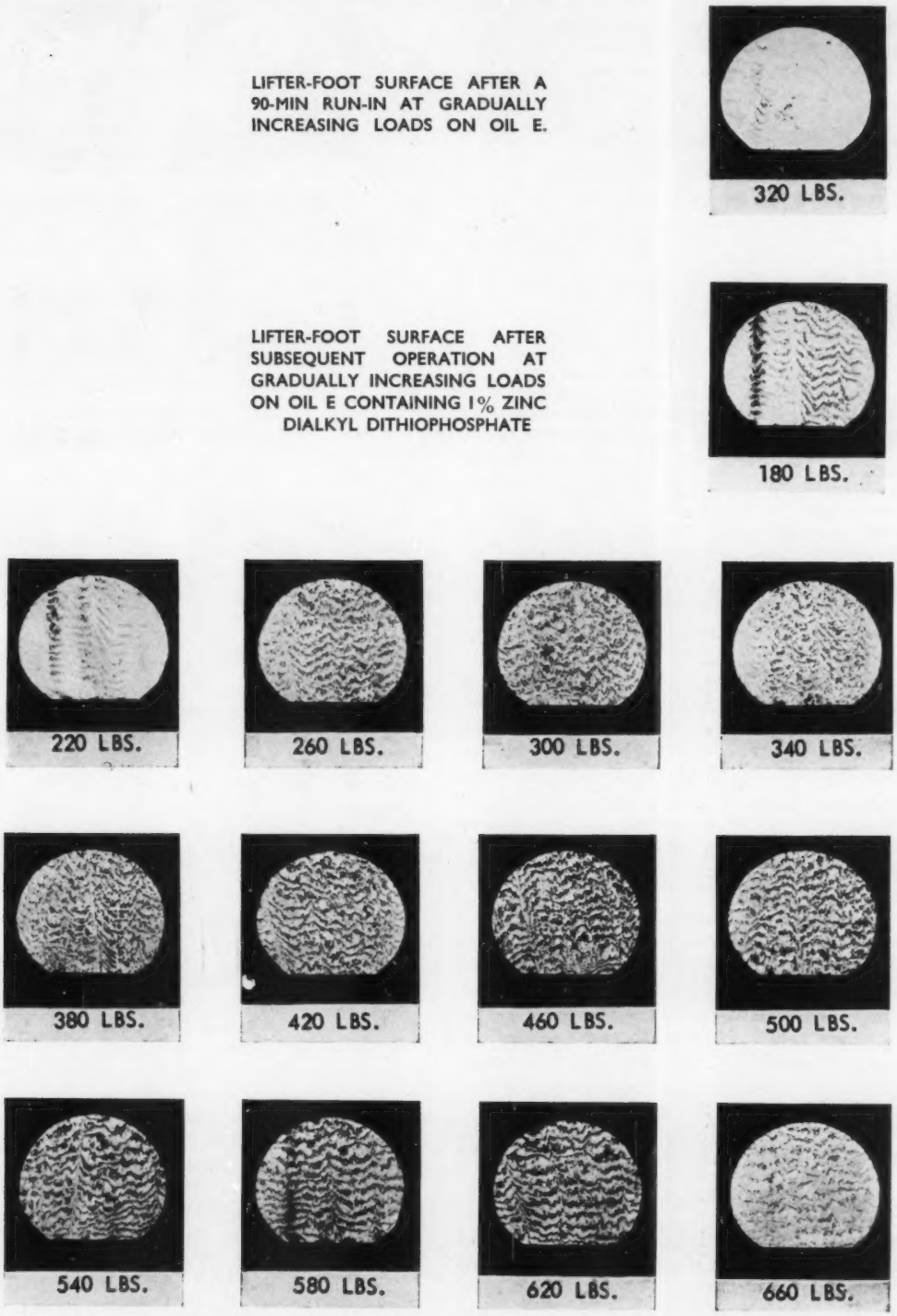

FIG. 10. Effect of load on lifter-foot surface microinterferogram. Bench test machine. Unlubrited hardened cast-iron valve lifter.

was somewhat irregular and suggestive of a random wiping away and re-establishment of the small-scale roughness. It was also observed that the wear-rate increased considerably as indicated by Table 2.

TABLE 2

Wear Rates Corresponding to Figure 9

Oil E with 1% zinc dialkyl dithiophosphate

Load, lb	Lifter wear-rate, mg/min.
200	0.004
300	0.008
400	0.013
500	0.019
600	0.062

Figure 10 presents results for an unlubrited HCI valve lifter comparable to the lubrited steel lifter data of Fig. 9. With the HCI valve lifter the increase in small-scale roughness is much more gradual. In addition, once a uniform finish was established (300–400 lb), the surface roughness did not change appreciably at high loads as contrasted with the results of Fig. 9.

Other General Observations

It has been shown that zinc dialkyl dithiophosphate can cause an increase in small-scale roughness of valve-lifter-foot surfaces in both bench and engine tests. However, this characteristic of the additive is not universally observed. Attempts to duplicate the data of Figs. 3 and 7 using a 1957 V-8 engine were unsuccessful. The lifter-foot surfaces differed only slightly in visual reflectivity when operated with non-zinc versus zinc-containing oils, and differences were not observed in the microinterferograms. In addition, both steel and HCI lifters may have highly reflective surfaces when run for 60–100 hr on zinc-treated oils in the 1954 6-cylinder engine.

In these latter cases the reflectivity of the parts was greater than that observed in the other work reported in this paper. Examples of this type of surface are shown in Fig. 11. The lifters shown in Fig. 11 were run in a 1957 V-8 engine using commercial Oil C, which contained a zinc dialkyl dithiophosphate additive similar to the one used in the work reported above. The engine was run on a dynamometer for 1000 hr at various speeds and loads. The foot surfaces of the lifters after this service were extremely reflective and very highly polished as is indicated by the records of Fig. 11.

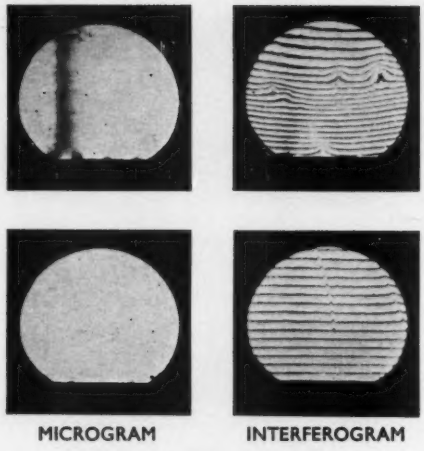

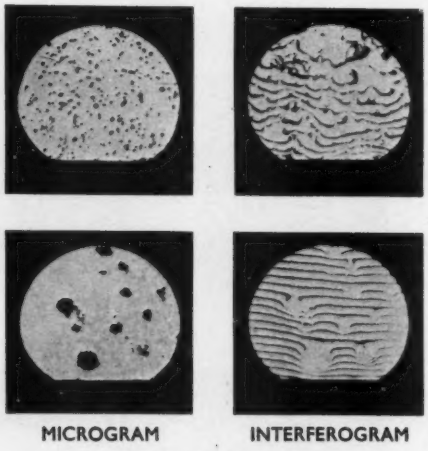

FIG. 11. Valve-lifter-foot surfaces. 1957 V-8 engine. 1000 hr of operation. Commercial oil C.

(a) 5120 steel valve-lifter-foot surface.
(b) Hardened alloy cast-iron valve-lifter-foot surface.

Discussion and summary

The literature (9, 10) has indicated that operation of engine parts on oils containing zinc dialkyl dithiophosphate additives results in the formation of chemically-combined films on metal surfaces. In addition, Loeser, Wiquist and Twiss (10) have reported that the phosphorus–zinc ratio in these films is a function of test temperature. This indicates that additive decomposition occurs and that competing reactions are taking place between the decomposition products and the surface. Thus, any change in the concentrations of the reactants, metallurgy, temperature, etc., would be expected to affect the kinetics of the system. This may account for the tendency of the additive to react more readily with the lubrited steel than the unlubrited HCI lifter-foot surface (Figs. 9 and 10).

The current work has established that the observed differences in lifter-foot reflectivity result from some action of the zinc dialkyl dithiophosphate additive (Figs. 7 and 8). Accordingly, it would seem that the changes in small-scale roughness observed could result from some combination of

additive decomposition products and the surface to form surface irregularities which can be detected by the interference microscope.

If the reaction of the additive and the surface results in a film which is not easily sheared or smeared, an appreciable amount of material may build up in areas of contact resulting in an increase in surface roughness. As this film builds up, the tendency for removal by normal wear processes increases. In addition, assuming that the additive has combined chemically with the surface, removal of the surface film would result in the removal of original surface material. This supposition is consistent with the observation (Fig. 9, Table 2) that high wear-rates accompanied the smoothing observed at loads above 500 lb.

Abowd (7) has reported that use of zinc dialkyl dithiophosphate additives can result in an increase in wear at high additive concentrations. Increased additive concentrations would be expected to increase the additive decomposition rate and the rate of formation of new film material. A high rate of film formation would also imply an increased rate of removal of film material by wear processes and accordingly an increase in metal removed from the surface.

The reduction in surface roughness observed after extended periods of operation may be partially explained on the basis of a gradual mating of the contacting surfaces resulting from a gradual build-up and removal of film material from the contact areas. Improved mating of the parts would act to reduce the surface temperatures, the additive decomposition rate, and thus the rate of deposition of new film material. Accordingly, after extended periods of operation, an improvement in surface smoothness could occur which may, in part, result from this combination of wear and a decrease in additive decomposition rate. On the other hand, this is a chemical problem and such factors as time and temperature may be very important in determining the equilibrium film composition. For example, the composition and properties of the film may change with time with more easily smeared films occurring at high test times. Accordingly, the reduction in surface roughness at high test times may simply reflect a filling in of the areas between the original asperities by the smearing of the film during operation.

Although a detailed explanation of the action of zinc dialkyl dithiophosphate additives is not available, it is believed that the mechanism involves additive decomposition as a result of the high temperatures produced by contact of the surfaces during operation to form a film which is chemically combined with the metal surface. This film can result in an increase in surface roughness of the contacting surfaces. Because of the complexity of the system, considerable additional work will be required to define completely a mechanism of action for these materials.

REFERENCES

1. Beeck, O., Givens, J. W. and Williams, E. C., "On the Mechanism of Boundary Lubrication II. Wear Prevention by Addition Agents," *Proc. Roy. Soc.* A, v. 177, 1940, p. 103.
2. Thorpe, R. E. and Larson, R. G., "Antiseizure Properties of Boundary Lubricants," *Ind. Eng. Chem.*, v. 41, 1949, p. 938.
3. Templeman, G. C., "A Dual-Purpose Film Strength Additive for Engine Crankcase Oils," *Lubrication Engineering*, March 1957, p. 141.
4. Prutton, C. F., Turnbull, D. and Dlouhy, G., "Mechanism of Action of Organic Chlorine and Sulfur Compounds in Extreme Pressure Lubrication," *J. Inst. Petroleum*, v. 32, 1946, p. 90.
5. Bidwell, J. and Williams, R. K., "The New Look in Lubricating Oils," *SAE Trans.*, v. 63, 1955, p. 349.
6. Ayres, Vincent, Bidwell, J. B., Pilger, A. C., Jr. and Williams, R. K., "Valve Train Wear as Affected by Metallurgy, Driving Conditions and Lubricants," SAE Annual Meeting, Detroit, Jan. 1957.
7. Abowd, R. G., Jr., "Chrome Face vs. Iron Side Wear—An Analysis of Some Radioactive Piston-Ring Wear Studies," *ASLE Trans.*, v. 1, n. 1, April 1958, pp. 91–95.
8. Loeser, E. H., Twiss, S. B. and Teague, D. M., "Cam and Tappet Test for Lubricants II—Wear Evaluation," *Lubrication Engineering*, May 1957, p. 269.
9. Furey, J. J. and Kunc, J. F., Jr., "A Radiotracer Approach to the Study of Engine Valve Train Lubrication," *Symposium on Nuclear Technology*, Division of Petroleum Chemistry, Amer. Chem. Soc., Miami, April 7–12, 1957, p. 81. (To be published in *Lubrication Engineering*.)
10. Loeser, E. H., Wiquist, R. C. and Twiss, S. B., "Cam and Tappet Lubrication. III—Radioactive Study of Phosphorus in the EP Film," *ASLE Trans.*, v. 1, n. 2, October 1958.
11. Roosa, M. B., "Application of Wear Resistant Phosphate Coatings to Ferrous Surfaces," *Lubrication Engineering*, June 1950, p. 117.
12. Robinson, G. H., "Bench Test Simplifies Search for Better Cam and Tappet Materials," *G. M. Engng. J.*, v. 3, n. 4.
13. Grube, W. L. and Rouze, S. R., "Application of the Two-Beam Interference Microscope to the Study of Surfaces," *J. Opt. Soc. Am.*, v. 44, n. 11, 1944.

DISCUSSION

P. A. Asseff:

Mr. Bennett's paper presents convincing engine and bench test data to show that oils containing zinc dialkyl dithiophosphate promote surface roughness of valve lifter-foot surfaces. He suggests that such surface roughness forms as the result of a chemical attack on the lifter surfaces by the additive or additive decomposition products. Although the mechanism of the attack is not known, it is believed to parallel mechanisms proposed in the literature for the action of phosphorus, sulfur, and chlorine compounds on ferruginous surfaces under boundary lubrication conditions.

Boundary lubrication conditions are known to produce high temperatures which heighten the activity of an additive and, in some instances, cause it to decompose. One would logically expect then that the thermal stability (i.e. resistance to decomposition on heating) of a zinc dithiophosphate must greatly influence its behavior as a lubricant additive.

It should be emphasized that many varieties of zinc

dithiophosphate are known to exist. They differ in composition from each other, principally with respect to the kinds of organic radicals (R) present in the molecular structure:

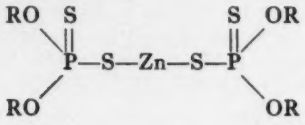

Experiments carried out in our laboratories using the Roxanna Model B Panel Coker apparatus clearly indicate that the kind of "R" group present in a zinc dithiophosphate has a profound effect on its thermal stability. In the Panel Coker test, droplets of the test lubricant are whipped against a heated panel maintained at a predetermined temperature. Depending on the thermal stability of the test lubricant, decomposition products in large or small amounts will adhere to the panel. The cleanliness of the panel is rated according to a numerical scale in which 10 indicates a perfectly clean panel and 0 indicates one which is heavily coated with decomposition products.

Table 1 (of this discussion) illustrates the substantial differences in thermal stability between various zinc dithiophosphates.

TABLE 1

Variation in Panel Appearance with Organic Content of the Zinc Dithiophosphate

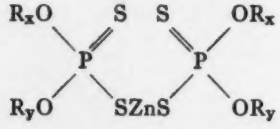

R_x and R_y represent a variety of alkyl and alkylaromatic radicals.

Compound	Panel rating
A	8.0
B	7.5
C	6.0
D	5.0
E	5.0
F	3.5
G	1.0
H	0.0

Dithiophosphates tested at 0.06% P wt. in SAE 30 Base Oil containing 0.67% wt. Ash Basic Barium Sulfonate

570° F—3 hours continuous splash

A number of mechanisms can be offered to explain these observed differences in thermal stability:

(A) When the R group is a secondary alkyl radical, the dithiophosphate is susceptible to decomposition due to the instability of the activated hydrogen atoms on the beta carbon atom. The decomposition may occur in the following manner:

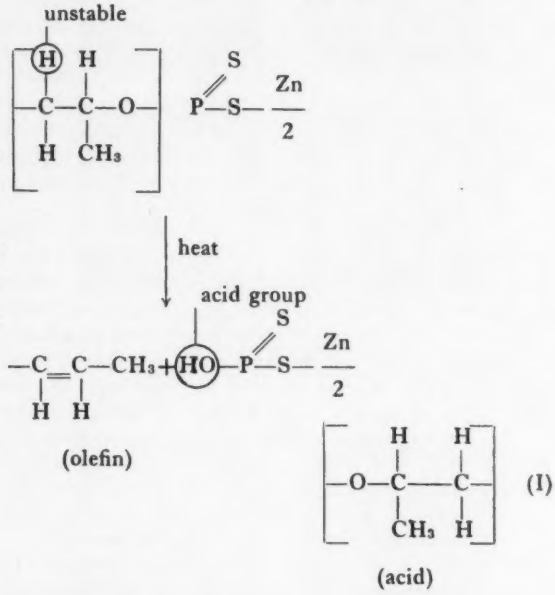

The strong acid (I) which is formed can react with iron to form the corresponding iron salt. Further decomposition at the point of the remaining secondary alkyl radical will result in the formation of a second acid group, which in turn can attack the iron surface.

(B) When the R group is a primary alkyl radical, the dithiophosphate is more stable than that in (A) above because there is less activation of the hydrogen atoms on the beta carbon atom:

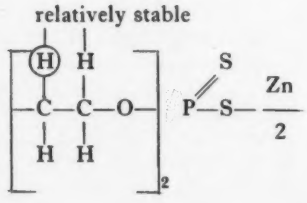

Decomposition, when it does occur, would take place at a higher temperature than for (A). The proposed mechanism for decomposition would follow the pattern previously given.

(C) When the R group is an aromatic radical, the resulting dithiophosphate is more stable than (A) or (B) because of

the very stably bonded hydrogen atoms on the beta carbon atom:

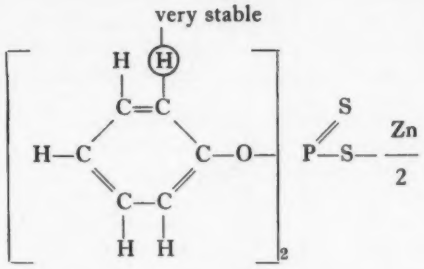

Decomposition of this compound according to the mechanism proposed under (A) would necessitate cleavage of the aromatic ring, an unlikely occurrence in view of the large amount of energy required for such a cleavage.

In conclusion, substantial differences in thermal stability have been observed for zinc dithiophosphates having dissimilar organic radicals. These differences are reflected in the behavior of such zinc dithiophosphates as additives in lubricating oils.

AUTHORS' REPLY:

We would agree with Dr. Asseff that one would expect "that the thermal stability (i.e. resistance to decomposition on heating) of a zinc dithiophosphate must greatly influence its behavior as a lubricant additive". Engine cam and lifter scuffing tests conducted at our laboratory have shown that relatively stable zinc dithiophosphate additives do not inhibit scuffing as readily as other less stable materials. Some of our data on this subject are currently being assembled and will be published in the near future.

M. Z. FAINMAN (*Inland Testing Laboratories, Division of Cook Electric Co., Morton Grove, Ill.*):

I want to compliment Messrs. Furey and Bennett on the presentation of a pair of fine papers. Their results point out some interesting and important phenomena and should aid substantially in clarifying the antiwear behavior of the substituted zinc dithiophosphates.

Dr. Asseff in his discussion of Bennett's paper presented some very interesting and useful data obtained at the Lubrizol Laboratories. However, I want to inject a note of caution on the use of the term thermal stability. This term is creeping into the literature in a practical sense and will soon lose its definitive meaning unless this trend is stopped. Dr. Asseff's discussion properly defines thermal stability as resistance to decomposition on heating. This would imply that as the temperature of a material is increased there is a temperature or energy level at which decomposition ensues. We must also bear in mind that there is a rate of decomposition associated with the degradation of an organic material as well as an activation energy for the process. If oxygen is introduced into a system, we are, in practically all instances, no longer observing a strictly thermal degradation, but a more complex reaction in which oxygen is now involved in the form of free radicals and peroxides.

Hence, if we are to understand the phenomena involved in the lubrication process we must define our terms more carefully. Say, for example, one was looking up the thermal stability of various organic structures in an attempt to understand the cracking reaction or to ascertain how a material might be expected to behave at high temperature in an inert atmosphere. I don't believe that the data in this discussion under the heading "Thermal Stability" would be very significant.

Now let us look closely at the discussion and the data presented.

> "Experiments carried out in our laboratories using the Roxanna Model B Panel Coker apparatus clearly indicate that the kind of "R" group present in a zinc dithiophosphate has a profound effect on its thermal stability. In the Panel Coker test, droplets of the test lubricant are whipped against a heated metal panel maintained at a predetermined temperature. Depending on the thermal stability of the test lubricant, decomposition products in large or small amounts will adhere to the panel. The cleanliness of the panel is rated according to a numerical scale in which 10 indicates a perfectly clean panel and 0 indicates one which is heavily coated with decomposition products."

The panel coker in this case was used with a panel temperature of 570° F and 3 hours' continuous splash. This may mean, under normal conditions, a sump temperature of about 200° F and a constant circulation of air. The amount of deposits on the panel are nothing more nor less than the amount of deposits formed by an oil containing additives, in this case barium sulfonate and a dithiophosphate tested at 0.06% P weight in the oil. Unfortunately, no relative rating is given for the base oil with only the basic barium sulfonate. However, we can list several reasons for the effects of different alkyl or aryl groups on the amount of deposits formed.

(1) The amount of deposit may depend upon the molecular weight of the zinc dialkyl dithiophosphate.

(2) The amount of deposits may depend on its efficacy as an oxidation inhibitor.

(3) The amount of coke may depend upon the solubility of the zinc dialkyl dithiophosphate in the oil blend.

(4) The amount of deposit may depend upon the structure of the zinc dialkyl dithiophosphate and its competition for the surface of the heated plate with the basic barium mahogany soap.

As the zinc dialkyl dithiophosphates are described only by letters of the alphabet, the above can only be a surmise, and fortuitously the ease of decomposition of the zinc dialkyl dithiophosphate may be intimately associated with one or more of the above mechanisms.

In the light of the above commentary and the apparatus used to obtain the data for this discussion, I do not believe the authors are warranted in their conclusion that "substantial differences in thermal stability have been observed for zinc dithiophosphates having dissimilar organic radicals. These differences are reflected in the behavior of such zinc dithiophosphates as additives in lubricating oils."

AUTHOR'S REPLY:

The author agrees with Dr. Fainman's remarks relative to the effect of a constant circulation of air and the introduction of oxygen into the system.

Under conditions of this experiment, however, there was very little oxygen present in the system. The openings in the coker reservoir were closed to eliminate circulation of air through the reservoir and hence it was felt that we were measuring primarily thermal degradation.

The items, other than oxidation stability listed by Dr. Fainman as being possible explanations for the effect of different alkyl or aryl groups on deposit formation, are quite interesting and might serve as possible subjects for future work.

Film Formation by an Antiwear Additive in an Automotive Engine

By M. J. FUREY[1]

Experiments carried out in a laboratory multicylinder gasoline engine with mineral oil lubricants containing radioactive (P^{32}-labeled) zinc di(C_6)alkyl dithiophosphate show that strongly attached films are formed by this compound on many of the rubbing metal surfaces of the engine. Results are presented on the effects of chemical treatments on the radioactivity of the metal surfaces and on a technique by which the films are removed and assayed with a Geiger counter. On the basis of radioactivity per unit of geometrical contact area, most of the active parts were the highly stressed components of the valve train mechanism. These included the cams, valve lifter faces, push rod ends, rocker arm bearing areas and valve stem ends. The activity of the valve lifter faces was found to be influenced by (a) lifter metallurgy, (b) degree of break-in and (c) the presence of a detergent-inhibitor additive in the lubricant. Autoradiographs show that practically all the activity on a cam surface is localized at the cam nose—the region of greatest stress, of greatest surface damage and where metal transfer is known to occur. It is estimated that the films found on the cams and valve lifters are several molecular layers thick. The data support the idea that the action of zinc dialkyl dithiophosphate in reducing valve train wear in automotive engines involves the formation of phosphorus-containing protective films by chemical reaction with the rubbing metal surfaces. In addition, the results of this study suggest that this radiotracer method may be useful for locating critical areas of boundary lubrication in other mechanical devices.

Introduction

ALTHOUGH the use of certain compounds in lubricants to reduce wear between rubbing metal surfaces is not new, little is known about the detailed mechanisms by which these additives function. Materials containing phosphorus, sulfur or chlorine account for the majority of the antiwear and antiseize additives described in the literature and in patents. Several theories have been offered to explain their action, the most generally accepted ones involving the formation of protective films such as iron phosphides, sulfides or chlorides. Although the existence of such films has been confirmed by chemical analyses and by electron and X-ray diffraction techniques, very little is known about the distribution and thickness of these films as actually formed in a dynamic system. However, in recent years, the increased availability of radioisotopes for use as research tools has helped considerably in studies of metal surface phenomena as shown in an admirable review by Simnad (1). Using radioactively-tagged compounds in lubricants, several static studies have been made of film formation on metal surfaces by additives known to reduce friction or wear (2–5). However, Borsoff and Wagner (4) were the first to investigate the formation of metal surface films in a dynamic system using a radioactively-labeled additive. Their work was carried out with gears operated on oils containing S^{35}-tagged dibenzyl disulfide.

It is known that zinc salts of certain dialkyl dithiophosphoric acids can be very effective lubricant additives for reducing the wear of the highly-loaded valve lifters and cams of automobile engines (5–7). In studies with Zn^{65}-tagged zinc di(C_6)alkyl dithiophosphate, Furey and Kunc (5) found appreciable quantities of tightly bound zinc on steel specimens which had been immersed in solutions of this compound. They also showed, however, that the nickel and iron salts of di(C_6)alkyl dithiophosphoric acid were at least as effective as the zinc salt in reducing valve lifter wear. The acquisition of zinc by valve lifters immersed in an oil containing zinc dialkyl dithiophosphate has also been reported in a recent paper by Loeser, Wiquist and Twiss (8), who used X-ray spectrometry to examine the surfaces. In addition, they showed evidence of film formation by P^{32}-labeled zinc dialkyl dithiophosphate in both static immersion tests and in a bench scale cam and valve lifter tester.

The present paper describes the results of studies carried out in a multicylinder gasoline engine with mineral oils containing P^{32}-tagged zinc di(C_6)alkyl dithiophosphate. The object of this investigation was fourfold, namely (a) to find out whether or not phosphorus-containing films formed on valve lifter and cam surfaces in an actual engine under normal operating conditions, (b) to determine the distribution and thickness of these films if they existed, (c) to study the effects of valve lifter metallurgy, degree of break-in and presence of a detergent-inhibitor additive on film formation and (d) to explore the use of this radiotracer technique as a tool to locate critical areas of boundary lubrication.

Presented as an American Society of Lubrication Engineers paper at the Lubrication Conference held in Los Angeles, Calif., October, 1958.

[1] Research Engineer, Esso Research and Engineering Co., P.O. Box 51, Linden, New Jersey.

Experimental

The selection of the apparatus and experimental conditions used in this study was made primarily on the basis of duplicating conditions under which zinc dialkyl dithiophosphate is known to reduce wear. Specifically, short-term tests were carried out in a laboratory multicylinder gasoline engine with lubricants containing radioactively labeled zinc dialkyl dithiophosphate. Upon completion of the tests, various engine parts were examined for radioactivity using both Geiger counting and autoradiographic techniques. In a designed experiment, the effects of (a) metallurgy, (b) degree of break-in, (c) a detergent-inhibitor additive, and (d) solvent treatment on the radioactivity of the highly loaded valve lifter faces were studied. The experimental details are described in the following paragraphs.

Preparation of the Radioactively Tagged Zinc Dialkyl Dithiophosphate

The zinc dialkyl dithiophosphate used in this study was tagged with radioactive phosphorus in the form of P^{32}—a strong beta particle emitter (1.7 MeV maximum energy) decaying with a half-life of 14.3 days. The zinc salt was prepared by reacting a mixture of non-radioactive and P^{32}-labeled P_2S_5 with 4-methyl-2-pentanol and converting the acid thus formed to the salt. The labeled P_2S_5, having a specific activity of about 4 millicuries per gram at the time of this study, was made by heating an intimate mixture of radioactive red phosphorus and sulfur in a CO_2 atmosphere.

Composition of the Test Lubricants

Two lubricants of the 10W-30 type, each containing 1.30% by weight of the radioactive zinc dialkyl dithiophosphate, were used in this study. These blends were based on a straight paraffinic type mineral oil plus polymeric viscosity index improvers and differed only in that one contained 5% by volume of a detergent-inhibitor additive.

Engine and Test Conditions

The engine used in this study was of the V-8 overhead valve type having a displacement of 331 cu. in. The camshaft was made of an alloy cast-iron, and the cams had a Rockwell C hardness of 50 and no surface treatment. Based on previous wear studies with radioactive valve lifters in a laboratory engine of the same make (5), the test conditions shown in Table 1 were chosen for film formation studies with the labeled zinc compound.

TABLE 1

Engine Test Conditions Used in Radiotracer Film-Forming Studies

Engine speed	1000 rpm
Engine load	Zero
Jacket water outlet temperature	180°F
Oil temperature (uncontrolled)	180–190°F
Time	3 hr

Under these conditions with "broken-in" valve lifters made of SAE 5120 carburized steel, the addition of 1.30 wt.% of zinc di(C_6)alkyl dithiophosphate (derived from the alcohol 4-methyl-2-pentanol) to each of the two test oils previously described markedly reduces valve lifter wear. This is shown by the data in Table 2.

TABLE 2

Effect of Zinc Dialkyl Dithiophosphate on Valve Lifter Wear

Detergent inhibitor →	None	5 vol. %
Relative Valve Lifter Wear		
Base lubricant alone	100	138
With 1.3 wt. % $[(RO)_2PSS]_2Zn$	12	7

In this study of film formation, the effects of valve lifter metallurgy and degree of lifter "break-in" were also determined using standard lifters which initially had been phosphate-treated. In each of the 3-hr engine tests with the two lubricants containing the P^{32}-tagged zinc dialkyl dithiophosphate, half or eight of the sixteen valve lifters were made of SAE 5120 carburized steel and had case and core hardnesses of 59 and 38 Rockwell C, respectively. The remaining lifters were made of an alloy cast-iron and had case and core hardnesses of 58 and 51 Rockwell C, respectively. In addition, within each metallurgy, half the lifters were new and half had been "broken-in" by 7 hr of engine operation on oils not containing any radioactive additives. The details of this test sequence and the actual arrangement of the valve lifters within the engine are shown in Appendix Table 1. It can be seen that the distribution of the lifters is also balanced with respect to the left and right sides of the engine, front and rear, and intake and exhaust valves.

Carrying Out the Engine Tests

The first radiotracer test in the engine was carried out with the 10W–30 base oil (mineral oil plus viscosity index improvers) containing the tagged zinc dialkyl dithiophosphate. A photograph of the engine and accessories is shown in Fig. 1. At the end of the test, the oil was drained and all sixteen valve lifters were removed, disassembled and rinsed in hexane to remove residual oil. The engine was then flushed with hydrocarbon solvent and the second set of valve lifters was installed. This was followed by two 5-min. flushes with a straight, non-additive mineral oil.

Using the same test conditions, the next radiotracer test was carried out with the 10W–30 oil containing the detergent-inhibitor and labeled additive. The oil was again drained and the lifters and camshaft were removed. The engine was then thoroughly flushed with hydrocarbon solvent and completely disassembled. All the parts were rinsed in hexane to remove the oil.

Examination of Engine Parts for Radioactivity

Using a collimated Geiger tube, a preliminary survey of several of the engine parts was made. This was useful for

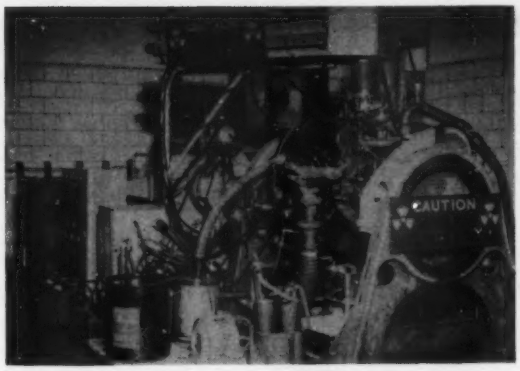

FIG. 1. Multicylinder engine and accessories used in radiotracer studies of film formation.

a qualitative examination, but the large differences in geometry still made comparisons between parts rather difficult. To overcome this problem, a technique of wiping a given area of an engine part with filter paper moistened with dilute acid was used. Specifically, the areas were wiped with small circles of filter paper moistened with dilute HCl. The circles were placed in stainless steel counting planchets and allowed to dry before being counted in a flow counter having a thin (¼ mil) metalized Mylar window and operating at 1400 V with a Geiger gas mixture consisting of 0.95% isobutane in helium. It was found that close to 100% of the radioactivity was easily removed by the first wipe and that little, if any, of the phosphorus was lost as a gas. Using this method, several of the engine parts, including most of the rubbing metal surfaces, were examined for activity. However, the activity of all the highly-loaded rubbing surfaces of the valve lifters was first determined directly in the flow counter. Although the lifters were initially rinsed in hexane to remove residual oil, some were treated with additional solvents which included acetone, pyridine and water. An aluminum valve lifter holder, shown with the flow counter in Fig. 2, was used to keep the geometry constant and to

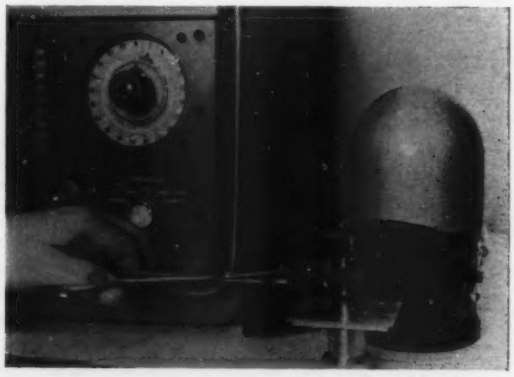

FIG. 2. Flow counter and valve lifter holder used for radioactivity measurements.

expose only the lifter face to the counter window. To obtain quantitative results of the amount of phosphorus present on the lifter faces, standard valve lifters containing known quantities of the P^{32}-tagged dithiophosphate deposited by hexane were also counted. This facilitated decay corrections and also minimized any errors due to back-scattering. The radiochemical purity of the standards and of the radioactive films on the lifter faces was checked by making half-life and absorption measurements.

To study the distribution of the radioactivity on the cam and valve lifter faces, autoradiographs were made by contacting these surfaces with X-ray film for approximately two weeks.

Results

General Engine Activity

The results of counting the various engine parts by the acid-wipe technique are shown in Appendix Table 2, where the average activity per part and the relative activity per unit of geometrical area are listed. A summary of these results is shown in Table 3. In general, it was found that films were formed by the zinc dialkyl dithiophosphate on most of the rubbing surfaces of the engine. It is seen that on the basis of activity per unit of area, the most active parts were the highly loaded rubbing surfaces of the valve train mechanism, a diagram of which is shown in Fig. 3.

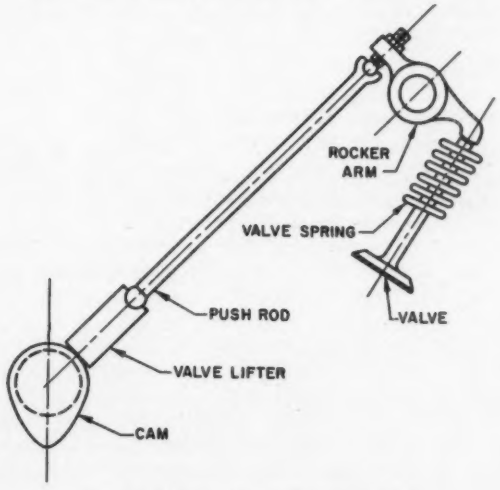

FIG. 3. Valve train—"V" type engine.

For example, the activity of the valve lifter faces or area that contacts the cam is at least a hundred times as great as the activity of the lifter side. Similarly, the activity on the push rods is concentrated at the ends—the rubbing areas under high load. Other active regions in the valve train mechanism included the cams, rocker arm bearing areas and valve stem tops. In a particular rocker arm bearing area, about 85% of the activity was in the scuffed half. Similarly, on the rocker arm shaft, only the scuffed half of the corresponding rocker arm bearing area had significant activity.

Areas of moderate but lower activity included the drive gear teeth on the distributor, piston rings, rubbing parts of the rocker arm shaft, the fuel pump eccentric and the sprocket teeth on the camshaft and crankshaft.

TABLE 3

Radioactivity of Various Engine Parts after Tests with Oils Containing P^{32}-labeled Zinc Di(C_6)Alkyl Dithiophosphate

Part or Section	Relative activity per unit of area[a]
Valve Train Mechanism	
Valve lifter face[b]	100
Valve lifter side[b]	1
Cam surface	44
Lower end of push rod	32
Push rod body	0
Upper end of push rod	8
Rocker arm socket	20
Inner bearing area of rocker arm	11
Bearing area of rocker arm shaft	3
Rocker arm pad	25
Valve stem top	66
Other Parts	
End of fuel pump push rod	43
Drive gear teeth on distributor	7
Piston ring flats	5
Piston ring face	3
Fuel pump eccentric	2
Camshaft sprocket teeth	2
Crankshaft sprocket teeth	1
Camshaft bearing	<1 but significant
Cylinder wall	
Wrist pin assembly	
Crankshaft connecting rod journal	
Connecting rod bearing inserts	No significant activity
Crankshaft main journal	
Non-rubbing section of crankshaft	
Part of rocker arm in contact with bracket	
Remaining non-rubbing areas of rocker arm	

[a] After 6 hr of engine operation unless otherwise noted.
[b] After 3 hr of engine operation.

Showing very low but significant activity were the camshaft bearings, cylinder walls, wrist pin assemblies, and the crankshaft connecting rod journals. No significant activity was found on other rubbing surfaces in the engine. Radioactivity was found on the steel crankshaft connecting rod journals but not on the mating bearing inserts which consist of babbitt over steel.

Appreciable radioactivity was found in the combustion chamber region of the engine in the form of brown deposits. Particularly active were the piston tops, valve faces, the combustion chamber domes and the spark plugs.

Films Formed on the Valve Lifters

The preliminary survey of the lifters made with the Geiger tube showed appreciable radioactivity on the faces of the lifters but very little, if any, on the sides. With a background of about 20 counts/min in the flow counter and lifter face activities ranging from 400 to 2000 counts/min, good counting precision (*ca.* 1–2%) was easily achieved without exceeding 30-min counts. Half-life and absorption measurements of the radioactive films on the lifters and of the standards confirmed the fact that the activity was due to phosphorus-32. The results of counting the hexane-rinsed lifter faces are summarized in Table 4 and shown in detail in Appendix Table 3. It is seen that metallurgy, break-in and the presence of the detergent-inhibitor all affect the pick-up of P^{32}.

TABLE 4

Influence of Metallurgy, Break-In and Detergent-Inhibitor on the P^{32} Activity Acquired by Valve Lifter Faces

	Activity of lifter faces[a] (net counts/min)			
Metallurgy:	Steel		Alloy cast-iron	
Break-in?	No	Yes	No	Yes
Detergent-Inhibitor				
None	440	550	1310	1434
5 vol. %	593	1669	796	1275

[a] Each activity shown is the average of four lifters and is corrected for decay.

If one treats all the results as a group, an analysis of variance shows that the following conclusions can be drawn:

(a) Lifter metallurgy has a significant (>95% confidence level) effect.

Steel (average) = 813
Cast-iron (average) = 1204

(b) There is a highly significant (>99% confidence level) interaction between metallurgy and the presence of the detergent-inhibitor.

	Averages	
	Steel	*Cast-iron*
No detergent	495	1372
Detergent	1131	1035

In other words, the detergent additive increases the amount of P^{32} pick-up by steel but decreases the amount retained by cast-iron.

(c) Lifter break-in has a highly significant (>99% confidence level) effect.

No break-in (average) = 785
Break-in (average) = 1232

(d) A significant (>95% confidence level) interaction exists between break-in and the detergent-inhibitor.

	Averages	
	No break-in	*Break-in*
No detergent	878	992
Detergent	694	1472

One way of expressing this interaction is to say that the effect of break-in is most striking in the presence of the detergent-inhibitor additive.

One of each of the eight groups of valve lifters was subjected to further solvent treatment to learn more about the nature of the phosphorus-containing film. This treatment

consisted of a vigorous 1-min scrub of each lifter face with cotton soaked in a particular solvent. It is recognized that this is not an easily reproducible procedure and that physical "wearing away" of the film could also have occurred. Nevertheless, the results indicate the effect of a rather intensive scrubbing action. Each of the eight lifters was treated this way and counted after each cleaning to determine the radioactivity removed. The sequence of solvents was the same for all lifters, namely hexane, acetone, pyridine and distilled water. As seen in Fig. 4,

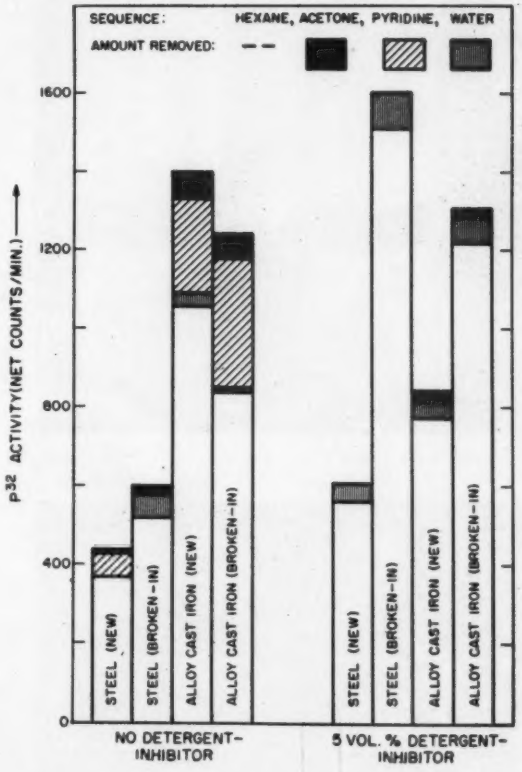

FIG. 4. Effect of solvent treatment on the P^{32} activity of valve lifters.

this type of solvent treatment generally removed only a minor portion of the P^{32} activity. It appears that the solvent effect varies with metallurgy, presence of the detergent-inhibitor and possibly the degree of break-in. For example, the amount of activity removed by acetone and pyridine is higher with cast-iron lifters and with those run in the absence of the detergent-additive.

By increasing the scrubbing time from one to five minutes with cotton soaked in distilled water, the amount of activity removed increased from about 5 to 19%. However, a 1-min scrub or immersion in dilute (3.8%) HCl removed all of the activity. This suggested the previously-described techniques by which the remaining parts of the engine were counted to determine the amount of radioactivity present. A prolonged (72-hr) immersion of the lifters in hexane, acetone or pyridine had no significant effect on the activity. It was reasoned that if the film contained an iron phosphate, then immersion in a solution containing phosphate ions should remove activity by an exchange process. Such an experiment showed that about 90% of the activity was thus removed in 72 hr but that slight rusting also occurred. Immersion in distilled water alone for the same period of time removed about $\frac{2}{3}$ of the activity and the amount of rusting was much heavier.

Autoradiographs of Cams and Valve Lifters

Examples of a cam autoradiograph and of two extremes in lifter face autoradiographs are shown in Fig. 5 where the dark areas represent the location of radioactive phosphorus. It is seen that most of the activity on a cam surface is localized at the cam nose. This was also verified by direct counting of the cam surface with a thin window Geiger tube ($\frac{3}{8}$-in. dia.) and aluminum shielding. There is also a curved non-radioactive area on each side of the cam nose, having the same pattern which can be observed visually on the cam. Furthermore, there is a slight concentration of activity in the regions corresponding roughly to the junction of the flank and base circles. It is seen that on the lifter faces, the active pattern can vary from a light, fairly uniform one to a highly localized ring.

The scattered dark dots on the cam autoradiograph are apparently not due to radioactivity since they do not appear on successive wrappings of the X-ray film as shown in Fig. 6. In each of the four cam autoradiographs shown, the area of first contact with the cam nose is on the right. The dark dots are probably due to a chemical activation of the film by the metal. Figure 6 also shows more clearly the presence of a light smear of activity on most of a cam surface, and again the abrupt change near the intersection of the flank and base circles. The top cam autoradiograph is somewhat lighter than the others because a 10-day rather than 2-week exposure was used.

The similarity between the physical appearance of the lifter faces and the distribution of radioactivity is shown in Fig. 7 where photographs and autoradiographs are compared. With the steel lifters, the central area was generally found to have less activity whereas the reverse was true for alloy cast-iron.

Discussion

This study with radioactively tagged zinc dialkyl dithiophosphate has provided conclusive evidence of film formation by an antiwear additive in an automotive engine, demonstrating the value of using radiotracers in lubricants to study metal surface phenomena in a complex, dynamic system. The high concentration of radioactive phosphorus found on the rubbing surfaces of the valve lifters and cams supports the idea that zinc dialkyl dithiophosphate reduces wear in this region by the formation of a protective, phosphorus-containing film. This idea is supported even further by the general similarity between the distribution of radioactive phosphorus on the cams and the previously shown (5) pattern of metal transfer from the valve lifters to

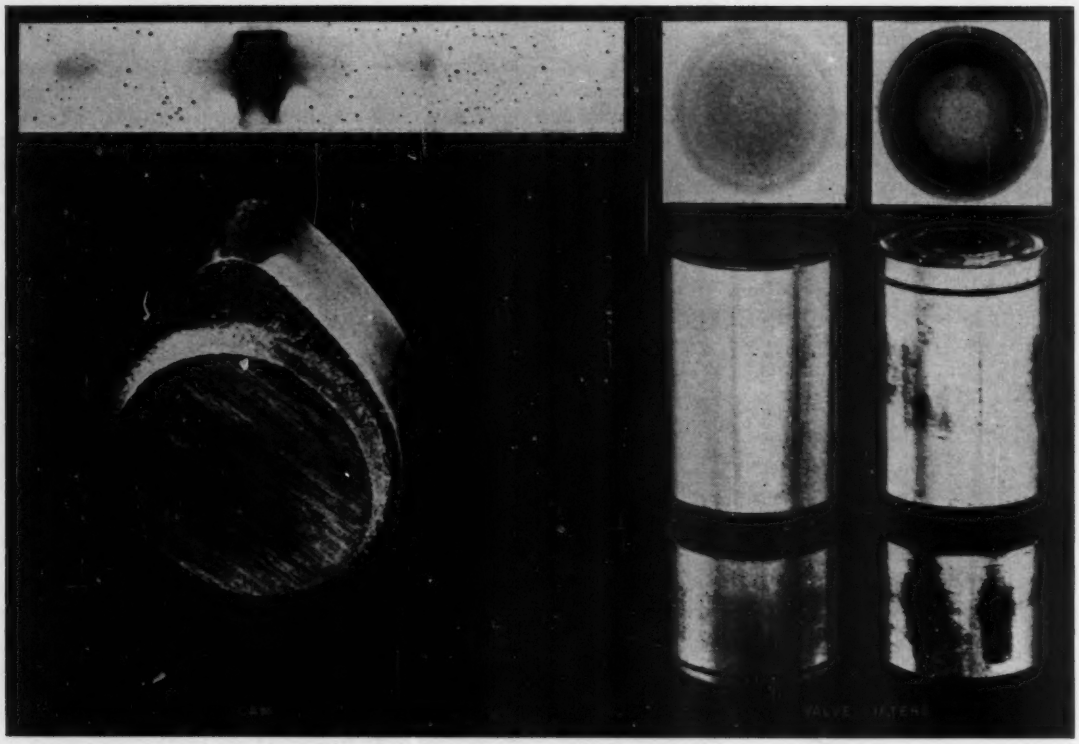

FIG. 5. Autoradiographs of a cam and valve lifters.

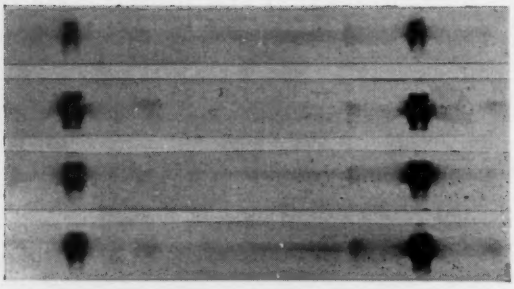

FIG. 6. Autoradiographs of four cams.

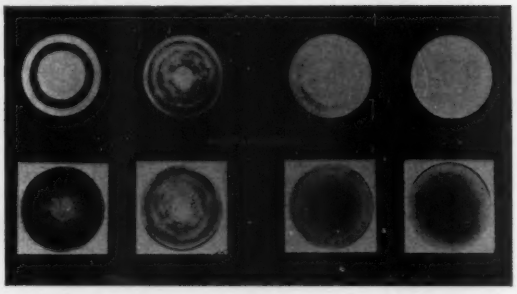

FIG. 7. Valve lifters run on oils containing P^{32}-labeled zinc dialkyl dithiophosphate.

the camshaft. Both film formation and metal transfer are localized at the cam nose where the contact stresses and wear are greatest. Further evidence of a relationship between film formation and contact stress is shown by the fact that most of the very active engine parts were components of the highly loaded valve train mechanism. The solvent treatment studies suggest that most of the film is chemisorbed or chemically reacted with the metal. Factors responsible for the concentration of the radiophosphorus on rubbing surfaces under high stress could include (a) localized temperature flashes due to the breakdown of the oil film and (b) the generation of naked, more reactive metal. One might, therefore, venture the idea that the dithiophosphate functions by thermally decomposing in this region to form a film which reduces the extent of metal transfer. The localization of radiophosphorus on rubbing surfaces under high stress and on scuffed sections also suggests that this technique may be useful in locating critical areas of boundary lubrication in other mechanical devices.

Metallurgy, Break-In and Lubricant Effects

The influence of metallurgy, break-in and presence of a detergent-inhibitor additive on the P^{32} activity acquired by the valve lifter faces demonstrates the complex nature of the process of film formation on metal surfaces. The first

point to be made, however, is that although the detergent additive has an effect on the activity acquired, appreciable activity is present in both cases. Wear data show that zinc di(C_6)alkyl dithiophosphate reduces the wear rate of the steel lifters under these conditions by about 90%, both in the absence and presence of the detergent-inhibitor. The absence of cam/lifter radioactivity in either or both of the two tests would have contradicted the idea that a phosphorus-containing film is involved at all in the antiwear process.

Before attempting to discuss the effects of metallurgy, break-in and detergent-inhibitor on lifter activity, it might be well to examine more closely the influence of the various solvent treatments on the removal of activity. First, immersion and scrubbing of the lifters in organic solvents removed only a minor amount of the radioactive material. This suggests that what remained—or most of the activity—was very strongly held, perhaps by chemisorption or by chemical reaction with the metal. However, some of the activity can be taken off with acetone, pyridine or water. In addition, the amount removed by a particular solvent seems to depend on metallurgy, the detergent and possibly the degree of break-in. Although this behavior could be a reflection of varying efficiencies of film removal because of physical differences (e.g. in surface roughness), it could also be due to the presence of phosphorus in several different forms. These could include, for example, (a) physically adsorbed zinc dialkyl dithiophosphate, (b) thermal decomposition products of the zinc additive, (c) varnish or lacquer deposits containing physically or chemically bound phosphorus, and (d) metal/phosphorus reaction products. Although exchange between the phosphorus in the metal and the phosphorus in the labeled additive could also have occurred, calculations show that this would account for only a minute fraction of the activity observed. The percent removal of activity by acetone and pyridine is decreased by the detergent additive, increased by cast-iron and decreased by break-in with steel lifters in the absence of the detergent. This behavior could conceivably be due to differences in the amount of phosphorus-containing debris, deposits, or varnish caught in small openings or valleys of the metal surfaces. The detergent could have decreased this deposit accumulation by either a surface or dispersant action. The lifters made of the alloy cast-iron, being much more wear-resistant, were not smoothed out as much during the engine tests and presented a rougher surface which one would expect to be more efficient for trapping deposits. This idea would also explain why the new steel lifters which were run on the non-detergent oil had activity removable by pyridine and acetone.

In this complex system, many other factors could also account for the observed effects of metallurgy, break-in and lubricant composition on the amount of P^{32} activity acquired by the valve lifter faces. These might include differences in (a) actual surface area, (b) chemical reactivity of the surfaces, and (c) the rates at which the metal and/or phosphorus-containing film is worn off. For example, the effect of break-in could be one of providing a more reactive underlayer of metal by removing the original surface treatment. Further studies are necessary to establish the reasons for these effects.

The effects of treating the lifters with water, water containing phosphate ions and dilute HCl are difficult to interpret since corrosion of the underlying metal may have been responsible for the removal of P^{32} activity.

Thickness and Distribution of the Films

From counts of standard valve lifters containing known quantities of P^{32}-tagged zinc dialkyl dithiophosphate, it is calculated that the amount of phosphorus present on the lifter faces ranges from 3.2 to 12.1 micrograms per lifter. This is equivalent to 0.75 to 2.85 micrograms of phosphorus per cm^2 of apparent geometrical area. From the cam autoradiographs and total cam activity, the average amount of phosphorus on the cam nose is calculated to be about 11.1 micrograms per cm^2 of geometrical area. If one assumes an effective density of 2.2 g/cm^3 for phosphorus, then the volume of a phosphorus atom is 23.2×10^{-24} cm^3 and one monolayer is equivalent to 6.36×10^{-8} g/cm^2. Therefore, if the phosphorus-containing films were in the form of phosphorus alone, then the amounts of radioactivity found represent an average thickness of about 12 to 44 molecular layers for the lifter faces and 174 molecular layers for the cam noses. Similarly, if the activity were due to an iron/phosphorus compound such as iron diphosphide, Fe_2P, then the amounts of phosphorus found would be equivalent to an average thickness of 16 to 60 molecular layers for the lifters and 235 molecular layers for the cam noses. Phosphorus present in the form of larger molecules could account for even thicker films.

Although the absolute area of these metal surfaces is not known, it is certainly greater than their geometric area. This, of course, would lower the above estimates of average film thickness. In studies by Erbacher (9) with metals subjected to finishing with fine or coarse emery paper, the ratio of absolute to geometric area—or roughness factor—was found to equal about 2.5. King (10) indicates that the common metals seldom have a roughness factor greater than 10. If the roughness factors of the valve lifter and cam surfaces were as great as 10, then the estimated average thickness of Fe_2P, for example, would be 1.6 to 6 molecular layers for the lifters and 23.5 molecular layers for the cam noses. In addition, the autoradiographs show very distinct localization of radioactivity on the lifter faces, thereby indicating that the actual film thicknesses encountered may be considerably greater than the estimates made on the basis of average activity per unit of area. This localization appears to coincide with the actual rubbing contact areas.

A more careful examination of the cam autoradiographs shows a curved, non-radioactive area on each side of the cam nose having the same pattern which is observed visually on the cam. It is believed that this corresponds to a region of "no-contact" due to the intentional slight taper (about an angle of 7′) of the cam with respect to its axis of rotation. There is also some activity in the regions corresponding roughly to the junction of flank and base circles. This could be explained on the basis of an added force of acceleration due to the sudden change from a rapid increase

in the speed of the lifter to a rapid decrease. With the mushroom-type of cam used in this study, the maximum speed of lift is reached in less than about 6° of cam rotation. Acceleration forces might also explain the apparent dual nature of the active area at the cam nose.

Comments on the Activity of Other Sections of the Engine

The radioactivity found in the combustion chamber zone in deposit form is believed to be due primarily to the burning of the lubricant in this region. Extraction of the deposits with hexane removed very little of the activity whereas water was completely effective, thus indicating an inorganic material (e.g. zinc phosphate).

The absence of radioactivity on the push rod body, crankshaft main journal, and other non-rubbing metal parts of the engine is particularly interesting. This suggests that physical adsorption may not play a part in the antiwear action of zinc dialkyl dithiophosphate. The presence of activity on the steel connecting rod journal and the absence of activity from the mating bearing inserts made of babbitt-coated steel may be another indication that the film-forming process involves a chemical reaction with the metal surface.

Further dynamic studies with zinc dialkyl dithiophosphate labeled with other radioisotopes (e.g. Zn^{65}, S^{35}) should be of value in learning more about the true nature of these phosphorus-containing films on rubbing metal surfaces.

REFERENCES

1. SIMNAD, M. T., "Radioisotopes in the Study of Metal Surface Reactions in Solutions," in *Properties of Metal Surfaces*, Monograph No. 13, Institute of Metals, London, 1st ed., 1953, pp. 23–58.
2. CLARK, G. L., GALLO, S. G. and LINCOLN, B. H., "Radiosulfur Tracer Study of Sulfurized Lubrication Addition Agents," *J. Appl. Phys.*, v. 14, 1943, pp. 428–434.
3. VINOGRADOV, G. V., KUSAKOV, M. M., SANIN, P. I., ZASLAVSKII, Yu. S., RAZUMOVSKII, E. A., UL'YANOVA, A. V. and RYABOVA, D. V., "Investigation of the Mechanism of Action of Organothiophosphorus Oil Additives by Means of Radioactive Tracers," *Khim. i tekhnol. Topliva*, n. 6, 1956, pp. 14–20.
4. BORSOFF, V. N. and WAGNER, C. D., "Studies of Formation and Behavior of an Extreme-Pressure Film," *Lubrication Engineering*, v. 13, n. 2, Feb. 1957, pp. 91–99.
5. FUREY, M. J. and KUNC, J. F., Jr., "A Radiotracer Approach to the Study of Engine Valve Train Lubrication," Symposium on Nuclear Technology in the Petr. and Chem. Ind., Preprint of Div. Petr. Chem., A.C.S. Meeting, Miami, April 1957, pp. 81–94.
6. ETCHELLS, E. B., THOMSON, R. F., ROBINSON, G. H. and MALONE, G. K., "The Interrelationship of Design, Lubrication, and Metallurgy in Cam and Tappet Performance," S.A.E. Golden Anniv. Passenger Car, Body, and Materials Meeting, Detroit, March 1955.
7. AYRES, V., BIDWELL, J. B., PILGER, A. C., Jr., and WILLIAMS, R. K., "Valve Train Wear as Affected by Metallurgy, Driving Conditions and Lubricants," S.A.E. Annual Meeting, Detroit, January 1957.
8. LOESER, E. H., WIQUIST, R. C. and TWISS, S. B., "Cam and Tappet Lubrication. III—Radioactive Study of Phosphorus in the E.P. Film" Paper, Annual A.S.L.E. Meeting, Cleveland, April 22–24, 1958.
9. ERBACHER, O., "A Method for the Determination of the Absolute Surface Area of Metals," *Z. physik. Chem.*, v. 163A, 1933, pp. 215–230.
10. KING, C. V., "Adsorption and Exchange in Metal–Metal Ion Systems," *Ann. N.Y. Acad. Sci.*, v. 58, art. 6, 1954, pp. 910–924.

APPENDIX

APPENDIX TABLE 1

Arrangement of Valve Lifters in Engine Tests with Oils Containing P^{32}-labeled Zinc di(C_6)Alkyl Dithiophosphate

Cam no.	Valve[a]	Lifter position[b]	Valve lifter identification[c]		
			Break-in (all new)	Test 1[d]	Test 2[e]
1	X	L-1	1	1	13 (new)
2	X	R-1	21	21	33 (new)
3	I	L-1	2	9 (new)	2
4	I	R-1	22	29 (new)	22
5	I	L-2	23	23	34 (new)
6	I	R-2	3	3	14 (new)
7	X	L-2	24	30 (new)	24
8	X	R-2	4	10 (new)	4
9	X	L-3	5	11 (new)	5
10	X	R-3	25	31 (new)	25
11	I	L-3	6	6	15 (new)
12	I	R-3	26	26	35 (new)
13	I	L-4	27	32 (new)	27
14	I	R-4	7	12 (new)	7
15	X	L-4	28	28	36 (new)
16	X	R-4	8	8	16 (new)

[a] X = exhaust, I = intake.
[b] Bank (L = left, R = right) and cylinder number.
[c] Lifter numbers: 1–16, alloy cast-iron; 21–36, carburized steel (SAE 5120).
[d] Lubricant composition: 1.3 wt. % P^{32}-labeled zinc dialkyl dithiophosphate in 10W–30 base oil.
[e] Lubricant composition: 1.3 wt. % P^{32}-labeled zinc dialkyl dithiophosphate plus 5 vol. % detergent-inhibitor in 10W–30 base oil.

APPENDIX TABLE 2

Radioactivity of Various Engine Parts after Tests with Oils Containing P^{32}-labeled Zinc di(C_6)Alkyl Dithiophosphate

Engine part or section	Average activity per part[a]	Relative activity per unit of geometrical area
Valve Lifters		
Face	1150[b]	100.0
Side	50	0.8
Camshaft		
Cam surface (complete)	1731	43.7
Fuel pump eccentric	109	2.4
Camshaft bearing	35	0.4
Sprocket teeth (for timing chain)	155	1.8
Push Rods		
Lower end	20	32.4
Upper end	16	7.7
Remaining area	NSA[c]	NIL
Rocker Arms and Brackets		
Socket (for push rod)	40	19.6
Complete inner bearing area of rocker arm	480	11.4
Lower half of one inner bearing area (scuffed)	351	16.7

Table 2—*continued*

Engine part or section	Average activity per part[a]	Relative activity per unit of geometrical area
Upper half of above bearing area (non-scuffed)	61	2.9
Rocker arm pad (against valve stem)	36	24.7
Area of rocker arm bracket in contact with rocker shaft	48	1.2
Rocker Arm Shaft		
Area in contact with rocker arm	134	3.2
Scuffed half of one contact area	159	7.7
Remaining non-scuffed half of above contact area	NSA	NIL
Area in contact with rocker shaft bracket	NSA	NIL
Remaining non-rubbing sections	NSA	NIL
Valve Stem Tops	111	66.0
Cylinder Walls		
All but lower non-rubbing area	253	0.2
Upper 1-in. wide strip (includes top of ring travel)	53	0.2
Lower 1-in. wide strip (includes bottom of ring travel)	155	0.6
Remaining area between the two above strips	225	0.4
Piston Rings		
Top compression ring		
Face	29	1.5
Top flat	83	5.1
Bottom flat	91	5.7
Second compression ring		
Face	39	2.1
Top flat	127	7.6
Bottom flat	51	3.1
Oil ring edges in contact with cylinder	71	3.6
Connecting Rod Assembly		
Connecting rod bearing inserts[d]	NSA	NIL
Wrist pin bearing area on connecting rod	10	0.3
Wrist pin center (against connecting rod)	14	0.4
Wrist pin ends (against piston)	67	0.5
Inner bearing area of piston pin holes (against wrist pin)	105	0.9
Crankshaft		
Main journal	NSA	NIL
Connecting rod journal	151	0.5
Crankshaft counterweight	NSA	NIL
Crankshaft sprocket teeth (for timing chain)	54	1.3
Miscellaneous		
Drive gear teeth on distributor	155	7.2
End of fuel pump push rod (against eccentric)	127	43.4

[a] Net counts/min corrected for decay to the same date and obtained by the acid-wipe method.
[b] All 32 valve lifter faces were counted directly, giving an average activity of 1008 net counts/min. Some were then counted by the acid-wipe method to arrive at a conversion factor.
[c] No significant activity.
[d] Steel-backed babbitt.

APPENDIX TABLE 3

Radioactivity of Hexane-Rinsed Valve Lifters after Engine Tests with Oils Containing P^{32}-labeled Zinc Dialkyl Dithiophosphate

	Activity of lifter faces (net counts/min)[a]			
Metallurgy:	Steel		Alloy cast-iron	
Break-in?	No	Yes	No	Yes
Detergent-inhibitor				
None	432	610	1425	1263
	438	397	1313	1924
	456	514	1050	1562
	434	679	1454	987
Average:	440	550	1310	1434
5 vol.%	606	1600	838	1310
	542	1906	647	1304
	584	1660	648	1200
	639	1512	1052	1285
Average:	593	1669	796	1275

[a] Corrected for decay to the same date. Calculated standard deviations equal to 1–2% of the activity.

DISCUSSION

MORTON ANTLER (*Ethyl Corporation, Detroit, Michigan*):

The study of EP mechanisms has until recently been concentrated on lubricant systems which do not contain metal as a constituent of the EP agent. Representative nonmetal EP compounds include carbon tetrachloride, dibenzyl disulfide, and triphenyl phosphate. With them, EP action is due to the formation of protective chloride, sulfide, and phosphide films by reaction of the additive or its thermal degradation products with the rubbing surface. In the case of EP compounds which contain metal, new mechanisms are possible. With the zinc dialkyl dithiophosphate-type additive, it is now known by radioactive tracer methods that zinc, in addition to sulfur and phosphorus, is a constituent of the protective surface films.

The chemical composition of the films formed from zinc dialkyl dithiophosphates is unknown. Mr. Furey has suggested that they might be resinous layers containing bound phosphorus or the reaction products of EP corrosion of the additive with the rubbing surface. There may be, however, another mechanism operating in cooperation with the mechanisms proposed by Mr. Furey. The thermal degradation of metal-containing lubricants on rubbing surfaces due to frictional heat might produce a variety of inorganic compounds in which all atoms in the film are derived wholly from the additive or the additive and the environment, i.e. solids produced without corrosive action of the

rubbing surface. This mechanism of film formation has been demonstrated in "Lubrication with Organometallics"[1]. In this paper, many systems in which this is the sole mechanism are described. Solids which could be formed from zinc dialkyl dithiophosphates include zinc oxide, zinc sulfide, zinc phosphide, and zinc phosphate. Even more complex inorganic compounds involving zinc, phosphorus, sulfur, and oxygen could be produced. Certainly, solid state reactions might occur between these solids and the usual oxides or metal of the rubbing surface to give yet new phases if the temperature level in rubbing is high enough. It is probable that the surface layer is a "fudge" involving basis metal and its oxides, EP corrosion solids, and the solids produced by the mechanism just described.

Mr. Furey has pointed out that zinc, nickel, and iron dialkyl dithiophosphates are all effective antiwear additives. This does not mean that the role of metal from the additive is unimportant in film formation; if we assume that the divalent metal oxide is formed initially in the thermal degradation of the additive as one of the products, then these oxides could react with α-Fe_2O_3 from the rubbing surface to give new species with the spinel crystal structure. $ZnO.Fe_2O_3$, $NiO.Fe_2O_3$ and $FeO.Fe_2O_3$ (usually written as Fe_3O_4) have identical structures[2]. Spinels are probably preferred on rubbing surfaces to solids having the corundum structure, such as α-Fe_2O_3; ferrous surfaces rich in Fe_3O_4 have long been known to be associated with relatively low friction and wear[3].

A large number of papers have been written in the past three years on lubrication of the internal combustion engine with zinc dialkyl dithiophosphates. However, there have not been serious attempts to determine the chemical composition of the surface films that are formed. This is surprising, since electron diffraction techniques are highly developed and have been shown many times to be applicable to the study of worn surfaces[4]. The appreciable thickness of films from zinc dialkyl dithiophosphate, found by Mr. Furey and others, suggests that sufficient material is present for electron diffraction work. Diffraction methods at their best can not only conclusively determine the species on surfaces, but can establish physical factors such as the average crystallite size and the orientation of surface films. A study of zinc dialkyl dithiophosphate anti-wear mechanisms in research-type bench machines, as opposed to engines, may allow better control of test variables. Worn specimens better suited to electron diffraction studies may, possibly, also be obtained.

Once we recognize the effective anti-wear compounds on worn surfaces, their physical structure, and their relationship to test variables, we will have a means which can allow us to more intelligently select new lubricants for EP applications.

---

[1] M. Antler; "Lubrication with Organometallics", Preprints of the Petroleum Division Symposia, 134th Meeting, American Chemical Society, Chicago, September 1958, v. 3, No. 4, pp. A153–170.

[2] A. F. Wells; *Structural Inorganic Chemistry*, 2nd ed., p. 380, Oxford, Clarendon Press, 1950.

[3] R. L. Johnson, D. Godfrey, and E. E. Bisson; "Friction of Solid Films on Steel at High Sliding Velocities", NACA Tech. Note 1578, April 1948.

[4] L. M. Niebylski, M. Antler, and L. O. Brockway; "Investigation of Wear by Electron Diffraction", Paper 58AM 3A-1, presented at the ASLE 13th Annual Meeting, Cleveland, April 1958. To be published in ASLE Transactions.

Testing and Operation of Ball Bearings Submerged in Liquefied Gases

By K. B. MARTIN[1] and R. B. JACOBS[2]

The demand for large quantities of liquefied gases has necessitated the development of liquefaction turbines and pumping systems. These developments have required studies of bearings and bearing materials suitable for operation in liquid hydrogen and other liquefied gases. The apparatus used to measure frictional torque, wear, and to make life tests on bearings submerged in liquefied gases is described. The information concerning ball bearings obtained from this equipment and some bearing information obtained from an apparatus designed to make basic pump studies is presented. Frictional torque data, wear data, and pictures showing a few of the test ball bearings are included.

1. Introduction

In the design of rotating machinery for operation at very low temperatures, the engineer faces a number of unique problems. Solution of these problems involves selection of materials, seals and bearings.

The selection of materials is usually determined by consideration of thermal expansion coefficients and mechanical properties; the former are important to the maintenance of clearances and to the control of thermal stresses; the latter, of course, determine the design stresses.

Certain materials show more desirable low-temperature properties than others. For instance, type 303 stainless steel has over twice the tensile strength at liquid hydrogen temperature than it has at room temperature. The notch toughness decreases with decreasing temperature but the impact strength is still adequate at liquid hydrogen and nitrogen temperatures. However, in the case of low carbon 1020 steel, although the tensile strength increases to about three times the room temperature value, the impact strength drops from about 15 ft lb to 2 to 3 ft lb. Thus ordinary carbon steel may be unsafe for some low-temperature applications.

A number of materials do have excellent low-temperature physical properties and so the selection of materials is usually not a difficult problem. The austenitic stainless steels, most of the aluminum alloys, and most copper alloys retain sufficient ductility at low temperatures. Thus, because an adequate amount of research has been done on strength of materials and thermal expansion coefficients at low temperatures, a selection of materials can usually be made at this time.

On the other hand, however, little work has been done on bearings and seals for low-temperature application. The purpose of the investigations reported here is to help remedy this situation with respect to bearings which operate submerged in liquid.

2. Performance of bearings in pumps

Since certain pump configurations require no seals, and pumps are commercially available in a number of satisfactory materials, the solution of the low-temperature bearing problem is of primary importance in the pumping of liquefied gases. As early tests showed that properly degreased ball bearings turn freely in liquid nitrogen, all pumps used in our work were either purchased with ball bearings or were modified to take ball bearings. The experience began with a single-row, radial ball bearing (type R-12) having a pressed steel separator in a pump testing apparatus similar to that shown schematically in Fig. 1. (It should be emphasized that all of the bearings

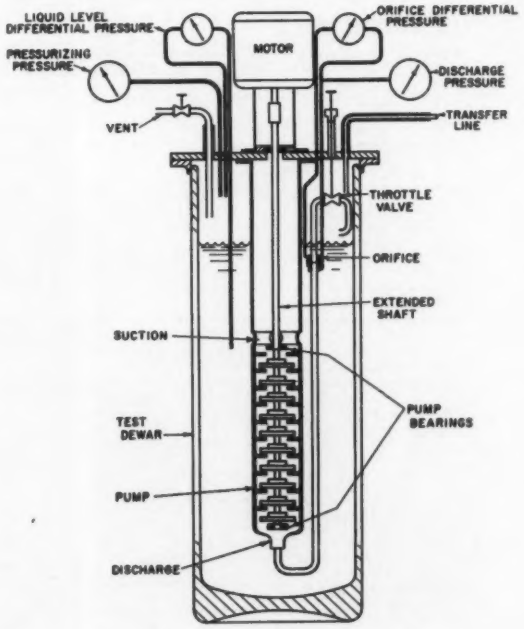

Fig. 1. Pump testing apparatus schematic.

Presented as an American Society of Lubrication Engineers paper at the Lubrication Conference held in Los Angeles, Calif., October, 1958.

[1] Research Engineer, Cryogenic Engineering Laboratory, National Bureau of Standards, Boulder, Colorado.

[2] Research Engineer, Cryogenic Engineering Laboratory, National Bureau of Standards, Boulder, Colorado.

TABLE 1A

Bearing Log for Single Stage Pump—Liquid Indication and Replacement.

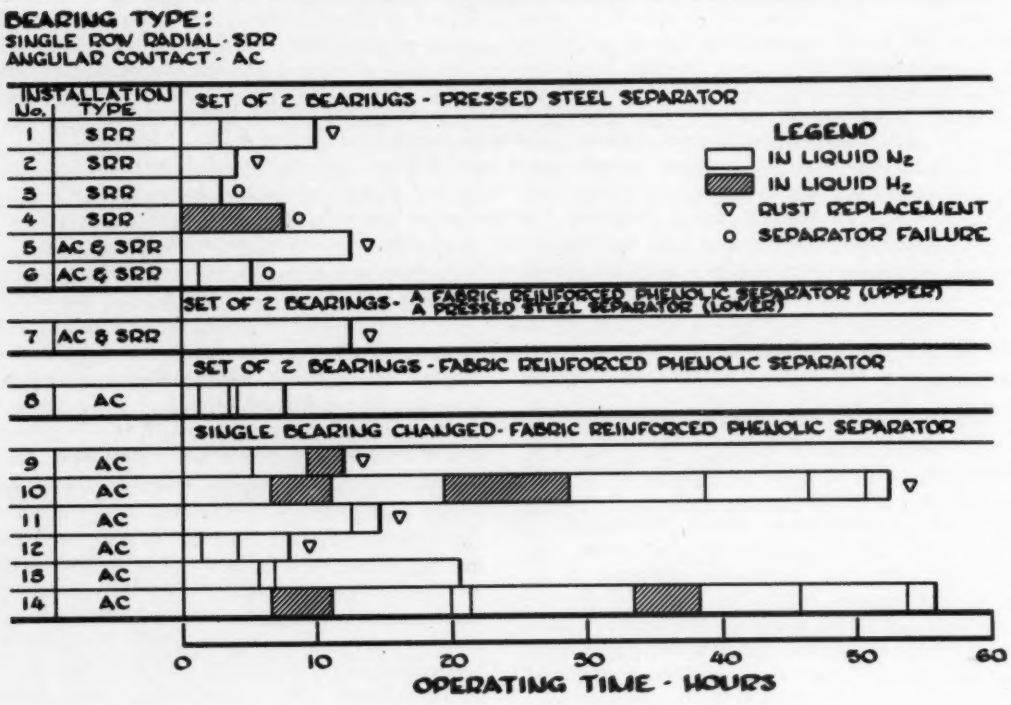

TABLE 1B

Bearing Log for Single Stage Pump—Speed and Bearing Size.

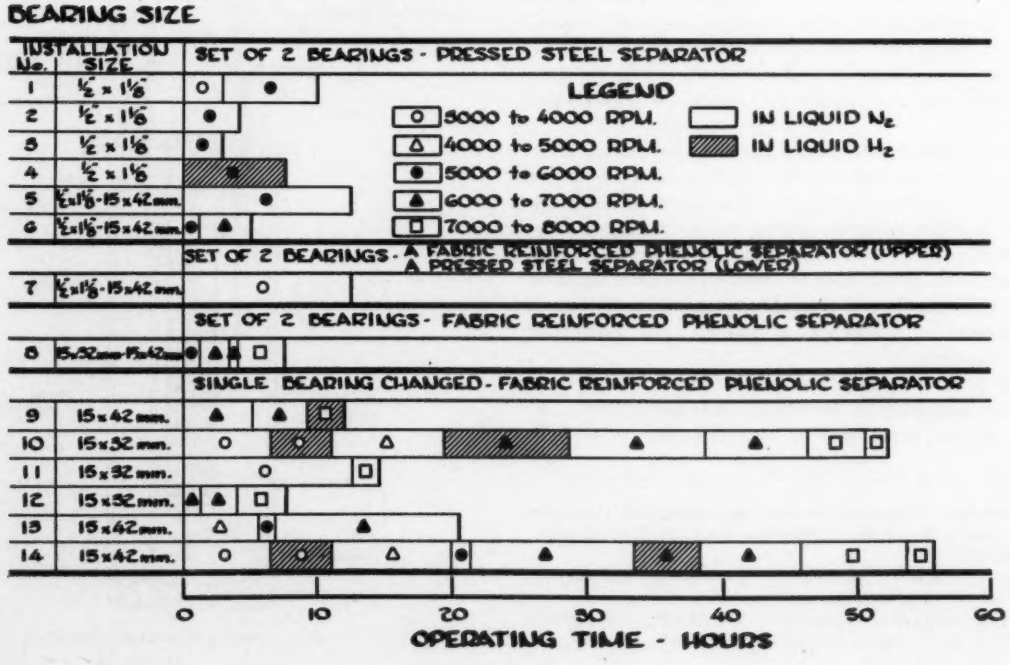

used in the work reported here were purchased "off the shelf"; no attempt has been made to control or determine specifications relating to ball and race dimensions, heat treatment, separator composition and treatment, etc.) In these initial tests the pump was driven by a long shaft, the motor operating at ambient temperature. Since that time it has been thoroughly demonstrated that induction motors can be designed to operate submerged in liquid at any low temperature. The bearings used in the first experiments were standard "off-the-shelf" 52100 series steel and from a number of different manufacturers. These single-row, radial bearings with pressed steel separators gave only limited service in liquid nitrogen and liquid hydrogen; the mechanical failures in all cases were in the separators.

Satisfactory performance, as shown in Tables 1A and 1B, has been obtained, however, in the pump testing apparatus with standard 52100 series angular contact bearings with fabric-reinforced phenolic separators. Some of these bearings have been operated at speeds ranging from 3300 to 8000 rpm. Of these bearings, no failures have occurred from separator wear. However, the bearing material does need careful handling to prevent rusting. Rusting did not occur during the tests; when the apparatus was shut down for reasons which were connected with the pump test, moisture was inadvertently permitted to condense upon the bearings. The rusting caused by this situation is what is referred to in Table 1A as "rust replacement". No bearings were run after they had become corroded and therefore rusting was not a factor in the failures which occurred. The loads on these bearings were those imposed by a conventional fuel booster pump.

In the most recent pumping work, a pair of type 440C stainless steel, single-row, radial ball bearings with two-piece fabric-reinforced phenolic separators (NDQSS 3202) operated very satisfactorily for 262 hr in liquid hydrogen at more than 12,000 rpm. The pump was removed and inspected at the end of this period. The bearings showed no visible wear, but three small cracks visible in the separators are indicated by arrows in Fig. 2. Even though the bearings ran smoothly, they were replaced to protect the pump rather than risk a failure.

3. Performance of bearings in the bearing-tester

3.1 *Description of Bearing Tester*

At the same time that the pumping experiments were being carried on, a project to evaluate bearings and seals was also begun. The apparatus designed to test bearings is shown schematically in Fig. 3. The figure shows a long vertical shaft extending from the ambient temperature region at the top where the drive mechanism is located to the low temperature region in the liquid bath. A commercial, cylindrical stainless-steel Dewar insulates the liquid sump from ambient temperature. Thermal conduction from the warm region is kept small by using stainless steel support tubes and shafts. (One support bearing, located at the lower end of the shaft, keeps shaft whip at a tolerable value.)

The test bearings are located in a test chamber in the sump. A stainless steel extension tube transmits the torque caused by the test bearings into the warm region where it is measured by a dynamometer. The dynamometer consists of two basic parts—a flat coil spring which opposes the frictional torque generated in the bearings and a variable capacitor which indicates the deflection caused by this torque. The dynamometer has no tare since it is supported only by the test bearings and no torque is generated in the variable capacitor. A self-balancing capacitance bridge continually indicates and records the torque generated by the test bearings.

Automatic liquid level controls shown in Fig. 4 maintain the liquid level in the sump so that the bearings are always submerged in liquid. The speed of the apparatus is indicated and recorded with an optical tachometer, frequency meter and recorder. The test apparatus, therefore, becomes an automatic device which requires an operator only to replace periodically the liquid supply vessel and to change charts on the recording instruments. Periodic maintenance

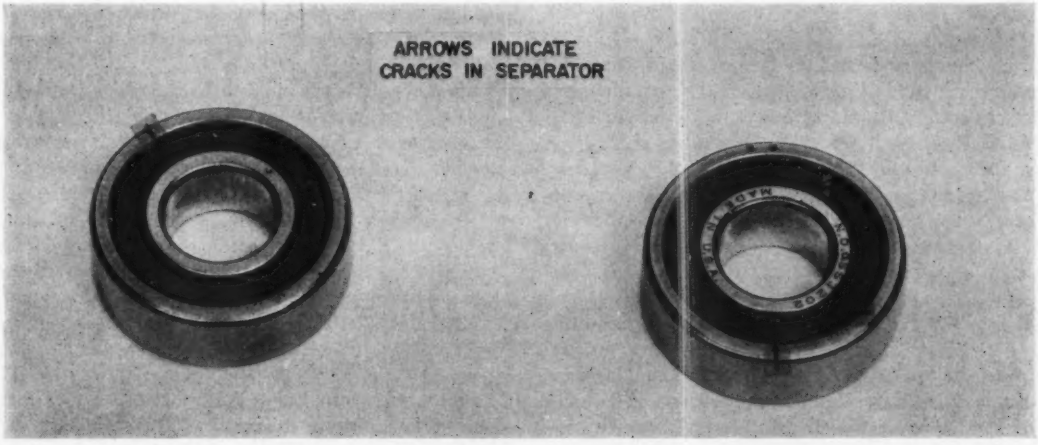

FIG. 2. Separator failure after 262 hr in liquid H_2 at 12,000 rpm.

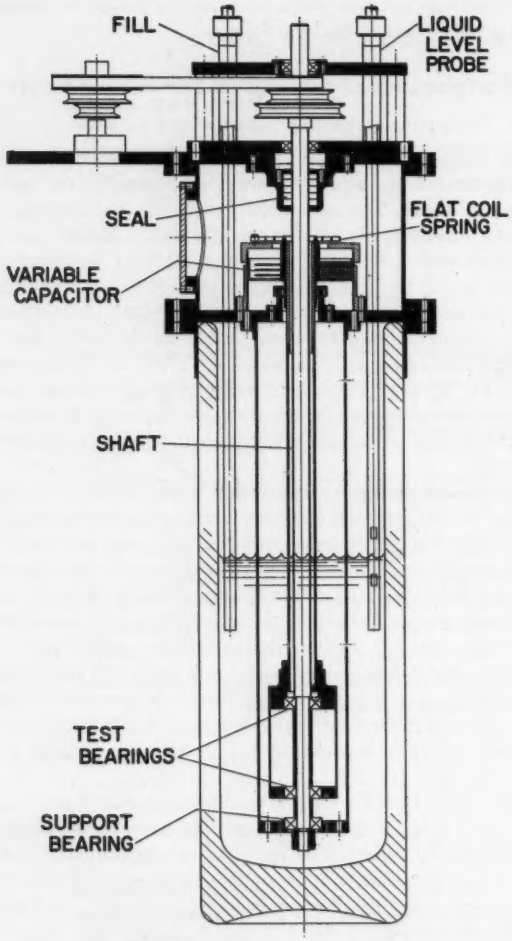

Fig. 3. Bearing tester schematic.

of the recording instruments makes the apparatus capable of operating continuously for months at a time.

3.2 *Test Results*

All of the bearings tested to date with this apparatus have been submerged in liquid nitrogen. The equipment is designed for testing in liquid hydrogen, but liquid nitrogen has been used in the initial tests because safety and ease in handling the fluid were desirable during the shakedown runs. The first runs with this apparatus were made primarily to perfect the apparatus, but useful information has been obtained from them. In test number 3 a single row radial bearing with a riveted pressed steel separator (type R-12) was run for 651 hr at 3300 rpm with but one interruption: the apparatus ran out of fluid and shut itself off automatically; the apparatus was refilled with liquid and the test resumed. At failure, the bearings seized and, because the apparatus did not stop quickly enough, it was severely damaged. The apparatus was therefore redesigned, employing shear pins and a mechanical stop to protect the equipment.

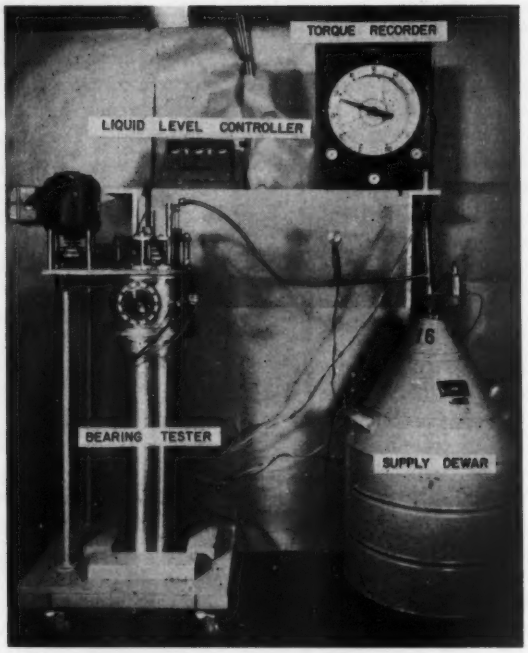

Fig. 4. Bearing tester and automatic controls.

At the completion of test number 3, tests numbers 4 and 5 were conducted to determine when the separators actually failed. Results of these tests indicate that failure or actual wear-through of the separators occurred at about 125 hr.

The loading of the test and support bearings consisted of the incidental loads imposed by the apparatus; during these initial tests, the bearings were not purposely loaded. The bottom test bearings had a slight radial load; the top test bearings had a slight radial load and 6.3 lb thrust load; the support bearings had a 10.9 lb thrust load and whatever radial load was due to imperfections in the shaft. The loading is one of the parameters which will be varied in later tests. As expected, greater thrust loads produced more wear.

Since separators seemed to be the major factor affecting the life of bearings submerged in cryogenic liquids, a ball bearing with a fabric-reinforced phenolic separator was selected for use in the pump testing experiments. These bearings operated so much better in the pump that tests were begun on these bearings in the bearing test apparatus. In test number 6, each of the three submerged bearings had operated for a total of 4772 hr at 3300 rpm when the test apparatus was shut off. The test was terminated when excessive wear of the shaft caused by slipping of the inner races of the room temperature drive bearings was discovered.

The torque history of test number 3 is shown in Fig. 5. The torque increase during the first period up to about 100 hr seems to be typical for the bearings run with pressed steel separators. After about 100 hr, the torque decreased

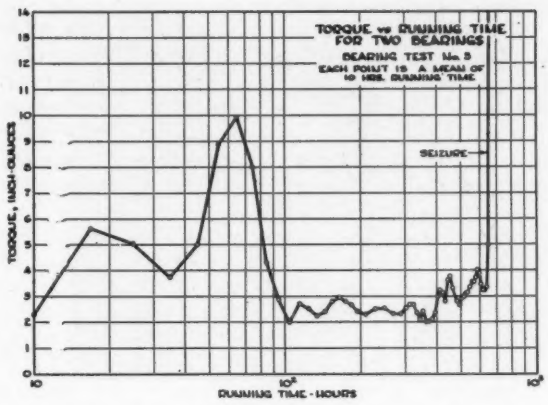

FIG. 5. Torque history of test 3 (pressed steel separator) at 3300 rpm in liquid N_2.

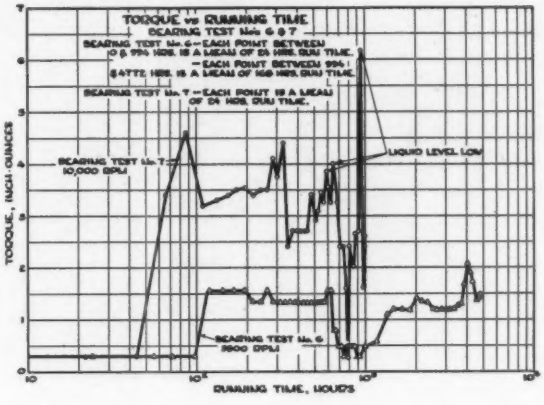
TORQUE vs RUNNING TIME
BEARING TEST Nos. 6 & 7
BEARING TEST No. 7 — EACH POINT IS A MEAN
OF 24 HOS. RUN TIME.
LIQUID LEVEL LOW
BEARING TEST No. 7
10,000 RPM
BEARING TEST No. 6
3300 RPM
TORQUE, INCH-OUNCES
RUNNING TIME, HOURS

FIG. 6. Torque history of tests 6 and 7 (fabric-reinforced phenolic separators) at 3300 rpm and 10,000 rpm in liquid N_2.

to about the value at the beginning of the test and remained nearly constant until the separators wore through. The test apparatus shut itself off apparently when a small part of the separator jammed the bearing.

The torque history of tests number 6 and 7 are shown in Fig. 6. The bearings used in both tests were 52100 steel angular contact bearings with fabric-reinforced phenolic separators. The torque at the beginning of both tests was about the same. Notice, however, that in the 10,000 rpm test, the torque increased much sooner, as might be expected, than in the 3300 rpm test.

At 310 hr of test number 7, the bearings were removed and inspected for wear. The upper test bearing and the support bearing which were thrust loaded sustained no visible wear on the balls by the end of 310 hr.

The bearings were replaced and the test resumed. At the end of 686 hr the test apparatus shut itself off when the liquid level ran low. The bearings were again removed and inspected for wear. The balls in both the upper test bearing and the support bearing showed from 0.006 in. to 0.007 in. wear. Visible wear was also noticed in the races but no quantitative value was determined.

At this point in test number 7 the support bearing was replaced and the test again resumed. From this time on until 1000 hr the torque record was very erratic. Continued trouble with the automatic liquid level device may have contributed, however, to this condition, because the test apparatus kept running low on liquid.

At the end of 1000 hr, the bearing test was again shut down not only for periodic inspection, but because it was known that the liquid had dropped below the usual operating level. The separator of the upper test bearing was worn through like the one shown in Fig. 8. The separator did, however, show signs that it had been very hot. The material around the ball holes was badly charred. The balls and races were also badly worn and discolored. The total wear on the balls from the beginning of the test was almost 0.010 in. Some of the balls even showed where a flat ring was worn around the ball. As the lower test bearing appeared to be in good condition, it is believed that the

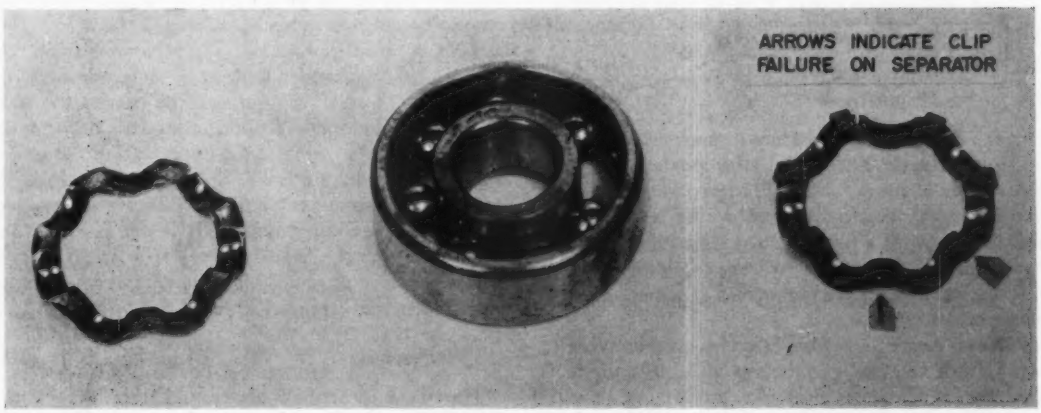

FIG. 7. Pressed steel separator failure after 103 min at 5600 rpm in liquid N_2.

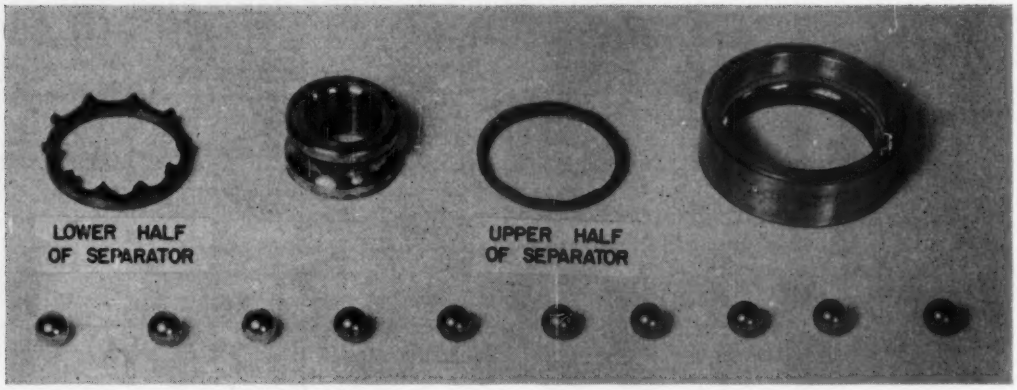

FIG. 8. Fabric-reinforced phenolic separator failure after 4772 hr at 3300 rpm in liquid N_2.

failure of the upper test bearing was caused by its operation out of the liquid.

During test 7, the bearing tester ran out of liquid several times due to malfunction of the liquid control system. The torque record shown on the daily charts indicates a rapid increase in torque, much more severe than is shown in Fig. 6; these high values of torques were masked when the average points shown in the figure were computed. In one instance the torque actually went from 3.3 in. oz to 17.5 in. oz; this gives an indication of the effect of the presence of liquid on the friction generated by the bearings. It is not known if this effect is due to the lubricating quality of the liquid or to the more effective cooling, or both. As the liquid level drops below the bearings, the lubricating quality of the liquid is lost, as well as the excellent heat transfer mechanism. The bearings immediately begin to warm up and as the temperature rises the friction also increases. On two such occasions the tester automatically shut off because of high torque. An increase in temperature was easily determined from inspection of the separators. The separators show where they had been scorched from overheating of the balls. It is concluded, therefore, that the cooling ability of the liquid is of primary importance. However, it is planned in future tests to conduct experiments to determine the actual effects of the presence of liquid.

4. Types of bearing failure

The types of bearing failure are an important aspect of the bearing experience. The only destructive failure of the bearings has been in the separators. The experience in both the pump testing apparatus and the bearing tester shows that a ball bearing with a pressed steel separator operating submerged in liquid nitrogen or hydrogen will not operate as long as the same ball bearing with a fabric-reinforced phenolic separator.

Tables 1A and 1B are logs of the bearings used in a single stage pump. Half the sets of bearings with pressed steel separators were replaced because of separator failure and half were replaced because they appeared rough; in all cases, the roughness was due to rusting which occurred as described above. The bearings with phenolic separators, on the other hand, suffered no separator failures, and were replaced only when rusting occurred, or if modifications were being made to the apparatus.

Table 1B shows operating speed in both liquid nitrogen and liquid hydrogen for the pump bearings. The last two bearings listed both had more than 50 hours' operating time at speeds up to 8000 rpm, at which time the project was terminated.

A bearing with a clipped pressed steel separator taken from the pump apparatus is shown in Fig. 7. The bearing operated for 103 min at 5600 rpm in liquid nitrogen. Fatigue of two of the clips at points of high stress concentration caused failure of the metallic separator. No visible wear occurred in the balls and races. The bearings from test number 3 at 3300 rpm were removed and visually inspected for wear. The riveted metal separator of the upper test bearing showed severe wear. Some sections of the separator had even worn through and dropped out of the bearing. The separator of the lower test bearing showed even more severe wear. The separator between three balls had dropped out of the bearing into the bottom of the test Dewar.

One of the bearings from test number 6 is shown in Fig. 8. This bearing was the first of the 52100 series angular contact bearings to be tested. After 4772 hr at 3300 rpm, the apparatus was disassembled. The separators of all the submerged bearings were found to be worn through between the balls. On all three bearings, the part of the separator which dropped away still had sharp points between the ball holes. The greater wear of the upper part of the separators, which rested on the balls, is readily seen. Possibly the presence of the upper part of the separators managed to keep the balls from jamming. It is not known when the separators actually failed. However, it is suspected that failure occurred after 3700 hr of operation when the torque temporarily rose from 1.4 in./oz to 2.2 in. oz.

5. Conclusions

The work described above indicates that, for some applications, thoroughly degreased ball bearings operate satisfactorily submerged in liquid hydrogen and liquid

nitrogen. It should be emphasized that this conclusion is based upon the results of tests which involved light loads and shaft speeds from 3300 rpm to 12,300 rpm (ND numbers ranging from about 40,000 to 185,000). Furthermore, the tests were performed on bearings which were obtained "off the shelf" from jobbers; detailed specifications such as ball and race materials, dimensions, heat treatment, internal clearance, and separator composition and history were not known. In spite of the lack of control of these details, the authors obtained relatively long and apparently satisfactory performance from bearings which were tested.

6. Acknowledgments

The authors wish to acknowledge the appreciable contributions to this work made by W. Harry Probert, William L. Olson and Lowell M. Anderson.

Effect of Fiber Orientation, Temperature and Dry Powder Lubricants on Rolling Contact Fatigue

W. J. ANDERSON[1] and T. L. CARTER[2]

The rolling contact fatigue spin rig was used to study the interrelation of fiber orientation and fatigue. In both balls and specially oriented races, a concentration of fatigue failures was observed in regions with the highest angle of intersection of fiber flow lines with the surface. In one race specimen fewer failures per unit area were obtained with increasing distance from the billet axis so that variations in cleanliness in the race may have been important. Further tests are necessary to determine the actual importance of cleanliness. In races, increase in fiber orientation angle also resulted in poorer fatigue life. The fatigue life of M-1 tool steel balls decreased with increasing temperature when using a synthetic lubricant, and was low with dry powder lubricants at 450°F, possibly due to the lubricant particles acting as mechanical stress raisers within the contact zone.

Introduction

A NECESSARY requisite to the improvement of bearing fatigue life in turbojet engine and other high-speed, high-temperature applications is the development of a better understanding of the nature and importance of the many factors influencing fatigue. One of the most important factors is temperature because it affects the properties of both the bearing material and the lubricant. At the bearing temperatures desired by designers of present and anticipated engines (1) the standard bearing material, SAE 52100, suffers from loss of hardness and dimensional stability and most conventional lubricants break down thermally and oxidize. New materials and lubricants are required and research is necessary to choose the best material–lubricant combinations from the standpoint of adequate rolling contact fatigue life. Since dry powder lubricants offer advantages at high temperatures because of their excellent thermal and oxidative stability, it was felt that information on the effect of dry powder lubricants on rolling contact fatigue would be invaluable. Some results of ball fatigue tests with solid lubricants are reported (2).

Another factor of importance in fatigue has been found to be the relation of the fiber orientation to the stressed surface. Reference (3) shows that, in SAE 52100 balls run with randomly oriented tracks, the frequency of failure in the polar areas is about twice that anticipated with a homogeneous material.

The investigation reported in this paper was conducted to determine the effect of temperature on fatigue with liquid and dry powder lubricants and to extend the results of (3) by studying the effect of fiber flow over the entire range of orientations using races with controlled fiber orientation. An estimate of the degree of these orientation effects in balls made of SAE 52100, M-1, M-10, M-50, MHT, TMT, H-15, and T-1 steel alloys is also presented. Some of the results are based on work reported (4, 5).

Apparatus

Figure 1 is a cutaway view of the rolling contact fatigue spin rig. The rig design and operation are described fully in (4, 5, 6). In this rig two balls are driven by air jets around

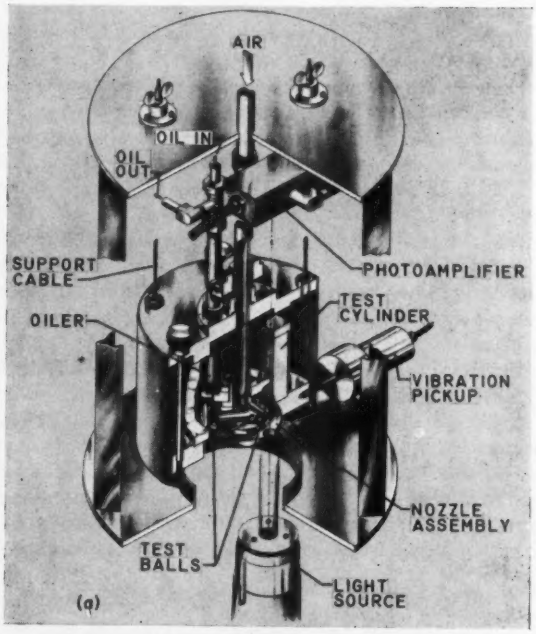

FIG. 1. Diagram of rolling contact fatigue spin rig. (a) Cutaway view.

Presented as an American Society of Lubrication Engineers paper at the Lubrication Conference held in Los Angeles, Calif., October, 1958.

[1] Head of Bearin Research Section, NASA, Lewis Research Center, Cleveland 11, Ohio.

[2] Aeronautical Lubrication Research Engineer, NASA, Lewis Research Center, Cleveland 11, Ohio.

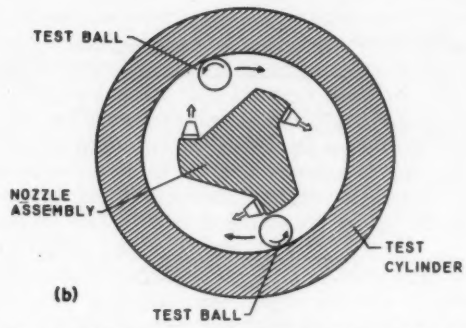

FIG. 1. Diagram of rolling contact fatigue spin rig. (b) Schematic.

the bore of a vertically mounted cylindrical race at orbital speeds to about 30,000 rpm. Each ball assumes a fixed axis of rotation so that all stresses are applied to one great circle track of the ball. Loading results from centrifugal force and is changed by adjusting speed. Speed and temperature are controlled automatically and a failure detection and automatic shutdown system is provided. Liquid lubricants, when used, are introduced through a capillary tube in droplet form and atomized by the high-speed air jets. The system used to introduce the solid particles in fluid suspension is described fully in (4). Flow rate was about 15 ml per hr for the liquid and suspension lubricants.

The test balls were hardened to Rockwell C-62 to C-64 and were all $\frac{1}{2}$ in. in diameter, except the SAE 52100 balls which were $\frac{9}{16}$ in. in diameter. The nominal composition and the cleanliness ratings for these groups of balls are given in Table 1. The running track on the balls was predetermined by randomly grinding two diametrically opposed $\frac{1}{8}$-in. flats on the ball surface.

Specimens with controlled fiber flow orientation were obtained by machining race cylinders from AISI T-1 (18–4–1 tungsten tool steel) billet stock at various angles to the direction of forging. Three cylinders were machined with axes parallel to, at 45° to, and perpendicular to the direction of fiber flow (Fig. 2). The first cylinder had fiber orientation parallel to the test surface, the second had fiber orientation ranging continuously from parallel to 45° to the test surface, and the third had fiber orientation ranging continuously from parallel to perpendicular to the test surface. The nominal composition and the cleanliness rating of this material are given in Table 1. Each of the cylinders was hardened to Rockwell C-62 to C-64.

In testing the special race cylinders, about 20 tracks could be run to failure before the cylinder bore was refinished to a 0.120 in. greater internal diameter. The vertical location of a running track was determined by the vertical position of the guide plate assembly in the bore of the test cylinder. Three bore surfaces (3.25, 3.37 and 3.49 in. diam.) were tested in each cylinder. Sufficient material was removed in each refinishing process to remove any effect of previous stressing. SAE 52100 steel balls, with a fatigue life long enough to ensure that the race failed first, were used in this race evaluation.

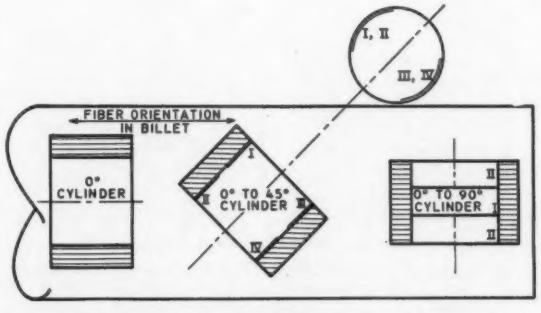

FIG. 2. T-1 tool steel cylinder orientation in billet stock.

RESULTS

Fatigue data were obtained at three different stress levels. Therefore results for different runs can be compared only after correcting for differences in stress level.

Fiber Orientation in Special Race Cylinders

The fatigue life results for the 0°, 0° to 45°, and the 0° to 90° cylinders are shown as Weibull plots in Figs. 3(a) to (c),

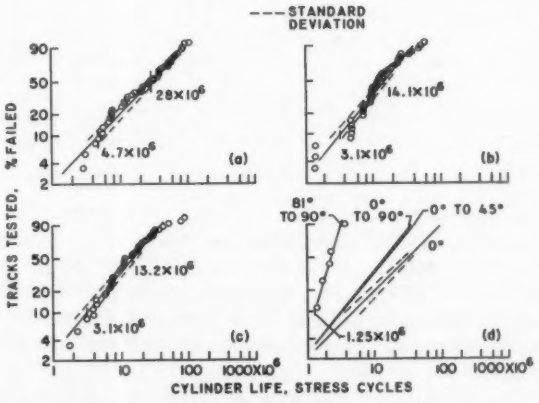

FIG. 3. Fatigue life data for specially oriented T-1 tool steel cylinders. Lubricant, SAE 10 mineral oil; maximum Hertz compressive stress, 750,000 psi.
(a) 0° cylinder.
(b) 0° to 45° cylinder.
(c) 0° to 90° cylinder.
(d) Comparison of 3 cylinders and data from the 81° to 90° zone of fiber orientation angles in the 0° to 90° cylinder.

respectively. Fatigue lives at failure probabilities of 10 and 50% are given in the figures, and the results for the three cylinders are shown for comparison in Fig. 3(d). The 0° cylinder had the best life. The 0° to 45° and 0° to 90° cylinders had approximately equal lives. The difference in L_{10} lives (4.7×10^6 stress cycles for the 0° cylinder and

TABLE 1

Analysis and Cleanliness of Specimens

Material	ASTM cleanliness		Analysis (specified)									
	A–	D–	C	P	S	Mn	Si	Al	Cr	V	W	Mo
SAE 52100 (air-melt)	1	1	1.00	0.025 max.	0.025 max.	0.35	0.28	—	1.45	—	—	—
AISI M-1 (air-melt)	1	1	0.80	0.030 max.	0.030 max.	0.23	0.23	—	4.00	1.00	1.50	8.50
MHT (air-melt)	1	1	0.98	0.025 max.	0.025 max.	0.40	0.54	1.25	1.38	—	—	—
TMT (air-melt)	1	1	1.00	0.025 max.	0.025 max.	0.50	1.00	0.08	1.45	—	—	0.30
AISI M-10 (air-melt)	1	1	0.85	0.030 max.	0.030 max.	0.23	0.03	—	4.00	2.00	—	8.00
AISI H-15 (vacuum-melt)	1	1	0.65	0.030 max.	0.030 max.	0.27	1.20	—	4.72	0.55	—	5.36
AISI T-1 (air-melt)	1	1	0.70	0.030 max.	0.030 max.	0.30	0.25	—	4.00	1.00	18.00	—
AISI MV-1 (air-melt)	1	1	0.80	0.030 max.	0.030 max.	0.30	0.25	—	4.10	1.10	—	4.25
AISI M-50 (air-melt)	1	1	0.80	0.030 max.	0.030 max.	0.30	0.25	—	4.00	1.10	—	4.0
AISI M-1 (vacuum-melt)	1	1	0.80	0.030 max.	0.030 max.	0.23	0.23	—	4.00	1.00	1.50	8.50
AISI T-1 (air-melt), cylinders	1	1	0.70	0.030 max.	0.030 max.	0.30	0.25	—	4.00	1.00	18.00	—

3.1×10^6 for either of the other two cylinders) represents about two standard deviations of either the 0° to 45° or the 0° to 90° cylinder data. Standard deviations were calculated by the method of (7). These data indicate that there is a significant difference in life between the 0° cylinder and the other two cylinders.

The life data for the three cylinders does not give a quantitative measure of the variation in life between the extremes of parallel and perpendicular grain because the 0° to 90° cylinder represents a composite value for a range of orientations. A Weibull plot for the portion of the 0° to 90° cylinder with fiber orientations near the perpendicular would give a more representative value. Such a plot is given in Fig. 3(d) for the 81° to 90° zone. As expected the L_{10} life (1.25×10^6 cycles) is lower than that for the cylinder as a whole (3.1×10^6 cycles). This plot is not entirely correct statistically since a failure in the remainder of the cylinder would be a runout in the zone under consideration, but five of the six lowest lived failures occurred in the 81° to 90° zone. Figure 3(d) was drawn using a sample size of six with five failures and one runout.

A second method of determining the effect of fiber orientation would be to examine failure density as a function of fiber orientation angle. In both the 0° to 45° and 0° to 90° cylinders there are four similar 90° quadrants so that the data could be condensed into one equivalent quadrant. The equivalent quadrant was then divided into four zones for the 0° to 45° cylinder and five zones for the 0° to 90° cylinder, and the number of failures in each zone counted. The resulting histograms are shown in Fig. 4. In

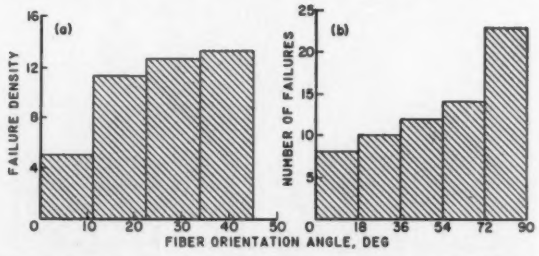

FIG. 4. Variation in failure density with fiber orientation angle in the 0° to 45° and 0° to 90° T-1 tool steel cylinders.
(a) 0° to 45° cylinder (corrected for unequal areas).
(b) 0° to 90° cylinder.

the 0° to 45° cylinder the variation of fiber orientation angle with rotation is not linear so that equal increments of fiber orientation angle mean unequal areas. It was therefore necessary to correct the number of failures for this variation in area. Figure 4 shows that, for both the 0° to 45° and 0° to 90° cylinders, the failure density is significantly higher in the regions of high fiber orientation angle than in the regions where the fibers are oriented almost parallel to the test surface. Thus, both the life and failure density data indicate that high fiber orientation angles are detrimental to rolling contact fatigue.

Material cleanliness is known to be an important factor in fatigue and it is also known that a billet is "dirtiest" along its axis. Because of the manner in which the race cylinders were machined from the billet (Fig. 2), cleanliness, as measured by distance from the billet axis, and not fiber orientation angle might be the important variable. Further analyses were therefore made in an attempt to answer this question. These are discussed in detail in the appendix. Briefly these analyses indicate that, in these tests, fiber orientation appears to be the more important variable but that more tests are required to obtain conclusive results.

Fiber Orientation in Balls

A large group of balls, of which 211 failed, was tested with randomly oriented tracks and was used to obtain data on failure location with respect to fiber orientation. This sample group consisted of sub-groups of ten different materials.

Since the tracks of the balls were randomly oriented with respect to fiber orientation, a random failure pattern should have been produced if the balls were of uniform fatigue strength over the entire surface area. Reference (8) contains a computation of the probability of failure occurring in a polar area under various limiting conditions; this computation shows that the percentage of failures theoretically anticipated in the polar areas (assuming homogeneous material) is 15. Table 2 is a comparison of the actual failure

TABLE 2

Experimental and Theoretical Failure Location Distributions in Randomly Oriented Balls[a]

Material	Location of failures	Experimental results		Theoretical fraction of failures (b)	Ratio of experimental to theoretical results
		Number of failures	Fraction of failures		
SAE 52100,[c]	Polar area	14	0.326	0.15	2.17
$\frac{1}{16}$ in. diam.	Non-polar	29	.674	.85	.79
AISI M-1	Polar area	15	0.205	0.15	1.37
$\frac{1}{4}$ in. diam.	Non-polar	58	.795	.85	.94
AISI M-1	Polar area	3	0.231	0.15	1.54
(vacuum-melt) $\frac{1}{4}$ in. diam.	Non-polar	10	.769	.85	.90
AISI MV-1,	Polar area	5	0.217	0.15	1.45
$\frac{1}{4}$ in. diam.	Non-polar	18	.783	.85	.92
AISI M-10,	Polar area	4	0.444	0.15	(d)
$\frac{1}{4}$ in. diam.	Non-polar	5	.556	.85	
AISI M-50,	Polar area	5	0.417	0.15	(d)
$\frac{1}{4}$ in. diam.	Non-polar	7	.583	.85	
MHT,	Polar area	2	0.167	0.15	1.11
$\frac{1}{4}$ in. diam.	Non-polar	10	.833	.85	.98
TMT,	Polar area	10	0.833	0.15	(d)
$\frac{1}{4}$ in. diam.	Non-polar	2	.167	.85	
AISI H-15	Polar area	5	0.500	0.15	(d)
$\frac{1}{4}$ in. diam.	Non-polar	5	.500	.85	
AISI T-1,	Polar area	2	0.500	0.15	(d)
$\frac{1}{4}$ in. diam.	Non-polar	2	.500	.85	
Total	Polar area	65	0.308	0.15	2.05
	Non-polar	146	.692	.85	.81

[a] All groups had an average pole half-angle of 40°.
[b] For a homogeneous material as calculated in (8).
[c] Includes 29 failures reported in (8).
[d] Computations omitted because track orientation was not approximately random.

locations with the 15% theoretical anticipated. The ratio of experimental to theoretical results is given only for the samples which showed an approximately random track orientation, that is, 63% of the total of the failed tracks passing through the polar areas. For the entire group the proportion of polar failures (30.8%) is approximately two times that which would be expected if the entire ball surface had uniform fatigue strength. This susceptibility of polar areas to failure indicates that the polar areas are significantly weaker in fatigue. The tendency for a larger than normal proportion of polar failures seems to hold for each of the ten individual materials investigated although some of the smaller samples were not randomly oriented and thus are difficult to analyse.

Table 3 gives the distribution of failures in the 144 balls, taken from the 211 in Table 2, which ran over the poles. If the ball surface had uniform fatigue strength, 23.4% of the failures should have occurred in the poles (8). For the total group of balls the actual result (45%) was about 1.9 times that number. For each of the 10 ball materials studied, the polar areas appear to be weak in fatigue because for each material the ratio of actual to theoretical fraction of polar failures is greater than unity.

Figure 5 is a plot of failure density on the ball surface as a function of the elevation from the equator toward the pole (i.e. ball latitude). This figure was compiled from the failure position data obtained from the 211 balls examined. The data were plotted by counting all the failures in each of nine 10° zones of ball latitude and dividing by a factor equal to the percentage of the total ball area in the zone. This gave a failure density for each zone. This plot shows a very marked increase in the density of failures at higher ball latitude, that is, the polar areas where the fiber orientation is approximately perpendicular. The area near the equator also shows an increase in failure density. This area also has perpendicular fiber orientation due to the

TABLE 3

Distribution of Failures in Randomly Oriented Balls which Ran over Polar Areas[a]

Material	Location of failures	Experimental results		Theoretical fraction of failures (b)	Ratio of experimental to theoretical results
		Number of failures	Fraction of failures		
SAE 52100,[c] ⅝ in. diam.	Polar area	14	0.560	0.234	2.39
	Non-polar	11	.440	.766	.57
AISI M-1, ½ in. diam.	Polar area	15	0.300	0.234	1.28
	Non-polar	35	.700	.766	.97
AISI M-1 (vacuum-melt) ½ in. diam.	Polar area	3	0.375	0.234	1.60
	Non-polar	5	.625	.766	.82
AISI MV-1, ½ in. diam.	Polar area	5	0.400	0.234	1.65
	Non-polar	8	.600	.766	.80
AISI M-10, ½ in. diam.	Polar area	4	0.572	0.234	2.44
	Non-polar	3	.428	.766	.56
AISI M-50, ½ in. diam.	Polar area	5	0.556	0.234	2.37
	Non-polar	4	.444	.766	.58
MHT, ½ in. diam.	Polar area	2	0.286	0.234	1.22
	Non-polar	5	.714	.766	.93
TMT, ½ in. diam.	Polar area	10	0.833	0.234	3.56
	Non-polar	2	.167	.766	.22
AISI H-15 ½ in. diam.	Polar area	5	0.500	0.234	2.14
	Non-polar	5	.500	.766	.65
18–4–1, ½ in. diam.	Polar area	2	0.667	0.234	2.85
	Non-polar	1	.333	.766	.44
Total	Polar area	65	0.451	0.234	1.93
	Non-polar	79	.549	.766	.72

[a] All groups had an average pole half-angle of 40°.
[b] For a homogeneous material as calculated in (8).
[c] Includes 16 failures from (8).

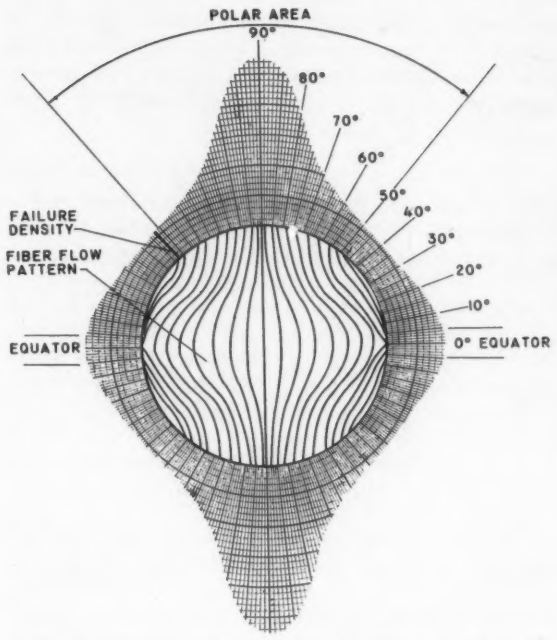

FIG. 5. Failure density as function of ball latitude (for 211 failures and 10 materials).

removal of flashing formed at the upsetting die parting line. These characteristic fiber orientation areas are illustrated in Fig. 6.

Effect of Temperature with the Sebacate Lubricant

The fatigue life result for three series of tests of M-1 balls run at 100°, 250° and 450°F with a synthetic sebacate lubricant are shown in Figs. 7(a) to (c). The lubricant used was di(2-ethylhexyl)sebacate with a viscosity of 13.5 cs at 100°F and 4.91 cs at 210°F. These results, summarized in Fig. 7(d), indicate a decrease in L_{10} life with increase in temperature. However, there appears to be an increase in L_{50} life in going from 250° to 450°F. At 450°F the sebacate tended to polymerize into a very viscous residue. The rate of formation was low, but in the longer test runs there was an appreciable accumulation of the residue on the ball track, and it is believed that this viscous film extended the lives of the longer running balls at 450°F.

The reduction in fatigue life with increasing temperature exhibited in these tests evolves partly from the decrease in lubricant viscosity and partly from the effects of temperature on the material and lubricant. In (9) fatigue life with mineral oil lubrication was found to increase with increasing viscosity. The viscosity–life relationship of (9) predicts a decrease in life (due to temperature lowering of viscosity over the temperature range, 100° to 450°F) smaller than that obtained in these tests; thus additional temperature-dependent factors evidently affect life.

The failures obtained at all three test temperatures were similar in appearance and origin and no evidence of chemical corrosion was present on any of the running tracks.

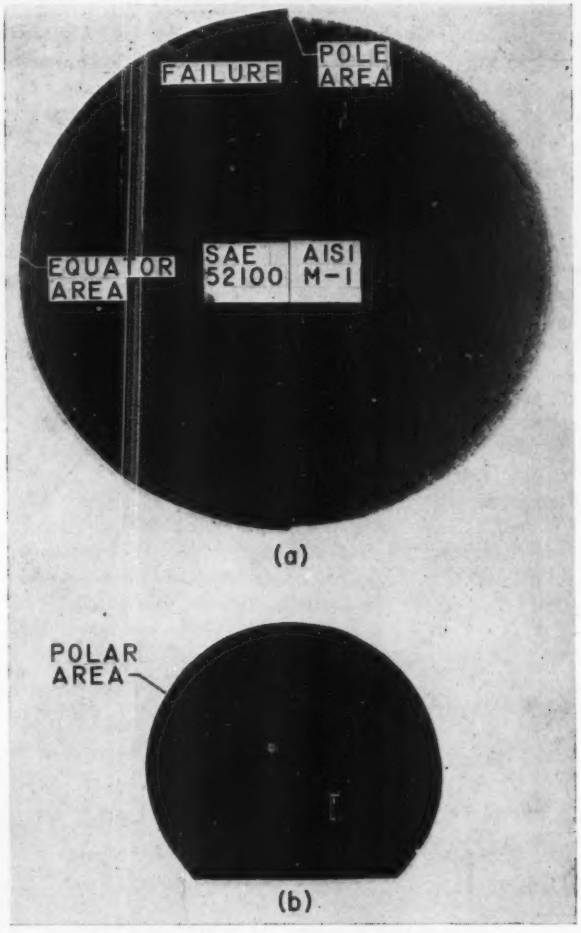

FIG. 6. Fiber orientation of SAE 52100 and AISI M-1 balls.
(a) Cross sections showing fiber orientation.
(b) Poles and equator.

The formation of a transformation product in the subsurface zone of maximum shear stress in M-1 balls was reported in (10) at room and 200°F test temperatures. Since these observations were for the same heat of material as used in this report, no further investigation was made for the 100° and 250°F specimens. Metallographic sections were made of the 450°F test specimens, and typical results are presented in Fig. 8. Only slight transformation or structural change was observed at room temperature, but at 200°F this transformation became more pronounced. At 450°F a further increase in this transformation was observed. The transformation increases with test temperature and with the number of stress cycles.

These results must be tempered by confidence in the statistical reliability of the data. For the sample sizes of 21, 16 and 8 balls each, used to produce the data in Figs. 7(a) to (c), these confidence limits are wide in relation to the observed difference in lives. However, if there exists no effect on life with increasing temperature, the probability

(a) 100°F.
(b) 250°F.
(c) 450°F.
(d) Summary.

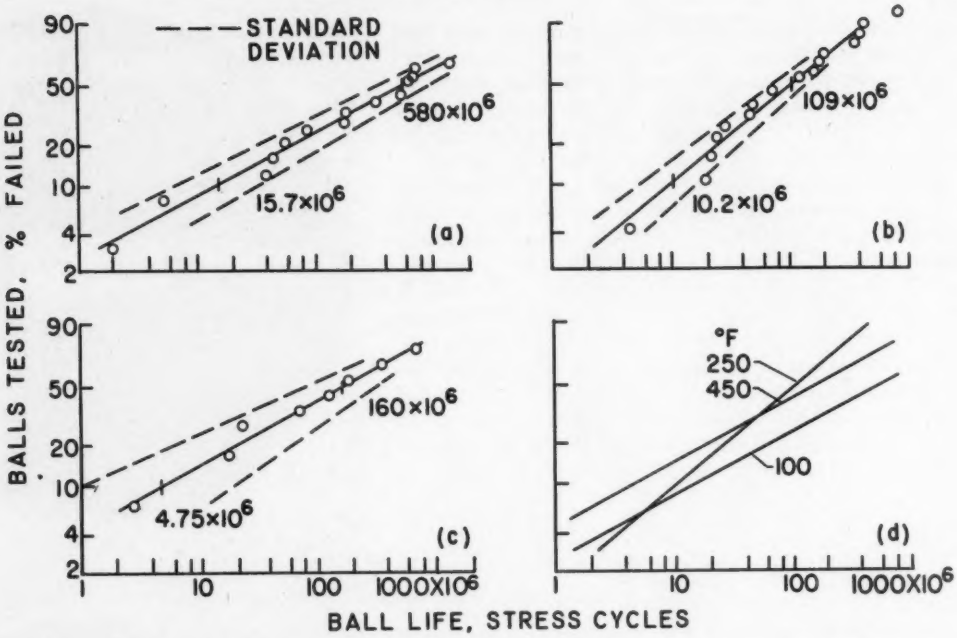

FIG. 7. Fatigue life for ½ in. AISI M-1 balls at various temperatures. Lubricant, di(2-ethylhexyl)sebacate; maximum Hertz compressive stress, 650,000 psi. (a) 100°F (b) 250°F (c) 450°F (d) Summary.

FIG. 8. Metallographic transformation in subsurface zone of maximum shear. AISI M-1 tool steel; test temperature, 450°F; maximum Hertz compressive stress, 650,000 lb per sq. in.; ×100 (reduced to 7/10ths).

(a) 21×10^6 stress cycles.
(b) 174×10^6 stress cycles.
(c) 261×10^6 stress cycles.
(d) 197×10^6 stress cycles; matrix damage in shear plane.

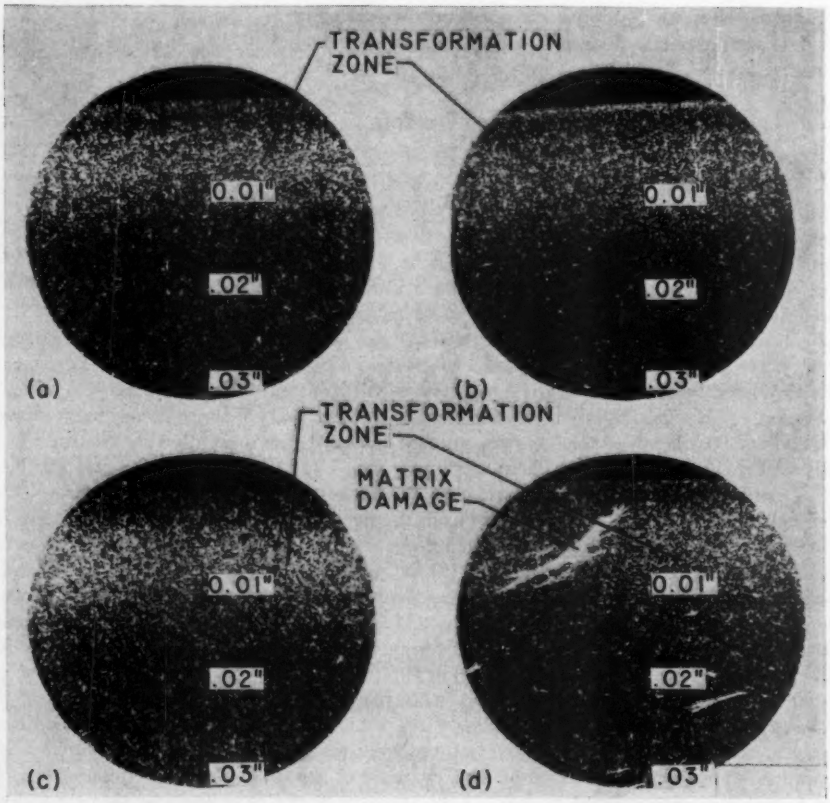

for the 10% lives of the three plots falling in ascending order is only 1 in 6. This is true because each of the lines was calculated by the least-squares, best-fit technique so that they are objective.

Dry Powder Lubricants

Dry powders were used in an attempt to find lubricants usable at test temperatures beyond 450°F. In preliminary test runs when powders were introduced as a dust in air, problems in metering during prolonged unattended periods were encountered so that, in subsequent tests, a suspension of the powder in a fluid that would evaporate at the test temperature was used. A polyalkylene glycol that evaporates at about 350°F and leaves little residue was chosen for the tests run at 450°F. The glycol had a viscosity of 8.75 cs at 100°F and 2.28 cs at 210°F. The MoS_2 powder had a maximum particle size of 25 microns.

Results at 100°F—Figure 9 shows the results of two test series run at 100°F with 0.2% MoS_2 suspension in glycol and with plain glycol for comparative purposes. Failure appearance and type of failure obtained with the plain glycol resembled those for other liquid lubricants except that the track surface did not have the characteristic darkening produced by an adherent oxide film. The life with the glycol was similar to that with the sebacate at 100°F after adjusting for differences in stress level.

The MoS_2 suspension produced results at 100°F which were quite different from those obtained with the plain glycol (Fig. 9b). A best fit straight line has been drawn through the data points of Fig. 9(b) but, obviously, two straight lines (dashed lines) are required to fit the data points reasonably well. At about 200×10^6 stress cycles, there appears to be a sharp increase in slope indicating a limit to ball fatigue life. An extensive metallographic investigation was conducted in an attempt to explain this change in slope. Figure 10 shows running track appearance and longitudinal cross-sections of the subtrack region for three specimens subjected to successively greater numbers of stress cycles. Figures 10(e) and (f) show a failed specimen with the complete fatigue spall. The spall appears to be subsurface in origin but the depth of origin of the spalls is confined to a zone less than 0.002 in. below the ball surface. A zone of 0.004 to 0.009 in. is considered normal for the failures observed in previous specimens run with simple fluid lubricants (10). A large amount of cracking was observed at a depth of much less than 0.001 in. Incipient cracking and matrix damage originating from carbides were more common and more agglomerated than in previous specimens. This result indicated both higher local stresses and non-uniform stressing. Structural changes characteristic of the subsurface zone of maximum shear tended to be less severe and closer to the surface.

A strong tendency for formation of surface cracking was observed in these specimens (Figs. 10(b), (d) and (f)). This condition is not typical of fluid lubricant fatigue failures. This cracking had a characteristic pattern that bore a definite relation to the relative sliding always encountered

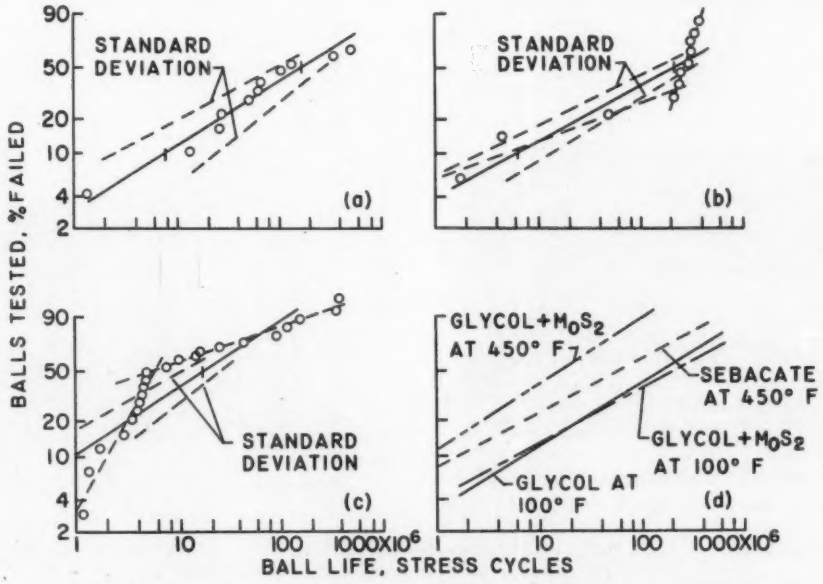

FIG. 9. Fatigue life for ½ in. AISI M-1 balls at 100° and 450°F with glycol and glycol–MoS_2 suspensions. Maximum Hertz compressive stress, 725,000 psi.

(a) Lubricant, polyalkylene glycol; 100°F.
(b) Lubricant, 0.2% MoS_2 suspension in polyalkylene glycol; 100°F.
(c) Lubricant, 0.2% MoS_2 suspension in polyalkylene glycol, 450°F.
(d) Summary.

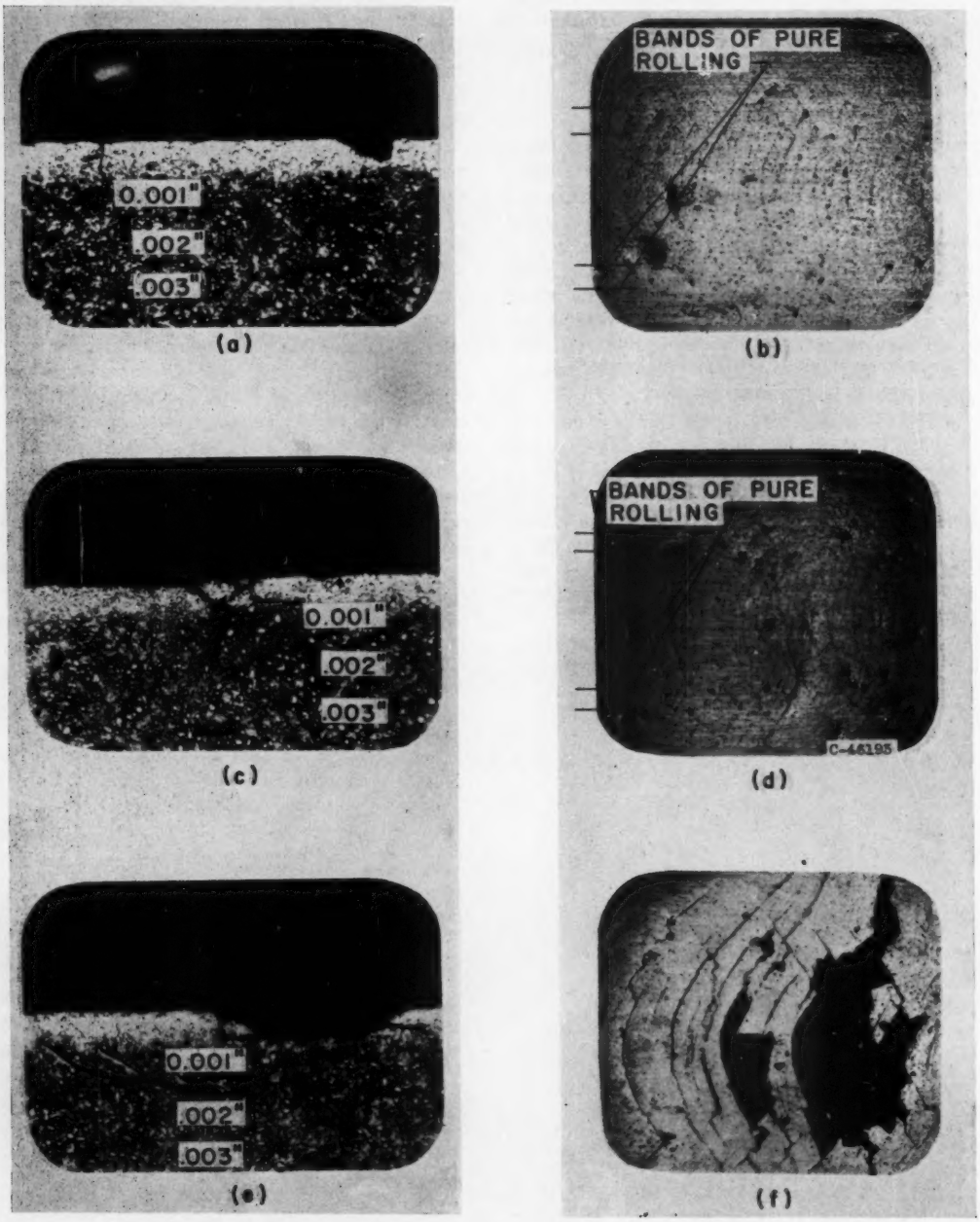

FIG. 10. Typical specimens. Lubricant 0.2% molybdenum disulfide suspension in polyalkylene glycol; M-1 tool steel; test temperature 100°F; maximum Hertz compressive stress 725,000 lb per sq. in.

(a) Longitudinal section; $\times 500$; 52×10^6 stress cycles.
(b) Ball surface; $\times 75$; 53×10^6 stress cycles.
(c) Longitudinal section; $\times 500$; 210×10^6 stress cycles.
(d) Ball surface; $\times 75$; 210×10^6 stress cycles.
(e) Longitudinal section; $\times 500$; 330×10^6 stress cycles.
(f) Track surface; 330×10^6 stress cycles.

in rolling contact of a ball with a race. The sliding motion against the ball surface is opposite the rolling direction at the center of the track and in the same direction at the track edges. Between the zones of sliding, pure rolling occurs on the track in two bands as noted in Fig. 10. The cracking in Figs. 10(b), (d) and (f) has an abrupt change in direction at these bands of pure rolling. Thus, it has a characteristic pattern relative to surface sliding.

The shallow depth of subsurface crack origin (Figs. 10(a), (c) and (e)) and the surface crack pattern (Figs.10 (b), (d) and (f)) indicate a much stronger skin effect in the suspension lubricated balls than that observed in fluid lubricated balls. High shear stresses are apparently generated at the surface by the relative sliding of the contact surfaces. This is in addition to the high shear stress that results from the compressive stresses and that is a maximum about 0.009 in. below the surface. Since the relative sliding and contact pressures are the same for this test run as for previous fluid lubricated runs, the effective friction coefficient apparently is higher for the solid-particle-suspension lubricant.

Evidence of corrosion at the contact surface was very strong in this test run. All previous fluid lubricated runs yielded very limited evidence of contact surface corrosion. Figures 10(b), (d) and (f) show this pitting and the tendency for it to align with the surface cracking. Apparently there is an interaction between surface corrosion and the cracking, with each one promoting the other. Cracking, or the high local stresses causing cracking, would facilitate corrosion, and a corrosion pit would provide the stress concentration for fatigue cracking. Figures 10(a) and (c) present a cross-section of the ball subsurface showing the penetration of corrosion cracking into the subsurface. The increase in depth with longer test time is apparent.

The formation of very small fatigue spalls is shown in Fig. 10(d). These fine spalls are too small to cause enough vibration for failure shutdown, but they are of interest because of their unique tendency to form at the bands of pure rolling. This indicates that some stress-raising effect, possibly the solid lubricant particles in the suspension, was acting in the bands of pure rolling.

The abrupt change in slope of the fatigue curve observed in Fig. 9(b) for the MoS_2 suspension appears to be caused by an interaction of stress corrosion and the high surface shear stresses due to skin effects. The higher shear stress generated by surface sliding would tend to move the maximum shear stress nearer the surface than would be normal for that resolved from compressive stresses alone. The corrosion cracking progresses from the surface at a relatively constant rate. When it reaches the critical zone (i.e. high shear stress) where fatigue spall cracking originates, the susceptibility for fatigue failure is greatly increased and a large fatigue spall will soon develop. The time for corrosion cracking to proceed to this depth corresponds to the running time for 2×10^8 to 4×10^8 stress cycles (regions of increased slope in Fig. 9b) and hence the concentration of the last eight failures within this range.

Results at 450°F—Figure 9(c) shows the results obtained at 450°F with the MoS_2 suspension. Since the glycol evaporated at 350°F only the dry powder was left at the test temperature. A best-fit straight line was drawn through the data points of Fig. 9(c), but again, as for the MoS_2 suspension at 100°F, it is obvious that two straight lines (shown as dashed lines) are required to fit the data points reasonably well. In these tests reaching the test temperature required about 30 min and this corresponds approximately to the intersection of the two dashed lines so that the lower dashed line corresponds to a transition from room temperature to 450°F. Once the test temperature was reached, the slope changed and produced the results considered to be a measure of M-1 tool steel lubricated with MoS_2 powder at 450°F. At 450°F it is possible that the corrosion damage observed at 100°F with the MoS_2 suspension is greatly accelerated. The decomposition of MoS_2 could form corrosive sulfur compounds. In order to evaluate chemical corrosion as a failure-causing factor, a limited number of tests were run at 450°F with dry graphite powder as a lubricant. These are reported in (4) and the results are similar in slope and intercept to the upper dashed line for MoS_2 powder at 450°F. These similar results obtained with two dry powder lubricants with markedly different chemical compositions indicate that physical, rather than chemical, factors are responsible for the poor fatigue life with the dry powder. Possibly the lack of a fluid film to hold corrosive substances at the contact surface prevented corrosion. Figure 11(a) shows no evidence of corrosion pitting as compared to that at 100°F (Figs. 10 (b) and (d)).

Comparison of Results with Fluid and Dry Powder Lubricants

Figure 9(d) shows the results with the glycol at 100°F, MoS_2–glycol suspensions at 100° and 450°F, and the sebacate at 450°F for comparative purposes. The decrease in fatigue life from 100° to 450°F with the MoS_2 suspension is apparent. Increasing temperature is detrimental to fatigue life with both liquid and dry powder suspensions. At 450°F better life was obtained with the sebacate than with the MoS_2–glycol suspension.

While the test runs with dry powder lubricants (both MoS_2 and graphite) at 450°F produced similar results, these results are much different from the results for any of the fluids or for the suspension at 100°F. Subsurface metallographic changes were similar for the runs with fluids and dry powders so that these do not appear to be the cause of lower life. The pattern of failures obtained with the dry powders seems to indicate that mechanical factors were responsible for the poor life.

Two annular bands of fine spalling coincident with the bands of pure rolling were observed on the ball track (Fig. 11a). These spalls in the bands of pure rolling are similar to the normal fatigue spall (Fig. 11c) except that they are on a much smaller scale. A tendency for small spalls to form in the bands of pure rolling was noted previously with the molybdenum disulfide suspension at 100°F (Fig. 10d). A metallographic examination showed that the incipient failures and matrix damage originating from carbides tended to be more common and more segregated than in previous examinations (10), which indicates that high localized stresses were present. Localized

matrix damage occurred under the bands of pure rolling in the region shown in Fig. 11(b). This indicates that a stress raiser was acting in the bands of pure rolling. Apparently the lack of relative sliding of the contacting surfaces at the bands of pure rolling enables the dry lubricant particles to retain some of their shape while the sliding in the remainder of the contact area smears the particles into a thin film.

The theory that the dry lubricant particles produce high, localized compressive stresses in the bands of pure rolling is a hypothetical one, but there is a substantial amount of evidence indicating that some type of localized stress raiser is present that was not present in fluid lubricants. The unique appearance of the spalling, intense localized incipient matrix damage confined to the region of the unique spalling, and the low life all indicate that this is the case. Since a complete bearing has better conformity between ball and race, hence greater relative sliding of the surfaces, the observed effect of dry powder lubricant particles acting as stress raisers may be reduced to a negligible role in normal rolling-contact bearing applications.

Summary of results

Three AISI T-1 tungsten tool-steel race cylinder specimens with controlled fiber orientation and a large group of balls with subgroups of 10 different materials were tested under rolling-contact fatigue conditions at room temperature to study the effect of fiber orientation on fatigue. AISI M-1 tool steel balls were run with a synthetic lubricant at temperatures of 100°, 250° and 450°F, and with a suspension of MoS_2 in water-base glycol at 100° and 450°F. The results of these studies are as follows:

1. In the races a concentration of fatigue failures was observed in that portion of the specimens with the greatest angle of intersection of fiber flow lines with the surface. In one race specimen, however, the concentration of fatigue failures also correlated with distance from the billet axis, fewer failures per unit area being obtained with increasing distance. Since billet material is usually dirtier at its axis, cleanliness may have been a factor. The geometry of the race specimens limits this analysis so that further tests will have to be conducted to determine the actual importance of fiber orientation.

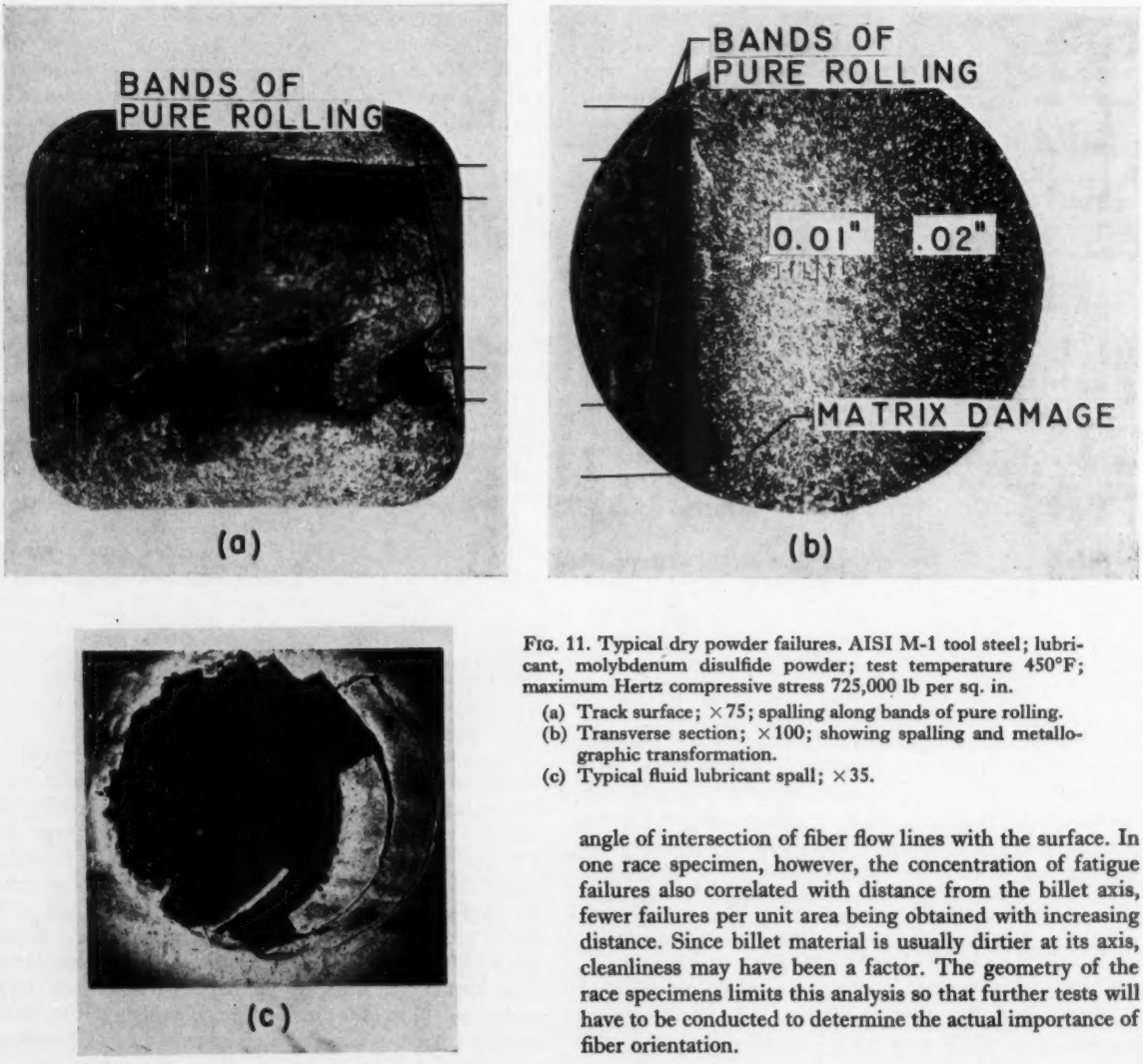

FIG. 11. Typical dry powder failures. AISI M-1 tool steel; lubricant, molybdenum disulfide powder; test temperature 450°F; maximum Hertz compressive stress 725,000 lb per sq. in.

(a) Track surface; ×75; spalling along bands of pure rolling.
(b) Transverse section; ×100; showing spalling and metallographic transformation.
(c) Typical fluid lubricant spall; ×35.

2. In balls, the polar or end grain areas were significantly weak in fatigue. A somewhat lesser weakness was observed for the equator area.

3. A trend toward lower fatigue life was observed with the race specimens as the fiber orientation varied from parallel to perpendicular.

4. Fatigue life for AISI M-1 balls lubricated with di(2-ethylhexyl)sebacate decreased with increasing temperature in the range studied.

5. Metallurgical transformation in the subsurface zone of maximum shear increased with both test temperature and the number of stress cycles.

6. With the dry powder lubricant at 450°F the failures appeared to be hastened by stress raisers localized in the bands of pure rolling. The stress raisers possibly were the dry lubricant particles. Fatigue life was lower than that observed with a fluid lubricant under the same test conditions. Corrosion at the track surface and metallographic transformations did not appear to play a significant role in the observed lowering of life.

7. The MoS_2–glycol suspension at 100°F produced results for short-lived balls in the same range as plain glycol and other fluid lubricants. An abrupt increase in slope of the fatigue life curve for the suspension was observed at 2×10^8 stress cycles. This change in slope appeared to be due to a combination of higher than normal surface shear stress and corrosion cracking. The corrosion cracking progressed from the track surface at an approximately constant rate until it reached the critical subsurface shear zone when failure quickly resulted.

APPENDIX

Analysis of the relative importance of fiber orientation and cleanliness (as measured by distance from billet axis) in race cylinders

The manner in which the race cylinders were machined from the billet (Fig. 2) led to questions regarding possible effects of variations in material cleanliness. Generally billet material is dirtiest at its axis and becomes cleaner as distance from the axis increases. An analysis of failure density as a function of distance from the billet axis produced the results shown in Fig. 12. Figure 12(b) indicates that, in the 0° to 90° cylinder, failure density decreased significantly with distance. This might lead one to conclude immediately that distance (or, equivalently, cleanliness) and not fiber orientation is the important variable affecting fatigue. However, Fig. 13(b) indicates that, in the 0° to 90° cylinder, close proximity to the billet axis generally means higher fiber orientation angles. Therefore, Figs. 4(b) and 12(b) show collectively that either fiber orientation or distance could be the important variable.

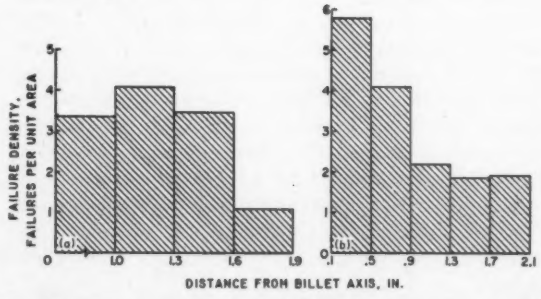

FIG. 12. Variation of failure density with distance from the billet axis in the 0° to 45° and 0° to 90° cylinders.
(a) 0° to 45° cylinder.
(b) 0° to 90° cylinder.

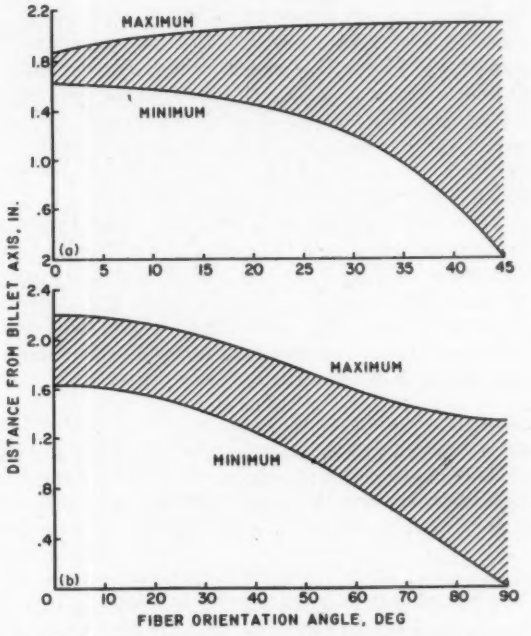

FIG. 13. Relationship between fiber orientation angle and distance from the billet axis in the 0° to 45° and 0° to 90° cylinders.
(a) 0° to 45° cylinder.
(b) 0° to 90° cylinder.

Figure 12(a) indicates that, in the 0° to 45° cylinder, there is no significant trend of failure density with distance. This is in contrast to Fig. 4(a) which shows that, in this cylinder, there is a trend of failure density with fiber orientation angle. Furthermore, Fig. 13(a) indicates that regions of high fiber orientation angle do not necessarily occur close to the billet axis. Thus, in this cylinder the two variables in question are more independent and the data seem to favor fiber orientation as the more important variable.

To determine which of the two variables is more important it is necessary to separate the data, keeping one of these variables constant while the other changed. It was possible to do this, on a limited scale, in two ways. First the 0° to 90° cylinder was divided axially into a zone symmetric about the billet axis (zone I, Fig. 2) and two zones outside this center zone (zones II). In zone I, 30 failures occurred with $L_{10} = 3.9\times10^6$ and $L_{50} = 14.2\times10^6$ stress cycles. In zones II, 37 failures occurred with $L_{10} = 3.5\times10^6$ and $L_{50} = 15\times10^6$. For each data point the range of fiber

orientation angles was the same but the average distance from the tracks to billet axis was less in zone I than in zone II.

A second analysis was made using the 0° to 45° cylinder. Here, four zones, each 1¼ in. long in the test cylinder axial direction and covering 80° circumferentially, were examined for failure density. As shown in Fig. 2, each of the four zones includes the same variation of fiber orientation, but zones I and IV are at a greater average distance from the billet axis than are zones II and III. If distance from the billet axis were the variable of prime importance, one would expect a greater number of failures to occur in zones II and III than in zones I and IV. Thirteen failures occurred in zones II and III and fifteen in zones I and IV.

These two analyses, while limited in scope by the race cylinder geometry and the necessity for treating fatigue data statistically, indicate that, for these tests, cleanliness (as measured by distance from the billet axis) is of lesser importance than fiber orientation angle. Considerable additional research is, however, required to determine the true effects of cleanliness and fiber orientation.

REFERENCES

1. SAE Panel on High-Speed Rolling-Contact Bearings, "Trends of Rolling-Contact Bearings as Applied to Aircraft Gas-Turbine Engines," NACA TN 3110, 1954.
2. SCOTT, D., "Some Studies of Pitting Failure in Rolling Contacts," Paper No. 54 presented at the Conf. on Lubrication and Wear, Inst. Mech. Eng. (London), Oct. 1957.
3. CARTER, T. L., BUTLER, R. H., BEAR, H. R., and ANDERSON W. J., "Investigation of Factors Governing Fatigue Life in the Rolling Contact Fatigue Spin Rig," *ASLE Trans.*, v. 1, n. 1, 1958, pp. 23–32.
4. CARTER, Thomas L., "Effect of Temperature on Rolling-Contact Fatigue Life with Liquid and Dry Powder Lubricants," NACA TN 4163, 1958.
5. CARTER, Thomas L., "Effect of Fiber Orientation in Races and Balls Under Rolling-Contact Fatigue Conditions," NACA TN 4216, 1958.
6. MACKS, E. F., "The Fatigue Spin Rig—A New Apparatus for Rapidly Evaluating Materials and Lubricants for Rolling Contact," *Lubrication Engineering*, v. 9, n. 5, Oct. 1953, pp. 254–258.
7. LIEBLEIN, Julius, "A New Method of Analyzing Extreme-Value Data," NACA TN 3053, 1954.
8. BUTLER, Robert H., BEAR, H. Robert and CARTER, Thomas L., "Effect of Fiber Orientation on Ball Failures Under Rolling-Contact Conditions," NACA TN 3933, 1957.
9. CARTER, Thomas L., "Effect of Lubricant Viscosity on Rolling-Contact Fatigue Life," NACA TN 4101, 1957.
10. BEAR, H. Robert and BUTLER, Robert H., "Preliminary Metallographic Studies of Ball Fatigue Under Rolling-Contact Conditions," NACA TN 3925, 1957.

Rolling Contact Fatigue Evaluation of Bearing Materials and Lubricants

By E. G. JACKSON[1]

Modern aircraft are pushing bearing temperatures beyond the limits of standard steels and lubricating fluids. Newer materials are introducing serious uncertainties into design life calculations. So many parameters and such a spread of statistical phenomena are involved that a "bench" type tester is essential as a substitute for full scale bearing tests to screen material-lube combinations. A high temperature tester has been built, and several months of testing at 400°F have emphasized the magnitude of the problem by showing that (a) the state of oxidation of diesters is a significant factor with several materials, (b) life can vary appreciably between apparently similar heats of steel, (c) hardness is an important factor that needs much more study, (d) standard cleanliness measurements do not seem to be sufficient to establish relative quality.

Introduction

FATIGUE of aircraft main shaft bearings has become an especially difficult design problem within the last few years. The development of higher loads and operating temperatures, with synthetic lubricants replacing mineral oils, and tool steels replacing older bearing metals, has resulted in significant reductions in observed fatigue life.

All the catalogs which provide methods of calculating the load capacities of bearings are based on experience with 52100 type steels and mineral lubricating oils. But, the use of oils other than mineral oils invalidates all the catalog data, and, unfortunately, the effect appears to be often in the direction giving less than calculated life.

For temperatures of 400F and beyond, tool steels are now being used. This change in material also causes deviations from the catalog value of the life, although in this case there is evidence that life can be better than with 52100 if the materials are carefully chosen.

A third factor, and the primary source of the trouble which results in great uncertainty in calculating the average life, is the increased temperature. The catalog values have all been determined at room or moderate temperatures. Very few data are available comparing fatigue over wide temperature ranges, and there are not enough tests to permit any reliable calculations. It is known that increased temperature gives reduced life, but whether due to lower viscosity of the lube oil, increased chemical corrosion, weakened metal structure, or all together, has not been established. Probably the mechanisms vary with the particular material–lube combination.

Therefore, in the light of the uncertainties in the calculation of bearing fatigue life introduced by changes in fluid lubricants, in bearing materials and increased temperatures, the designer is in the very unhappy state of being unable to predetermine a reliable value for the life of a bearing under a given load.

This is especially difficult for aircraft designers because the B10 or 10% life, i.e. the life exceeded by 90% of a sample of bearings, has an even wider statistical distribution than the median life, B50.

Therefore, a large number of test bearing failures must be obtained to bring the confidence in a given value within limits near enough for designers of such critical apparatus. This is very expensive, particularly when it is desirable to study each of the various significant factors by itself. Even using the best statistical techniques requires a very large number of tests, and these non-standard bearings are costing hundreds of dollars apiece.

One way of collecting a lot of data in a shorter time and relatively inexpensively is by the use of simpler devices than complete bearings. This report describes some of the experiences of the first few months with such a machine designed for rolling contact fatigue evaluation at the higher temperatures which are being experienced and which are anticipated. It includes the mechanism shown in Fig. 1 very closely simulating that obtained in ball and roller bearings, and is a derivation of the Barnes rig (1) which uses two rolls and a single ball. Adding the third roll eliminates cage rubbing in one direction as well as increases the rate of stress cycling.

It is believed that by utilizing this type of machine, a large number of factors such as the type of oil, the vendor, the state of oxidation of the oil, the hardness, cleanliness and grain size, as well as the chemical constituents of metals may be evaluated on a relative basis, thereby screening out many combinations which are inferior, and saving the more expensive bearing fatigue tests for those materials which offer the best opportunity for successful operation.

Presented as an American Society of Lubrication Engineers paper at the Lubrication Conference held in Los Angeles, Calif., October 1958.

[1] Supervisor, Bearings and Lubrication, Small Aircraft Engine Dept., General Electric Co., West Lynn, Mass.

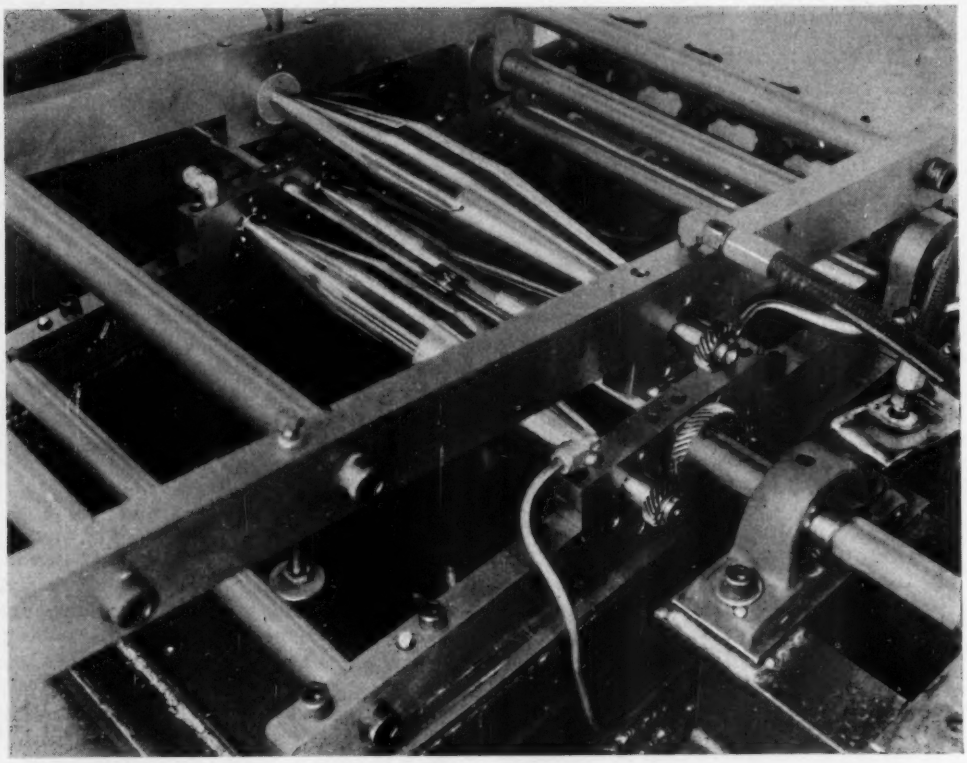

FIG. 1. Thomson laboratory single ball fatigue tester showing three cylinders, single ball in retainer, loading frame and drive mechanism.

Test equipment and procedure

The Thomson Lab Single Ball Fatigue Tester consists essentially of a 2.5 in. cylinder resting on a 0.5 in. ball which is in turn rested on two other cylinders. The bottom cylinders drive the ball which drives the top roll. The top roll is loaded by a dead weight cantilevered off its supporting frame. The cylinder and ball assembly is located in an oven capable of maintaining 1000F.

The machine is designed to run fatigue tests on materials with as few variables as possible, while still reproducing a rolling contact fatigue. Sliding is minimized by eliminating the need for cage guidance in all but one direction, and that is against the axis of spin where surface speeds are low. A little of the lube flow is also fed to this spot. A non-scavenging drip system of lubrication eliminates the variation in the lubricant which occurs during a test with circulating high temperature oil systems. About sixty drops per minute have provided adequate lubrication of both rolling path and cage.

Under the heavy loads of these first tests, no evidence of slipping has been detected on the ball paths. Stroboscopic observation of the top roll speed showed it to be identical with that of the lower two, even without the originally designed positive gear drive. Removal of the top gear reduced vibration and permits regrinding the rolls without having to rematch the gear mesh.

Balls are flatted on two sides so that the cage guides can maintain a constant spin axis. Running on a constant ball path permits accurate count of stress cycles, which are generated at a rate of 9×10^6 per hr (50,000 ball rpm).

Tests are started under full load when the ball temperature as measured by a thermocouple impinging on a pole of the spin axis is at test temperature. No effect of friction heat is observed, and ball temperature is usually within 10 degrees of the oven temperature.

Failure is promptly signaled by a vibrating crystal pick-up which automatically shuts down the machine at the first small pit. The next ball is tested on a new path by moving the cage $\frac{3}{64}$ in. Roll failures occur very infrequently. Such tests are treated as suspended samples since the ball may have been damaged by the roll pit.

All the reported tests were run at 400F with 730,000 psi maximum and 486,000 mean Hertz stresses. A few original tests were run with a circulating (C) oil system. The majority were run with a drip feed of unused fresh (F) or used oxidized (O) oil. The oxidized samples were from

previous ball or ball bearing tests at elevated temperatures. While neutralization (acid) numbers were high, viscosities were essentially unchanged.

The number of balls per run is generally determined by replotting on Weibull paper (2) after each failure and cutting off that series when the curve seems to steady in one position. In one case, series 4, failures were so rapid that the series was stopped at 3. This set of balls was later found to have been improperly heat treated. A new sample will be run later.

Results and discussion

Results are presented in Table 1 and representative plots in Figs. 2–6. Series numbers refer to tests of several balls under identical conditions; Lot numbers refer to the ball material. Tables 2 and 3 show results of metallographic studies and compositions of balls.

Many gaps in the information provided by these results become obvious on study. They emphasize the need for such a quick test in order to be able to examine each of the many parameters involved, some of which may be unexpectedly important, such as the effect of oxidized MIL-L-7808. Future testing will attempt to plug these gaps.

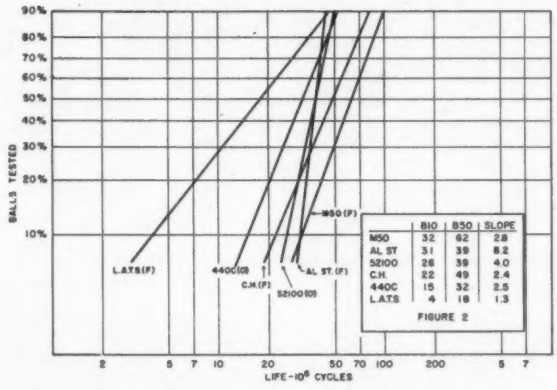

FIG. 2. Best results obtained with each of six materials tested.

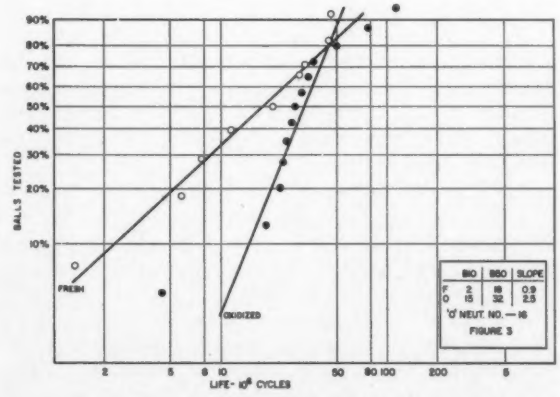

FIG. 3. Effect of oxidized 7808 on 440C (lot no. 18).

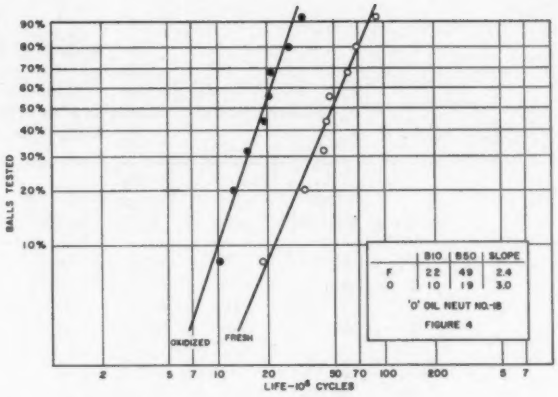

FIG. 4. Effect of oxidized 7808 on Case Hardened (lot no. 29).

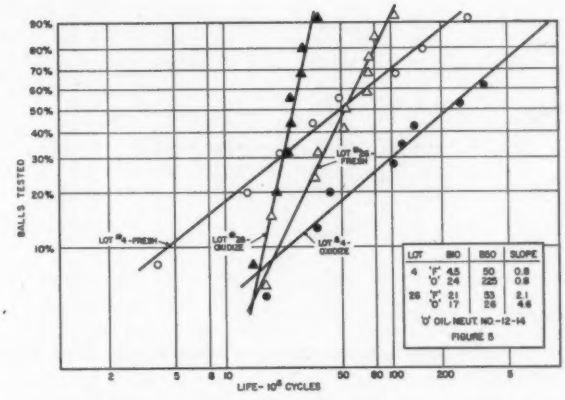

FIG. 5. Effect of oxidized 7808 on M50 (lots nos. 4 and 26).

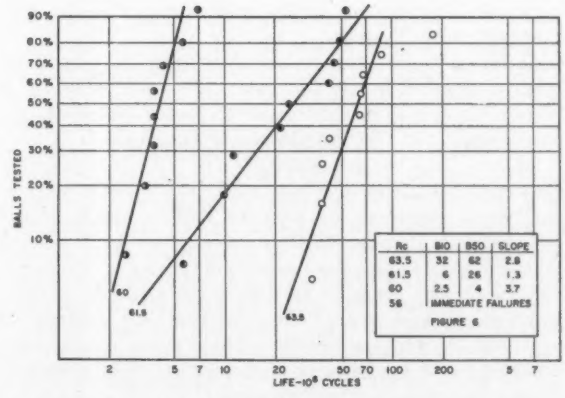

FIG. 6. Effect of hardness. One lot of M50 (no. 25) retempered with fresh MIL-L-7808C.

TABLE 1

Single Ball Fatigue Tests, 400F

9×10^6 cycles per hour, 730,000 psi max. and 486,000 psi mean Hertz stress.
MIL-L-7808C fluids in circulating system (C) or fresh (F) or oxidized (O) in drip-feed system.
Rolls—Halmo VM (Rc 62.5).

Series	Ball material	Lot no.	Room Temp. Rc	Oil, batch	Oil, condition	Neut. no.	Life in 10^6 cycles			No. of balls
							B10	B50	Slope	
1[a]	52100	1	58	A	C	1	21	44	2.6	9
3	52100	1	58	A	C	4	26	39	4.0	9
16	52100	19A	60	B	O	14	19	30	3.9	4
2	52100	—	60	A	C	1	10	25	2.1	8
17	Al St.	21A*	61.5	B	F	0.1	31	39	8.2	7
4	Al St.[b]	2	62	A	C	4	1.5	3	3.7	3
11	440C[c]	18	61.5	B	F	0.1	2	18	0.9	11
13	440C	18	61.5	A	O	16	15	32	2.5	13
23	C.H.	29	59.5	C	F	0.1	22	49	2.4	8
24	C.H.	29	59.5	B	O	18	10	19	3.0	8
10	L.A.T.S.	3*	62.5	B	F	0.1	4	18	1.3	7
9	L.A.T.S.	3*	62.5	A	O	12	3	8	1.7	7
5	L.A.T.S.	3*	62.5	A	C	4–7	3	18	1.1	9
20A & B	M50	23	63.5	B	F	0.1	30	48	4.0	13
22	M50	25	63.5	C	F	0.1	32	62	2.8	11
19	M50	25A	61.5	B	F	0.1	6	26	1.3	9
25	M50	25C	60	C	F	0.1	2.5	4	3.7	8
26	M50	25B	56	C	F	0.1	Immediate failures			2
7	M50	4	63.5	B	F	0.1	4.5	50	0.8	8
6, 8	M50	4	63.5	A	O	12	24	225	0.8	13
18	M50	26*	63	B	F	0.1	21	53	2.1	11
21	M50	26*	63	B	O	14	17	26	4.6	8

[a] Rolls were two 52100 (Rc 60) and one M1 (Rc 62).
[b] Later examination by the vendor showed improper heat treatment.
[c] Special heat treatment.
* Vacuum melted.

It is apparent, however, that when any one factor is being considered, all the others should be held constant. For instance, if hardness is the question, the batch of material and oil should be the same to ensure that only the hardness is effecting whatever differences are found.

So far, however, the results presented in Table 1 may point out the following:

52100—The first two series listed show the reproducibility obtainable. While both were with circulating oil, it was oxidized in a short time at 400F, so the two series are comparable; and they give about the same lives.

Al St.—The vacuum melted (VM) Al St. was better than any of the 52100 samples, which might not have been anticipated simply on the basis of 400F hardness of the two materials because the lives are so short in these tests that softening doesn't have much time to occur. However, while all tested materials have been more or less "clean", this was the least clean. This combined with information provided by personal communication from others casts some doubt on the validity of cleanliness as an assurance of long life, even on a relative basis.

440C—The 440C tests plotted in Fig. 3 present one of the cases of no change in parameters except oil. Here, it is assumed that the state of oxidation is more important than the source, but the latter question is still to be investigated. Less difference between the two oils might have been anticipated on a corrosion basis since 440C is a stainless steel, and so more corrosion-resistant.

C.H.—This material differs from all others in being case hardened, having a 0.075 in. case of Rc 60 and a core of Rc 42. As seen in Fig. 4, with fresh oil it did fairly well compared to most others, but with oxidized oil, the B10 was halved. Failed balls showed a wide track which was not apparent in balls examined after 50 million cycles before failure. This is interpreted as progressive collapsing of the case after initial fracture.

L.A.T.S.—In the case of L.A.T.S. three tests were run with the same Lot 3 but differing oils, fresh, oxidized and circulating. They all give the same B10, with the oxidized drip-feed giving half the B50 of the fresh and circulating. Again, different oil sources may have confused the issue. The L.A.T.S. which shows so little difference between fresh and acid oil, is also the material which showed least corrosion by 7808 in bomb tests of 21 materials (3). This may be evidence of the significance of chemical corrosion in the fatigue problem, contrary to that of 440C. It is also

TABLE 2

Metallurgical Observations

Lowest and highest life balls from each series

Material	Lot. no.	Series[a] no.	Cleanliness[b] rating	Grain[c] size	Carbide dist.	Polarity[d]	Life $\times 10^{-6}$
52100	19A	16	2 D thin	20	None	60	0.1
	19A	16	2 D thin	20	None	60	35
Al St.	21A	17	3 D thick	20	Light	45	32
	21A	17	3 D thick	20	Light	90	45
440C	18	11	2 D thin	13	Light	0	1.3
	18	11	2 D thin	13	Light	0	47
L.A.T.S.	3	10	1 D thin	8	Heavy	30	11
	3	10	1 D thin	7	Heavy	75	41
M50	23	20 A & B	Very clean	10	Heavy	30	26
	23	20 A & B	Very clean	10	Medium	45	103
	25	22	Very clean	10	Light	60	33
	25	22	Very clean	10	Light	45	176
	25A	19	1 C thin	10	Heavy	30	6
	25A	19	1 C thin	10	Heavy	75	53
	4	6, 8	Very clean	13	Light	15	17
	4	6, 8	Very clean	15	Light	0	116
	26	18	Very clean	13	Light	45	35
	26	18	Very clean	13	Medium	0	80
	26	21	Very clean	13	Light	0	15
	26	21	Very clean	13	Light	30	37

[a] Lowest lived ball in each series in listed first.
[b] By comparison with ASTM E45-51 charts.
[c] Intercept method.
[d] Degrees between failure pit and pole as determined by deep etch.

possible that this sample was such a poor one that nothing else could make it much worse. This will be checked by running other samples.

M50—M50 is one of the most promising of materials and several tests have been run, while many more are planned. There are two pairs of tests of "F" vs. "O" oil, using two lots, one vacuum melt and one air melt (AM), both plotted in Fig. 5. Both are around Rc 63 in hardness. The VM Lot 26 has about the same B10 with both "F" and "O" oils, while the "O" reduces the B50 by half. With the AM Lot 4, both B10 and B50 are significantly reduced by "F" oil. This suggests that something in the oil that accelerates fatigue is eliminated by oxidation, and that, whatever it is, it is more serious when there may be more inclusions to initiate fatigue cracking, which then is acclerated by the oil. Both lots, however, rated as very clean.

Comparing the VM with the AM using the same oils, it is found that the two "O" tests give about the same B10, but show a much steeper slope with VM. With "F" oils, the VM and AM have the same B50 but VM has much higher B10. This is the usual result in comparing the two, assuming that the VM is a cleaner steel.

Where two supposedly similar lots, 4 and 23, are compared with "F" oil, a large difference (6 to 1) in B10 is detected.

Lots 23 and 25 are identical except for a deep freeze treatment of Lot 23, which was to transform any retained austenite. The results do not suggest any significant effect on fatigue life, although the initial low percentage of austenite present makes it difficult to measure changes.

Hardness requirements for bearing steels are still a matter of dispute. Two excellent authorities have given the author minimums of Rc 55 and of Rc 60. And it has been recently suggested that 58–60 is the optimum.

So, batches from Lot 25 which have a hardness of Rc 63.5 were retempered at various temperatures to soften them. These Lots 25A, B and C were run under the same conditions as 25. Results shown in Fig. 6 were startlingly in favor of the hardest balls. The softest, Lot 25B, Rc 56, was attempted twice, one ball fatigued in a few minutes and the other picked up in the cage almost immediately. Both paths were three to five times as wide as usual. This series indicates that the fatigue life improves sharply with hardness, at least up to Rc 63.5. This, like other conclusions will be tested on other samples for confirmation.

As a check on the instrument when the Rc 60 balls started failing in minutes instead of hours, a Lot 25 ball was run in the middle of series 25. It ran to 90 million cycles (10 hr) before failing, indicating that tester variation was not responsible for the reduced lives of softer balls.

TABLE 3

Compositions of Ball Specimens

Material	Lot no.	C	Mn	Si	P	S	Ni	Cr	Mo	Co	V	W	Al	Cu	Fe
52100	1														
	19A	0.95–1.10	0.25–0.45	0.2–0.35	0.025	0.025		1.30–1.60		(Nominal values)					R
Al St.	2	1.03		0.34				1.50					1.36		R
	21A	0.95/1.10	0.25/0.45	0.25/0.55	0.025M	0.025M		1.30/1.60			(Nominal)		0.75/1.25		R
440C	18	1.03	0.48	0.41	0.018	0.014	0.20	17.27	0.50		0.14				R
C.H.	29	0.13*	0.53	0.33	0.010	0.011	2.77	1.67	5.12						R
L.A.T.S.	3	0.56	0.34	1.21	0.003	0.007		4.57	5.18		0.53				R
M50	4	0.80	0.30	0.25				4.10	4.25		1.10		(Nominal)		R
	23	0.82	0.29	0.16	0.006	0.005		4.10	4.23		1.04			0.08	R
	25	,,	,,	,,	,,	,,		,,	,,		,,			,,	R
	26	0.80	0.30	0.18	0.018	0.010		4.13	4.22		1.01	0.23			R

* Case to 0.075 in. runs around 1.25%.

Table 2 presents the results of metallurgical examination of the lowest and highest life ball from most series. They do not throw much light on any relationship between cleanliness or any other such factor and fatigue life. Part of the trouble may lie in the difficulty of making precise determinations of such a factor as cleanliness in which the size, distribution, shape and chemical identity of inclusions may all play a part.

Table 2 also shows a random distribution between polarity and failure, with some long-lived failures at the poles and short-lived balls completely out of polar areas. This is in agreement with unpublished results from one bearing manufacturer. However, NACA Spin Rig results on both balls and race cylinders show a pronounced high failure incidence at polar areas (4). This question is still unresolved, although one explanation put out by the manufacturer is that fatigue initiating inclusions will congregate at polar areas, and, therefore, poorer steels will show the polarity effect while better ones will not.

All failure balls showed overheating and work hardening of the running surface which was missing from balls suspended before failure.

The metallurgical type of analysis obviously needs much more investigation before it can be useful in anticipating fatigue life capabilities.

The results of Table 1 are more preliminary than it was originally expected in that so many parameters have been found to influence rolling fatigue. This means that more tests in which only one parameter at a time has been changed are needed. It is obviously not enough to compare one sample of M10 with one sample of M50 and thereby draw the conclusion that one is definitely superior to the other. Furthermore, even the conclusions so far reached must be confirmed by more tests. Much more work is needed and is planned.

Sometime in the future, it is hoped that a comparison of single ball results and full bearing tests may be made.

Conclusions

Some of the conclusions which may be presented based on the results of the single ball fatigue tests are as follows:

1. The state of oxidation of the diester type oil, at least at 400°F, has a very significant effect on the B10 life, and, furthermore, this effect results in improved life with the oxidized oil and some materials and a poorer life with some other materials.
2. In the one series of varying hardnesses, M50 of Rc 63.5 was distinctly superior to Rc 61.5, which was better than Rc 60.
3. Hard M50 (Rc 63.5) did best of all tested, although one sample of Al St. (Rc 61.5) did almost as well.
4. A deep freeze treatment on one portion of one lot of M50 had no significant effect on fatigue life.
5. No evidence of a relationship between cleanliness and life was observed.
6. No evidence of any influence of polarity of flow lines in the balls was detected in initial tests. Fatigue occurred randomly over the ball surface.

Acknowledgments

The assistance of C. F. Muench, E. H. Scott and T. H. Cooke of the Thomson Laboratory is gratefully acknowledged. Also, appreciation is expressed for the support provided by the Component Engineering Section of the Jet Engine Department, General Electric Company, Evendale, Ohio.

REFERENCES

1. BARNES, G. C. and RYDER, E. A., "A Look at Some Turbine Bearing Problems," Preprint No. 693, SAE, 1956.
2. JOHNSON, L. G., "Ball Bearing Engineers' Statistical Guide Book," New Departure, April 1957.
3. MOORE, C. C. and LEWIS, P., "Current Development Problems in High Temperature Aircraft Roller Bearings," Preprint No. 57-Lub-4, ASME, October 7, 1957. (*Note:* A misprint in Table 5 shows M50 as most resistant. Actually this would show L.A.T.S. as first on the list and M50 as No. 11.)
4. CARTER, T. L., "Effect of Fiber Orientation in Races and Balls Under Rolling Contact Fatigue Conditions," NACA TN 4216, 1958.

DISCUSSION

P. M. Ku (*Southwest Research Institute, San Antonio, Texas*):

In Dr. Jackson's ball fatigue tester, the test ball is loaded by three rotating drums disposed 120° apart around the ball. The three drums are supported at both ends. This arrangement gives inherently stable balance of forces on the ball. In the Barnes ball fatigue tester, the test ball is loaded by two rotating drums placed on opposite sides of the ball, and the drums are carried on shafts supported only at one end. Experience at Southwest Research Institute (SwRI) with the Barnes tester indicates that obtaining really precise control over the conditions imposed upon the test ball is exceedingly difficult. The fact that Dr. Jackson is apparently able to obtain significant results with about 10 to 15 tests, as compared with about twice as many tests found necessary with the Barnes rig at SwRI, gives tangible evidence of the improvement brought about by the author's arrangement. Another important advantage of the author's apparatus is its ability to operate at high temperatures. Dr. Jackson is to be congratulated for having developed this fine research tool.

Dr. Jackson does not show some of the details of his rig. For example, it would be of interest to know how he applies side restraint to the test ball (if needed), and how the lubricant supply jet is located.

The paper states that it is planned to compare the test results obtained from this rig with full-scale bearing test results. One question which can immediately be raised is the degree of correlation of results from several of the known ball fatigue testers. It is noted that some of Dr. Jackson's results are in rather good agreement with those obtained at SwRI, and some are at variance. In general, the results obtained by NASA (Lewis Flight Propulsion Laboratory), SwRI and Dr. Jackson agree in some respects, but disagree in others. Unless these discrepancies are ironed out, there can be reasonable doubt on the validity of all such tests. It is believed that some basic data on Dr. Jackson's rig to show the effect of lubricant viscosity, ball speed, ball load, etc., will help clarify the over-all picture.

In some of Dr. Jackson's tests the Weibull lines cross each other so that the trends based on B–50 life are opposite to those based on B–10 life. This is a point that is theoretically rather difficult to reconcile. It is wondered how results of this sort should be interpreted.

Clinton C. Moore (*General Electric Co., Cincinatti, Ohio*):

The author is to be congratulated for his effort in operating and assembling data from a new type of rolling contact fatigue tester. We believe that the development of this device will eventually bring an understanding of the rolling fatigue problem not possible before, due to the length of time necessary to accumulate data by conventional testing of full scale bearings.

From the standpoint of aircraft gas turbine design, the paper is useful for the following reasons:

1. It confirms and extends full scale testing results indicating that M50 vacuum or consutrode melt steel consistently makes the best race and ball material when run at elevated temperatures with diester lubrication.
2. It shows that R_c 63.5 produces the best fatigue life over lower hardness. We have been allowing as low as R_c 61 in our material specifications of M50.

From the standpoint of academic interest, the author's conclusion that the oxidation level of diester oils greatly affects fatigue life is noteworthy. It supports the view that chemical attack of the bearing surface by the lubricant, independent of either bulk viscosity or pressure viscosity properties, is a parameter of great magnitude in the fatigue problem. It is disappointing that some correlation between grain size, cleanliness, and carbide distribution and fatigue life was not evident and I submit that the reason for this may be that either (1) the narrow range of these variables or (2) the overpowering effect of corrosion properties of the diester oil obscured their effect.

From the engine-builder's standpoint, fatigue life of bearings is assuming an even greater concern than in the past. As turbo-jet machinery gains more and more commercial acceptance, so does the problem of maintaining longer overhaul periods and increased reliability. Research and development can help the industry most in the following directions.

1. Find better materials for rolling bearings which permit longer fatigue life with less scatter.
2. Develop a non-destructive method of inspection which will permit selection of B90 bearings.

I feel that Dr. Jackson's efforts have materially aided us in this direction by providing a rapid means of ranking materials.

E. G. Jackson (*General Electric Company, West Lynn 3, Massachusetts*):

I wish to thank Messrs. Ku and Moore for their remarks and discussion.

In reply to Mr. Ku's questions: The test ball is restrained from axial movement by the cage device shown in Fig. 1. The oil is fed through the left hand hollow arm of the cage support. The smaller tubes that straddle the ball are also hollow and through holes in these, oil is dripped directly onto the rolling path.

As Mr. Ku points out, there are many areas yet to be studied with this machine. These data are the first obtained with it, and the particular tests undertaken were aimed almost as much at evaluating the apparatus as studying the fatigue phenomenon. Therefore, no parameter was exhaustively examined. This will be done in future programs. As of now, there would appear to be no serious discrepancies between this and other devices. The conclusion on polarity effects has been withdrawn on the basis of the analysis of the data by W. J. Anderson of NASA Lewis Research Center presented at the Conference.

As for the crossing of Weibull lines, all we can suggest right now is that the theoretical Weibull slope is based essentially on a mechanical analysis of stresses. If chemical effects are superimposed, as may be the case with more active oils and at high temperatures, the slopes may be expected to vary. Then, of course, reversals of relationship at B50 and B10 may also be anticipated.

In any event, we expect that much more work of our own and others in the field may be the means of more clearly defining the answers to these questions.

Materials in Rolling Element Bearings for Normal and Elevated (450°F) Temperature

By T. W. MORRISON[1], H. O. WALP[2] and R. P. REMORENKO[3]

The effect of vacuum melting has been under investigation by the author's company for several years. Fatigue testing has been conducted on races and balls in full-sized bearings, so that the results can be interpreted directly into bearing performance.

Studies have been made of both induction and consumable electrode vacuum melted steel. Material inspection has shown a more consistently high level of cleanliness in consumable electrode vacuum steel than that melted by induction.

Improvement in life of bearings made of vacuum melted steels does not appear to be commensurate with the improvement in cleanliness. This is regarded as confirming evidence to a long-held view that cleanliness is not the only factor involved in the fatigue property of steel. Fatigue studies have been made of both 52100 and high temperature steels. Bearing ratings range from 17% less than the AFBMA basic load rating to 23% greater than this rating for vacuum melted 52100 steel. In a test of vacuum melted tool steel (M–1), the bearing load rating was 22% greater than the basic load rating for 52100 steel.

There is no indication that vacuum melting has served to reduce the number of early failures more proportionately. Where there has been a change in life, the curve of bearing lives has been displaced, but retains the same general shape.

Introduction

AISI 52100 STEEL, or slight modifications of this analysis, have been most commonly used in rolling element bearings. Production and heat treatment of this steel have been very extensively investigated over the years, resulting in a high quality, dependable bearing material.

With the rapid development of high performance gas turbines during the last decade, there has been a necessity for operating bearings at ever higher temperatures. Although its performance suffers to some degree in the upper range of temperature, 52100 steel has performed adequately up to 350°F and even slightly higher, if suitably heat treated.

Many years of testing and service experience have indicated that a minimum hardness of approximately 58 Rockwell C at the operating temperature is desirable. Hardness is a function of both temperature and time. Increasing temperature causes almost immediate reduction of hardness, and increasing time a slow, relatively small, reduction in hardness. Suitable materials must have sufficient hardness up to the maximum service temperatures for a service life of the order of at least 1000 hr.

A great amount of effort has gone into exploring steel analyses suitable for temperatures beyond 350°F. It has become obvious that additional quantities of alloys are required—alloys such as molybdenum, chromium and vanadium.

Hot hardness tests, in which the specimens were held at temperature for only one or two hours have been made on several steel analyses. A more extended study of hot hardness for times up to 1000 hr has been made by Bhat and Nehrenberg (1). Consideration of all data that have been reviewed by the authors led to the recommendation of:

52100 up to 350°F
M50 up to 600°F
M1 up to 800°F.

These recommendations were made not only on the basis of hot hardness but on the endurance testing of bearings described later in this paper.

Introduction to the high temperature problem came when a British turbine was to be manufactured in this country under license. The British were using T1 (18–4–1) for the high temperature bearings. This seemed to be a flagrant waste of critical tungsten. Recommendation of M2 based primarily on acceptable hot hardness for these bearings was adopted and successful performance resulted. Early in the Korean conflict, Washington pointed out the necessity for cautious use of critical alloys. Hot hardness tests on M10 indicated it might be a satisfactory steel.

The nominal analyses of the five steels mentioned above, are:

	C	Mn	P	S	Si	Cr	W	Mo	V
52100	1.00	.35	.025[a]	.025[a]	.30	1.45	—	—	—
M50	.81	.35[a]	.015[a]	.015[a]	.25[a]	4.00	—	4.25	1.00
M1	.80	.30	.030[a]	.030[a]	.30	3.85	1.50	8.50	1.10
M2	.83	.30	.030[a]	.030[a]	.30	3.85	6.15	5.00	1.90
M10	.88	.25	.030[a]	.030[a]	.30	4.15	—	8.15	2.00

[a] = maximum

Presented as an American Society of Lubrication Engineers paper at the Lubrication Conference held in Los Angeles, Calif., October, 1958.

[1] Manager, Research Laboratory, SKF Industries Inc., Front and Erie Avenue, Philadelphia 32, Penna.

[2] Supervising Metallurgist, SKF Industries Inc., Front and Erie Avenue, Philadelphia 32, Penna.

[3] Supervising Research Engineer, SKF Industries Inc., Front and Erie Avenue, Philadelphia 32, Penna.

The limits for Mn, P, S, and Si, as shown for M50, are those currently used for vacuum melted material. It will be noted that no tungsten is specified for M10.

Some experimental bearings made of M10 steel for engine builders were rig tested and gave reasonable success. However, the grindability of M10 is so poor that there would be insufficient existing capacity in the bearing industry to produce at rates sufficient to meet high military demands. Attention was turned to M1 steel, which was found to have relatively good grindability and low tungsten content, as noted above. Grinding experiments indicate the following grindability for the M steels referred to 52100 as a base:

52100	1.0
M1	1.8
M2	3.0
M10	4.0

It has been found more recently that the grindability of M50 is very similar to M1.

Steel melting methods and cleanliness

Basic electric arc melting has been the source of most domestic rolling element bearing steels. While there will probably be further improvement in the quality of 52100 and M series steels produced by this method, vacuum melting currently offers the most promise of markedly increasing fatigue characteristics of these steels.

Some of the earliest vacuum melted 52100 steel to be made in this country was obtained and tested as rotating beam specimens. The results were very promising and were reported by Styri (2).

The early vacuum melted steels were made by the induction method. The average level of cleanliness of these induction vacuum steels is much higher than for the commercial basic arc product. However, the induction vacuum method requires that the charge be melted in a refractory lined crucible and poured over a refractory spout into a substantially conventional ingot mold coated with a refractory mold wash. As a result, induction vacuum melted heats, and finished parts made from such heats, have shown more non-metallic inclusions of rather larger sizes than is desirable.

The more recently introduced method of consumable electrode vacuum melting has shown considerable promise, both on initial inspection of material and on final inspection of parts. In this method an electrode is progressively melted under vacuum by the heat of the electric arc and the ingot is built up continuously in a water cooled copper mold. Therefore, no exogenous non-metallics are added, and considerable quantities of the non-metallics in the electrode are eliminated by disassociation and by cropping. Those not eliminated are broken up into a very fine dispersion.

Inspection results have shown a negligible number of consumable ingots rejected at inspection. The following table gives some statistics for magnetic particle inspection, after finish grinding, of bearing rings made of 52100 steel. The rejections noted are for non-metallic inclusions only:

	Rings examined	Rejected Rings	%	Maximum length of permissible non-metallic inclusions on Groove	Other surfaces
Induction vacuum	3864	146	3.8	$\frac{1}{32}$ in.	$\frac{1}{4}$ in.
Consumable vacuum	1847	74	3.5	$\frac{1}{64}$ in.	$\frac{1}{64}$ in.
Basic arc	3089	401	13.0	$\frac{1}{32}$ in.	$\frac{1}{4}$ in.

On the basis of the percentages rejected, it would appear that the vacuum melted materials were about equally clean. However, the specification to which the induction vacuum rings were inspected permitted indications for non-metallics on the raceways (running surfaces) to $\frac{1}{32}$ in. and on non-operating surfaces to $\frac{1}{4}$ in., while those made from consumable electrode were rejected for indications larger than $\frac{1}{64}$ in. on any surface.

For comparison, results are shown on some rings of recent manufacture made of basic arc steel. These rings were inspected to $\frac{1}{32}$ in. limit for the grooves and $\frac{1}{4}$ in. for non-operating surfaces.

Evaluation of bearing materials

Fatigue studies have been made of basic electric and vacuum melted 52100 and M1, M10 and M50 tool steels.

Table 1 shows the melting practice, heat numbers, type of steel and size of bars used for preparing the test parts for which data are herein presented.

The analyses of the heats used are shown in Tables 2 (a, b).

Table 3 gives the record of fracture inspection for non-metallics. The lower incidence of slag in the inspection disks of the vacuum melted heats is apparent.

Micro ratings according to ASTM E45, shown in Table 4, are noticeably lower for the vacuum melted heats. The lines marked "worst field" represent the worst field for each type of slag, for both the thin and heavy series, that were found in all specimens from the heat.

Heat treatment given the samples is shown in Tables 5 (a, b). All 52100 rings and balls were oil quenched. Except for the 1309 outer rings of Group 11 and the 6309 inner rings of Group 7, which were heated in a controlled atmosphere furnace, all 52100 rings and balls were hardened from gas fired continuous production furnaces. All rings and balls of M1, M10 and M50 steels were heated in and quenched into molten salt baths at the temperatures shown in the table. This is generally considered the most suitable method for heat treating such steels.

The Rockwell C hardness of the finished parts is given in Table 6.

The results of magnetic particle inspection of the grooves of the test rings appear in Table 7. The number of rings, the total number of indications, total length of indications and longest indication, are shown. The large number and great length of indications for Heats 1P114 and 1P115 were due mostly to segregation and not to non-metallics. Therefore, these two heats cannot be compared

with the others in Table 7 in which indications were known to represent slag. The M1 inner rings made from Heat 28446 were turned directly from 2½-in. bar stock, while the outer rings from the same heat were individual forgings. Likewise, the M1 inner rings from Heat 1C142 were turned from bar stock and the outer rings made as individual forgings from Heat 02131. This explains why the indications were more numerous in the inner rings than in the outer rings, as the fiber direction for the inners was axial, whereas in the outers it was irregular due to forging.

Fatigue Testing

For evaluating the endurance characteristics of materials the endurance results for complete bearings have been utilized. The test rings have been for either a 6309 or 1309 size bearing shown in Fig. 1. The configurations are such that inner ring failures predominate in the 6309 size and outer ring failures in the 1309 size. Therefore it is possible to prepare only these parts of the test material, when it is scarce.

It is recognized that non-test element failures, considered when analysing the test results for groups of failed bearings, result in values which underestimate the rating of the test element. However, this effect is minor and does not justify detailed analysis since only in Group 1 were there more than two non-test element failures before the test median life had been attained.

Balls have been tested in 1309 size bearings since there are thirty ½-in. balls in a complement, permitting testing of a large number at one time, again under full-scale bearing conditions.

These bearings have been tested on standard endurance testing machines, Fig. 2. Each machine accommodates two test bearings. The loading is applied radially through a lever and dead weight system, so that the magnitude is known with certainty at all times. Each test bearing can be mounted and aligned independently; therefore, when a failure occurs there is no need to disturb the other bearings.

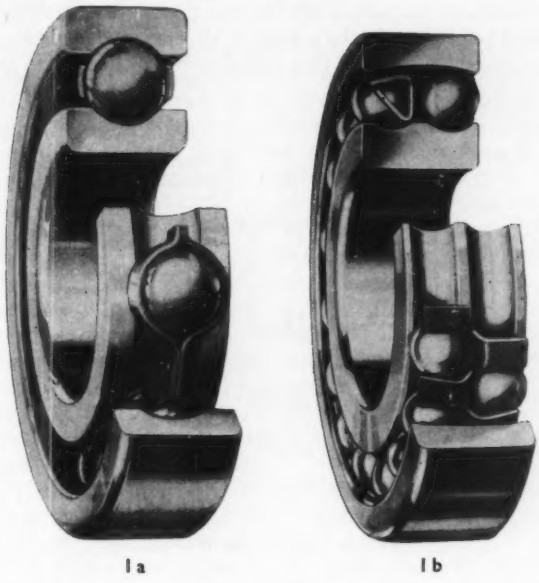

FIG. 1. Representative test bearing views.
(a) 6309 size.
(b) 1309 size.

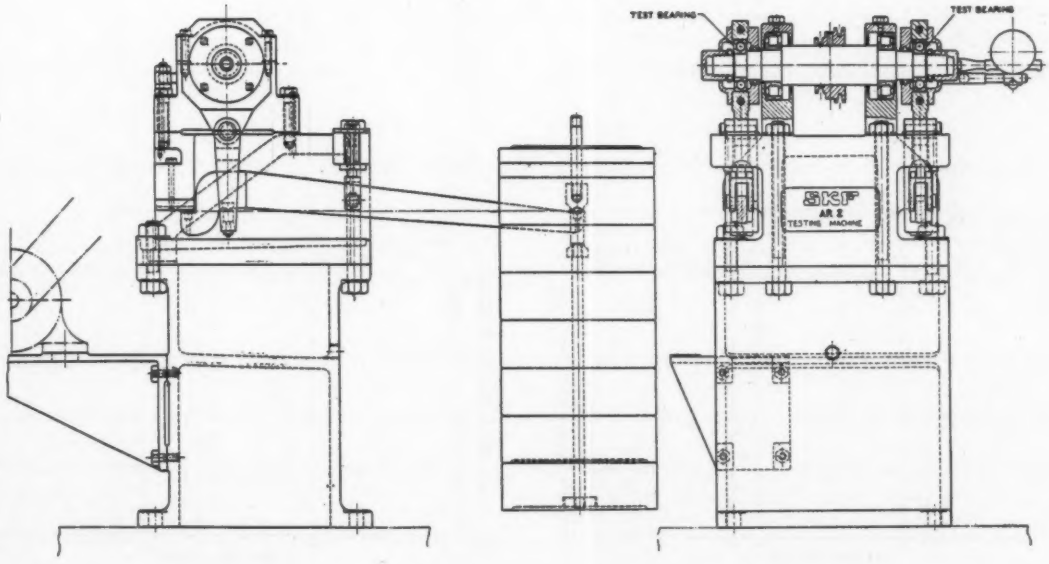

FIG. 2. Endurance testing machine.

Provision has been made for testing at elevated temperatures by placing electric resistance heaters in the test bearing housings (Fig. 2a). Thermocouples bear directly on the outer ring, to measure temperature, and actuate thermostats to control temperature. Lubrication may be by grease, usually applied to the test bearing once each eight hours, or by drop fed fluid to a closure surrounding the bearing. The fluid passed through the bearing to a drain in the housing and was not reused.

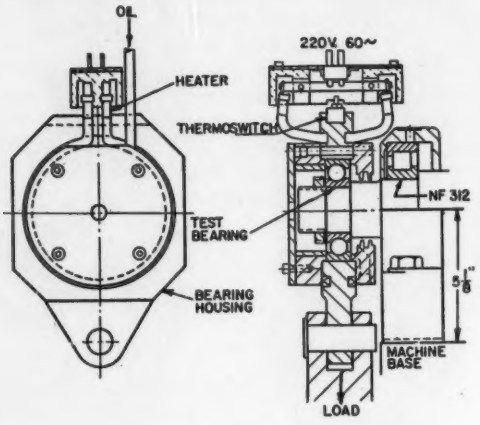

FIG. 2a. Test bearing housing.

52100 Steel

The results of testing bearing parts from a number of ingots of vacuum melted 52100 steel in 11 groups of bearings (22 to 42 bearings per group) are presented in Table 9. The individual bearing lives for representative test groups are shown in Fig. 3 (using a cross to designate inner ring failure, a plus-sign for outer ring failure, a zero for ball failure and a zero with horizontal arrow for unfailed bearings). These are called Weibull (4) plots after the originator. The Weibull distribution was applied to the theory of rolling contact bearings by Lundberg and Palmgren (5). Load ratings based on the Weibull Plots and on the method of calculation given in the Appendix are tabulated in Table 10.

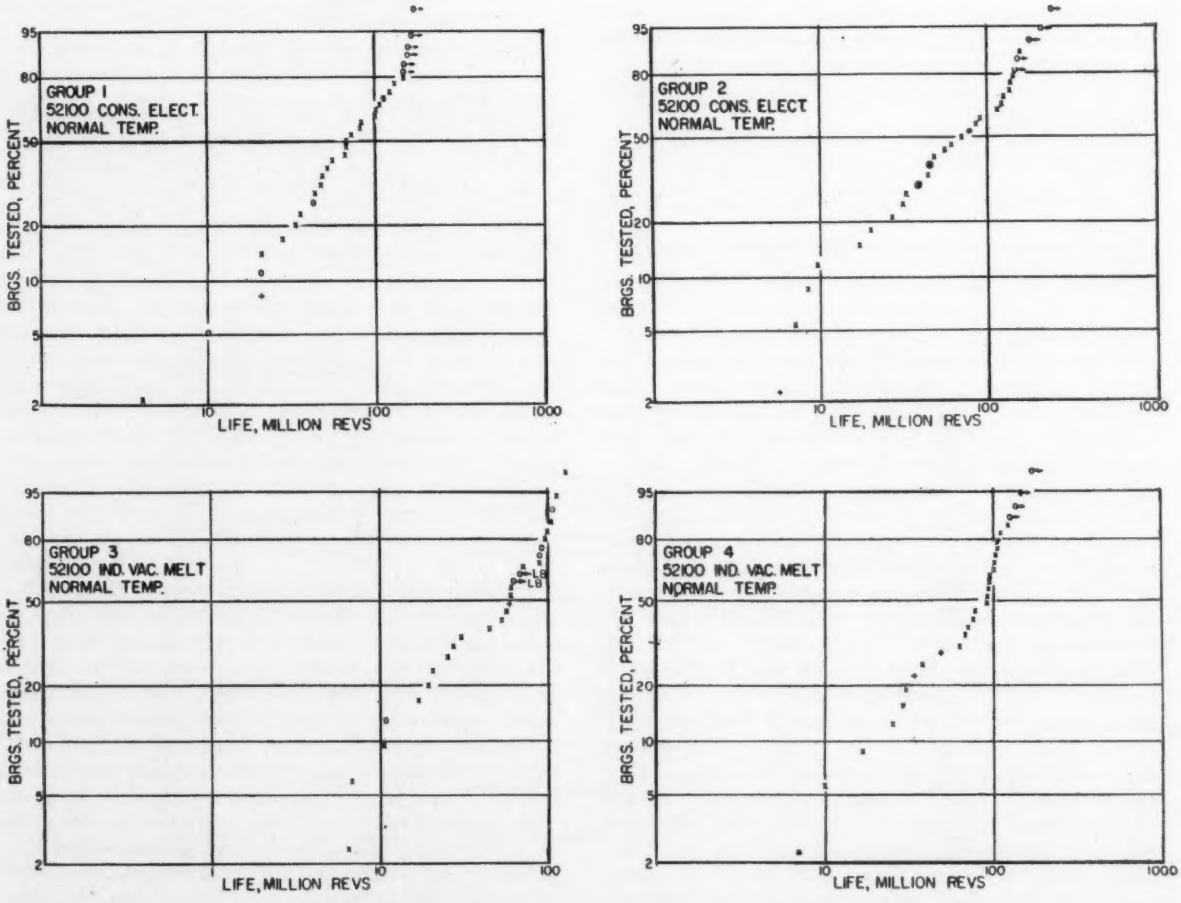

FIG. 3. Endurance of bearings made of vacuum melted 52100 steel.

It is interesting to note that there is considerable spread in capacities even with vacuum melted material. Considering all the groups of vacuum melted 52100 steel, capacities based on test median lives, L_{50}, ranged from 83 to 123% of the value expected from the AFBMA Standard (3).

L_{50} and L_{10} are the lives which 50 and 90%, respectively, of the bearings will exceed. It is felt that the L_{50} test lives are more reliable since they are least affected by sample variations.

Table 10 is arranged to facilitate comparing load ratings by steel lot. There is the indication from the table that the variation in fatigue characteristics of the vacuum melted material has been from lot to lot of material rather than within a lot. Conclusive evidence as to why this should have been the case is not yet available. The ingot size may have had an effect. It is known that some reduction from the original ingot size is necessary but the percentage has not been defined with certainty. There is further indication later in this paper that the degree of reduction of the ingot is a factor affecting fatigue.

Referring to the difference in load ratings of Table 10, there is also the possibility that improvement in the art of making 52100 steel has permitted better fatigue characteristics, since the order of numbering is also the order of purchasing.

For comparison with the results obtained for vacuum melted steel, Weibull plots of the lives for the poorest (Group 12) and best (Group 13) of 11 groups of bearings made of domestic basic arc steel (14 to 50 bearings in a group) are shown in Fig. 4. Load ratings calculated from the Weibull plots are shown in Table 11.

It is evident from a comparison of Tables 10 and 11 that vacuum melted material has not resulted in bearing load ratings greater than attainable with good quality 52100 steel. However, from the consistent results obtained from steel lots 3 and 4, there is the possibility that a greater percentage of heats will permit bearings having load ratings in the higher range, provided large ingots are used.

Ball fatigue life

Results are presented for two quantities of ½-in. diameter balls made from induction vacuum melted 52100 steel, and tested in 1309 bearings. Material for one of the quantities was from the same ingot (1P115) used for making the inner races of Group 10. There were no races made from the ingot (1P58) material used for the other quantity of balls.

Lives attained by these two groups of balls are shown in Table 12 together with a summary of data collected in testing balls of domestic and Swedish commercially melted 52100 steel over a long period of time. It will be seen that the lives of the balls made of vacuum melted material greatly exceeded the lives obtained with the balls made of domestic material. Since only one ball failed in the sets made of Swedish material, it cannot be concluded with certainty that these would not give as good life as the balls made of vacuum melted material, but the probability is high that they would not.

The greater ball lives obtained with Swedish steel, as compared with domestic material, is typical of the difference in fatigue characteristics of these steels.

The lives of the balls made of vacuum melted material are even more impressive than the values indicate when it is realized that these were run in so many different races, which failed in the testing. With a flaked race, some fragment denting of the balls cannot be avoided. Experience with air melted 52100 steel has been that such fragment dents cause premature fatigue failure.

Effect of forging and carbon content

From the original ingots of vacuum melted material the following test pieces were made:

6309 inners 1309 outers ½-in. balls

The test races are identified as Groups 7 and 11. From the analysis of test results as shown in Table 10 it is evident that the 6309 inners had lower ratings than the 1309 outers. However, lives of these components do not indicate ratings

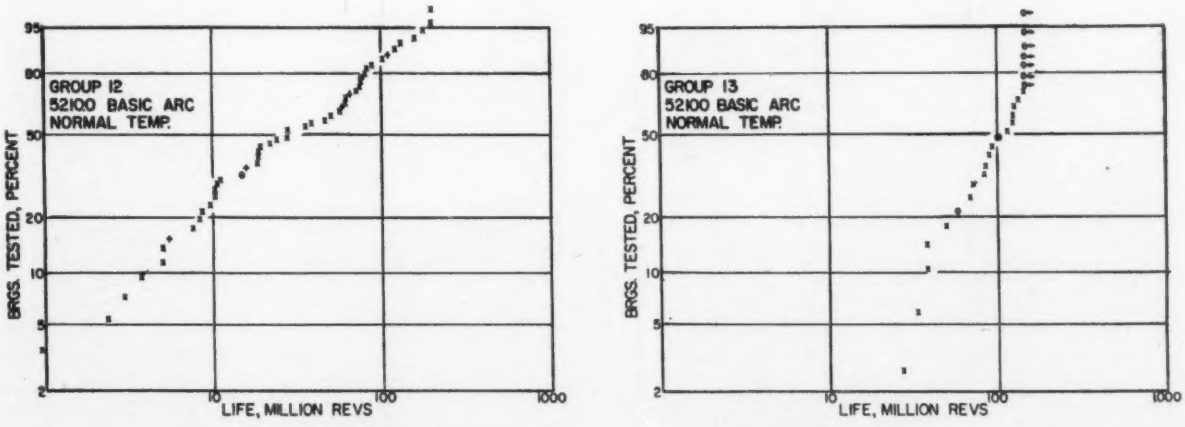

FIG. 4. Endurance of bearings made of basic arc melted 52100 steel.

as high as would be obtained on the basis of the ball lives.

In searching for an explanation of the relative disparity in life for the 6309 inners, 1309 outers, and balls made of vacuum melted material, it was evident that one difference in their processing was the degree of reduction, or working, of the original ingot material.

The ingots from which the material was obtained were 5½ in. in diameter. The ingot material was reduced to 0.358-in. diameter wire for making the balls; to 2½-in. diameter round bars for the 6309 inners; and to 2½-in. square bars for the 1309 outers. The 6309 inners were turned directly from the bars. Pieces of suitable length were cut from the square bars, pierced, upset and mandrel forged into rings from which the 1309 outers were turned. Thus, it was possible that there may have been a relationship between the endurance of the three different type test pieces and the degree of forging or working the material received.

To further investigate the effect of forging, two groups (No. 8 and No. 9) of 6309 inner races were made of material from the same 6-in. square ingot (1P112) of induction vacuum melted 52100 steel forged in the following manner:

1. The inner races of Group 8 were machined from a 2½-in. bar, material of which was obtained in the following manner:
   (a) Side forged from the 6-in. square ingot to a 4-in. square.
   (b) The 4-in. square upset to 6-in. square.
   (c) The 6-in. square side forged to 4-in. square.
   (d) The 4-in. square upset to 6-in. square.
   (e) The 6-in. square forged to 3-in. round.
   (f) The 3-in. round further reduced to the 2½-in. round.
2. The inner races of Group 9 were machined from a 2½-in. bar side forged directly from the ingot.

From the load ratings shown in Table 10, it appears that the increased working had no effect upon the fatigue characteristics of the material. It is recognized that the type of working given the material for the races of Group 8 is not the same as reducing an ingot directly to a small diameter bar. Therefore, possible effects of a relationship of ingot size to final stock size will be further investigated.

Although the steel from which the races of Groups 8 and 9 were made had lower carbon content than the other vacuum melted material tested, the load ratings for the two groups are not lower than for Groups 5, 6 and 10, for which the carbon was higher.

Effect of sulfur

Since the vacuum melted materials are relatively free of inclusions and gases, and, therefore, should contain a minimum of variables which affect fatigue life, they are felt to be suited for investigating the effects of certain residual elements.

One test has been run to determine the effect of high sulfur content. One vacuum melted ingot, with sulfur content of 0.050%, was obtained, whereas the specified maximum of 52100 steel is 0.025%, and the value is usually much lower than this. Two groups of 6309 inner races were made from the high sulfur material, Group 5 inners were made from a 2½-in. bar side forged directly from the 6-in. square ingot. Group 6 inners were prepared from a 2½-in. bar, which had been multiply upset, forged from the 6-in. square ingots as described above. The results of testing bearings containing these races are shown in Table 10. The bearing load ratings are comparable to those of other groups made of vacuum melted 52100 steel.

High temperature steels

With the obvious necessity of obtaining materials which will permit higher operating temperature than can be sustained by 52100 steel, endurance tests have been run on tool steels appearing to be most likely candidates for rolling element bearing service.

Results of endurance testing two statistically similar groups each of basic electric arc melted M-1 and M-10 steel, Groups 14, 15, 17 and 18 are shown in Fig. 5. In addition, Group 16 gives endurance test results of bearings having basic arc M-1 inners and 52100 outers.

Three of these groups were tested at room temperature (normal rise above room temperature for the conditions of operation-temperatures are given in Table 9), and two were tested at a controlled temperature of 450°F. The testing at room temperature was conducted to provide a basis of comparison with the fatigue characteristics of 52100 steels. The elevated temperature testing was to evaluate the bearing capacity under anticipated service conditions. Capacities calculated from the Weibull plots are tabulated in Table 13. It will be seen from the tabulation that the test bearing load ratings ranged from 54% to 91%, based on L_{50} of the basic load rating determined from the AFBMA Standard. The AFBMA value is, of course, based on the load rating of 52100 steel bearings operated at room temperature.

The bearing load ratings obtained with these high temperature steels at room temperature ranged below those expected for 52100 steel.

Since, in the past, tool steels have not been required to perform in such demanding applications as 52100 steel, they have not been afforded the same quality improvements. It was felt that vacuum melting might, in one big advance. bring the quality of the tool steels up to that of 52100 steel, M1 analysis was selected for vacuum melting and testing, based upon the advantages previously discussed for this material. Two quantities of statistically similar bearings (Groups 19 and 20), were prepared. Weibull plots of the bearing lives are shown in Fig. 6 and load ratings in Table 13. It will be seen that the bearing load ratings were greater than for any other tool steels previously tested at room temperatures and were comparable to those obtained with 52100 steel.

M50 tool steel has been reported from several sources to have exhibited rather good fatigue characteristics. Two statistically similar groups of 6309 bearings prepared from consumable electrode vacuum melted M50 steel are being tested. While the required number of bearings have not been run to failure, the results shown in Fig. 6 and Table 13 indicate that this material will provide high bearing load ratings.

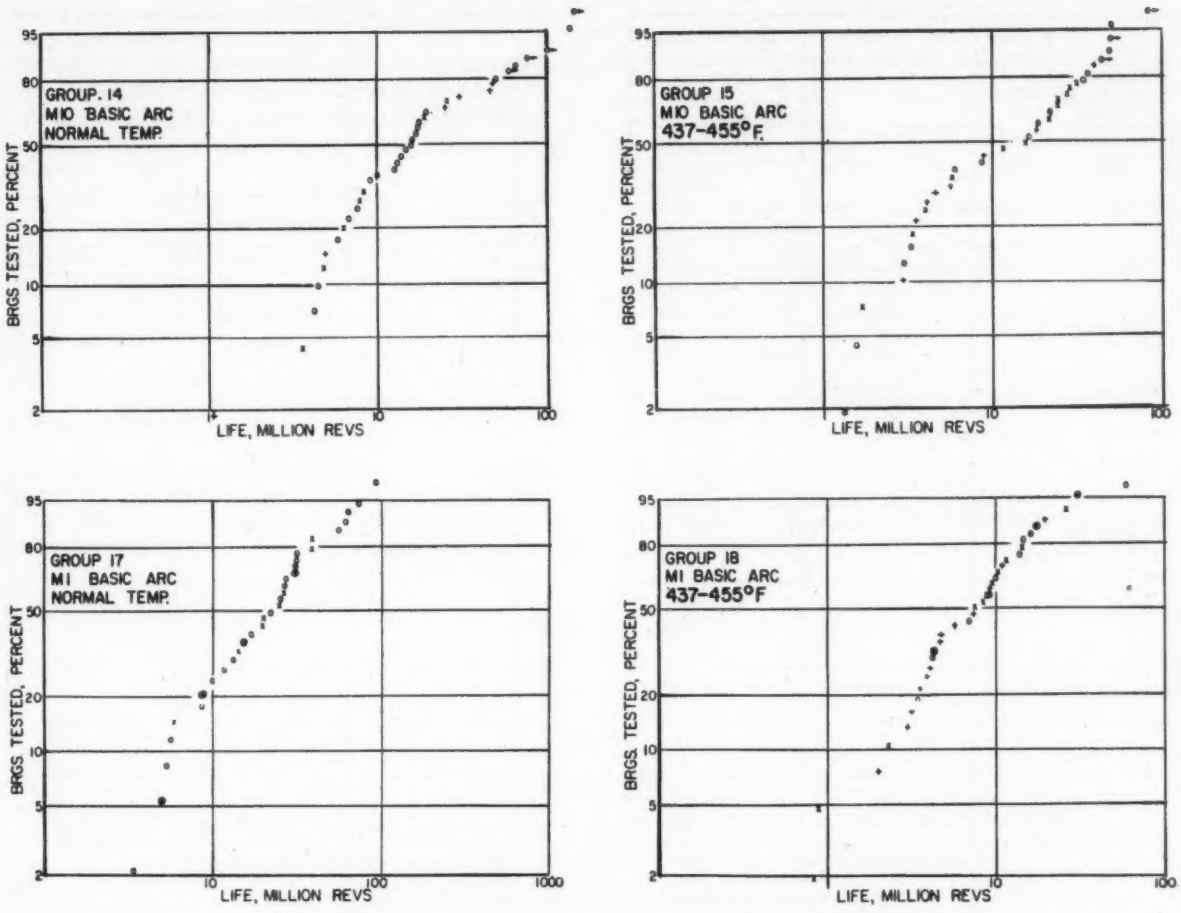

FIG. 5. Endurance of bearings made of basic arc melted M1 and M10 steels.

Discussion

The reduction in load rating of bearings made of M1, M10 and M50 materials, at a temperature of 450°F, is believed to be caused principally by the lubricant. The effect of lubricants on endurance has been shown in (6), (7) and (8).

Reduction in life was demonstrated on a few of the test bearings used. An effort was made to lubricate with MIL-L-7808B fluid, bearings statistically similar to those of Group 17 run at room temperature but the lives obtained were so much shorter than expected from the AFBMA Standard that the test was discontinued. A Weibull plot of the lives of the few bearings tested at room temperature with the 7808 fluid is shown in Fig. 7. The load rating calculated from the L_{50} life was 57% of the AFBMA value.

In addition to the life data, there was evidence of lubrication distress in the form of wear and glazing observed in a considerable number of bearings tested at 450°F and lubricated with 7808. It seems reasonable to conclude that these conditions resulted from insufficient film thickness, permitting some degree of metal to metal contact between the rings and balls. Such metal to metal contact must surely increase the tangential stress. The resulting wear also tends to destroy the surface geometry and leads to localized increase of stresses for this reason. All of these effects reduce endurance life.

The principal concern of the aircraft builders is to increase the lives before the first bearing failure. This was accomplished with the groups of bearings showing improved load ratings, but there was no evidence that vacuum melting was effective in reducing the early failures when the L_{10} and L_{50} lives were not improved (as evidenced by Weibull plots of Figs. 3 and 6).

It is recognized that with materials available in the past, fatigue life of rolling element bearings has shown a wide scatter (the order of 50:1). The slope of the Weibull plot is an indication of the scatter. The slopes for the Weibull plots of the bearings made of vacuum melted material range from 0.86 to 1.36, as shown in Table 9, Groups 1 through 11 and 19 through 22. Slopes for the bearings

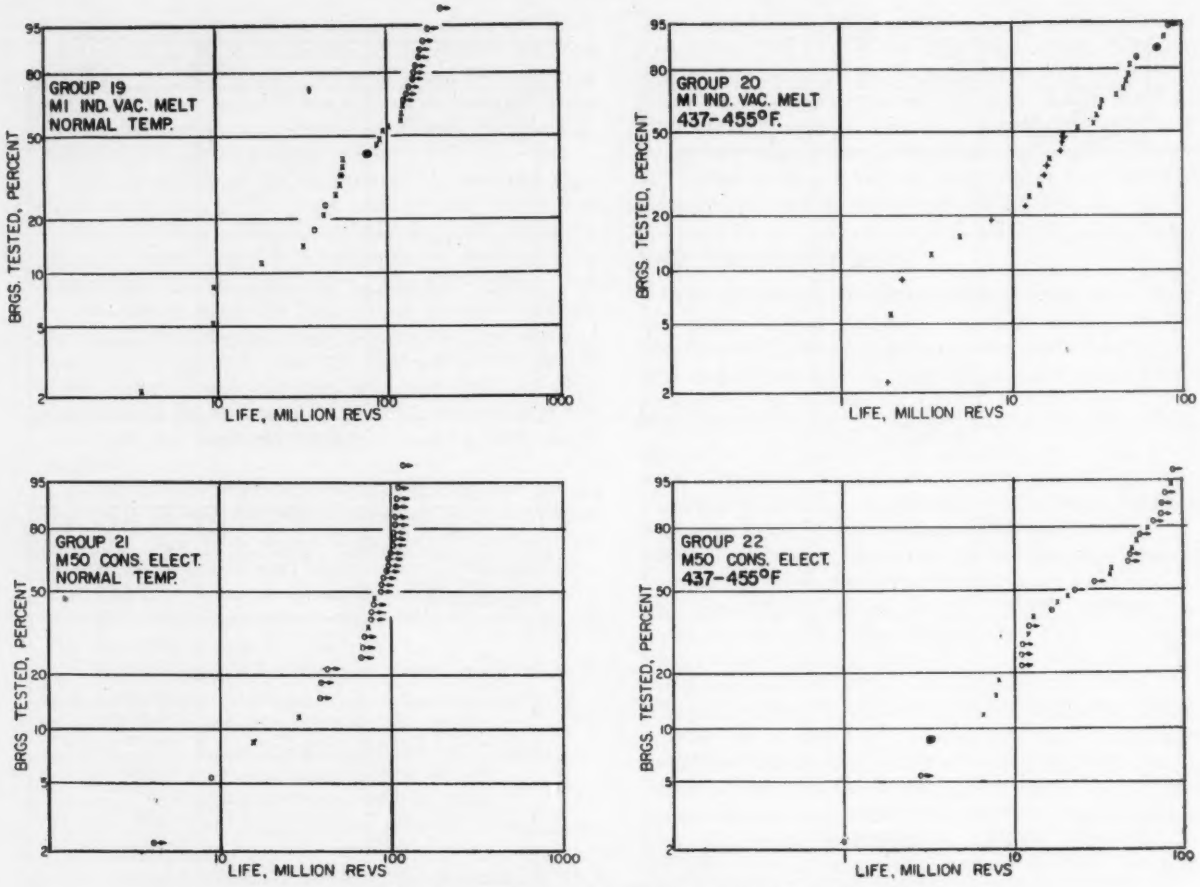

Fig. 6. Endurance of bearings made of vacuum melted M1 and M50 steels.

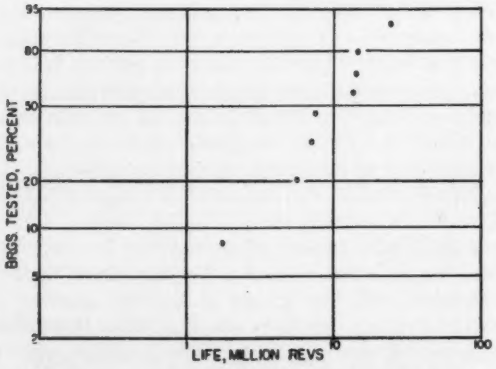

Fig. 7. Endurance of bearings of vacuum melted M1 steel lubricated at room temp. with MIL-L-7808B fluid.

made of basic arc 52100, M10 and M1 steels range from 0.93 to 1.76, as shown for Groups 12 through 18 of Table 9. From these results it appears that there is no reduction in bearing life scatter from the use of vacuum melted steel.

While there is no common denominator with which to compare material cleanliness and bearing life, it is felt that the increase in life of bearings made of vacuum melted steel is considerably less than the relative improvement in cleanliness. This is further evidence that there are factors other than cleanliness alone which bear upon the fatigue life of steel in rolling element bearings.

Conclusions

The load rating of bearings made of vacuum melted 52100 steel has not been increased beyond the range experienced with good quality air melted 52100 steel. There is the indication of a higher percentage of heats which will permit long-lived bearings.

Evidence is strong that ball life is appreciably increased with vacuum melted steel.

Basic electric arc melted tool steels have resulted in bearing load ratings noticeably lower than obtained with 52100 steel produced by the same process. Vacuum melting these tool steels has resulted in bearing load ratings at least comparable to those obtained with the best 52100 steel.

Load ratings of bearings made of tool steels are considerably lower at 450°F than at normal temperature. It is believed that the major factor in reducing bearing life at the

elevated temperature is the effect of the lubricants which are currently available.

There is no reduction in the life scatter of bearings made of vacuum melted material and, as a result, the lives of the first failures are only improved in the same proportion that the load rating determined for the entire population is increased.

Consumable electrode vacuum melted steel permits as long bearing life as obtained with induction vacuum melted material and is less likely to contain rejectable non-metallic inclusions.

Acknowledgment

The authors acknowledge, with thanks, permission of the United States Air Force to present in this paper a portion of the data collected during the investigations under Contract AF33(600)22860.

REFERENCES

1. Bhat, G. K. and Nehrenberg, A. E., "A Study of the Metallurgical Properties that are Necessary for Satisfactory Bearing Performance and the Development of Improved Bearing Alloys for Service Up to 1000°F," W.A.D.C. Technical Report 57–343, November 1957.
2. Styri, H., "Fatigue Strength of Ball Bearing Races and Heat Treated 52100 Steel Specimens," *Proc. ASTM*, v. 51, 1951, pp. 682–700.
3. AFBMA Standards, "Method of Evaluating Load Ratings of Annular Ball Bearings,"
4. Weibull, W., "A Statistical Theory of the Strength of Materials," IVA Handlingar (Royal Swedish Academy of Engineering Sciences, *Proceedings*), n. 151, 1939.
5. Lundberg, G. and Palmgren, A., "Dynamic Capacity of Rolling Bearings," *Acta Polytechnica* 7 (1947), Mechanical Engineering Series, v. 1, n. 3.
6. Morrison, T. W., "Some Unusual Conditions Encountered in the Lubrication of Rolling Contact Bearings," *Lubrication Engineering*, Nov.–Dec. 1955, pp. 405–411.
7. Cordiano, H. V., Cochran, E. P. and Wolfe, R. J., "Effect of Combustion Resistant Hydraulic Fluids on Ball Bearing Fatigue Life," ASME Paper No. 55-Lub-21
8. Otterbein, M. E., "The Effect of Aircraft Gas Turbine Oils on Roller Bearing Fatigue Life," *ASLE Trans.*, v. 1, n. 1 April 1958, pp. 33–39.

Table 1

Steel Identification

Test groups	Steel type	Melting practice	Brg. size	Brg. part	Bar size	Heat no.
1, 2	52100	Cons. vac.	6309	Inner	2½ in.	6X578
3, 4	,,	Ind. vac.	,,	,,	,,	02699
5, 6	,,	,,	,,	,,	,,	1P114
7	,,	,,	,,	,,	,,	1P59
8, 9	,,	,,	,,	,,	,,	1P112
10	,,	,,	,,	,,	,,	1P115
11	,,	,,	1309	Outer	,,	1P59
14, 15	M10	Basic arc	6309	Inner	1⅞ in.	1825
14, 15	,,	,,	,,	Outer	3 in.	1761
14, 15	,,	,,	,,	Balls	½ in.	15024
16	,,	,,	,,	Inner	,,	64127
17, 18	M1	,,	,,	,,	2½ in.	28446
17, 18	,,	,,	,,	Outer	3½ in.	,,
17, 18	,,	,,	,,	Balls	½ in.	,,
19, 20	,,	Ind. vac.	,,	Inner	2½ in.	1C-142
19, 20	,,	,,	,,	Outer	3½ in.	02131
19, 20	,,	,,	,,	Balls	½ in.	1C-142
21, 22	M50	Cons. vac.	,,	Inner	2½ in.	W-21535
21, 22	,,	,,	,,	Outer	,,	,,
21, 22	,,	,,	,,	Balls	½ in.	,,

1. Cons. vac. = Consumable electrode vacuum.
2. Ind. vac. = Induction vacuum.

TABLE 2A

Chemical Analysis

Test groups	Heat no.	C	Mn	P	S	Si	Cr	W	Mo	V	Ni	Cu
1, 2	6X578	1.05	0.26	0.010	0.013	0.25	1.45		0.06		0.05	0.09
3, 4	02699	1.06	0.37	0.002	0.007	0.27	1.54					
5, 6	1P114	0.95	0.32	0.001	0.050	0.32	1.41					
7, 11	1P59	0.98	0.40	0.001	0.013	0.32	1.55					
8, 9	1P112	0.86	0.20	0.001	0.007	0.35	1.42					
10	1P115	0.97	0.28	0.001	0.007	0.34	1.45					
14, 15	1825	0.86	0.25	0.019	0.016	0.31	3.85		7.84	1.98		
14, 15	1761	0.86	0.33	0.020	0.012	0.35	3.83		8.17	1.95		
14, 15	15024	0.88	0.26	0.020	0.013	0.28	3.89	0.63	7.99	2.00		
16	64127											
17, 18	28446	0.81	0.25	0.018	0.011	0.27	3.98	1.59	8.98	1.09		
19, 20	1C142	0.75	0.34	0.022	0.008	0.28	3.60	1.47	9.35	1.22		
19, 20	02131	0.81	0.25	0.005	0.007	0.39	3.75	1.54	8.58	1.22	0.03	0.01
21, 22	W21535	0.79	0.26	0.010	0.003	0.27	4.17	0.031	4.20	1.03	0.05	0.09

TABLE 2B

Gas Analysis

Heat no.	O_2	H_2	N_2
1P59	0.0018	0.00003	0.0018
1P112	0.0012	0.000093	0.00018
1P114	0.0013	0.00016	0.00087
1P115	0.00092	—	0.0013

TABLE 3

Fracture Inspection for Slag

Test groups	Heat no.	No. of disks	No. of streaks in fractures	Total length slag in fracture, $\frac{1}{32}$ in.	Largest streaks
1, 2	6X578	8	0	0	—
3, 4	02699	6	,,	,,	—
5, 6	1P114	4	,,	,,	—
7, 11	1P59	3	,,	,,	—
8, 9	1P112	4	,,	,,	—
10	1P115	,,	,,	,,	—
14, 15	1825	,,	2	4	$\frac{1}{16}$ in.
14, 15	1761	,,	3	5	,,
14, 15	15024	14	2	4	,,
16	64127		NOT AVAILABLE		
17, 18	28446	16	18	28	$\frac{1}{4}$ in.
19, 20	1C-142	4	1	3	$\frac{3}{32}$ in.
19, 20	02131	,,	,,	2	$\frac{1}{16}$ in.
21, 22	W21535	76	,,	1	$\frac{1}{32}$ in.

TABLE 4

Micro Slag Ratings

Test group	Heat no.		No. sample rated	A	B	C	D
1, 2	6X578	Avg.	8	1.3–1	1.6–0	0–0	1.3–0.8
1, 2	,,	W.F.	,,	1.5–0.5	3–0	0–0	1.5–1
3, 4	02699	Avg.	6	0.9–0	0.8–0	0–0	1–0
3, 4	,,	W.F.	,,	1.25–0	1–0	0–0	1–0
5, 6	1P114	Avg.	4	3.4–1.2	0–0	0–0	1.0–0
5, 6	,,	W.F.	,,	3.5–1.5	0–0	0–0	1–0
7, 11	1P59	Avg.	6	0.6–0	0.4–0	0–0	1.3–0
7, 11	,,	W.F.	,,	1–0	1.5–0	0–0	1.5–0
8, 9	1P112	Avg.	4	1.2–0	0–0	0–0	1–0
8, 9	,,	W.F.	,,	1.25–0	0–0	0–0	1–0
10	1P115	Avg.	,,	1.25–0	0.8–0	0–0	1–0
10	,,	W.F.	,,	1.5–0	3–0	0–0	1–0
14, 15	1825	Avg.	15	0.07–0	0.07–0.13	0.2–0	1.5–0.4
14, 15	,,	W.F.	,,	1–0	1–2	1–0	2–0.5
14, 15	1761	Avg.	12	0.3–0	0.5–0	0.3–0	1.9–0.6
14, 15	,,	W.F.	,,	1–0	2.5–0	1–0	2–1
14, 15	15024			NOT AVAILABLE			
16	64127			,,	,,		
17, 18	28446	Avg.	10	0–0	1.9–0.6	0.7–0.5	1.5–0
17, 18	,,	W.F.	,,	0–0	3–3	1.5–2	1.5–0
19, 20	1C142	Avg.	8	0–0	1.7–0	0–0	1.3–0
19, 20	,,	W.F.	,,	0–0	3.0–0	0–0	1.5–0
19, 20	02131	Avg.	4	0–0	0.8–0	0–0	1–0.1
19, 20	02131	W.F.	,,	0–0	1–0	0–0	1–0.5
21, 22	W21535	Avg.	8	0–0	1.2–0	0–0	1.4–0.3
21, 22	,,	W.F.	,,	0–0	1.5–0	0–0	1.5–1.5

W.F. = Worst field.

TABLE 5A

Heat Treatment of Parts: All Parts 52100 Steel

Test group	Brg. size	Part[a]	Quench[b]			Tempering	
			Soak, min.	Oil temp., °F	Emerg. temp., °F	Temp., °F	Time, hrs.
1, 3	6309	I	18	104	302–311	357	1
2, 4	,,	,,	18	104	302–311	455–464	4
5, 6, 8, 9, 10	,,	,,	20–25	113–131	266–302	455–464	4
7	,,	,,	20–25	125–131	260–284	455–464	4
11	1309	O	20–25	125–131	260–284	338–357	¾

[a] I = Inner, 0 = Outer.

[b] Quench temp. was 1562°F on all groups, except for 5, 6, 8, 9 and 10 which was 1572–1580°F.

TABLE 5B

Heat Treatment of Tool Steel Parts: Salt Bath Heat and Quench of 6309 Bearings

Test group	Steel	Preheat, °F	High heat, °F	Quench[a] salt, °F	Temp., °F
14, 15 Inner	M10 (Basic arc)	1544	2202	1112	1051
14, 15 Outer	,,	1552	2202	1102	1051
14, 15 Balls	,,				
16 Inner	M1 (Basic arc)	1526	2202	1122	1051
17, 18 Outer	,,	1508	2182	1148	1051
17, 18 Inner	,,	1508	2182	1148	1051
17, 18 Ball	,,	1526	2210	1130	1051
19, 20 Outer	M1 (Ind. vac.)	1508	2182	1148	1051
19, 20 Ball	,,	1552	2192	1130	1051
19, 20 Inner	,,	1508	2182	1148	1051
21, 22 ,,	M50 (Cons. elec.)	1502	2032	1148	1004
21, 22 Outer	,,	1552	2030	1148	1004
21, 22 Ball	,,	1552	2042	1148	1004

[a] Air cooled after quench, tempered twice, one hour each.

TABLE 6

Hardness of Parts

Test groups	Bearing		Steel	Rockwell C		
	Size	Part		Avg.	Min.	Max.
1	6309	Inner	52100 Cons. vac.	64.0	63.8	64.2
2	,,	,,	,,	61.2	61.1	61.6
3	,,	,,	52100 Ind. vac.	63.3	63.2	63.6
4	,,	,,	,,	60.2	60.1	60.4
5, 6	,,	,,	,,	59.9	59.6	60.3
7	,,	,,	,,	61.2	60.6	61.5
8, 9	,,	,,	,,	59.7	59.1	60.2
10	,,	,,	,,	59.1	59.0	60.3
11	1309	Outer	,,	61.0	60.0	62.0
14, 15	6309	Inner	M10	63.3	62.2	63.8
14, 15	,,	Outer	,,	63.8	62.5	64.2
14, 15	,,	Balls	,,	63.2	62.5	63.8
16	,,	Inner	M1 Commercial			
17, 18	,,	,,	,,	64.0	63.0	65.0
17, 18	,,	Outer	,,	64.5	63.8	64.8
17, 18	,,	Balls	,,	64.5	63.5	66.0
19, 20	,,	Inner	M1 Vac.	62.8	61.8	63.5
19, 20	,,	Outer	,,	64.0	63.4	64.7
19, 20	,,	Balls	,,	65.3	64.7	66.0
21, 22	,,	Inner	M50	64. 7	64.2	65.3
21, 22	,,	Outer	,,	64 ·3	62.5	65.2
21, 22	,,	Balls	,,	64· 6	63.8	65.2

TABLE 7

Results of Magnetic Particle Examination upon Finished Rings

Test group	Steel	Heat no.	Melt. pract.[a]	Part[b]	No. rings	Total no. indications in grooves	Total length indications in $\frac{1}{32}$ in.	Longest indication
1, 2	52100	6X578	C.V.	I	94	1	2	$\frac{1}{16}$ in.
3, 4	,,	02699	I.V.	,,	82	2	3	$\frac{1}{32}$ in.
5, 6	,,	1P114	,,	,,	31	38	53	,,
7	,,	1P59	,,	,,	26	rings not examined		
8, 9	,,	1P112	,,	,,	34	1	1	$\frac{1}{32}$ in.
10	,,	1P115	,,	,,	43	47	112	$\frac{1}{4}$ in.
11	,,	1P59	,,	O	22	0	0	—
14, 15	M10	1825	B.A.	I		rings not examined		
14, 15	,,	1761	,,	O				
16	M1							
17, 18	,,	28446	,,	I	83	59	70	$\frac{1}{16}$ in.
17, 18	,,	28446	,,	O	83	2	2	$\frac{1}{16}$ in.
19, 20	,,	1C142	I.V.	I	77	9	10	$\frac{1}{16}$ in.
19, 20	,,	02131	,,	O	77	1	1	$\frac{1}{32}$ in.
21, 22	M50	W21535	C.V.	I	102	0	0	—
21, 22	,,	,,	,,	O	,,	,,	,,	—

[a] C.V. = Consum. vac., I.V. = Ind. vac., B.A. = Basic arc.
[b] I = Inner, O = Outer.

TABLE 8

Test Group Details

Test group	Material and test element	Melt.[a] pract.	Test[b] temp., °F	URL[c]	Arbor interf. microns	Inner ring groove conf'ty	Outer[d] ring groove conf'ty
1	52100 inners	C.E.	Room	17.6	23.5	51.44	51.74
2	,,	,,	,,	18.6	23.3	51.40	51.79
3	,,	I.V.	,,	17.0	22.0	51.47	51.75
4	,,	,,	,,	17.4	21.9	51.46	51.77
5	,,	,,	,,	11.0	19.6	51.8	51.8
6	,,	,,	,,	,,	20.7	51.7	,,
7	,,	,,	,,	25.0	22.3	,,	51.7
8	,,	,,	,,	11.0	19.7	51.9	,,
9	,,	,,	,,	9.0	,,	,,	,,
10	,,	,,	,,	15.0	19.0	51.7	51.4
11[e]	52100 outers	,,	,,	28.0	19.6	52.0	—
12	52100 brgs.	B.A.	,,				
13	,,	,,	,,				
14	M10 brgs.	,,	,,	16.7	18.2	51.82	51.75
15	,,	,,	450	15.9	16.0	51.80	51.73
16	M1 inners	,,	Room	17.5	21.4	51.87	51.79
17	M1 brgs	,,	,,	9.9	21.6	51.81	51.79
18	,,	,,	450	8.0	20.3	51.77	51.78
19	,,	I.V.	Room	7.9	17.3	51.94	51.75
20	,,	,,	450	8.1	18.8	51.98	51.77
21	M50 brgs.	C.E.	Room	10.0	20.7	51.57	51.78
22	,,	,,	450	11.1	20.3	51.58	51.80

[a] C.E. = Cons. elec., I.V. = Ind. Vac., B.A. = Basic arc.
[b] Room temperature indicates normal temperature rise above room ambient for test condition of load and speed.
[c] Unmounted radial looseness, microns.
[d] As percentage of ball diameter.
[e] Group 11 are 1309 bearings, all other groups are 6309.

TABLE 9

Results of Testing at 1500 rpm, 4240 lb Load

Test group	No. of brgs.	Lube	L_{10} mill revs.	L_{50} mill revs.	Weibull slope e	Outer race temp., °F
1	33	Grease	19	78	1.35	210
2	31	,,	12	70	0.99	207
3	28	,,	11	54	1.17	209
4	30	,,	20	92	1.23	206
5	24	,,	3.6	28	0.92	198
6	27	,,	10	46	1.24	187
7	26	,,	8.6	36	0.99	182
8	27	,,	8.4	40	1.21	190
9	31	,,	7.4	41	1.17	190
10	42	,,	5	36	0.95	199
11	22	,,	4.7	26.2	1.23	178
12	50	,,	4.2	32	0.93	
13	26	,,	37.5	112	1.76	185
14	38	,,	4.5	17	1.41	185
15	36	7808B[a]	2.6	13	1.17	446
16	26	Grease	5.6	37	0.99	199
17	32	Oil	4.3	24	1.10	203
18	35	7808B, C	2.1	8	1.40	446
19	32	Oil	23	90	1.36	185
20	30	7808C	2.6	23	.86	446
21	,,	Grease	~30	>100	—	199
22	,,	7808C	~8	~50	—	446

[a] Group 15 and first 11 bearings of Group 18 were run with MIL-L-7808B fluid having an SOD Lead Corrosion loss of 7.9 mg/sq. in. per MIL-C-8188B. Test Groups 18, 20 and 21 were lubricated with MIL-L-7808C from a single shipment having SOD Lead Corrosion loss of 0.24 mg/sq. in. or less.

TABLE 10

Vacuum Melted 52100 Steel

Steel lot no.	Approx. ingot size	Melt. pract.	Ingot (heat)	Brg.[a] group	Rating as % of AFBMA basic load rating, based on L_{10}	L_{50}
1	5½ in. dia.	Ind.	1P59	7	95	90
		,,	,,	11	108	112
2	6 in. sq.	Ind.	1P114	5	71	83
		,,	,,	6	100	97
		,,	1P112	8	95	93
		,,	,,	9	91	94
		,,	1P115	10	80	90
3	9½ in. sq.	,,	02699	3	103	103
		,,	,,	4	126	123
4	16 in. dia.	C.E.[b]	6X578	1	124	116
		,,	,,	2	106	112

[a] Test components are 6309 inner rings except for Group 11, which are 1309 outer rings.

[b] Consumable electrode.

TABLE 11

Domestic Basic Arc 52100

Brg. group	Melting practice	Test brg.	Rating as % of AFBMA basic load rating, based on L_{10}	L_{50}
12	Basic arc	6309	75	86
13	Basic arc	6309	155	131

TABLE 12

Test Results ½-in. Diameter Balls

Material	Ball set lives, millions of inner race revolutions Max.	Min.	Avg.	Failed inner races	Failed outer races[a]	No. of ball sets[b]	No. of ball failures
Vacuum melted ingot 1-P-58	169.2	121.0	143.0	60	79	5	0
Vacuum melted ingot 1-P-115	143.1	99.2	126.0	49	71	6	0
Commerc'ly melted domestic 52100	74.4	1.6	16.5	79	82	95	74
Commerc'ly melted Swedish 52100	58.1	12.4	28.7	20	20	12	1

[a] Each ball set consists of thirty ½-in. balls.

[b] These outers had 1, 2 or 3 failures by indexing 120°.

TABLE 13

Test Results for Tool Steels

Brg. group	Melting practice	Material	Temp., °F	Rating as % AFBMA basic load rating, based on L_{10}	L_{50}
14	Basic arc	M10	Room	77	70
15	,,	,,	450	64	64
16	,,	M1	Room	83	91
17	,,	,,	,,	76	78
18	,,	,,	450	60	54
19	Ind. vac.	,,	Room	132	122
20	,,	,,	450	64	77
21	Cons. vac.	M50	Room	144	126
22	,,	,,	450	93	100

APPENDIX

For convenient reference, the test results in this paper have been analysed in a consistent manner with "AFBMA Standard Method of Evaluating Load Ratings of Ball Bearings", Section No. 9, Revision No. 2, dated August 1957, published by the Anti-Friction Bearing Manufacturers' Association, Inc.

The above publication says that "'the rating life' (L_{10}) of a group of apparently identical ball bearings is the number of revolutions that 90% of a group of bearings will complete or exceed before the first evidence of fatigue develops. As presently determined, the median life (L_{50}) which 50% of the group of ball bearings will complete or exceed is approximately five times this rating life." Hence, in this paper the test capacities are based upon the test rating life and/or one fifth of the median life read from the Weibull plots.

In addition, the Standard defines the "basic load rating" "as that constant stationary radial load which a group of apparently identical ball bearings with stationary outer ring can endure for a rating life of one million revolutions of inner ring."

The basic Load Rating, C, for radial ball bearings of the type reported here is given by the formula

$$C = f_c(i\cos\alpha)^{0.7}Z^{2/3}D^{1.8}$$

where i = the number of rows per bearing

α = the nominal angle of contact

Z = number of balls per row

D = ball diameter

f_c = a factor which depends on the geometry of the bearing components

The values for the quantities listed above in inch-lb units for 6309 and 1309 bearings are:

Brg.	f_c	i	α	Z	D	C
6309	4480	1	0	8	$\frac{11}{16}$ in.	9120
1309	2345	2	9° 25′	15	$\frac{1}{4}$ in.	6600

For comparing test results with the AFBMA capacity, the capacity corresponding to test results is taken as

$$C_{\text{Test}} = F_R(L_{\text{Test}})^{1/3}$$

where L_{Test} is the 10% life from the Weibull plots or one-fifth the median life in millions of revolutions.

For these tests $F_R = 4240$ lb.

DISCUSSION

WILLIAM J. DERNER (*Curtis-Wright Corporation, Wright Aeronautical Division*):

The authors are to be congratulated on making a straightforward approach to the problem of improving the reliability and capacity of rolling contact bearings. This problem, which is complicated by the effects of high temperature and lubricant properties, must be solved in a practical, conclusive manner if we are to capitalize on material and processing improvements now available to us. Due to the upsurge in the commercial aircraft applications of gas-turbine engines, an added impetus has been given to the demands for better bearings.

Though the effects of high temperature and lubricant properties must be dealt with before the overall bearing material problem is fully solved, I feel that we cannot permit the basic issue to be sidetracked or confused by them. This primary objective is to develop bearing materials which will improve the reliability and capacity of rolling contact bearings.

This paper makes a significant addition to the data now available, but of itself does not permit a proper conclusion to be drawn. Since the issue is clouded when we attempt to account for the effects of temperature and lubricant, I should like to restrict my discussion to the consideration of bearing material alone.

We have all waited for the introduction, by the steel industry, of production batches of "clean" vacuum-melted steel. Though the advent has been painful, the last twelve months has seen one or more steel companies demonstrate an ability to consistently produce practical lots of bearing steels which meet or surpass the highest cleanliness standards. Though these lots are generally consumable electrode batches, a significant number have been from induction vacuum-melts. Detailed metallurgical examination has shown them to be more uniform and cleaner than the induction vacuum-melted and consumable-electrode batches offered in previous years. At the writer's company, a distinct improvement has been noted in cleanliness ratings of 52100 batches produced in early 1958 over those procured in mid-1956. Inclusion frequency, size, and segregation have been bettered. As an example the following illustrations are offered (Figs. 1, 2 and 3).

This information is in agreement with the suggestion by the authors that improvement in the art of making 52100 steel has permitted better fatigue characteristics. Though cleanliness alone does not necessarily account for the difference, it is expected that the "cleaner" steels also show the benefits of improved grain size, alloy distribution, segregation, inclusion particle dispersion, and other desirable properties.

The data presented in this paper represents the condition of the original material samples but not the results of post-test chemical and metallurgical examination. If these have been made, was it possible to account for the causes of failure? Though it would seem repetitious and only slightly

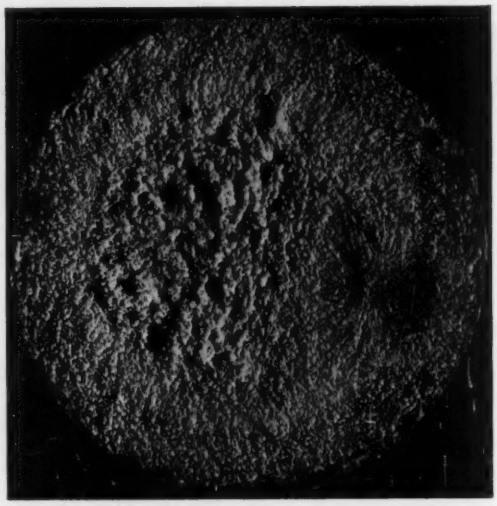

FIG. 1. Inclusion of fatigue nucleus.

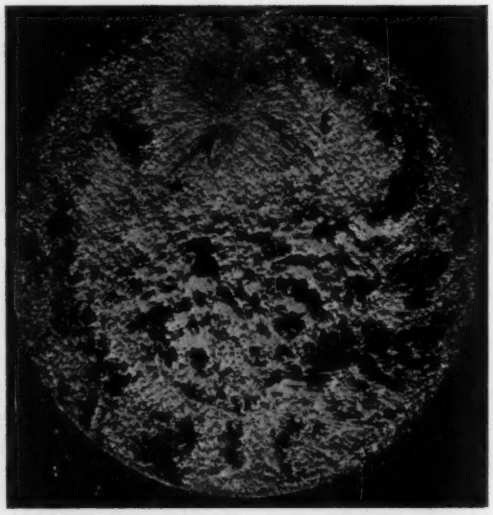

FIG. 2. Inclusion of fatigue nucleus.

relevant to some, it may be possible to account for the early failures by such a detailed examination. I should like to hear the author's comments on this, since there is no other explanation offered to account for the performance of the vacuum-melted balls (Table C) which was so paradoxically superior to that of races made from similar material.

In addition, I should like to have them answer the following:

1. What precautions were taken to verify dimensions of the various bearing components?
2. Was a post-test examination made to cull out those failures not attributable to normal fatigue?

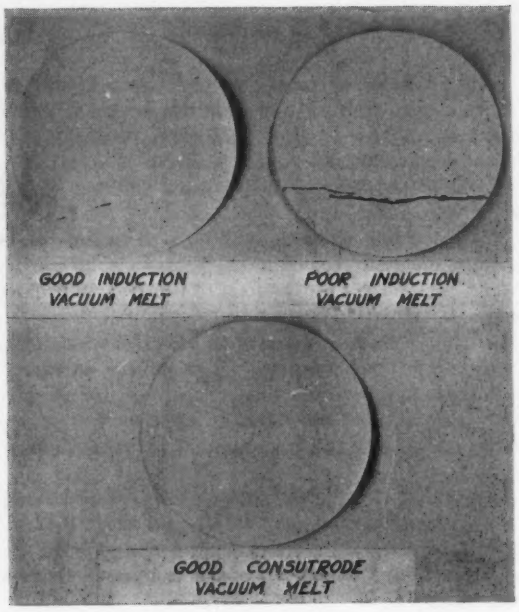

FIG. 3.

Since other investigators have reported a definite improvement in average life and a reduction in early failures resulting from the application of cleaner steels, I feel that we can be more optimistic in our appraisal of such material. (See H. HANAU, New Departure as reported in *Machine Design*, November 15, 1956, page 103, as shown by the Weibull plot on Fig. 4, and another competitive bearing firm which has noted a reduction in early failures resulting from the testing of bearings made from "premium quality steels".) I would suggest that a stricter surveillance of material batches, with the purpose of holding all to closer standards, would result in more uniform results.

It should be noted that the authors, as well as Lundberg and Palmgren (as stated in *Acta Polytechnica* 7/1947 "Dynamic Capacity of Rolling Bearings",) appreciate the attributes of "Swedish bearing steel". As these steels have exhibited a superiority over commercial 52100, it is again indicated that we have reason to be optimistic.

In this latter reference, the authors have referred to the fatigue characteristics of the Swedish 52100 steels. Perhaps, before we continue our work, we should consider the answers to the following questions:

1. What are the fatigue characteristics which Lundberg and Palmgren mention?
2. Is the variation in fatigue life from lot to lot due to cleanliness?
3. Is the reported superiority of vacuum-melted balls over vacuum-melted races due to grain orientation, processing or some other phenomena?
4. If it can be concluded from this testing that vm balls are more resistant to sub-surface damage during denting,

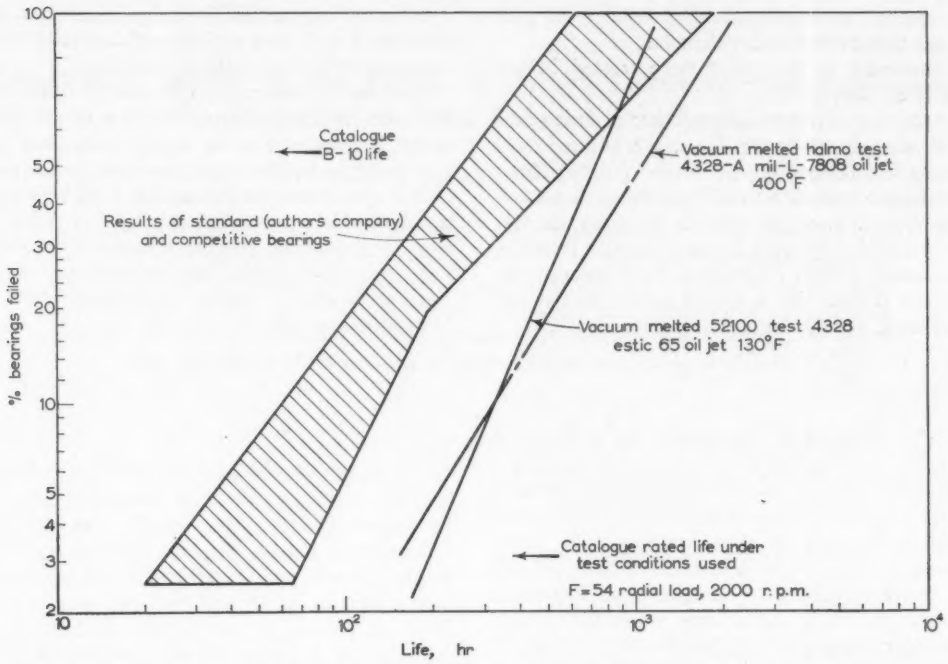

FIG. 4. Weibull life distribution curves. Comparison of standard vs. vacuum melted steels under radial load.

can we attribute this to some characteristic of the VM material (such as resiliency or ductility)?

5. Have we given proper cognizance to the "microscopic shapes of the weak points" and to the "dispersion in the number of weak points" as pointed out by Lundberg and Palmgren? (p. 9 of *Acta Polytechnica* 7/1947).

6. If we agree with the authors, that there is no reduction in life scatter resulting from the use of cleaner steels (as represented by the consumable electrode batches they tested), can't we still agree on the reduction in early failures or in the shift of the characteristic Weibull plot?

7. Can we add to the data, submitted by the authors, that collected by other investigators, to the end that the performance of up-to-date consumable-electrode steels is firmly substantiated?

In conclusion, I should like to state that it is my opinion that sufficient data is now available, if properly collated, to prove the superior performance of modern premium quality "clean" bearing steels. This proof must be assembled, concurred-in, and published as a coordinated bearing industry effort so that full advantage may be taken of the benefits offered. From this should come a new basic bearing material specification which will insure that improved performance and reliability can be guaranteed in the immediate future. This practical end is necessary before we in the aircraft engine field can solve the high temperature problem confronting us.

Therefore, it is apparent that the bearing industry should re-appraise their requirements for clean material and set about to make use of the better steels that are available.

AUTHORS' REPLY (*SKF Industries, Inc., Front Erie Ave., Philadelphia 32, Penna.*):

An attempt will be made to answer, insofar as possible, the various questions raised by Mr. Derner.

In conducting an endurance test on bearings in the laboratory with which the authors are associated, the following procedures are normally used. The material to be tested is first investigated for cleanliness and other pertinent metallurgical characteristics. The parts are carefully followed through the factory to insure that all phases of manufacture are properly performed. After heat treatment and grinding, parts are appropriately etched to detect the presence of possible grinding damage. Parts are checked for hardness and magnaflux tested, and the results recorded. Dimensional measurements of important characteristics are made and recorded.

After completion of the endurance test, representative parts throughout the life range are thoroughly investigated. Usually, in the case of rings, by the time a detectable spall or flaking occurs, there is very little chance of finding the initiation of failure. In balls and rollers, however, the flakings usually exhibit a pattern of successive removal of metal which clearly defines the origin. In low life ball failures, this is frequently a slag streak. Balls seem to be more sensitive to failure at slag streaks than other bearing elements. It is probably for this reason that the greater

cleanliness achieved by vacuum-melting shows more gain in life for balls than other bearing elements.

Bearings discussed in the paper were treated in the manner described above.

With the exception of rare occasions where a bearing fails from some obvious abuse—in which case it is omitted from the test results—all failures are by normal fatigue. However, normal fatigue follows the well established dispersion shown in the Weibull plots. As stated in the paper, the test results do not indicate any reduction in dispersion from the use of vacuum-melted steel. Where there has been improvement in life, the Weibull line is shifted so that lives at any level are increased, but the dispersion is not reduced.

Certainly fatigue does not always initiate at non-metallics. Whether it may start at unfavorable crystal boundaries or crystal imperfections remains to be seen.

Thus far, any attempts to correlate endurance of bearing steel with mechanical characteristics of the material have failed. Reference is made to the work done at Syracuse University under the direction of George Sachs for NACA.

It is agreed that the publication of all bearing endurance test data which might shed any light on this general problem of improvement in life and reliability is highly desirable. From the present state of our knowledge, it is not believed possible to write a bearing steel specification that would control bearing life.

A Theoretical Study of the Effect of Offset Loads on the Performance of a 120° Partial Journal Bearing

By A. A. RAIMONDI[1]

Reynolds' equation for a 120° partial journal bearing of the clearance type having an L/D ratio of 1 is solved numerically to determine the effect of positioning circumferentially the line of action of the load at various points along the bearing arc. The influence of the load position (α/β) on film thickness, eccentricity, journal position, friction, flow, temperature rise, and maximum film pressure is investigated and performance curves given. It is shown that the position of the load has a significant effect on bearing performance.

Introduction

PARTIAL journal bearings can be conveniently classified into two distinct types depending upon the location of the line of action of the load. These two categories consist of (a) offset bearings and (b) centrally loaded bearings. In the centrally loaded partial bearing the line of action of the load is located so as to bisect the bearing arc whereas in the offset bearing (or eccentrically loaded bearing as it is sometimes called) the load line can occur at any angular position other than that yielding central loading. Offset bearings may be further subdivided depending upon the direction of offset relative to the direction of rotation (Fig. 2). This paper is mainly concerned with the properties of offset bearings.

In the past, only a few workers have concerned themselves with offset bearings. During the years 1928–29, Howarth (1) and Boswall (2) described respectively the theoretical behavior of offset bearings with arcs of 120° and 90°. These analyses, however, were limited to bearings of infinite length and did not rigorously account for the effects of rupture of the lubricant film. In 1932 Boswall and Brierly (3) conducted some tests which were qualitatively compared with the limited theoretical data then available. From 1932 to date very little work on offset bearings is reported other than that of Pinkus (4) who treats a bearing of special design and Boswall (5) who gives limited data on finite bearings and Howarth (6) who summarizes the results of his earlier work. It is noteworthy that all the recent texts on lubrication have neglected this aspect of bearing performance presumably because of lack of sufficient data.

Most treatments of partial journal bearings have been devoted mainly to the case of the centrally loading bearing (7–12). This type of loading is widely prevalent in practice since it maintains symmetry regardless of the direction of rotation, simplifies the bearing design, and ensures that some portion of the bearing arc will be available to carry the load should the line of action of the load shift in either direction in the application. However, it is of interest to the designer to determine whether or not other load positions are desirable and to ascertain their influence on such performance characteristics as film thickness, friction, flow, temperature rise, etc. It is the purpose of this paper to provide such fundamental information. A partial journal bearing of the clearance type having an arc of 120° and a length-to-diameter ratio of one ($L/D = 1$) was chosen for this study since this design is representative of present bearing practice. However, the results are qualitatively valid for partial bearings having other proportions and arcs. As Howarth (1) employed a 120° bearing in his study, the present paper can in some respects be considered as an extension of his work.

Nomenclature

The nomenclature used is identical with that previously employed (10, 11, 12) and is repeated on the following page. Some of the terms are shown diagrammatically in Fig. 1.

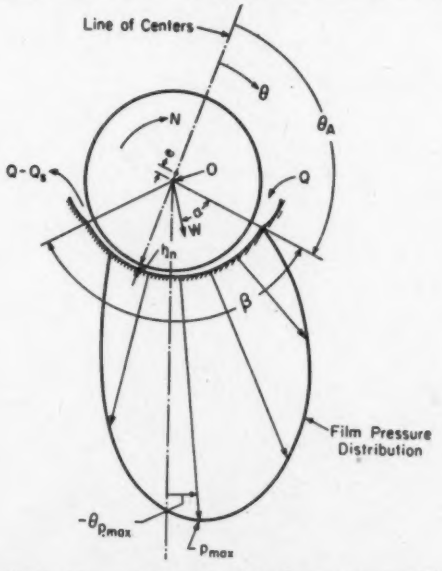

FIG. 1. Nomenclature (bearing drawn for $\epsilon = 0.8$, $\theta_A = 100°$, $\alpha/\beta = 0.408$).

Presented as an American Society of Lubrication Engineers paper at the Lubrication Conference held in Los Angeles, Calif., October, 1958.

[1]Research Engineer, Westinghouse Research Laboratories, Churchill Borough, Pittsburgh 35, Penna.

W = load, lb
N = speed, rps
R = journal radius, in.
D = journal diameter, in.
L = axial length of bearing, in.
$P = W/2RL$ = load per unit projected bearing area, psi
μ = viscosity in reyns, lb sec/in^2
h_n = minimum film thickness prevailing in bearing arc, in.
C = radial clearance = bearing radius—shaft radius, in.
e = journal displacement or eccentricity, in.
$\epsilon = e/C$ = eccentricity ratio, dimensionless
F = friction force on journal, lb
$f = F/W$ = coefficient of friction, dimensionless
Q = flow of lubricant drawn into clearance space by journal, in /sec.
Q_s = flow of lubricant out both sides of bearing, in^3/sec.
β = angular extent of bearing arc, deg
θ = angular coordinate, measured in direction of rotation, deg
θ_A = angle from line of centers to leading edge of bearing, measured in direction of rotation, deg
α = load angle, measured from leading edge to the line of action of the load, deg
$\theta_{p_{max}}$ = position of max. film pressure, deg
p = film pressure, psig
p_{max} = max. pressure developed in lubricant film, psig
$S = (R/C)^2 \mu N/P$ = bearing characteristic number, dimensionless
t_1 = lubricant inlet temp., deg F
t_2 = lubricant outlet temp., deg F
Δt = temp. rise = $t_2 - t_1$, deg F
c = specific heat of lubricant, Btu/lb deg F
γ = weight per unit volume of lubricant, lb/in^3
J = mechanical equivalent of heat = 9336 in lb/Btu

Type of loading

The various types of loading that can be experienced with a partial bearing are illustrated in Fig. 2 for a bearing having the arc β. Figure 2(b) shows the "centrally loaded" case where the load line bisects the bearing arc giving $\alpha/\beta = 0.500$; Figs. 2(a, c) show the "offset" cases. In Fig. 2(a) the load is offset counter to the direction of rotation and the load angle α is less than one-half the bearing arc, i.e., $\alpha/\beta < 0.500$. However, in Fig. 2(c) the load is offset in the direction of rotation and the ratio α/β exceeds 0.500.

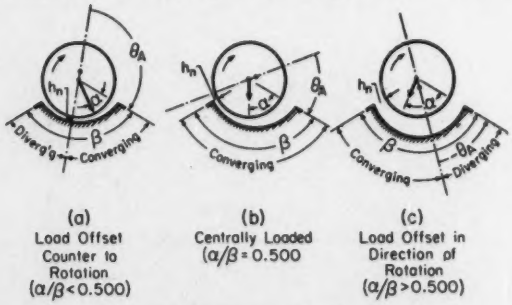

FIG. 2. Types of loading.

Figure 2, drawn for a fixed value of the eccentricity ratio ϵ, shows that as the load line shifts, the position of the journal which is characterized by the "entrance angle" θ_A will vary thus altering the shape of the lubricant film. A change in the film shape will in turn rearrange the distribution of the film pressures (Fig. 1) so that the resultant film pressure will coincide with the line of action of the load in order that equilibrium be restored. As a consequence of the altered film shape, the performance characteristics, to be discussed subsequently, are affected.

The lubricant film shape can fall into one of three classifications. These classifications are illustrated respectively in Figs. 2(a, b, c) as: (a) converging-diverging, (b) wholly converging, (c) diverging-converging. It can be seen from Fig. 2(c) that negative values of θ_A[2] will cause the film to be diverging at the leading edge while positive values of θ_A will result in converging films at the bearing entrance.

It should be mentioned that the film shape is not always related to the type of loading in the manner shown in Fig. 2. The exact relationship may be determined from either Fig. 4 or Fig. 14 which will be discussed subsequently.

Analysis

The results given in this paper were obtained by solving numerically the fundamental lubrication equations by means of a digital computer. The method of attack, the mesh sizes employed, and other pertinent information have been reported elsewhere (12) and need not be repeated. However, mention should be made of the two main assumptions used:

(a) The viscosity of the lubricant was assumed to be constant as was done before in (10, 11, 12) in order that the present paper be a logical and consistent extension of previous work, thus permitting comparisons and inferences to be made readily.

(b) The effects of rupture of the lubricant film in the diverging regions were accounted for by using the boundary conditions that were discussed in detail in (12)[3].

Results

Pressure Distributions

With converging-diverging film shapes such as that illustrated by Fig. 2(a) cavitation or film rupture was found to occur in the diverging portion of the film, that is, near the trailing edge. A typical pressure distribution taken from the results for such an operating condition is drawn in Fig. 3(a) for $\epsilon = 0.8$, $\theta_A = 100°$. With wholly converging film shapes (Fig. 2b) no film rupture was experienced; a typical pressure distribution is shown in Fig. 3(b). On the other hand, with the diverging-converging film shape

[2] θ_A is taken positively in the direction of rotation (see Nomenclature).

[3] Namely, that $dp/d\theta = p = 0$ at point of film rupture.

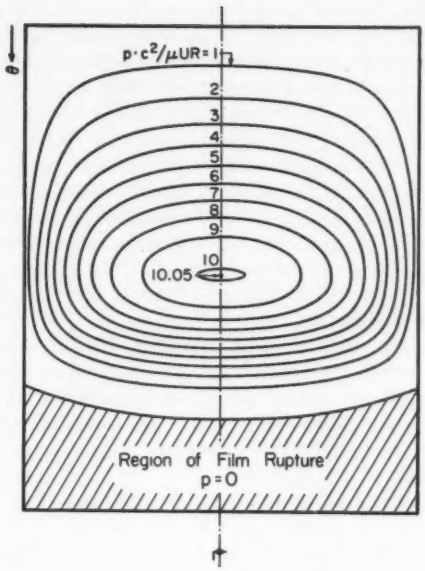

FIG. 3(a). Typical pressure distribution for converging-diverging film shape ($\epsilon = 0.8$, $\theta_A = 100°$, $\alpha/\beta = 0.450$).

such as that shown by Fig. 2(c), film rupture would tend to occur near the leading edge of the bearing. A typical pressure distribution for such a case is given in Fig. 3(c), drawn for $\epsilon = 0.8$ but $\theta_A = -40°$. An interesting result of this study was the discovery that for all the eccentricity ratios investigated (up to and including $\epsilon = 0.97$), no film rupture was experienced near the entrance of the bearing as long as the entrance angle θ_A was greater than $-30°$.

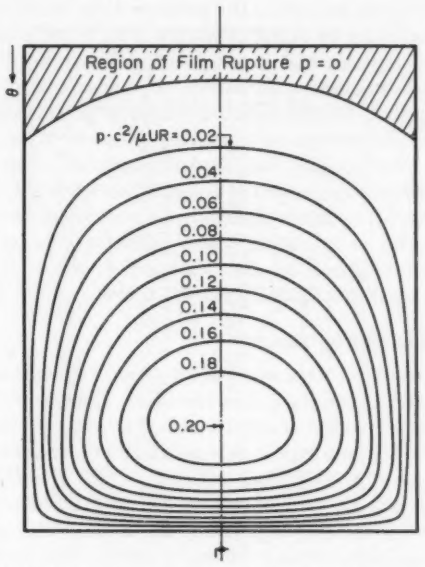

FIG. 3(c). Typical pressure distribution for diverging-converging film shape ($\epsilon = 0.8$, $\theta_A = -40°$, $\alpha/\beta = 0.676$).

Figure 3(d) shows the negligible rupture areas existing near the sides of the bearing for $\epsilon = 0.8$ and $\theta_A = 30°$. Thus, it can be seen that a diverging film embracing, say, the first 30 degrees of the bearing arc can exist before extensive film rupture (Fig. 3c) would be incited.

There is presently some question as to whether or not the pressure distribution shown in Fig. 3(c) could prevail in an actual bearing as it has been contended that the

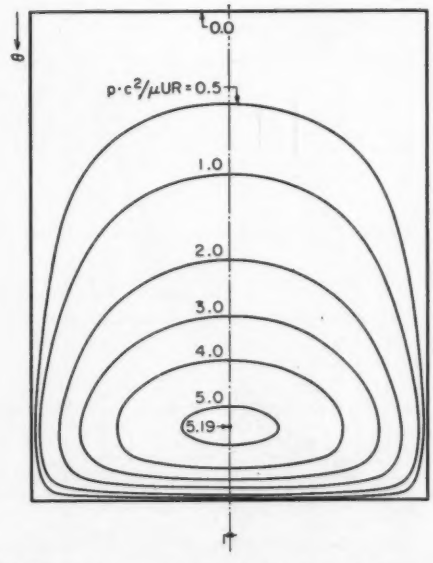

FIG. 3(b). Typical pressure distribution for wholly converging film shape ($\epsilon = 0.8$, $\theta_A = 40°$, $\alpha/\beta = 0.706$).

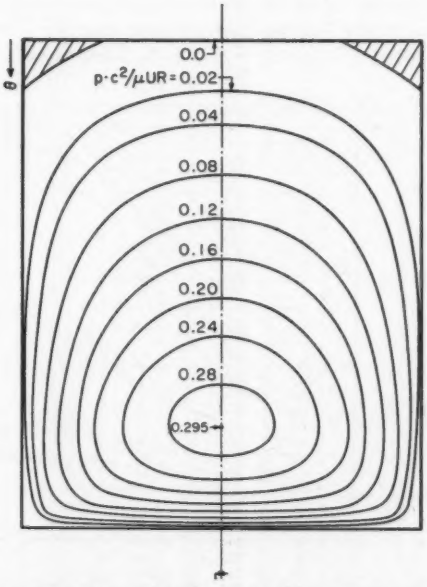

FIG. 3(d). Illustration of small area of film rupture at entrance ($\epsilon = 0.8$, $\theta_A = -30°$).

ruptured area, preceding the pressure area, could interfere in the building up of the pressures. This is one aspect that requires experimental investigation. Chamfering the inlet edge to promote film formation, or pressurizing the lubricant supply at the entrance could delay or perhaps eliminate cavitation in the entrance region. There is some experimental evidence (13) that the latter approach does inhibit rupture depending upon the design of the bearing. However, there is need for more experimental work along these lines. The region of operation where extensive rupture occurs near the entrance of the bearing (i.e., $\theta_A < -30°$) is shaded on all the figures discussed below.

Method of Plotting Results

The results of the numerical solutions of the fundamental lubrication equations are tabulated in Table 1. While the data may be plotted in any manner, the author has preferred the use of the bearing characteristic number, or Sommerfeld number as it is sometimes called, $S = (R/C)^2 \mu N/P$ as the abscissa and the type of loading α/β as the plotting parameter as illustrated in Figs. 4–13. Such plots have the advantage of presenting the performance characteristics as a function of those variables over which the designer or analyst can exercise some control, namely, the radius R, the radial clearance C, the lubricant viscosity μ, the speed N, the unit loading P, and sometimes the type of loading α/β. The effect of design or operational changes in S and α/β on bearing performance thus become more obvious and meaningful. It was first necessary to plot all the performance characteristics against the entrance angle θ_A as shown in Figs. 14 and 15 and to cross plot from these in order to prepare Figs. 4–13.

Entrance Angle θ_A

The manner in which the position of the line of centers varies with the bearing characteristic number S and the load position α/β is given in Fig. 4. As S increases from zero to infinity, for any given value of α/β, the line of centers swings about in the direction of rotation thereby changing the shape of the lubricant film. For example, for $\alpha/\beta = 0.6$, the film shape passes successively through the following three stages: (a) converging-diverging, (b) wholly converging, (c) diverging-converging. Typical pressure distributions accompanying these three film shapes are indicated in Figs. 3(a, b, c) respectively. It can be seen from Fig. 4 that bearings with $\alpha/\beta < 0.500$ remain in the "convergent-divergent" region throughout the entire range of operation and that changes in S have relatively little effect on the journal position θ_A as compared to those bearings operating with $\alpha/\beta > 0.500$.

It is interesting to note from Fig. 4 that as the load sweeps across the arc in the direction of rotation (α/β increasing) the line of centers also moves in the same direction (θ_A decreasing); this is the case for any given value of S and is a useful property that becomes easy to remember.

When the bearing is operating at values of S greater than, say, $S = 0.10$, Fig. 4 shows that small deviations from central loading are responsible for very large movements in the journal position. As these movements greatly alter the film shape and hence the film pressure distribution, it is to be expected they will be accompanied by drastic changes in the performance characteristics. That this is the case is shown in the following discussion.

Minimum Film Thickness and Eccentricity Ratio

In Fig. 5 the minimum film thickness variable h_n/C is plotted for various values of α/β. It should be made clear that the quantity h_n appearing in Fig. 5 represents the least

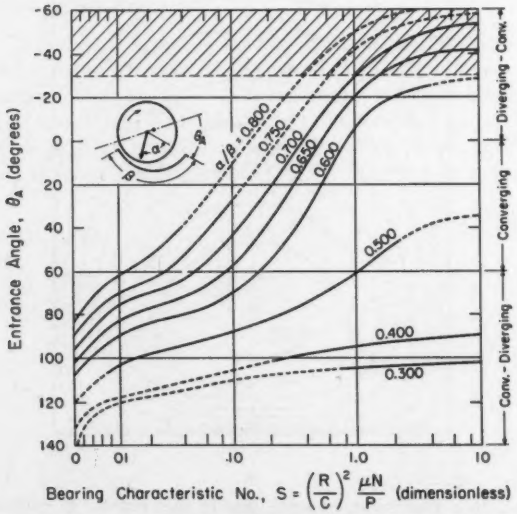

FIG. 4. Entrance angle vs. Bearing characteristic number.

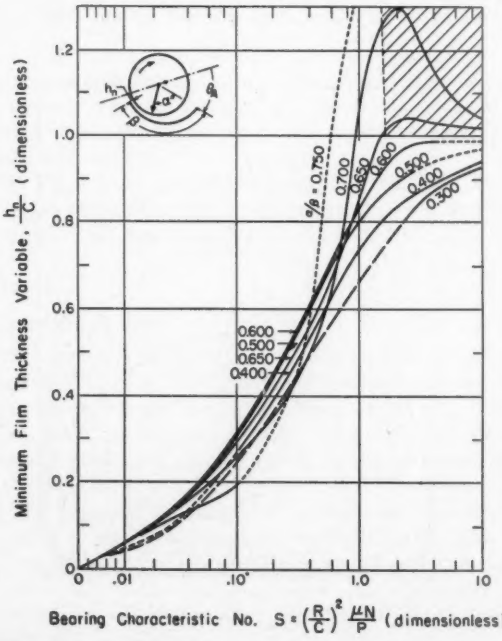

FIG. 5. Minimum film thickness variable vs. Bearing characteristic number.

TABLE 1

Computer Results for 120° Offset Journal Bearings, L/D = 1

ϵ	θ_A	α/β	h_n/C	S	$\frac{R}{C}f$	$\frac{Q}{RCNL}$	$\frac{Q_s}{Q}$	$\frac{Jyc\Delta t}{P}$	$\frac{P}{p_{max}}$	$\theta_{p_{max}}$
0.1	-40	.651	1.1017	6.88	42.1	3.3822	.0342	159.	.347	25.4
	-30	.615	1.00	4.98	30.6	3.41	.0452	115.	.375	22.2
	-20	.586	.9826	3.85	23.9	3.41	.0573	90.5	.396	19.1
	-10	.568	.9658	3.18	19.9	3.40	.0682	76.2	.409	16.5
	0	.554	.9500	2.74	17.4	3.38	.0773	67.2	.418	14.0
	20	.532	.9234	2.27	14.8	3.32	.0886	58.6	.428	9.10
	40	.510	.9060	2.12	14.2	3.24	.0900	57.9	.430	3.36
	60	.482	.9000	2.25	15.5	3.14	.0809	64.6	.424	-3.65
	80	.438	.9000	2.85	20.1	3.05	.0613	85.4	.400	-12.1
	100	.360	.9000	4.70	33.6	2.97	.0370	145.	.348	-21.7
0.2	-40	.656	1.0347	4.09	23.4	3.6229	.0652	83.9	.347	27.1
	-30	.622	1.0000	2.90	16.8	3.68	.0857	59.8	.372	24.3
	-20	.597	.9653	2.20	13.0	3.68	.108	46.8	.392	22.2
	-10	.581	.9316	1.77	10.7	3.66	.129	39.2	.404	20.3
	0	.570	.9000	1.48	9.18	3.62	.147	34.4	.411	18.5
	20	.552	.8468	1.15	7.54	3.49	.170	29.7	.421	14.9
	40	.532	.8121	1.00	6.98	3.32	.175	29.0	.425	9.62
	60	.502	.8000	.998	7.32	3.13	.160	31.9	.422	1.98
	80	.451	.8000	1.20	9.19	2.95	.124	41.8	.400	-8.12
	100	.367	.8000	1.89	14.8	2.79	.077	69.6	.347	-18.7
0.4	-40	.664	1.0694	2.80	14.2	4.1042	.119	46.5	.343	29.6
	-30	.634	1.0000	1.91	10.0	4.22	.156	32.3	.367	28.2
	-20	.616	.9305	1.39	7.58	4.21	.196	25.1	.382	27.4
	-10	.607	.8632	1.07	6.09	4.15	.235	20.9	.390	26.9
	0	.602	.8000	.844	5.10	4.05	.268	18.3	.394	26.4
	20	.594	.6936	.569	3.90	3.77	.318	15.4	.397	24.9
	40	.579	.6241	.426	3.33	3.42	.337	14.7	.402	21.5
	60	.547	.6000	.369	3.32	3.04	.319	15.9	.405	13.6
	80	.484	.6000	.401	3.79	2.69	.256	20.3	.390	0.776
	100	.383	.6000	.574	5.68	2.39	.169	32.6	.342	-14.0
0.6	-40	.670	1.1042	2.46	11.4	4.5855	.163	33.8	.340	32.0
	-30	.646	1.0000	1.63	7.86	4.75	.213	23.3	.360	31.5
	-20	.633	.8958	1.14	5.86	4.72	.271	18.0	.370	31.7
	-10	.630	.7948	.834	4.62	4.62	.325	15.0	.371	32.2
	0	.632	.7000	.620	3.76	4.46	.374	13.1	.369	32.9
	20	.637	.5404	.355	2.68	4.00	.454	10.9	.362	33.7
	40	.634	.4362	.219	2.08	3.44	.498	10.1	.360	32.1
	60	.605	.4000	.160	1.84	2.86	.488	10.7	.368	25.2
	80	.526	.4000	.155	2.03	2.34	.410	13.7	.364	10.5
	100	.408	.4000	.200	2.77	1.93	.289	21.0	.325	-7.24
0.7	-40	.674	1.1216	2.40	10.6	4.8262	.183	30.3	.338	32.9
	-30	.651	1.0000	1.57	7.28	5.01	.239	20.8	.356	32.8
	-20	.641	.8784	1.08	5.40	4.97	.304	16.1	.363	33.4
	-10	.641	.7606	.766	4.21	4.84	.366	13.4	.362	34.5
	0	.646	.6500	.550	3.39	4.65	.424	11.6	.357	35.6
	20	.660	.4638	.287	2.32	4.09	.522	9.64	.342	37.6
	40	.667	.3422	.155	1.70	3.41	.583	8.82	.331	37.2
	60	.643	.3000	.0998	1.41	2.73	.584	9.15	.338	31.2
	80	.553	.3000	.0925	1.52	2.14	.504	11.9	.338	15.6
	100	.425	.3000	.112	1.96	1.67	.370	18.1	.309	-3.24
0.8	-40	.676	1.1389	2.38	10.0	5.0668	.202	27.7	.336	33.8
	-30	.655	1.0000	1.53	6.88	5.27	.263	18.9	.352	34.0
	-20	.648	.8611	1.03	5.06	5.22	.335	14.6	.357	35.0
	-10	.652	.7264	.714	3.91	5.06	.405	12.2	.352	36.5
	0	.660	.6000	.495	3.11	4.83	.471	10.6	.343	38.1
	20	.685	.3872	.230	2.04	4.17	.590	8.72	.317	41.6
	40	.706	.2482	.104	1.38	3.36	.675	7.78	.294	42.3
	60	.691	.2000	.0559	1.05	2.58	.693	7.83	.298	37.4
	80	.588	.2000	.0494	1.12	1.91	.617	10.7	.302	21.3
	100	.450	.2000	.0563	1.37	1.39	.479	16.2	.282	1.94
0.9	-40	.679	1.1562	2.38	9.67	5.3075	.219	25.6	.335	34.6
	-30	.660	1.0000	1.51	6.58	5.53	.285	17.4	.348	35.1
	-20	.656	.8437	1.00	4.81	5.46	.364	13.5	.350	36.5
	-10	.662	.6922	.673	3.69	5.28	.442	11.3	.342	38.4
	0	.675	.5500	.449	2.89	5.00	.517	9.79	.329	40.5
	20	.712	.3106	.182	1.81	4.23	.659	8.01	.289	45.5
	40	.755	.1543	.0626	1.09	3.29	.776	6.82	.246	48.0
	60	.762	.1000	.0232	.697	2.39	.822	6.23	.241	44.4
	80	.640	.1000	.0197	.756	1.65	.763	9.31	.237	27.0
	100	.490	.1000	.0210	.861	1.08	.647	14.8	.227	7.26
0.97	-40	.681	1.1684	2.39	9.47	5.4760	.230	24.5	.333	35.7
	-30	.663	1.0000	1.50	6.42	5.71	.300	16.6	.346	36.3
	-20	.660	.8316	.982	4.68	5.64	.384	12.9	.346	37.5
	-10	.669	.6682	.649	3.56	5.43	.467	10.8	.336	39.6
	0	.685	.5150	.420	2.77	5.12	.548	9.35	.318	41.9
	20	.733	.2569	.152	1.66	4.26	.709	7.59	.268	47.2
	40	.803	.0885	.0372	.878	3.22	.855	5.98	.197	51.9
	60	.854	.0300	.00588	.374	2.24	.931	3.93	.151	51.4
	80	.712	.0300	.00487	.428	1.45	.904	6.77	.155	32.9
	100	.552	.0300	.00493	.455	.846	.843	11.7	.156	13.1

film thickness *prevailing in the bearing arc*. If the line of centers, when projected backwards, intersects the bearing arc as shown in Fig. 2(a), then h_n must necessarily occur along the line of centers. This condition will always exist as long as the film shape is convergent-divergent[4]. However, when the journal assumes a position such as that shown in Fig. 2(c) and the insert in Fig. 5 where the line of centers, when projected backwards, does not intersect the bearing arc, then the least film thickness *prevailing in the bearing arc* does not occur along the line of centers but at the trailing edge of the bearing, i.e., h_n equals the outlet film thickness. This condition will exist for all film shapes other than converging-diverging[5]. When the minimum film thickness is defined in this manner, no limit need be placed on its maximum value in contrast to the case of the full journal bearing where the maximum value cannot exceed the radial clearance because of physical limitations. This discussion is based on the assumption that the bearing has no cap (or top half), or that the cap is relieved sufficiently so as not to interfere with the movement of the journal.

With regard to minimum film thickness it can be seen from Fig. 5 that bearings with loads offset counter to the direction of rotation are inferior to the centrally loaded bearing over the entire range of S. This is analogous to stating that for a given value of h_n these bearings possess less load capacity than centrally loaded bearings. Therefore, in any given application it can be concluded that as the load shifts toward the entrance edge, the load capacity of the bearing is diminished.

On the other hand, Fig. 5 shows that loads offset in the direction of rotation can be either beneficial or detrimental depending upon the magnitude of the offset and the range of S in which operation takes place. For offsets up to $\alpha/\beta = 0.6$, the minimum film thickness is improved over that of the centrally loaded bearing although the improvement is rather slight over most of S. For offsets such that $\alpha/\beta > 0.6$, the minimum film thickness is reduced considerably at the lower values of S at which most bearings usually operate. However, at the higher values of S, it is remarkable that offsetting the load in the direction of rotation will result in a tremendous improvement in the minimum film thickness *prevailing in the bearing arc* and that the greater the offset, the larger the minimum film thickness. However, large film thicknesses in the bearing arc require that the journal operate with large eccentricities as can be seen from Fig. 6 in which the eccentricity ratio $\epsilon = e/C$, where e is the displacement of the journal center relative to the bearing center as measured along the line of centers and C is the radial clearance, is plotted against S for various values of α/β. Indeed, it can be seen from Fig. 6 that when α/β exceeds 0.665, the bearing must operate with eccentricity ratios exceeding unity (and with negative values of θ_A as shown in Fig. 4). This is more evident

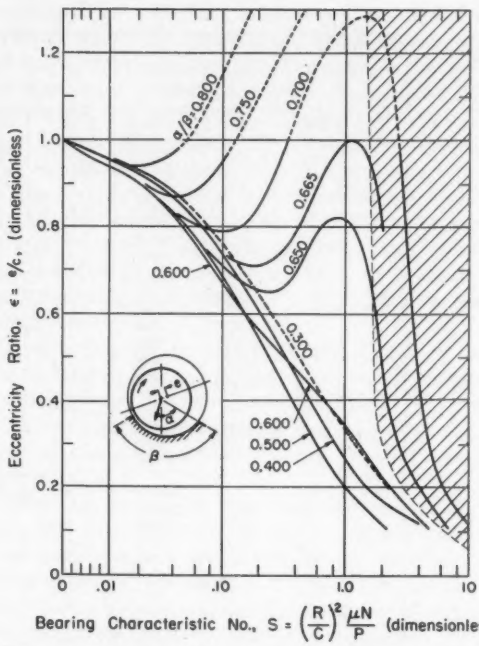

FIG. 6. Eccentricity ratio vs. Bearing characteristic number.

from Fig. 7 where the locus of the journal center is plotted for various offset loads. Lines of constant S are also drawn in Fig. 7. At $S = 0$, the journal is in contact with the bearing ($\epsilon = 1.0$) and at $S = \infty$ the journal center is coincident with the bearing center ($\epsilon = 0$). For intermediate values of S, the journal center will assume a position on the locus curve depending upon the value of α/β. At the

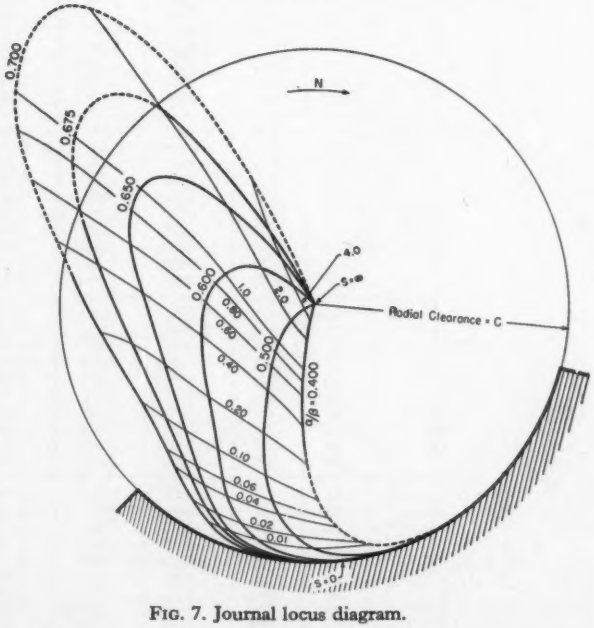

FIG. 7. Journal locus diagram.

[4] That is, as long as $0° < \theta_A < 60°$.

[5] The least film thickness prevailing in the bearing arc could also occur at the leading edge of the bearing when large divergent films are encountered, that is when θ_A is less than $-60°$. However, this range of operation is not taken up in this paper.

higher values of the bearing characteristic number S, it is readily evident from Fig. 7 that small shifts of the load line from central loading toward the trailing edge can result in tremendous swings of the line of centers. It is also interesting to note, as did Howarth (1), that at $S = \infty$, the journal and bearing centers always become coincident regardless of the direction of the load[6].

Other Performance Characteristics

Figures 8, 9, 10 and 11 illustrate the effect of the type of

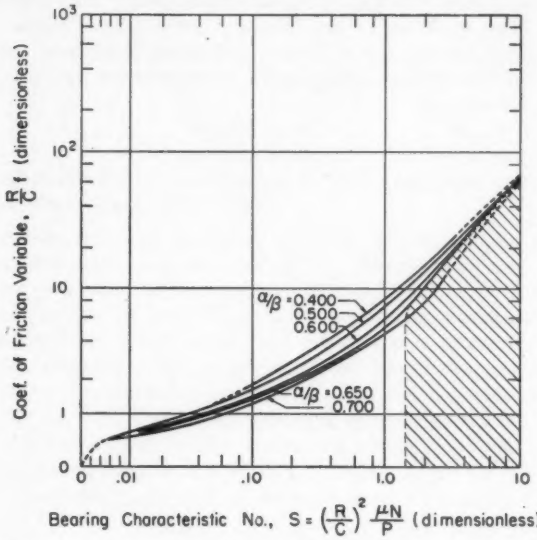

FIG. 8. Coefficient of friction variable vs. Bearing characteristic number.

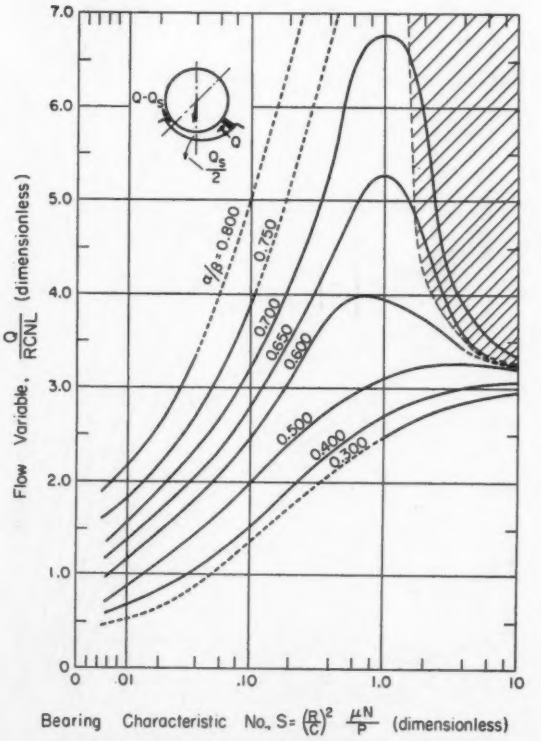

FIG. 9. Flow variable vs. Bearing characteristic number.

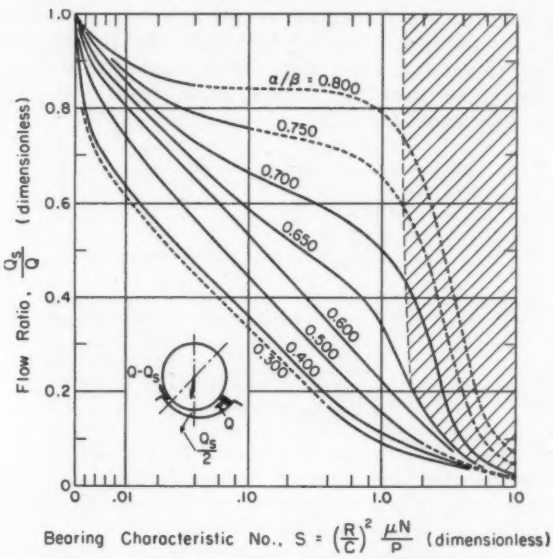

FIG. 10. Flow ratio vs. Bearing characteristic number.

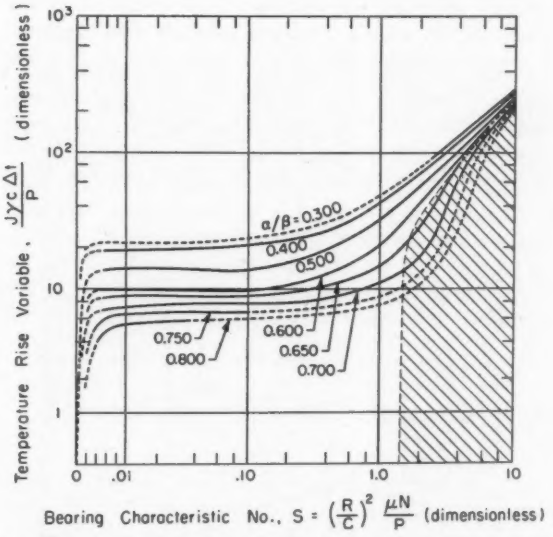

FIG. 11. Temperature rise variable vs. Bearing characteristic number.

[6] This will be true as long as the effect of the friction forces is assumed to be negligible as was done in this paper. When such tractive forces are accounted for, the curves for various α/β's will not necessarily converge at $\epsilon = 0$ when $S = \infty$ but will meet at some point displaced vertically downward from the bearing center by a small amount.

loading on the friction, flow and temperature rise of the bearing. It is very evident from these figures that changes in α/β will influence substantially the performance of the bearing. Using the centrally loaded bearing as a standard for comparison, it can be concluded that bearings with loads offset counter to the direction of rotation develop more friction and higher temperature rises but require less flow. On the other hand, bearings with loads offset in the direction of rotation have less friction, considerably lower temperature rises but require much more flow than centrally loaded bearings.

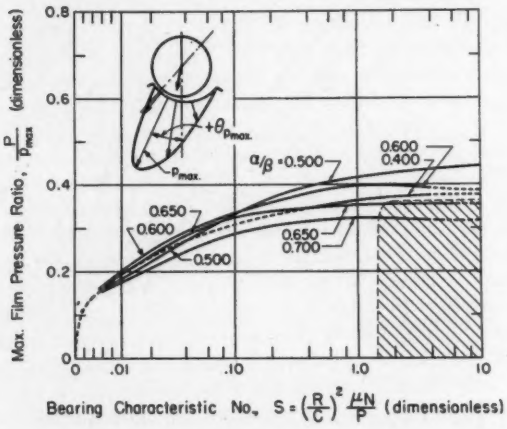

FIG. 12. Maximum film pressure ratio vs. Bearing characteristic number.

Figure 12 illustrates that the peak pressure developed in the lubricant film will, in general, be higher for offset bearings than for centrally loaded bearings at the higher values of S. The manner in which the location of the peak pressures varies with α/β and S is shown in Fig. 13. As would be expected, for any given value of S the maximum film pressure moves across the arc in the same direction as the load line.

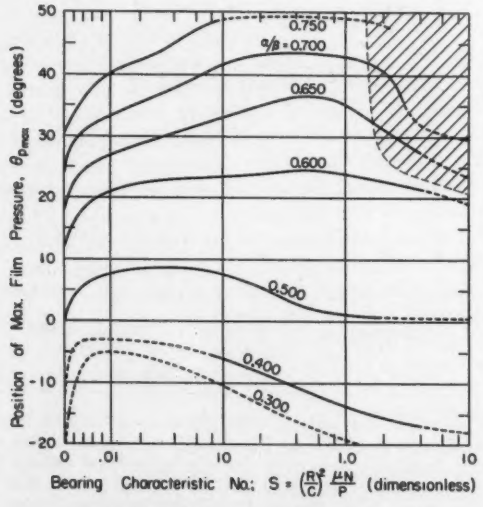

FIG. 13. Location of max. film pressure.

Discussion

(a) *Design Example*—The implications of the data given in Figs. 4–13 can be amplified by considering a specific bearing having the following operating conditions for which the effect of changing the position of the load is to be determined:

$\beta = 120°$	$P = 200$ psi
$L = D = 6$ in.	$C = 0.006$ in.
$N = 3600$ rpm	Lubricant = SAE 20 oil with 110°F inlet temperature.

As the data in Figs. 4–13 are plotted in a manner similar to that given in (10, 11, 12) the method of computation illustrated in (10) may be employed. The results of the calculations are shown in Figs. 16 and 17 where the performance characteristics are plotted against the type of loading α/β. Figure 16 shows that as α/β is increased, h_n increases and has an optimum value at about $\alpha/\beta = 0.6$; this is accompanied by large changes in the journal position θ_A and the eccentricity ratio ϵ which exceeds unity at $\alpha/\beta = 0.7$. It is shown in Fig. 17 that a small change in α/β results in a large variation in flow requirements and

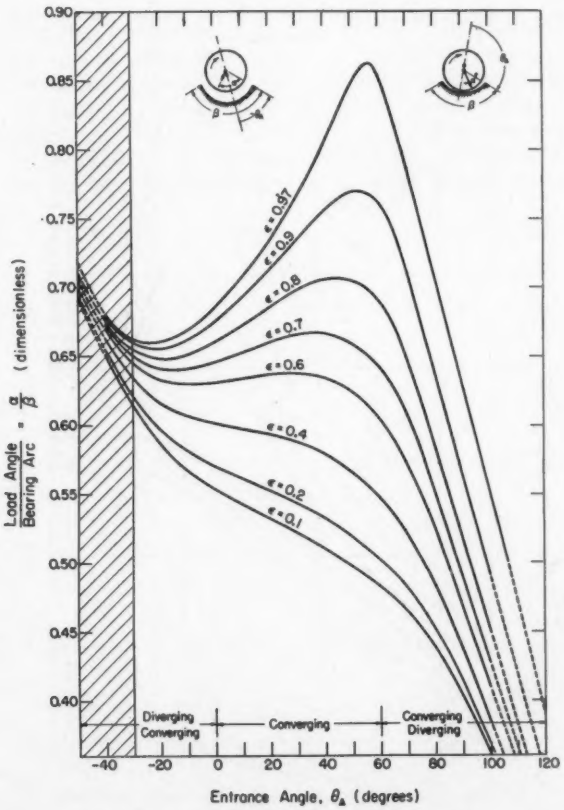

FIG. 14. Type of loading vs. Entrance angle.

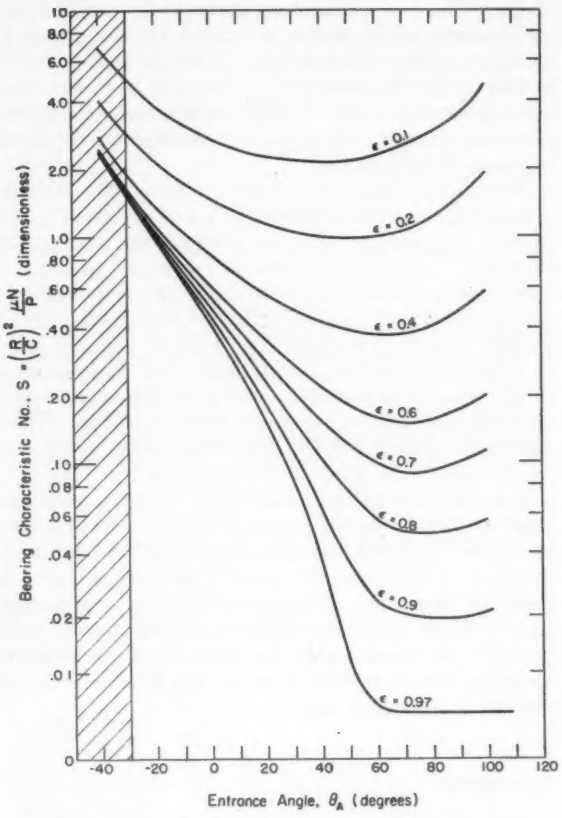

FIG. 15. Bearing characteristic number vs. Entrance angle.

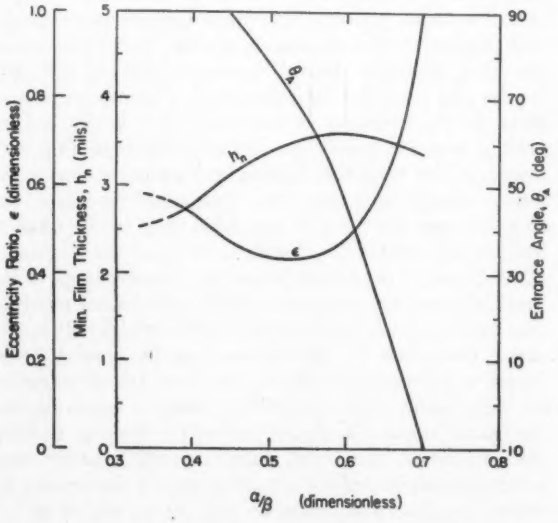

FIG. 16. Effect of type of loading on performance (illustrative problem).

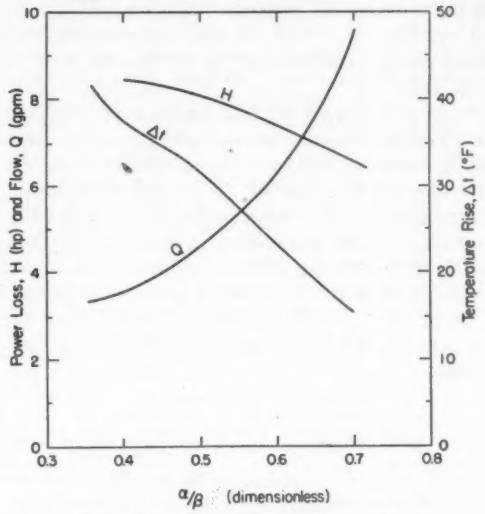

FIG. 17. Effect of type of loading on performance (illustrative problem).

temperature rise and a moderate change in power loss. For example, shifting the load in the bearing from $\alpha/\beta = 0.4$ to 0.6 will decrease the temperature rise by about 100% and require 85% more flow. This increase in flow requirement would not be critical in those applications where an abundant supply of oil was available such as in turbine type bearings. However, in applications where the oil supply is limited such as ring-oiled bearings, drop-fed bearings, wick-fed bearings, etc., a shift of the line of action of the load towards the trailing edge could cause the bearing to operate under starved conditions. Results such as those given in Figs. 16 and 17 can be easily obtained by utilizing the curves given in Figs. 4–13.

(b) *Influence of L/D and Variable Viscosity*—The data presented in the figures and Table 1 are directly applicable to a 120° bearing having a length-to-diameter ratio of 1($L/D = 1$). Complete solutions for other L/D ratios have not yet been obtained[7]. The influence of L/D ratio on the journal locus diagram can be inferred, however, from Fig. 18, where the path for $L/D = \infty$ based on Howarth's

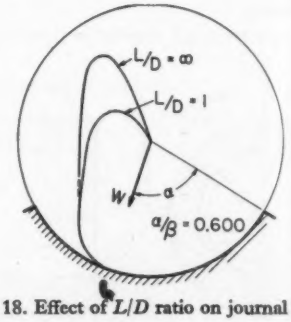

FIG. 18. Effect of L/D ratio on journal locus.

[7] Howarth (1) gives data for $L/D = \infty$ for values of ε up to 0.6, Boswall (5) gives limited data based on an approximate solution of Reynold's equation for $L/D = 2$, 1.5 and 1.0.

work (1) is compared with the path for $L/D = 1$ for the offset bearing $\alpha/\beta = 0.60$. It can be seen that narrower bearings exhibit less tendency for the journal to operate in the top half.

The present analysis is based on the assumption that the viscosity of the lubricant is constant. With such lubricants as oil the viscosity will vary throughout the film, and it is known that this will influence the location of the resultant of the film pressures. For a fixed position of the resultant pressure (i.e., a fixed value of α/β), a change in lubricant viscosity will alter the journal position. This is shown in Fig. 19 by the dotted line whose path is estimated from the work of Boswall (14) and Christopherson (15). A more detailed treatment accounting for viscosity effects is underway.

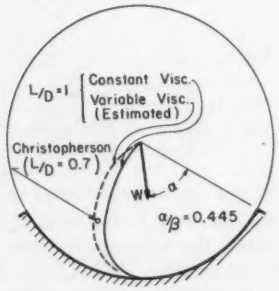

FIG. 19. Effect of variable viscosity on journal locus.

(c) *Effect of Cap*—Since by definition a partial bearing embraces an arc of 180° or less, there is theoretically no physical limitation as to the distance that the journal can travel vertically. Hence, partial bearings with offset loads possess the unique property of being able to operate with eccentricities greater than the radial clearance. This characteristic was borne out in the previous discussion. However, many partial bearings are constructed in practice with caps to exclude entry of foreign material into the bearing arc. The data in this paper will be applicable directly, therefore, if the cap is made so as not to interfere with the movement of the journal. This is readily accomplished by relieving the cap over the entire length of the bearing, the relief being of the order of three or four times the radial clearance.

If the cap is constructed similar to that shown in Fig. 20

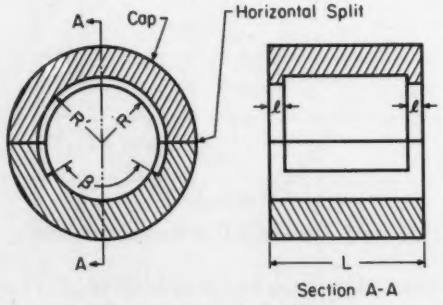

FIG. 20. Typical bearing design.

with small lands "l" extending along the full periphery of the bearing, which design is typical of many turbine bearings and ring-oiled bearings, the data will be applicable as long as the eccentricity ratio ϵ is equal to or less than unity for it is evident that the radial movement of the journal is limited by the lands to a value equal to the radial clearance of the bearing.

Moreover, the least film thickness in the bearing will now necessarily always occur along the line of centers (Fig. 2a) because the lands encircle the journal; its value can be calculated from the equation $h_n = C(1-\epsilon)$, where ϵ is given in Fig. 6. Since the hydrodynamic forces developed over the lands will be negligible the journal can contact the cap. As contact will take place when $\epsilon = 1.0$, the range of S where contact is likely to occur can be determined from either Fig. 6 or Fig. 7. These figures show that operation with α/β exceeding, say, 0.665, should be avoided with bearings similar to Fig. 20 in order to prevent rubbing on the lands in the top half of the bearing.

In some bearings the lands could be made relatively large so that the hydrodynamic forces developed thereon would aid in preventing contact with the cap. However, this subject is beyond the scope of the present paper as there are potentially an infinite number of cap designs, each of which would require analysis. The present paper provides the fundamental data necessary for a complete understanding of bearing behavior and for extending the analysis to treat other cases.

Summary

The effect of the position of the load with respect to the bearing arc on the theoretical performance of a 120° journal bearing of the clearance type with an L/D ratio of 1 is illustrated. It is shown that small deviations from the central loading condition can have significant effects on the performance. Bearings with loads offset counter to the direction of rotation ($\alpha/\beta < 0.500$) show inferior performance with regard to film thickness, friction, and temperature rise than centrally loaded bearings ($\alpha/\beta = 0.500$) but require less flow. On the other hand, bearings with loads offset in the direction of rotation ($\alpha/\beta > 0.500$) exhibit marked superiority over the centrally loaded bearing with regard to film thickness, friction and temperature rise but require considerably more flow. This superiority, however, depends upon the range of operation (that is, the value of the bearing characteristic number S) and the degree of offset. Superior performance over an extensive range of the bearing characteristic number can be experienced provided that the ratio α/β does not exceed 0.600. At high values of S larger minimum film thicknesses can be obtained with values of α/β exceeding 0.600, but these are accompanied by high values of the eccentricity ratio necessitating that the journal operate in the top half of the bearing. In addition, operation with high values of α/β requires large diverging film shapes at the leading edge of the bearing for which condition the operation may be unreliable or unstable. Curves are given from which the performance of offset bearings can be calculated.

Acknowledgment

The author would like to express his appreciation to Mr. John Boyd for his interest and for his sponsorship of the study, and to Mr. Carl Saalbach of the Analytical Section of the Westinghouse Electric Corporation for programming and carrying out the required computer solutions.

REFERENCES

1. Howarth, H. A. S., "Journal Running Positions," *Trans. ASME*, v. 51 (1), 1929, APM-51-3, pp. 21–33.
2. Boswall, R. O., "The Theory of Film Lubrication," Longmans Green New York, 1928, Chapter 9.
3. Boswall, R. O., and Brierly, J. C., "The Film Lubrication of the Journal Bearing," Inst. Mech. E., Excerpt Minutes of Proceedings of the Meetings of the I.M.E. in London and Manchester on 22nd April and 17th March, 1932.
4. Pinkus, O., "Analysis of Journal Bearings with Arbitrary Load Vector," ASLE–ASME Lubrication Conference, Atlantic City, N.Y., October, 1956 ASME Paper No. 56-LUB-2.
5. Boswall, R. O., "Characteristics of the 120 Deg. Journal Bearing," Inst. Mech. E., *Proc. General Discussion on Lubrication and Lubricants*, v. 1, October 1937, pp. 17–22.
6. Howarth, H. A. S., *Kent's Mechanical Engineers Handbook*, 11th ed., *Design: Shop Practice*, John Wiley, New York, pp. 13–03 to 13–58.
7. Needs, S. J., "Effects of Side Leakage in 120° Centrally Supported Journal Bearings," *Trans. ASME*, v. 56, 1934, pp. 721–732; v. 57, 1935, pp. 135–138.
8. Sassenfeld, H., and Walther, A., "Journal Bearing Calculations," *VDI Forschungsheft* 441, Ausgabe B, Band 20, 1954.
9. Boyd, J., and Raimondi, A. A., "Applying Bearing Theory to the Analysis and Design of Journal Bearings, I and II," *J. App. Mech., Trans. ASME*, v. 73, 1951, pp. 298–310.
10. Raimondi, A. A., and Boyd, J., "A Solution for the Finite Journal Bearing and Its Application to Analysis and Design, I," *ASLE Trans.*, v. 1, n. 1, 1958, pp. 159–174.
11. Raimondi, A. A., and Boyd, J., "A Solution for the Finite Journal Bearing and Its Application to Analysis and Design, II," *ASLE Trans.*, v. 1, n. 1, 1958, pp. 175–193.
12. Raimondi, A. A., and Boyd, J., "A Solution for the Finite Journal Bearing and Its Application to Analysis and Design, III," *ASLE Trans.*, v. 1, n. 1, 1958, pp. 194–209.
13. Cole, J. A., and Hughes, C. J., "Oil Flow and Film Extent in Complete Journal Bearings," I. Mech. E., Paper presented on 10th Feb., 1956.
14. Boswall, R. O., and Brierly, J. C., *loc. cit.*, pp. 441–443.
15. Christopherson, D. G., "A new Mathematical Method for the Solution of Film Lubrication Problems," *Proc. Inst. Mech. Engrs.* (London), v. 146, 1942, pp. 126–135.

Pergamon Press are also the publishers of the following journals:

JOURNAL OF NUCLEAR ENERGY (*including* *THE SOVIET JOURNAL OF ATOMIC ENERGY) Part A: REACTOR SCIENCE; Part B: REACTOR TECHNOLOGY; Part C: PLASMA PHYSICS

REACTOR TECHNOLOGY (*Journal of Nuclear Energy, Part B*)

HEALTH PHYSICS (*The Official Journal of the Health Physics Society*)

JOURNAL OF INORGANIC AND NUCLEAR CHEMISTRY

TETRAHEDRON (*The International Journal of Organic Chemistry*)

TALANTA (*An International Journal of Analytical Chemistry*)

INTERNATIONAL JOURNAL OF APPLIED RADIATION AND ISOTOPES

BIOCHEMICAL PHARMACOLOGY

*BIOPHYSICS

*JOURNAL OF MICROBIOLOGY, EPIDEMOLOGY AND IMMUNOBIOLOGY

*PROBLEMS OF HEMATOLOGY AND BLOOD TRANSFUSION

*PROBLEMS OF VIROLOGY

*PROBLEMS OF ONCOLOGY

*SECHENOV PHYSIOLOGICAL JOURNAL OF THE U.S.S.R.

*ELECTRIC TECHNOLOGY, U.S.S.R.

*RADIO ENGINEERING

*RADIO ENGINEERING AND ELECTRONICS

*TELECOMMUNICATIONS

*PHYSICS OF METALS AND METALLOGRAPHY

*THE ABSTRACTS JOURNAL OF METALLURGY

*APPLIED MATHEMATICS AND MECHANICS

CHEMICAL ENGINEERING SCIENCE

JOURNAL OF ATMOSPHERIC AND TERRESTRIAL PHYSICS

PLANETARY AND SPACE SCIENCE

GEOCHIMICA ET COSMOCHIMICA ACTA

BULLETIN GÉODÉSIQUE

ANNALS OF THE INTERNATIONAL GEOPHYSICAL YEAR

SPECTROCHIMICA ACTA

JOURNAL OF THE MECHANICS AND PHYSICS OF SOLIDS

ACTA METALLURGICA (*for the Board of Governors of Acta Metallurgica*)

INTERNATIONAL JOURNAL OF THE PHYSICS AND CHEMISTRY OF SOLIDS

DEEP-SEA RESEARCH

JOURNAL OF NEUROCHEMISTRY

JOURNAL OF PSYCHOSOMATIC RESEARCH

JOURNAL OF INSECT PHYSIOLOGY

JOURNAL OF AIR POLLUTION

INTERNATIONAL ABSTRACTS OF BIOLOGICAL SCIENCES (*for Biological and Medical Abstracts Ltd.*)

RHEOLOGY ABSTRACTS

VACUUM

OPERATIONAL RESEARCH QUARTERLY

ANNALS OF OCCUPATIONAL HYGIENE

* Translations of Russian Journals published on behalf of Pergamon Institute, a non-profit-making foundation.

Leaflets giving further details and subscription rates for each of these journals are available on request

---

PERGAMON PRESS, INC.

122 EAST 55TH STREET, NEW YORK 22, N.Y. 4 & 5 FITZROY SQUARE, LONDON W.1

24 RUE DES ÉCOLES, PARIS V^e^ P.O. BOX 47715, LOS ANGELES, CALIFORNIA

Vol 2 #1

CONTENTS—*Continued*

Page

Fein, R. S., Rowe, C. N. and Kreuz, K. L., Transition Temperatures in Sliding Systems 50

Wisander, D. W., Maley, C. E. and Johnson, R. L., Wear and Friction of Filled Polytetrafluoroethylene Compositions in Liquid Nitrogen 58

Kaufman, H. N. and Boyd, J., The Conduction of Current in Bearings 67

Bennett, P. A., A Surface Effect Associated with the Use of Oils Containing Zinc Dialkyl Dithiophosphate 78

Furey, M. J., Film Formation by an Antiwear Additive in an Automobile Engine 91

Martin, K. B. and Jacobs, R. B., Testing and Operation of Ball Bearings Submerged in Liquefied Gases 101

Anderson, W. J. and Carter, T. L., Effect of Fiber Orientation, Temperature and Dry Powder Lubricants on Rolling Contact Fatigue 108

Jackson, E. G., Rolling Contact Fatigue Evaluation of Bearing Materials and Lubricants 121

Morrison, T. W., Walp, H. O. and Remorenko, R. P., Materials in Rolling Element Bearings for Normal and Elevated (450°F) Temperature 129

Raimondi, A. A., A Theoretical Study of the Effect of Offset Loads on the Performance of a 120° Partial Journal Bearing 147